NASA/CR—2015-218879/VOL1 Honeywell Report No. 21–15066(10)

Acoustic Database for Turbofan Engine Core-Noise Sources, Volume I—Final Report

Grant Gordon
Honeywell Aerospace, Phoenix, Arizona

September 2015

NASA STI Program . . . in Profile

Since its founding, NASA has been dedicated to the advancement of aeronautics and space science. The NASA Scientific and Technical Information (STI) Program plays a key part in helping NASA maintain this important role.

The NASA STI Program operates under the auspices of the Agency Chief Information Officer. It collects, organizes, provides for archiving, and disseminates NASA's STI. The NASA STI Program provides access to the NASA Technical Report Server—Registered (NTRS Reg) and NASA Technical Report Server—Public (NTRS) thus providing one of the largest collections of aeronautical and space science STI in the world. Results are published in both non-NASA channels and by NASA in the NASA STI Report Series, which includes the following report types:

- TECHNICAL PUBLICATION. Reports of completed research or a major significant phase of research that present the results of NASA programs and include extensive data or theoretical analysis. Includes compilations of significant scientific and technical data and information deemed to be of continuing reference value. NASA counter-part of peer-reviewed formal professional papers, but has less stringent limitations on manuscript length and extent of graphic presentations.

- TECHNICAL MEMORANDUM. Scientific and technical findings that are preliminary or of specialized interest, e.g., "quick-release" reports, working papers, and bibliographies that contain minimal annotation. Does not contain extensive analysis.

- CONTRACTOR REPORT. Scientific and technical findings by NASA-sponsored contractors and grantees.

- CONFERENCE PUBLICATION. Collected papers from scientific and technical conferences, symposia, seminars, or other meetings sponsored or co-sponsored by NASA.

- SPECIAL PUBLICATION. Scientific, technical, or historical information from NASA programs, projects, and missions, often concerned with subjects having substantial public interest.

- TECHNICAL TRANSLATION. English-language translations of foreign scientific and technical material pertinent to NASA's mission.

For more information about the NASA STI program, see the following:

- Access the NASA STI program home page at http://www.sti.nasa.gov

- E-mail your question to help@sti.nasa.gov

- Fax your question to the NASA STI Information Desk at 757-864-6500

- Telephone the NASA STI Information Desk at 757-864-9658

- Write to:
  NASA STI Program
  Mail Stop 148
  NASA Langley Research Center
  Hampton, VA 23681-2199

NASA/CR—2015-218879/VOL1 Honeywell Report No. 21–15066(10)

Acoustic Database for Turbofan Engine Core-Noise Sources, Volume I—Final Report

Grant Gordon
Honeywell Aerospace, Phoenix, Arizona

Prepared under Contract NNC10BA07B, Task Order NNC11TA40T

National Aeronautics and
Space Administration

Glenn Research Center
Cleveland, Ohio 44135

September 2015

Acknowledgments

This is the Final Report for the "Acoustic Database for Core Noise Sources Program," which was sponsored by the NASA Fundamental Aeronautics Program, Fixed-Wing Project, under Contract No. NNC10BA07B, Task Order NNC11TA40T. The NASA Technical Monitor was Dr. Lennart S. Hultgren, NASA Glenn Research Center. The editor thanks the staff of the NASA Glenn Research Center for their support and technical insights.

A project of this magnitude and complexity is indebted to the contributions of many team members. In particular, the editor thanks the following Honeywell technical staff for their efforts:
Bill Schuster, Co-Principal Investigator Don Weir, Co-Principal Investigator
Ed Yaple, Development Shop Gary Meshew, Engine Testing
Harvey Niska, Lead Instrumentation Engineer Henry Gruenemeier, Engineering Test Services Hugh McDowell, Engineering Test Services Israel Picazo, Design
John Gerrard, Fabrication John Konves, Design Lead
Joshua Furner, Instrumentation Kaleb Lopez, Design
Marvin Springer, Engineering Test Services Ronald Goodwin, Lead Engine Test Engineer Ronald Swecker, Engineering Test Services Taylor Marotta, Data Analysis
Thomas Gajdecki, Instrumentation Tom White, Engineering Test Services Travis Sorenson, Control Engineer William Landram, Development Shop

This work was sponsored by the Fundamental Aeronautics Program at the NASA Glenn Research Center.

Level of Review: This material has been technically reviewed by NASA technical management.

Available from

NASA STI Program
Mail Stop 148
NASA Langley Research Center
Hampton, VA 23681-2199

National Technical Information Service
5285 Port Royal Road
Springfield, VA 22161
703-605-6000

This report is available in electronic form at http://www.sti.nasa.gov/ and http://ntrs.nasa.gov/

TABLE OF CONTENTS

TABLE OF CONTENTS (CONT)

LIST OF FIGURES

LIST OF FIGURES (CONT)

LIST OF FIGURES (CONT)

LIST OF FIGURES (CONT)

LIST OF TABLES

LIST OF TABLES (CONT)

ACRONYMS

APU	Auxiliary Power Unit
CAD	Computer Aided Design
CEL	Cleveland Electric Labs
CTA	Constant Temperature Anemometry
DGTMS	Dynamic Gas Temperature Measurement System
DTP	Dual Thermocouple Probe
EVNERT	Engine Validation of Noise and Emission Reduction Technology
FFT	Fast Fourier Transform
FPI	Fabry Perot Interferometry
GRC	Glenn Research Center
HP	High Pressure
HPT	High Pressure Turbine
ITD	Inter-Turbine Duct
LP	Low Pressure
LPT	Low Pressure Turbine
NIST	National Institute of Standards and Technology
OASPL	Overall Sound Pressure Level
PRT	Platinum Resistance Thermometers
PSDs	Power Spectra Densities
RMS	Root Mean Square
SOW	Statement of Work
SW	Small Wire
T/C	Thermocouple
TRL	Technical Readiness Level
UFF	Universal File Format

1.0 EXECUTIVE SUMMARY

In this program, a database of dynamic temperature and dynamic pressure measurements were acquired inside the core of a TECH977 turbofan engine to support investigations of indirect combustion noise. Dynamic temperature and pressure measurements were recorded for engine gas dynamics up to temperatures of 3100°F and transient responses as high as 1000 Hz. These measurements were made at the entrance of the high pressure turbine (HPT) and at the entrance and exit of the low pressure turbine (LPT). Measurements were made at two circumferential clocking positions. In the combustor and inter-turbine duct (ITD), measurements were made at two axial locations to enable the exploration of time delays. The dynamic temperature measurements were made using dual thin-wire thermocouple probes. The dynamic pressure measurements were made using semi-infinite probes.

Prior to the engine test, a series of bench, oven, and combustor rig tests were conducted to characterize the performance of the dual wire temperature probes and to define and characterize the data acquisition systems. A measurement solution for acquiring dynamic temperature and pressure data on the engine was defined. A suite of hardware modifications were designed to incorporate the dynamic temperature and pressure instrumentation into the TECH977 engine. In particular, a probe actuation system was developed to protect the delicate temperature probes during engine startup and transients in order to maximize sensor life. A set of temperature probes was procured and the TECH977 engine was assembled with the suite of new and modified hardware. The engine was tested at four steady state operating speeds, with repeats. Dynamic pressure and temperature data were acquired at each condition for at least one minute. At the two highest power settings, temperature data could not be obtained at the forward probe locations since the mean temperatures exceeded the capability of the probes.

The temperature data were processed using software that accounts for the effects of convective and conductive heat transfer. The software was developed under previous NASA sponsored programs. Compensated temperature spectra and compensated time histories corresponding to the dynamic temperature of the gas stream were generated. Auto-spectral and cross-spectral analyses of the data were performed to investigate spectral features, acoustic circumferential mode content, signal coherence, and time delays. The dynamic temperature data exhibit a wideband and fairly flat spectral content. The temperature spectra do not change substantially with operating speed. The pressure spectra in the combustor and ITD exhibit generally similar shapes and amplitudes, making it difficult to identify any features that suggest the presence of indirect combustion noise.

Cross-spectral analysis reveal a strong correlation between pressure and temperature fluctuations in the ITD, but little correlation between temperature fluctuations at the entrance of the HPT and pressure fluctuations downstream of it. Temperature fluctuations at the entrance of the low pressure turbine were an order of magnitude smaller than those at the entrance to the high pressure turbine. Time delay analysis of the temperature fluctuations in the combustor was inconclusive, perhaps due to the substantial mixing that occurs between the upstream and downstream locations. Time delay analysis of the temperature fluctuations in the ITD indicate that they convect at the mean flow speed. Analysis of the data did not reveal any convincing indications of the presence of indirect combustion noise. However, this analysis has been preliminary and additional exploration of the data is recommended including the use of more sophisticated signal processing to explore subtle issues that have been revealed but which are not yet fully understood or explained.

2.0 INTRODUCTION

This report, prepared by Honeywell Aerospace, Phoenix, AZ, hereinafter referred to as Honeywell, presents the final report for the NASA sponsored program Acoustic Database for Core Noise Sources covering the period October 2011 through August 2014. This document covers the Phase I base effort, the Phase II engine test and posttest data reduction effort.

2.1 Document Organization

This document is organized according to the Statement of Work (SOW) tasks:

- Section 2 summarizes the SOW elements
- Section 3 covers the Planning and Instrumentation task
- Section 4 covers the TECH977 Engine Modifications
- Section 5 covers the Data Analysis Methodology
- Section 6 covers the TECH977 Engine Test
- Section 7 covers the Data Processing and Distribution task
- Section 8 provides Conclusions and Recommendations for the overall effort

2.2 Program Task Definition – As Defined in the Statement of Work

2.2.1 Task 1: Planning and Instrumentation

Honeywell shall investigate the technology needed to acquire the dynamic gas temperature fluctuations with peak measurements potential of 2,000°F and frequency responses up to 1000 Hz. To perform this task Honeywell shall:

1. Configure data system to obtain the unsteady temperature fluctuations from sensor signals.

2. Design probes and define installation requirements.

3. Provide thermocouple material for probe fabrication.

4. Identify, acquire, and test in a burner rig a limited number of probes.

5. Provide replacement hardware for the TECH977 engine as required for the instrumentation for unsteady temperature.

6. Develop and deliver a detailed work plan for the base effort.

7. Develop and deliver a draft test plan containing a description of the test objectives and success criteria, requirements to be satisfied, schedule, test description and test conditions, number of tests and duration, and organizations involved with the respective responsibilities identified for the Optional Effort (Phase II).

2.2.2 Task 2: TECH977 Engine Modifications

Honeywell shall perform design modifications to the TECH977 engine for mounting the unsteady temperature and pressure sensors. This task also covers development of instrumentation to acquire the dynamic gas temperature fluctuations with peak measurements potential of 2000°F and frequency responses up to 1000 Hz. To perform this task Honeywell shall:

1. Prepare an instrumentation layout; Honeywell shall seek NASA's advice and concurrence on needed measurements and probe locations.

2. Modify engine hardware and fabricate sensor mounts as required per design.

3. Configure measurement system.

4. Setup, checkout, and calibrate sensor system.

5. Provide estimates of unsteady temperature and pressure measurement uncertainties.

6. Coordinate test schedule and required data acquisition and test support equipment.

7. Refine, finalize and deliver a test plan containing a description of the test objectives and success criteria, requirements to be satisfied, schedule, test description and test conditions, number of tests and duration, and organizations involved with the respective responsibilities identified for the optional Effort (Phase II).

2.2.3 Task 3: Data Analysis Methodology

Honeywell shall identify all of the signal processing and analysis methods needed to process the data to characterize the noise. Techniques shall be configured to process unsteady temperature and pressure fluctuations time history data collected at multiple locations from within the engine. These techniques shall include consideration of circumferential acoustic modes and their axial propagation as well as the characterization of the levels of temperature and pressure fluctuations at the combustor exit plane. Honeywell shall seek NASA's concurrence and advice on the selected data-analysis methods. To perform this task Honeywell shall:

1. Identify existing methods needed for the analysis.

2. Configure and validate the analysis methods required by the instrumentation.

3. Document the selection and configuration of analysis methods.

2.2.4 Task 4: TECH977 Engine Test

Honeywell shall conduct the TECH977 engine test to collect unsteady temperature and pressure fluctuations time history data at multiple locations from within the TECH977 engine. To perform this task Honeywell shall:

1. Rebuild the engine with all modified hardware.

2. Perform an engine health check.

3. Install and terminate the instrumentation.

4. Collect unsteady time histories of temperature and pressure data in the area of the combustor and turbine at various engine operating conditions; Honeywell shall seek NASA's advice and concurrence on measurement locations and engine operating conditions.

5. Develop and deliver a test report providing a record of the testing performed, an analysis and assessment of the test results, and the rationale for decisions.

2.2.5 Task 5: Data Processing and Distribution

Honeywell shall process and distribute the data. This task includes the application of analytical techniques to extract the core-noise components from the unsteady temperature and pressure time history data collected at multiple engine locations during the test runs. To perform this task Honeywell shall:

1. Process temperature and pressure data.

2. Perform acoustic modal analysis of the data.

3. Calculate spectra and root mean square (RMS) levels of the temperature and pressure fluctuations at the combustor exit plane.

4. Distribute the data and analysis results; Honeywell shall provide a data package to NASA with all resulting unsteady databases, including intermediate data sets, unsteady sensor time histories, and documentation.

3.0 TASK 1: PLANNING AND INSTRUMENTATION

3.1 Identification of Candidate Techniques

At the beginning of this program, three technologies were identified as candidate sensors for the measurement of dynamic temperature: constant temperature anemometry (CTA), two wire thermocouple probes, and Fabry Perot Interferometry (FPI). These approaches were investigated to determine their ability to measure fluctuating temperatures at mean temperatures up to 2000°F. The candidates were ranked according to criteria that included frequency bandwidth, measurement accuracy, spatial resolution, sensor life, technical maturity, and technical readiness level (TRL). Table 1 summarizes the rankings of the candidate technologies. From among these alternatives it was determined that the two-wire thermocouple probe was the best approach by a significant margin when considering a variation of attributes.

Table 1. Sensor Evaluation Matrix.

	Importance	Dual thermocouple e.g NASA /PW	Single wire Current driven anemometer e.g. TSI	Thin film Current driven anemometer e.g. TSI	Fabry Perot Interferometer e.g. Prime Photonics
Bandwidth/Response	7	9	9	7	9
Temperature limitation	7	9	5	7	9
Accuracy/resolution	8	8	9	8	9
Spatial resolution	5	9	9	7	7
Sensor life/robustness	9	9	3	5	8
TRL	5	7	7	7	3
HW maturity/risk	3	7	7	9	5
Totals		372	298	304	335

A constant temperature anemometer measurement system can be purchased as a commercial off-the-shelf package from TSI Incorporated, but the fragility of the probe and the lack of high temperature maturity posed significant risk. The Fabry Perot Interferometer holds great promise for these types of measurements, but these systems are not of sufficient maturity to warrant their use on this program. On the other hand, the dual thermocouple approach has been well characterized and documented during previous research and development test programs. Several of these past investigations are documented in NASA technical memoranda and contactor reports (References 1, 2, 3, 4, 5, 6, and 7). This previous work provided an excellent background of the measurement technique and sensor capabilities. Furthermore, the data compensation software used to determine the fluctuating gas temperatures from the two-wire probe measurements had already been developed in previous NASA programs. Thus, the two-wire approach had reached a high level of maturity, and was selected as the measurement technique for this program. In addition, NASA had available a sample temperature probe that could be used to validate the operation and robustness of the two-wire technique for the Honeywell engine application. This probe was loaned to Honeywell to develop experience and gain confidence with this measurement approach.

For the measurement of dynamic pressure, the high temperatures in the combustor and turbine limit the type of instrumentation that can be employed. In the combustor, extreme temperatures preclude the direct mounting of transducers on the combustor wall. For example, water cooled piezoresistive pressure transducers are generally limited to mean temperatures below 1300°F. In such high temperature environments, the semi-infinite tube configuration is a mature and proven technique for measuring dynamic pressure. The sensor is mounted away from the hostile measurement zone. Acoustic waves are carried through a sensing tube past the sensor

and then dissipated beyond the sensor by means of a long coil. Honeywell has gained experience with this method on several past engine test programs. To achieve higher accuracy for engine core measurements, where the mean pressures are very high, differential pressure sensors such as the Kulite XTE-190-10D model have been used. Semi-infinite probes using a minute nitrogen purge flow have been successfully used in previous turbine engine combustor tests to keep the transducers cool and protected from hot combustion gases. In addition to measuring dynamic pressure at a point, circular arrays of these semi-infinite tubes have been used to determine the circumferential mode content at a single axial station in the combustor of a Honeywell APU and a Honeywell propulsion engine (Reference 8). The amplitude and phase response of the transducers and the coils have been studied in these previous programs, and for the frequency ranges of interest in this program, excellent amplitude and phase response can be obtained. One alternative measurement option was considered. Kulite recently introduced the XTEL-SD-625 model transducer, which is a dual dynamic and static transducer with temperature capability to 900°F. The sensor incorporates an innovative mechanical filtering system, which takes the place of the semi-infinite tube, making it much more compact. However, this sensor was not used since the mean temperatures in the TECH977 combustor and turbine exceed its capability.

3.2 Definition of Data Acquisition Systems

NASA Glenn Research Center (GRC) loaned Honeywell a dual fine wire Type B thermocouple probe to assist with the design of the Honeywell probes and definition of the signal conditioning and data acquisition equipment. The probe was received from NASA GRC and used in a bench test to evaluate candidate arrangements. An initial instrumentation setup was proposed and evaluated. Two data acquisition systems readily available at Honeywell were identified as candidates for recording the temperature and pressure time history data. The first system was a Dewetron system, Model 801, configured with 64 channels of dynamic differential amplifiers, series MDAQ-SUB-ACC, and 24-bit delta-sigma analog-to-digital cards, model Orion 1624. The second system was Brüel and Kjær Pulse system, configured with 48 channels of 24-bit analog-to-digital modules, using eight 6-channel LAN-XI Type 3050-A-060 cards, and driven with Pulse Labshop software. Both of these systems provide high-speed simultaneous acquisition of multiple data channels and have excellent dynamic range. The software driving the data systems also provides certain data analysis functionality. The Dewetron system has the capability to perform real time mathematical calculations on the data stream. Particularly useful in this test program was the ability to convert the instantaneous voltages from the temperature probes into physical units. The millivolt readings from the Type B thermocouples were converted to degrees Fahrenheit using National Institute of Standards and Technology (NIST) coefficients that were entered as calculation routines. This is quite helpful during engine testing, as it provides a check that the measured temperatures are in the expected ranges and provides feedback on the engine operation and probe deployment. The Pulse system does not have similar calculation capability, but it does provide the capability to perform real time auto and cross spectral analysis. The Dewetron system was selected as the primary data recorder, with the Pulse system functioning as a backup recorder.

The primary challenge with the temperature measurement is that the voltages produced by Type B thermocouples are very small, typically on the order of a few millivolts. Furthermore, there is a need to resolve the small fluctuating voltages superposed on these mean levels, since this corresponds to the dynamic temperatures of interest. These voltages are on the low end of what the data acquisition systems are designed to record. This introduces two concerns. First, there is a concern about low signal-to-noise ratios due to the voltages being close to the electronic noise floor of the equipment. Second, there is a concern regarding signal

quantization due to the analog-to-digital converters being optimized for a larger voltage range. An obvious solution to overcome these issues is to amplify the signals with a low noise amplifier prior to analog-to-digital conversion.

Figure 1 shows the preliminary signal conditioning and data acquisition setup that was envisioned for the bench, rig, and engine testing. The Type B thermocouple wires are connected to a reference junction and a distribution amplifier, and the amplified signals are then routed into both the Dewetron and Pulse data acquisition systems. During bench testing of the temperature probes, it was determined that the signal-to-noise ratio of the amplified signals was actually degraded when readily available amplifiers were used (e.g. Vishay model 2310), due to the electronic noise associated with the signal amplifiers. It was determined that direct recording of the voltages from the temperature probes would provide a better overall signal-to-noise ratio and still provide acceptable signal quantization. As a result of the bench testing, direct recording of the thermocouple voltages was used in the rig and engine tests.

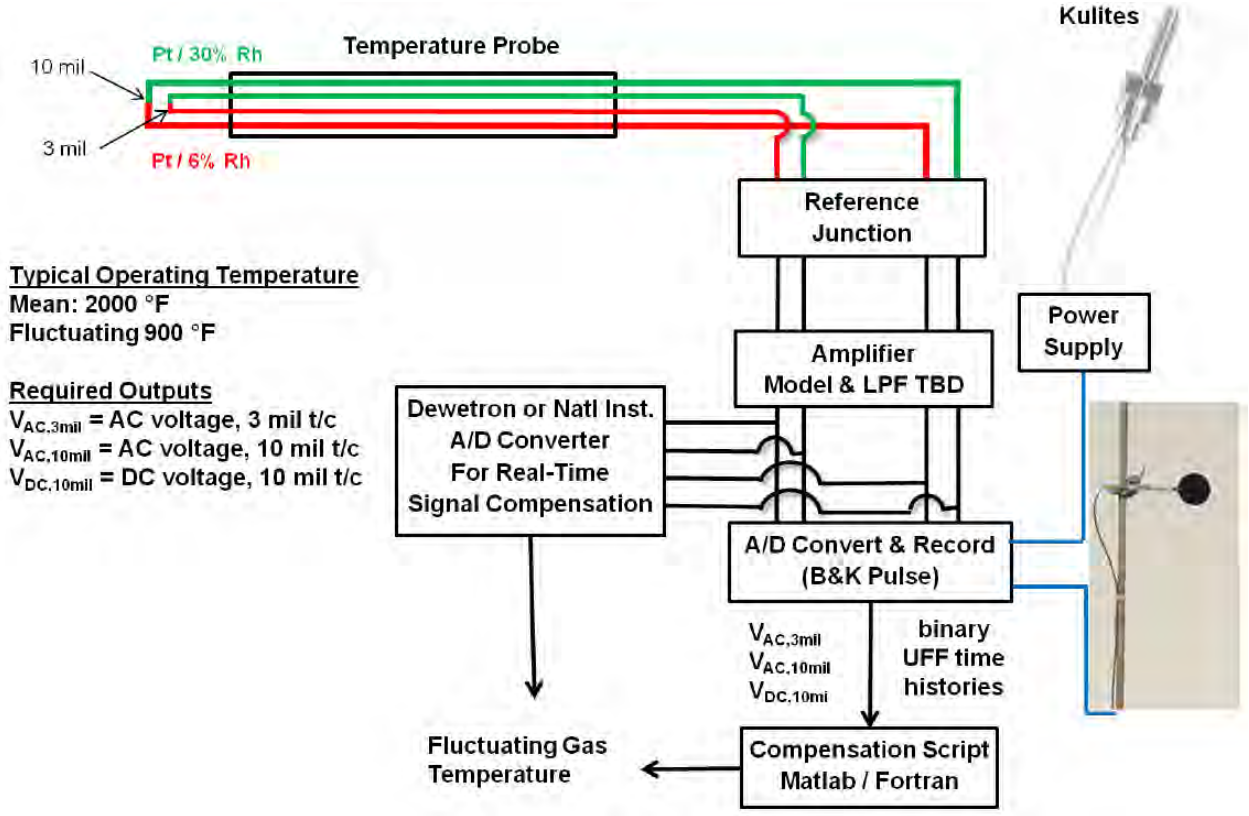

Figure 1. Preliminary Signal Conditioning and Data Acquisition Setup.

3.3 Development Probe Fabrication

Honeywell needed to fabricate temperature probes for the bench and engine tests. Because the thermocouple wires used on these probes are quite small, special care is needed to assemble the thermocouple junctions and weld them to their supporting wires. In order to develop and gain experience with the probe fabrication process, two Type B dual-wire temperature probes were ordered from Cleveland Electric Labs (CEL) in Tempe, AZ. The probes feature two closely spaced beadless thermocouple junctions of different diameter. We

had intended to manufacture the probes using the same diameter thermocouple elements that were used on the NASA probe, namely 0.003-inch and 0.010-inch. However, because the vendor could not locate a commercial source of 0.003-inch diameter Type B wire, the probes were built with 0.004-inch and 0.010-inch diameter wire. The thermocouple junctions were welded to support wires which are installed inside a ceramic stick. The development probes were designed with a thick Inconel housing so that they could be used in a rotating carousel test. These probes, shown in Figure 2, were used in the burner rig test to acquire dynamic temperature measurements and gain experience with the data acquisition systems and data reduction software.

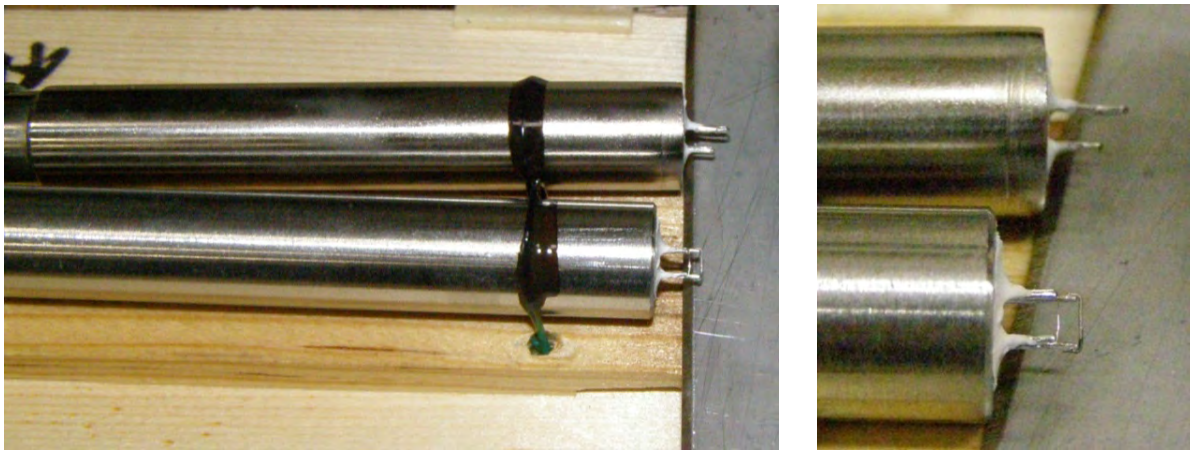

Figure 2. Dual Thermocouple Probes Used in the Bench and Burner Rig Tests.

3.4 Development Probe Rig Testing

Bench, oven, and burner rig tests were constructed to accomplish a number of objectives, including defining the optimal signal conditioning and data acquisition hardware, gaining experience in using the probes and data reduction software, and performing semi-quantitative quality checks on the data collected by the probes. For these tests, Honeywell procured two dual thermocouple probes (DTPs) from CEL. Special limits-of-error Inconel sheathed Type B thermocouples were also purchased for use as reference and control sensors for the oven test. For comparison purposes, NASA provided a DTP constructed with a 0.003-inch/0.010-inch wire diameter combination. NASA also provided the Fortran-based data reduction software routines.

A test plan describing bench, oven, and burner rig testing of the Dynamic Gas Temperature Measurement System (DGTMS) was compiled and reviewed with NASA personnel. The DGTMS consists of (1) a DTP and (2) a collection of data processing software subroutines. The DTP consists of two closely spaced beadless Type B (platinum and 30 percent rhodium, platinum and 6 percent rhodium) thermocouple junctions installed in a ceramic stick, with one junction having a large diameter and the other having a small diameter. Each junction generates a small voltage that is related to the fluctuating temperature of the wire. The software processes these voltage signals and produces an estimate of the dynamic temperature of the gas convecting past the probe. The software uses the measured frequency response of the voltage signals produced by the two wire junction, along with the predicted frequency responses derived from an analytical model of the convective and conductive heat transfer in the probe, to compute a compensation spectrum that is applied to the measured data.

3.5 Development Probe Bench Test

The purpose of the bench test was to determine the signal conditioning and recording equipment that would be used to acquire data from the DGTMS probes. Some of the subtasks were to identify system hardware components and connectivity, evaluate the benefits and limitations of signal amplification, quantify the electronic background noise level and the impact of data system settings on the noise level, and identify and resolve any issues with cables and connectors. One of the challenges in acquiring data from the probes is that the voltage output from Type B thermocouples is very small (Figure 3), which places stringent demands on the signal conditioning and recording equipment.

The bench testing was conducted by evaluating the voltage signal quality and electronic noise floor of various combinations of hardware. The capabilities of the data systems to measure very small voltages were examined by a couple of different methods. The first method was to directly inject low amplitude dynamic voltage signals into the data system inputs using a calibrated signal generator. The second method was to connect the probes to the data system inputs and use a heat gun to generate moderate temperature fluctuations at the probe ends, thus generating small fluctuating voltages (Figure 4).

It was originally envisioned that signal amplification would be required, due to the very low voltage levels that are generated by the thermocouples and the desire to maximize the input range of the analog-to-digital converters on the data acquisition systems. However, it was found that use of the readily available signal amplifiers resulted in a decrease of the overall dynamic range due to increased electronic noise. Measurement of non amplified signals was determined to be a simpler and preferable solution, and provided a signal noise floor on the order of 20μV. Also, it was originally envisioned that a thermocouple reference junction would be used, but this was found to be unnecessary with the Type B thermocouples. The instrumentation setup that was defined as a result of the bench testing is indicated in Figure 5. This setup worked well in the subsequent oven and burner rig tests and was also used during the engine test.

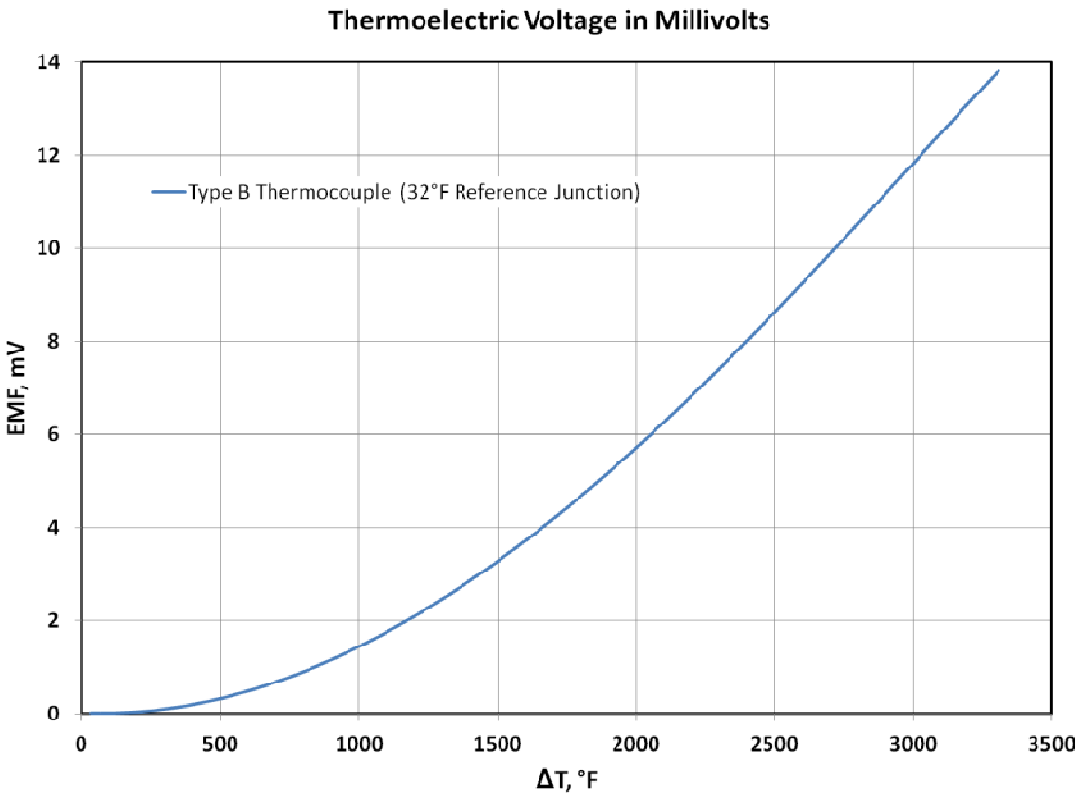

Figure 3. Voltage Output of Type B Thermocouples as a Function of Temperature.

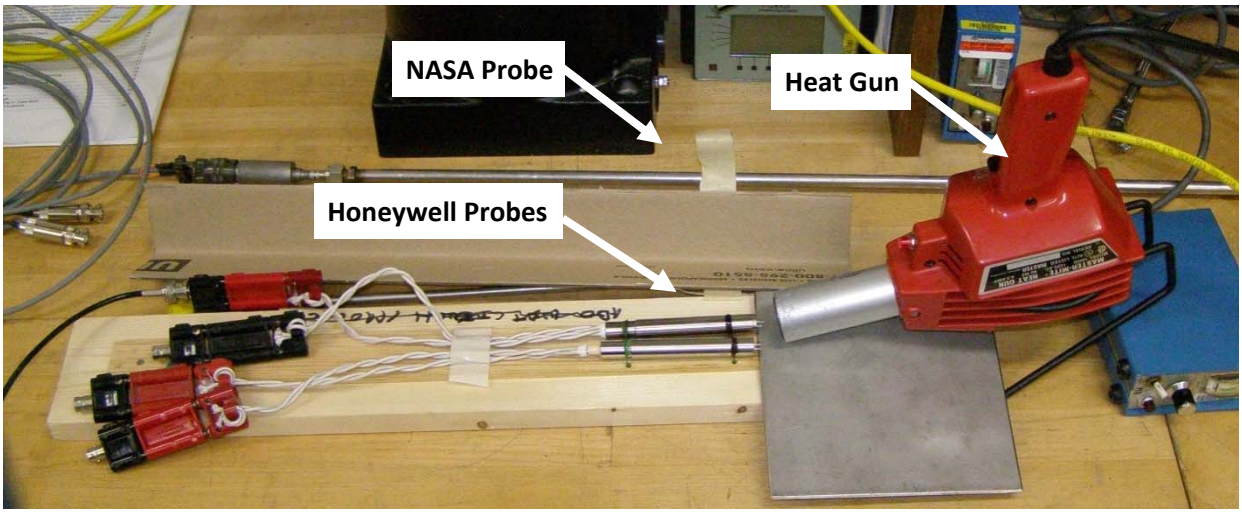

Figure 4. A Heat Gun Was Used to Generate Small Voltage From the Probes.

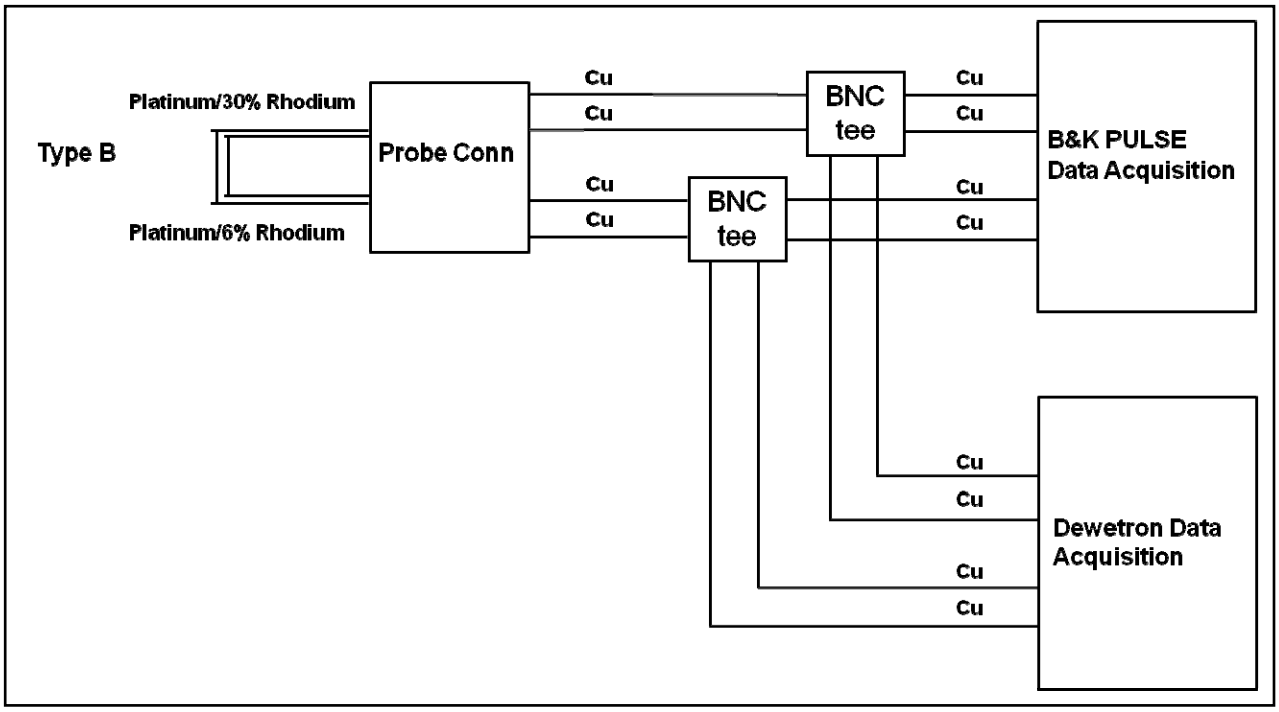

Figure 5. Final Signal Conditioning and Data Acquisition Setup.

3.6 Development Probe Oven Test

The main purpose of the oven test was to verify that the Type B thermocouples used in the DTPs produce the same DC output as a reference Type B thermocouple when placed in a constant temperature environment. This would enable a comparison of the probes DC output against a known reference, ensure that the correct material was used in probe fabrication, and allow a comparison of the Honeywell and NASA probes. In addition, it was of interest to determine whether any additional noise is encountered in a laboratory test cell where there is more extraneous electrical noise, and when the probes are operating at higher mean temperatures. This test was accomplished by placing the NASA probe, the two Honeywell procured probes, and a commercially procured NIST traceable reference Type B thermocouple all together inside an oven. A Type K reference thermocouple was also used for an additional comparison. The probes were inserted through access holes in the back of the oven, and placed in close proximity to one another (Figure 6). The collection of probes were also surrounded by a small metal box, with an insulating material placed at the front and back, in order to minimize the impact of any convection currents generated inside the oven by the resistive heating elements in the oven walls. Steady state temperature tests were conducted with the oven set to provide a stabilized constant temperature in the range of 500°F to 2000°F, in steps of 150°F. Transient temperature tests were also conducted with the oven temperature slowly increasing or decreasing. The DC voltage readings from the large and small diameter thermocouple wires on the DTPs were compared to the voltage output from the reference Type B thermocouple.

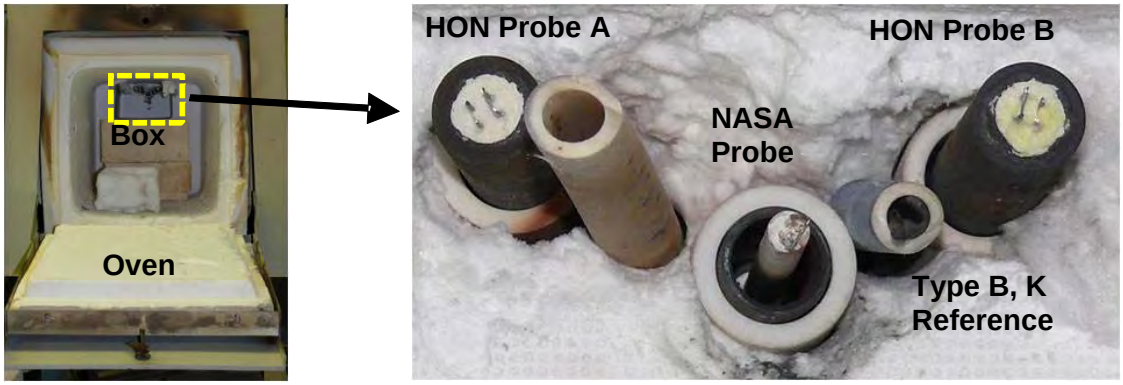

Figure 6. An Oven Test Was Conducted to Measure the DC Output of the Probes.

At the steady state conditions, the voltage outputs of the Type B thermocouples were fairly similar, though not identical. At transient conditions, the voltage outputs from the Honeywell and NASA probes lagged behind the output of the Type B reference. Figure 7 shows a typical result during a continuous oven warm up from 1000°F to 1800°F, where the voltage outputs of the Type B and Type K thermocouples have been converted to temperature units using the appropriate NIST conversion coefficients. The temperature measured by the Type K beaded thermocouple was very similar to the temperature measured by the Type B beaded thermocouple. However, the temperatures measured by the small and large wires on the Honeywell and NASA DTPs lagged behind the Type B reference. This is illustrated more clearly in Figure 8, which plots the temperature difference from the Type B reference. The temperature differences were greater than what was expected. The rate of change of the oven temperature was sufficiently gradual (quasi steady state) that one would expect all thermocouples to read nearly the same temperature. A conclusive explanation for the difference was not determined. One possibility is that the mass of the ceramic stick and the cylindrical metal sheath on the Honeywell DTPs acts as a thermal source or sink during transients. However, this explanation is not entirely satisfactory. The response of Honeywell probe #1 is very similar to the NASA probe, which has a smaller diameter ceramic stick and no metal sheath near the tip. Another possibility is that the there might be some manufacturing differences in the thermocouple junctions. A second oven calibration test was made using a metrology thermocouple calibration device to further investigate the differences and is reported on in Section 3.8.

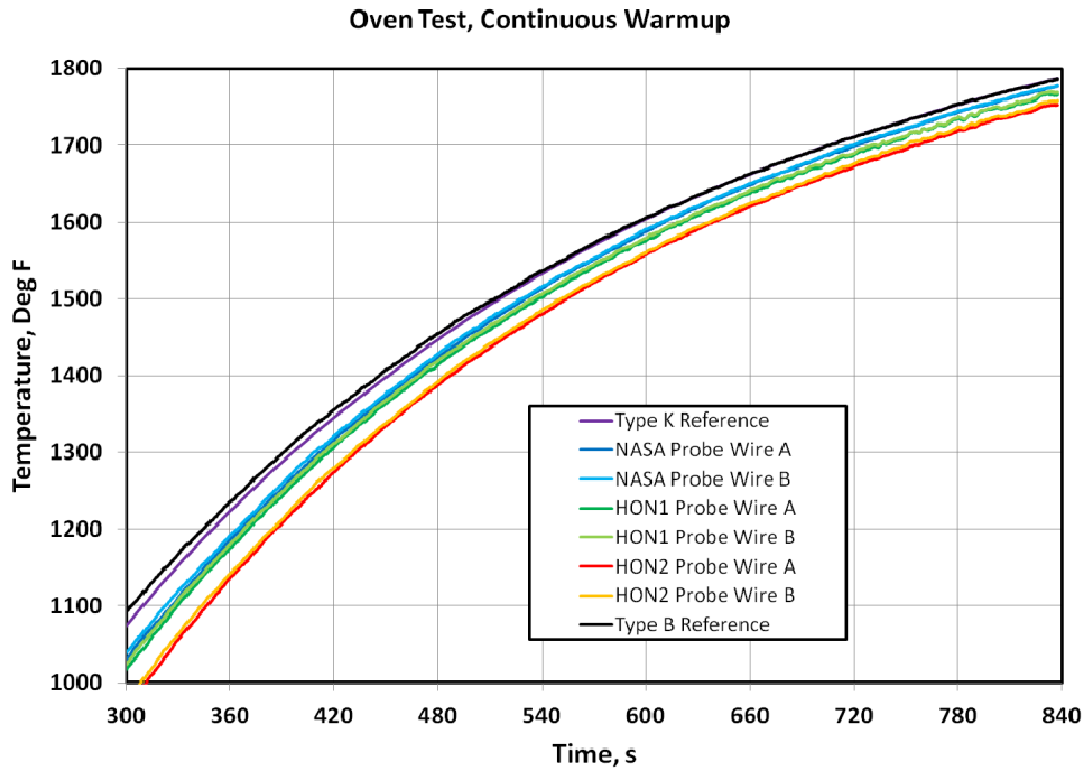

Figure 7. Temperature Measured by the Thermocouples During an Oven Warmup.

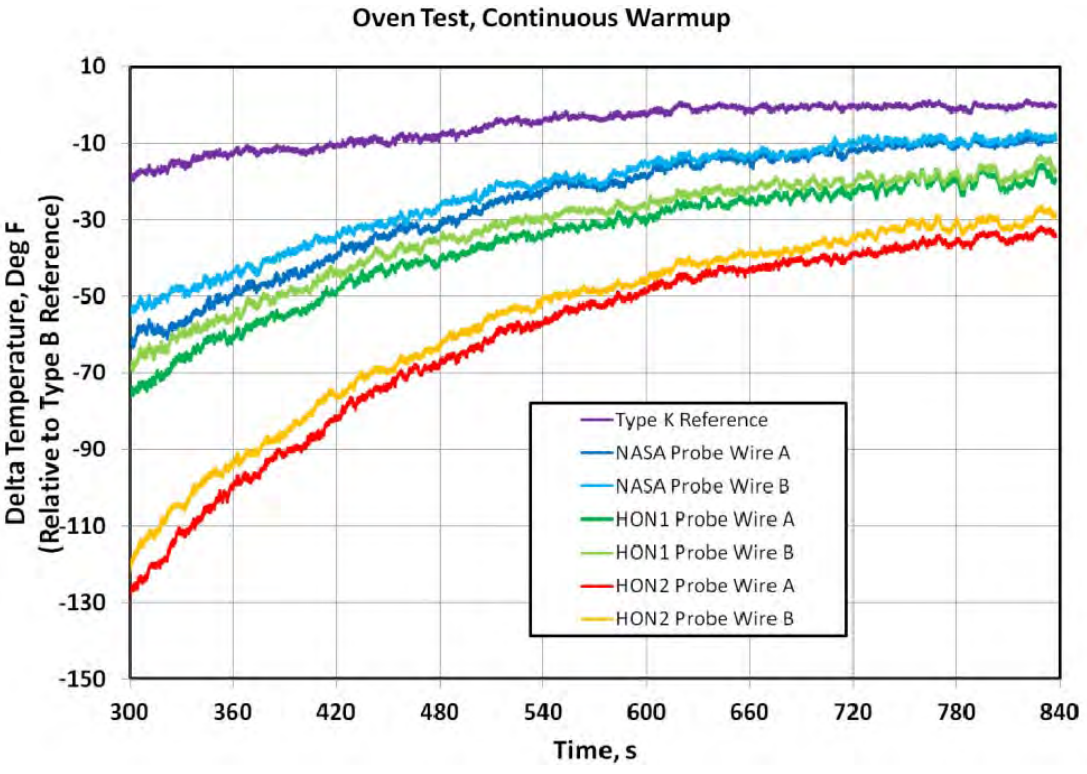

Figure 8. Temperature Differences Measured During the Oven Warmup.

3.7 Development Probe Burner Rig Test

The purpose of the burner rig test was to collect dynamic temperature data to support an evaluation of the data acquisition systems, the DTPs, and the DGTMS data processing software. Two types of tests were conducted. The first type was a test intended to collect "large-temperature-fluctuations" data by periodically exposing the Honeywell probes to a high a temperature burner rig gas stream, using a spinning carousel installed with rods. The second type was a test intended to collect "small-temperature-fluctuations" data by placing a one or more DGTMS probes in a fixed position in the burner gas stream and allowing the temperature fluctuations to arise naturally by the unsteady burning and turbulent mixing of the gas.

Figure 9 shows a photo of a typical "large-temperature-fluctuations" test burner rig test setup. A stationary Honeywell DGTMS probe was positioned in the center of carousel that is installed with 12 rods. The carousel was positioned in front of the burner rig gas stream, and rotated at a fixed speed, thereby periodically exposing the probes to high temperatures. As the probes are periodically exposed to, and blocked from, the gas stream, large fluctuations in temperature of a semi-sinusoidal nature at a known frequency were created. The rotational speed of the carousel was varied to change the frequency of the main temperature oscillation. Data were collected at rotational speeds near 500, 1000, 1500, 2000, and 2800 rpm, corresponding to fundamental temperature fluctuations ranging from to 100 Hz to 560 Hz. Measurements were also made with the carousel stationary, and with the probe either directly behind a rod or in between two rods. Measurements were acquired for each of the Honeywell probes. A minimum of 60 seconds of data was recorded to provide sufficient averaging of the dynamic temperature spectra.

As a side note, the original proposal for this test was to install the Honeywell DTP on the carousel and rotate the probe in and out of the burner flame, using slip ring to transfer the data from the rotating to stationary frames. This would provide a very large amplitude temperature fluctuation, with essentially two cycles per revolution. However, the maximum obtainable frequency of this large fluctuation would only be about 90 Hz, and the slip ring system would introduce additional noise. By holding the probe stationary in the center of a carousel that could accommodate 12 rods, temperature fluctuations at a much higher frequency (albeit with a lower amplitude) could be generated without any additional noise issues from the slip ring system. This latter approach was selected.

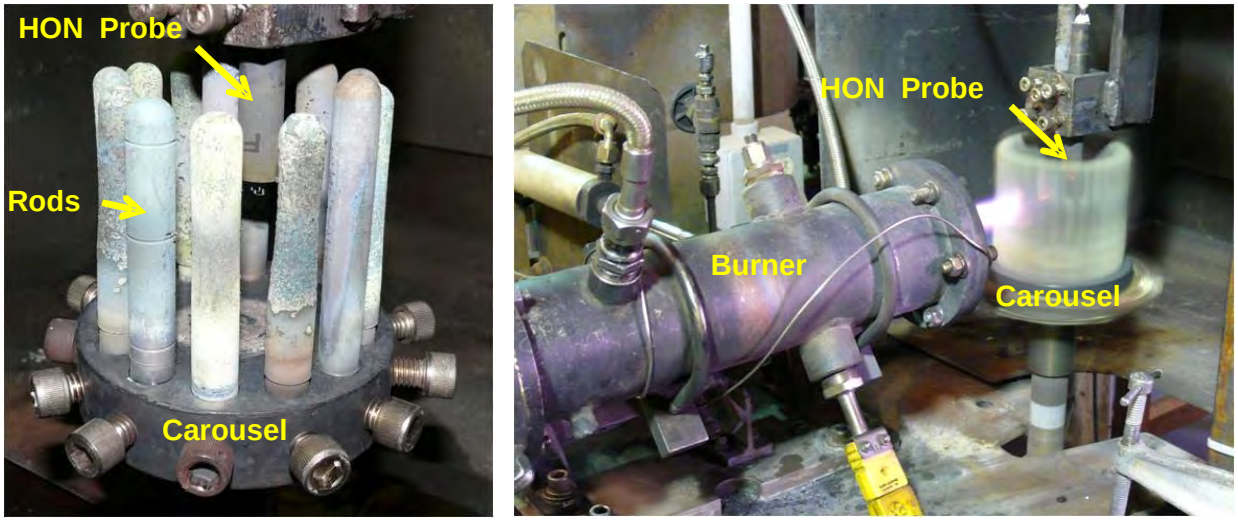

Figure 9. "Large Temperature Fluctuations" Burner Rig Carousel Test.

Figure 10 shows a photo of a typical "small-temperature-fluctuations" burner rig test setup. The NASA DTP, a Honeywell DTP, and a Kulite probe (semi-infinite coil arrangement) were placed at a fixed location in a hot gas stream. The probes were placed in the core of the gas stream with the intent of obtaining modest temperature fluctuations around a high mean temperature, with the fluctuations driven by turbulence and unsteady burning. The probes were also placed in the mixing region of the flow, with the intent of obtaining slightly larger temperature fluctuations around a lower mean temperature. The concept is that the observed temperature fluctuations arise naturally from the turbulent burning of the gas and from the turbulent mixing of the hot gas and surrounding air, with the expectation that this type of data might be representative of a measurement in the combustor or turbine in an engine test.

Measurements were made for two fuel flow rates corresponding to mean gas flow temperatures near 1200°F and 1500°F, at two probe locations corresponding to the hot core and mixing region. The NASA probe and Honeywell probe #1 were installed simultaneously and placed in as close proximity as possible. One objective of this arrangement was to compare compensated frequency responses of the 0.003-inch/0.010-inch NASA probe and the 0.004-inch /0.010-inch Honeywell probe, under the assumption that both probes experience comparable temperature fluctuations. A Kulite dynamic pressure probe was also installed next to the Honeywell DTP probe so that temperature-pressure cross spectra could be evaluated, after taking into account the time delay associated with propagation of pressure fluctuations in the Kulite probe tip. One observation was that the combustor flame front was very dynamic, so that it was not easy to identify the "edge" of the mixing region. The results of the burner rig test are discussed in Section 5.4, after a review of the data analysis methodology and software.

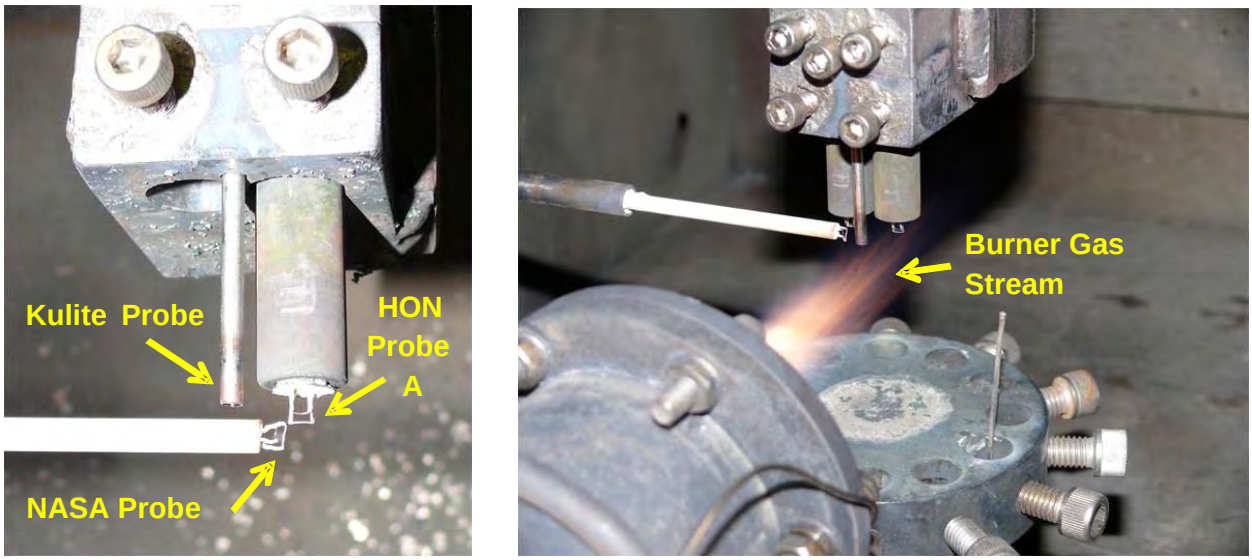

Figure 10. "Small Temperature Fluctuations" Burner Rig Test.

3.8 Development Probe Oven Calibration Test

A follow-on DC temperature calibration test of the Honeywell and NASA probes was conducted using a metrology thermocouple calibration device to more carefully compare the mean outputs when the probes are placed in a uniform temperature environment. As described in Section 3.6, the initial oven test of the probes indicated that the voltage output (or temperature) of the Honeywell and NASA probes lagged substantially behind that of a reference Type B thermocouple during a slow oven warmup. The differences were larger than would be expected, especially since the small and large wires on the probes used the same Type B junction material as the reference thermocouple. The differences might have been due to convection currents or temperature stratification in the test chamber, due to the thermal mass of the ceramic stick and/or metal shroud of the probes acting as a source or sink of heat, or due to some other effect. Because the discrepancies were larger than expected, a second DC calibration test was proposed using a more controlled thermal environment.

The Honeywell metrology department provided an Isotech Pegasus dry block thermocouple calibration device for this second evaluation. The Pegasus unit provides a much more controllable and uniform test environment than the oven. The device features a central well that is heated by a surrounding block to a precise, automatically controlled temperature. An 80mm deep metal insert sits inside the well, on top of which sits a 50mm ceramic insert that acts as a thermal insulator. The metal and ceramic inserts are drilled with holes to accommodate the installation of temperature sensors, whose sensing elements are positioned to an appropriate depth inside the metal insert. The available inserts had four holes with a diameter of 8mm (0.315-inch). The holes were large enough to accommodate the NASA probe (0.188-inch OD), but not the Honeywell burner rig "A" and "B" probes (0.5-inch OD). Although it was feasible to procure new inserts with larger holes that could accommodate the Honeywell development probes, this was not considered to be a value-added activity, since the probes considered for the engine test used a much different design, having a smaller diameter ceramic stick and no

metal shroud near the sensing tip, similar to the existing NASA probe. The NASA dual thermocouple probe was tested in the Pegasus unit, along with three references, namely a Type B thermocouple (used in the oven test), a Type S thermocouple (used by metrology as a reference standard), and a platinum resistance thermometer (PRT, used per NASA request). The installation of the probes in the Pegasus unit is shown in Figure 11.

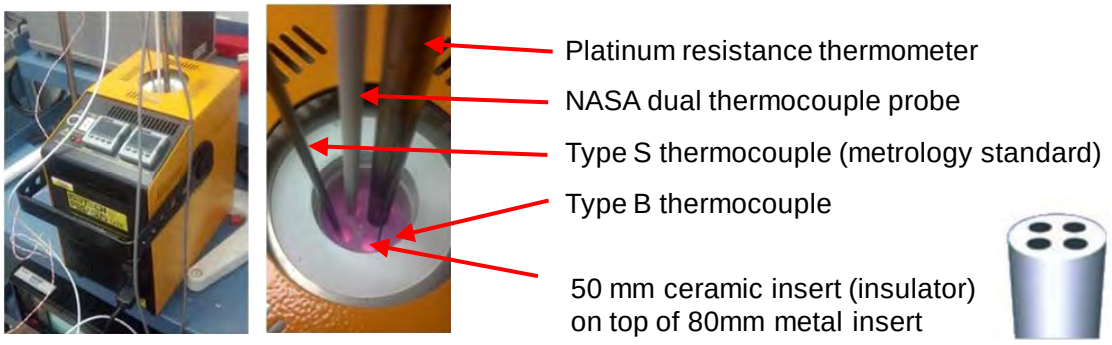

Figure 11. An Isotech Pegasus Dry Block Calibrator Was Used to Evaluate the NASA Dual Thermocouple Probe Output Against Reference Standards.

The four temperature sensors were placed in the calibrator, with each probe inserted into a hole in the ceramic and metal blocks, and with the sensing elements positioned in the metal block at approximately the same height above the bottom of the well. Ideally, when using a dry block calibrator, there should be a very close fit of the sensor within its hole, within a few thousandths of an inch if possible. In the present test, since standard size inserts were used, the fit was looser than ideal. The Type B reference had the loosest fit, with the Type S, NASA probe, and Platinum Resistance Thermometers (PRT) having tighter fits, in succession. The different gaps between the probes and their holes might have a small impact of the measurement (e.g. due to differences in conduction between the metal block and the probes, or differences in thermal gradients due to convective effects).

A gradual heating and cooling cycle covering the range of 1000°F to 2000°F was performed, which lasted several hours. During the warmup, the unit was allowed to stabilize for 10 minutes at set point temperatures of 1000°F, 1500°F, and 2000°F. The voltage outputs of the NASA probe (small and large diameter thermocouple wires) and the Type B thermocouple were recorded on a Dewetron system and converted to temperature using the standard NIST coefficients. The temperature output of the Type S reference, which the metrology department normally uses as their standard reference for this unit, was recorded by a Fluke Black Stack thermometer readout. The temperature output of the PRT was recorded by a Hart Scientific (Fluke) Super Thermometer. The temperatures measured by the four probes during the warmup and cooldown are shown in Figure 12. The temperature measured by the NASA probe, Type S reference, and Type B reference all tracked closely together. The PRT, however, lagged behind significantly. Although PRTs are generally known for their accuracy, this particular PRT design is not very compatible with making measurements in the Pegasus device. The sensing element is not located at the very tip of the device, but an inch or so up the probe, so it is not exposed to the hottest part of the dry well. Because of this, the metrology department does not use the PRT as a reference standard with the Pegasus unit. Instead, the Type S thermocouple is used as a calibrated reference.

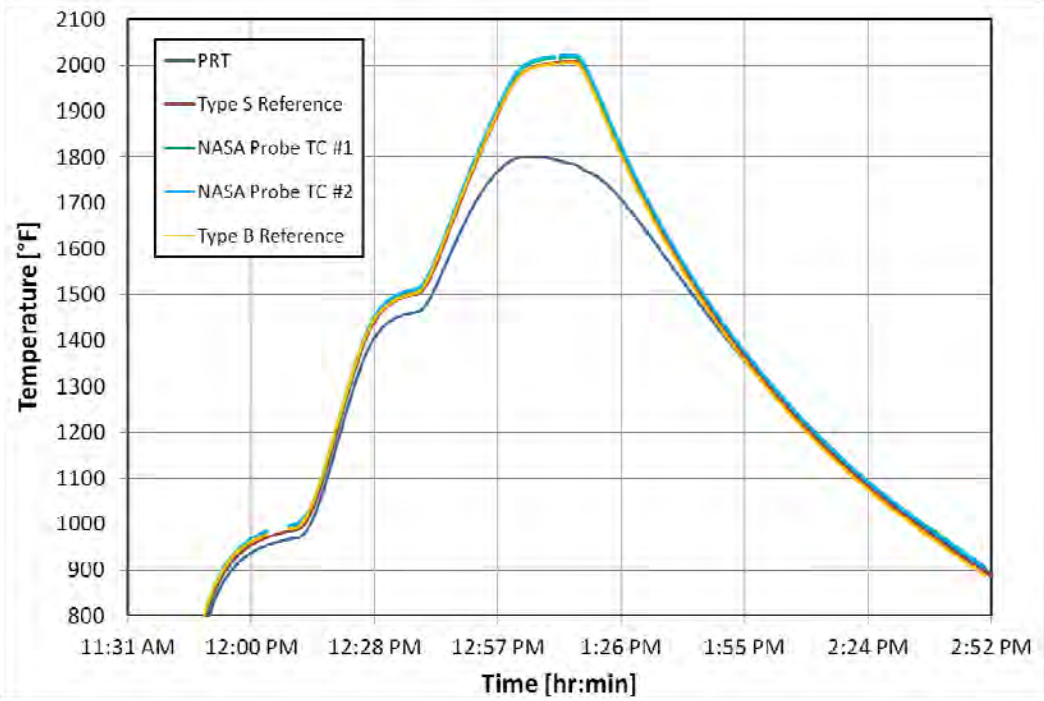

Figure 12. Comparison of the Temperature Measured by Four Temperature Probes During a Warmup and Cooldown in the Isotech Pegasus Unit.

Close-up comparisons of the readings from the probes at mean temperatures near 1500°F and 2000°F are shown in Figure 13. The difference between the Type S and the Type B reference thermocouples is typically less than 5°F. The difference between the large and small thermocouples on the NASA probe is on the order of 5°F, and the difference between the Type S reference and NASA probe is typically less than 15°F. The results of the metrology test are very satisfactory. The magnitude of the observed differences in mean temperature will not have a significant impact on the computation of the compensated dynamic temperature spectra. The small differences between the NASA probe, the Type S reference, and the Type B reference could be caused by a number of factors, including: vertical or lateral variation of the temperature field inside the metal block; differences in pocket clearance; differences in data acquisition systems; and differences in the probes. A more refined test could identify what differences are due to the test setup as opposed to the actual probes. A more precise vertical alignment of the sensors might improve the agreement, along with longer stabilization times. Also, the agreement might be improved by fabricating a metal/ceramic inserts with closer tolerance holes that minimizes the gap between the sensors and the inserts. However, because the measured temperature differences would not have a significant impact on the compensated dynamic temperature spectra, it was not necessary to investigate these issues further.

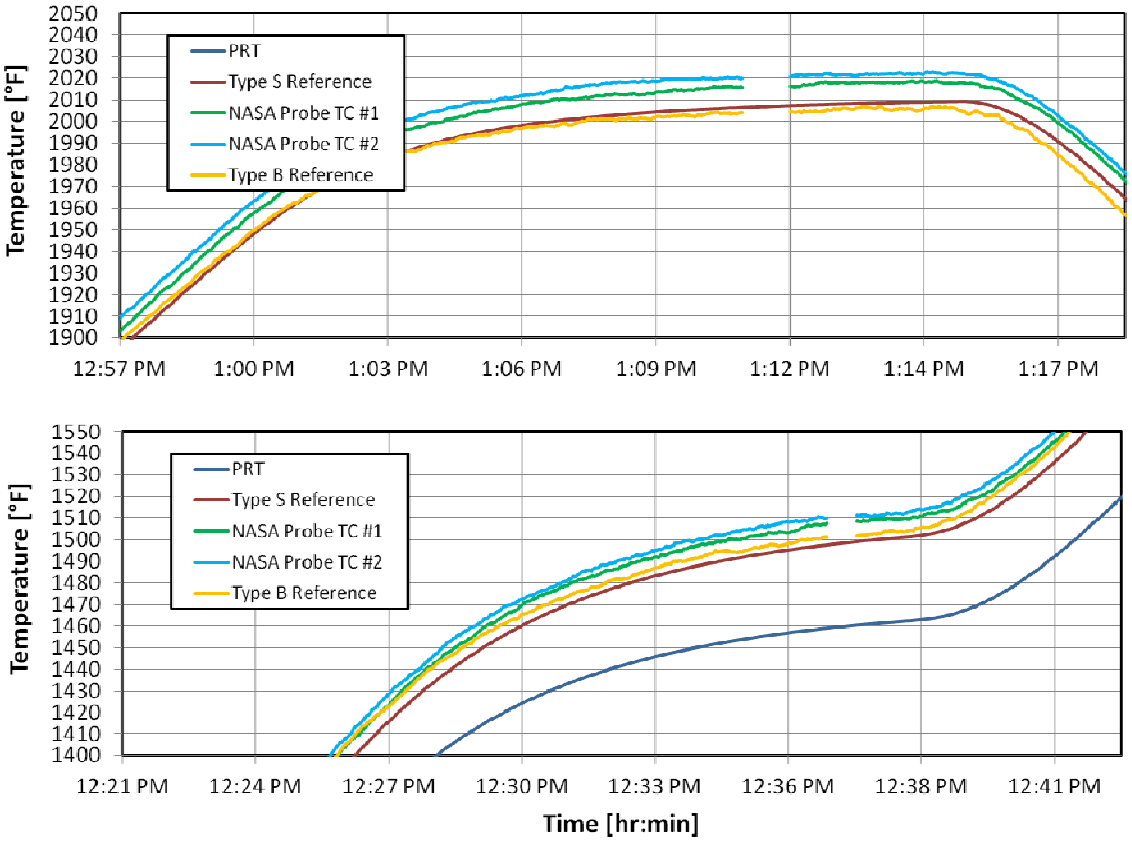

Figure 13. Comparison of the Probe Temperature Readings Made in the Dry Block Calibrator at Temperatures Near 1500°F [Bottom] and 2000°F [Top].

3.9 Engine Probe Design

The dual thermocouple probes were critical components of the engine test program and required special attention. The probes designed for the engine test were very similar to the NASA probe and the probes used in previous NASA/P&W programs (Reference 4, 6). The design criteria considered for the dual thermocouple temperature probes were much the same as those considered in previous reports (Reference 4). For this program, the design criteria were:

1. Be able to operate in mean temperatures as high as 2000°F
2. Provide a frequency response up to 1000 Hz
3. Have a compact size (don't want probe to affect temperature field)
4. Minimize adverse thermal conduction effects (no metal shroud near sensing tip)
5. Survive several hours of testing
6. Tolerate aerodynamic, thermal, and vibratory loads
7. Build on previous lessons learned

The first criteria dictated the use of Type B sensing elements (at least for the combustor zone). The second criteria dictated the use of 0.003-inch/0.010-inch or 0.004-inch /0.010-inch wire combinations. The first, third, and fourth criteria dictated the use of a small ceramic stick to hold sensing elements.

Figure 14 provides a schematic of the preliminary probe design. In addition to the metrology studies discussed in the previous section, the mechanical integrity of the probe during engine testing was a critical concern. Mechanical considerations for engine testing included (1) aerodynamic loading, (2) vibratory loads, and (3) thermal loads. Regarding aerodynamic loads, both the ceramic support element and the wires need to survive aerodynamic loads of the immersed flow field. Regarding vibratory loads, one needs to ensure that the ceramic sticks do not crack due to a resonant excitation from engine N1 or N2 shaft vibrations or from excitation induced by vortex shedding off of the probes. Regarding thermal loads, welds and wire arrangements must accommodate dramatic temperature changes without breaking.

A mechanical analysis was performed to evaluate the aerodynamic loading of the probe at all measurement locations, since the probe protrudes into the operating engine gas stream like a cantilevered beam. A 3/16-inch diameter ceramic stick was found to be an acceptable size for the probe providing sufficient mechanical strength while minimizing the influence of the probe on the aerodynamic flow. Relative to the NASA probe design, two design changes were made based on recommendations in NASA CR-168267. The Honeywell probe (1) modifies the ceramic stick at the tip to allow more complete packing of ceramic cement into the holes, and (2) keeps the support wires straight to avoid introducing stress concentrations with bent wires which may lead to probe failure at high temperature. In addition, a reference Type B thermocouple was added to each probe in order to measure the mean temperature at the probe location with an independent thermocouple sensor.

The typical operating range for Type B thermocouples is 400°F to 3100°F. The melting point of the platinum elements is near 3200°F. The ceramic stick, with 99.8 percent alumina content, has a maximum use, no load temperature of 3272°F. The Resbond ceramic adhesive has a maximum service temperature of 3000°F. The Inconel shroud supporting the ceramic stick, which remains outside of the combustor and turbine flow, has a melting point of about 2400°F.

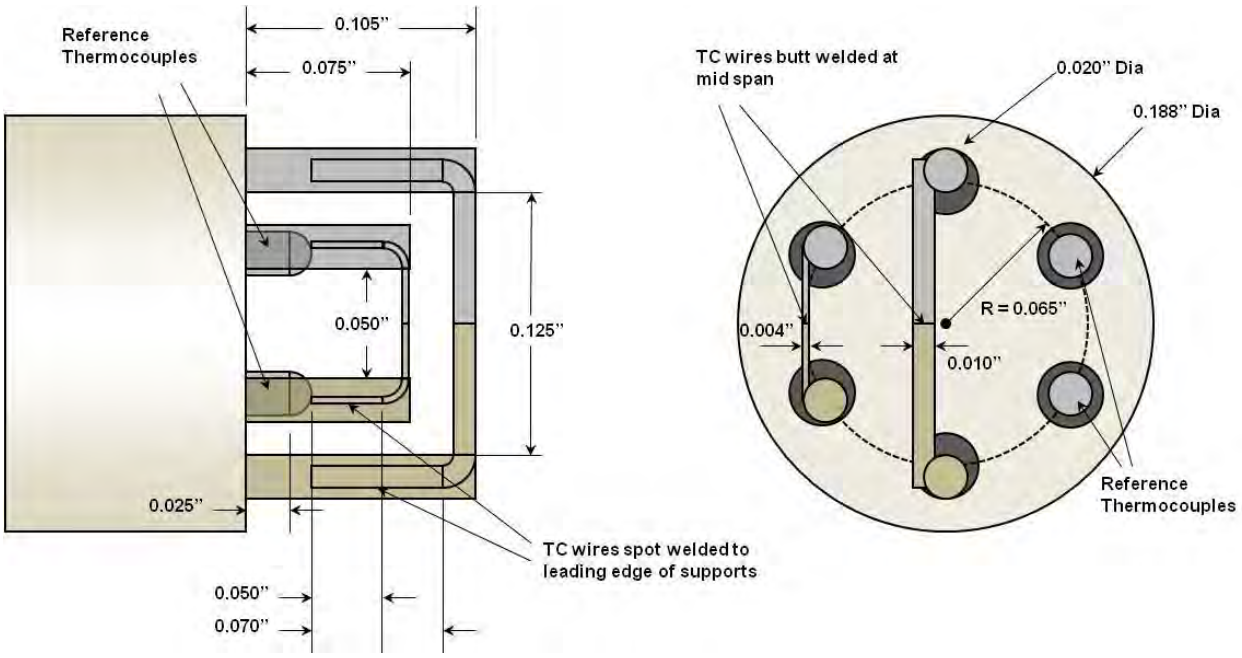

Figure 14. Preliminary Dual-Thermocouple Probe Design for the TECH977 Test.

After the design criteria had been addressed, the design of the probe was finalized and an assembly drawing (70642386-1) was completed. A source of supply for 0.003-inch diameter Type B thermocouple wire was located, so the final design used 0.003″ and 0.010″ diameter wires for the small and large sensing elements, respectively. This combination of wire diameters enabled a good frequency response to be obtained for measurement of the dynamic temperature to a frequency of at least 1000 Hz. This combination was also used for most of the probes tested in the previous NASA/P&W program. Figure 15 shows the first page of the probe drawing, which defines the dimensions of the sensing elements and their 0.020-inch diameter support wires. The heights of the support wires and lengths of the sensing elements are similar to those used in previous test programs. The sensing elements are welded to the upstream side of the support wires. The support wires have been left straight to minimize the possibility of inducing local stress concentrations that could contribute to premature failure of the elements. An Inconel-sheathed Type B thermocouple was installed as a reference to cross-check the mean temperature measured by the fine wires.

The thermocouple wires egress through a 15-inch long, six hole, 0.188-inch diameter alumina stick, and are terminated in a connector where the wiring transitions from platinum/rhodium to copper. The connector design, defined by the second page of the probe drawing (Figure 16), provides easy access for termination of the wires, and repair, if necessary. For structural support, the ceramic stick is housed in a 0.375-inch diameter Inconel tube, except for the last 2.5-inch on the sensing end, which is inserted into the hot gas flow.

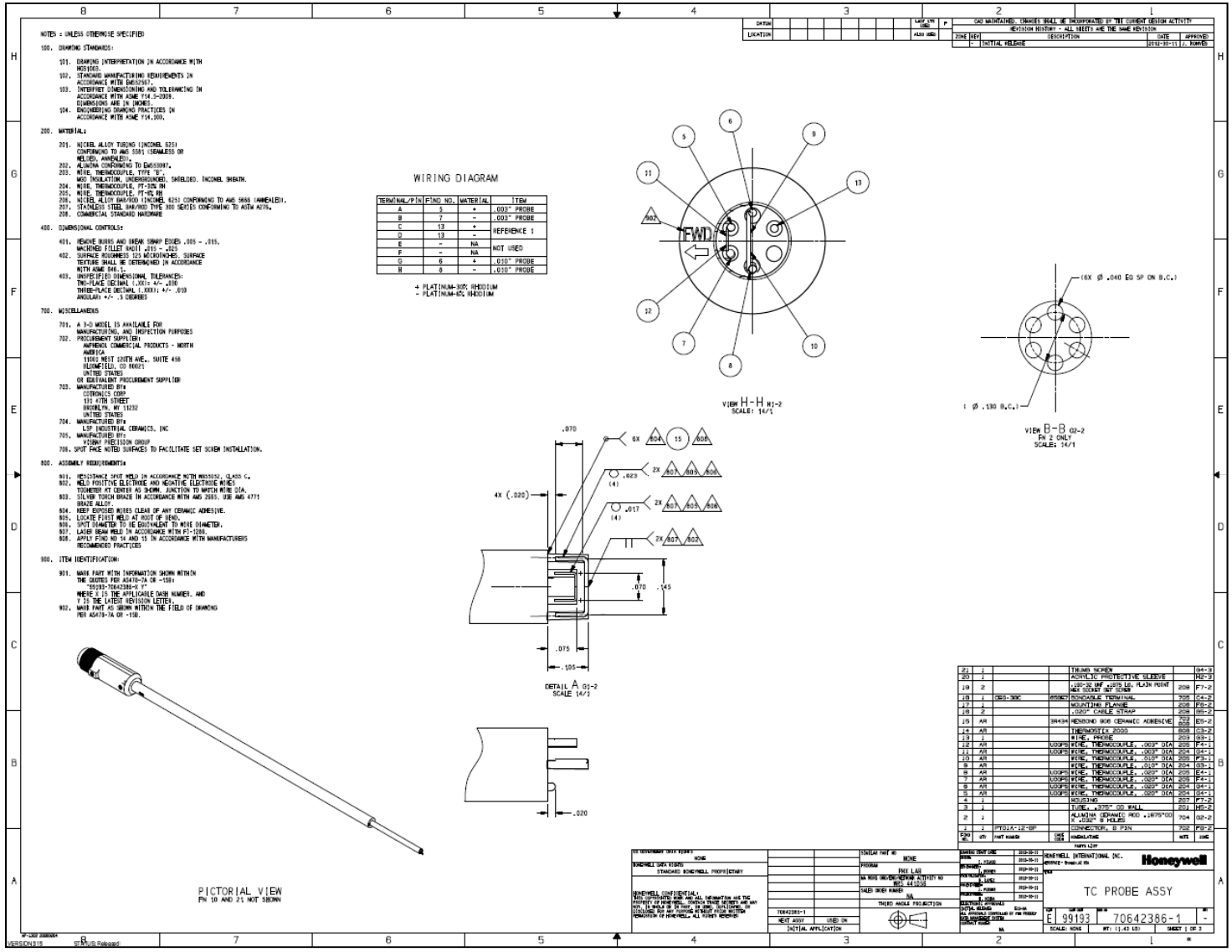

Figure 15. A Drawing (70642386-1) Was Created for the Dual Thermocouple Probes for the Engine Test.

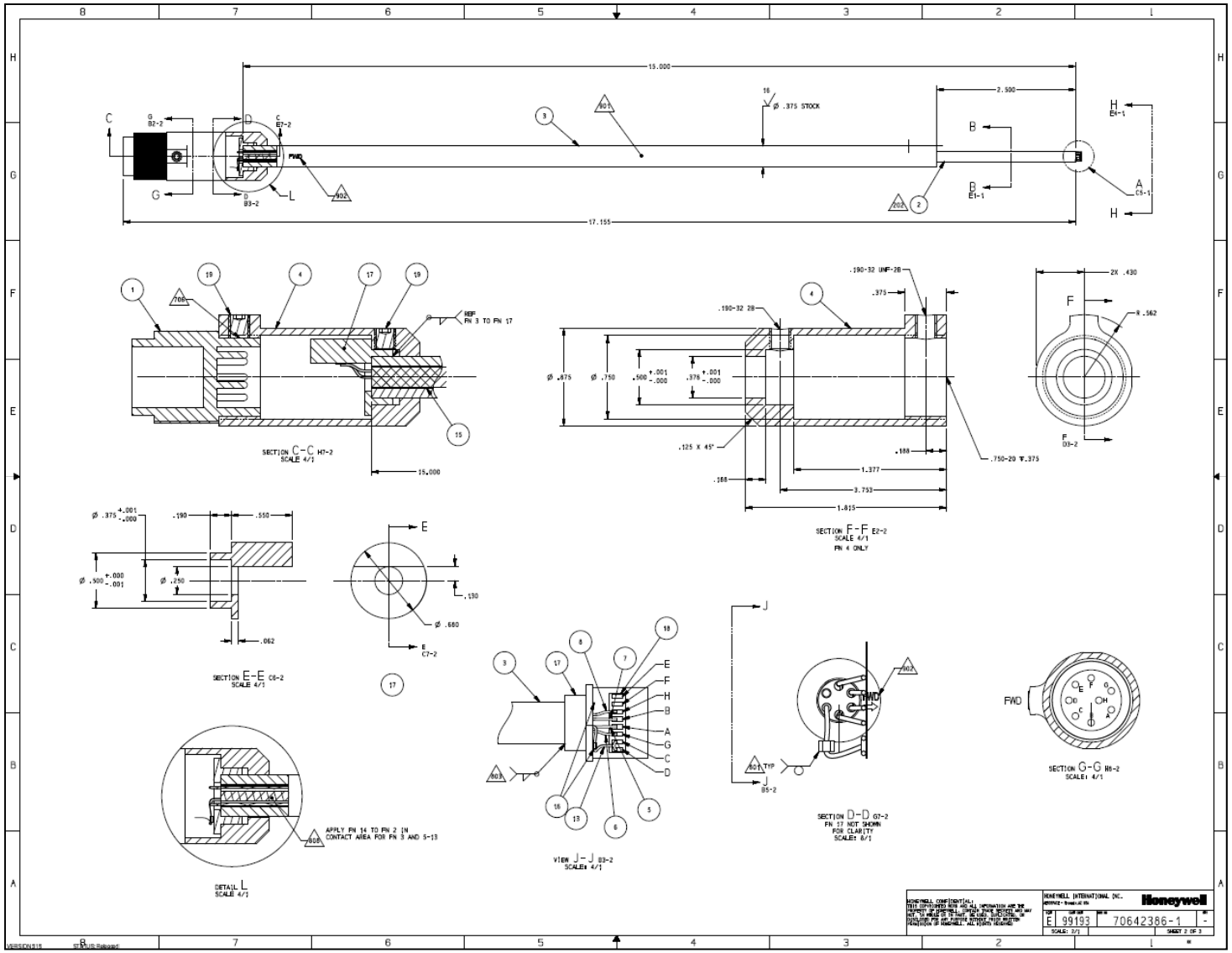

Figure 16. The Thermocouple Wires Egress Through an Alumina Stick and Are Terminated in an Easily Accessible Connector.

4.0 TASK 2: TECH977 ENGINE MODIFICATIONS

4.1 Engine Identification and Preparation

The TECH977 engine S/N P119123 was located in engineering stores and was prepared for use in the engine test program. In Phase I, a draft engine test plan was prepared and design discussions were held to determine what modifications of the engine hardware would be required to mount the temperature and pressure instrumentation.

4.2 Preliminary Instrumentation Layout

A preliminary instrumentation layout was developed for the TECH977 engine test. The instrumentation consisted of 14 dynamic pressure Kulite probes, 10 dynamic temperature probes, and 2 external microphones, as shown in Figure 17. In the combustor, an array of 4 Kulite probes at azimuthal positions of 0°, 90°, 180°, and 270° were planned to measure the circumferential mode content. The 4-probe array represents a subset of the 16-probe array that was previously used during the NASA EVNERT program (Reference 8). The purpose of this sub-array was to reaffirm the circumferential mode content that was previously measured (Reference 9). The modal content was reaffirmed and is discussed in Section 7.2.1.

At the combustor exit, upstream of the high pressure turbine (HPT) a pair of dynamic temperature probes, spaced 2 inches apart axially (and offset azimuthally to avoid wake interference), would be located at 0°, with dynamic pressure probes located close to the temperature probes. Another pair of dynamic temperature and dynamic pressure probes, spaced 2.7 inches apart axially, would be located at 100° at the combustor exit. Similar pairs of probes would be located at the entrance to the low pressure turbine (LPT) at 0° and 100°. At the exit of the low pressure turbine, dynamic temperature and dynamic pressure probes would be located at 0° and 100°. Two external microphones would be located in the test cell. During the detailed design of the engine modifications, the instrumentation layout evolved and specific positions of the instrumentation were adjusted as manufacturing or installation constraints were identified. However, the general concept was maintained.

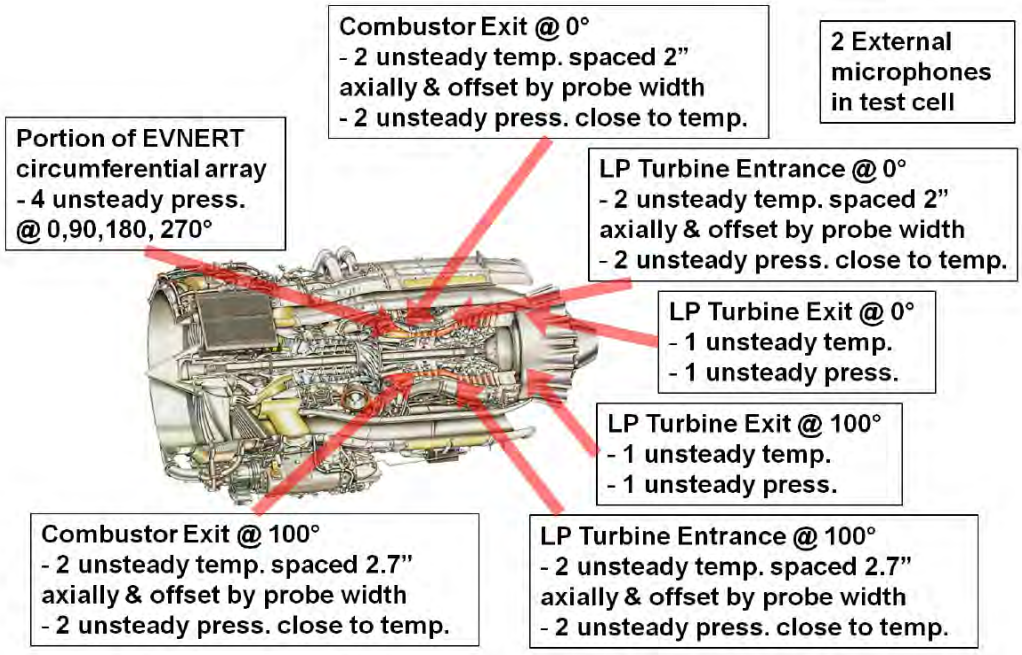

Figure 17. Preliminary Instrumentation Layout for the TECH977 Engine Test.

4.2.1 Engine Mechanical Design

The overall goal of the engine mechanical design activity was to design a solution for incorporating the pressure and temperature instrumentation into the engine. This was a combined effort requiring input and coordination of multiple engineering disciplines, including instrumentation, computer aided design, engine project, manufacturing, mechanical analysis, acoustics, assembly and test. Numerous aspects were considered, including engine accessibility and sensor routing; availability and capabilities of actuator systems; impact of modifications on mechanical integrity of engine hardware; and modifications of engine assembly sequences to accommodate instrumentation. There were numerous challenges that had to be overcome, and numerous design iterations were required to meet the technical objectives. Rather than describe the full evolution and history of the design process, this section describes the final engine design solution, and provides salient comments on the design decisions and challenges encountered.

4.3 Design Criteria

The objective of the engine test was to collect unsteady time histories of temperature and pressure data in the area of the combustor and turbine at various engine operating conditions. The design criteria that went into the decision on the placement of the 10 temperature probes were:

1. Measure at the combustor exit to acquire data relevant to HPT indirect noise generation
    a. Two circumferential locations, to quantify azimuthal variation
    b. Two axial positions, to quantify convection speeds

2. Measure downstream of HPT to acquire data relevant to LPT indirect noise generation

c. Two circumferential locations, to quantify azimuthal variation
d. Two axial positions, to quantify convection speeds

3. Measure downstream of LPT for residual temperature fluctuations
   e. Two circumferential locations, to quantify azimuthal variation

The upstream and downstream probe pairs in the combustor exit and LPT entrance were azimuthally offset so that the downstream probe was not in the direct wake of the upstream probe, which could affect the fluctuating temperatures. The general schematic depicting the temperature probe placement relative to some engine hardware is shown in Figure 18.

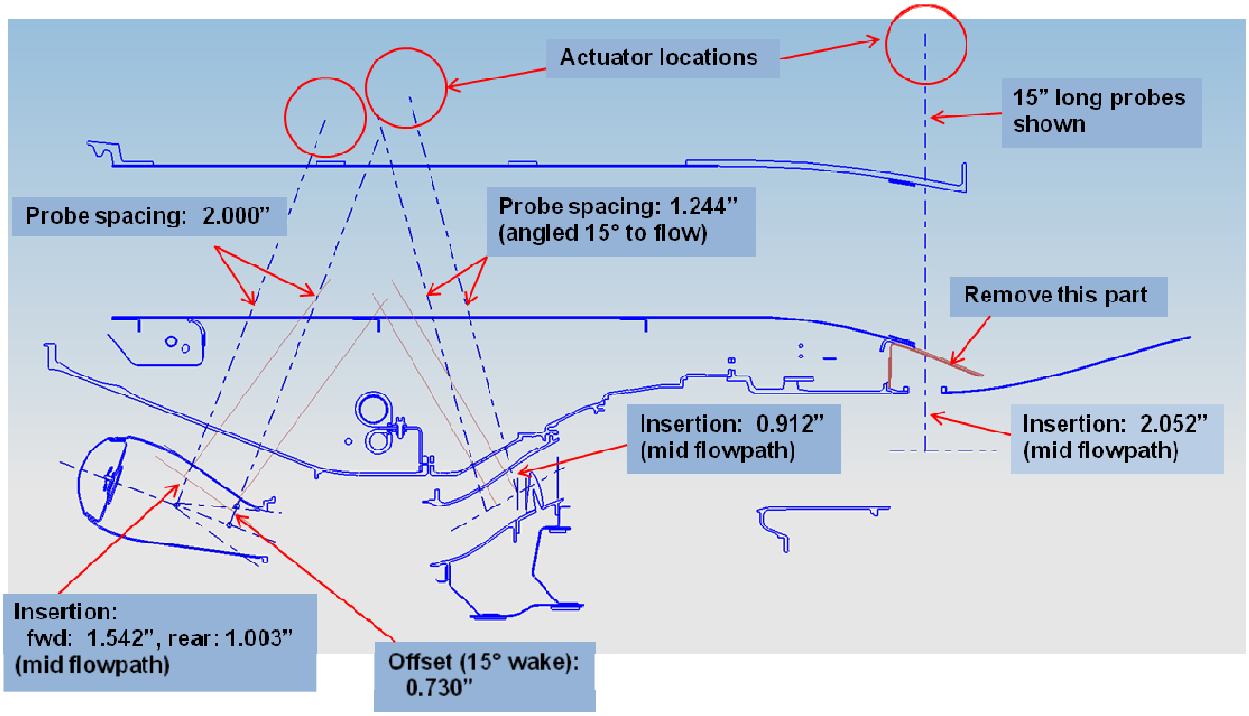

Figure 18. Schematic of Temperature Probe Placement (at 273° CCW ALF).

Early in the program it was decided to use an actuation system to deploy the temperature probes. This decision was motivated in part by recommendations from previous testing of dual thermocouple probes on an F100 engine. The conclusions and recommendations from Reference 4 stated:

> "A second area requiring further investigation concerns probe durability and obtaining increased probe life. The F100 engine test series demonstrated about one hour probe life for the present design. As described in the Task IV section of this report, the structural design of the probe was more than adequate for conditions in the engine. It is believed that the sensor element durability is extremely sensitive to particulate content in the airstream, especially during engine transients, and, at this time particulate content in the airstream is the hypothesis for failure. Increase in probe durability could be obtained by reducing sensor element and support wire lengths. Also, it is recommended that (1) the ceramic stick be modified at its tip to allow more complete packing of ceramic cement into the holes; and (2) the support

wires be left straight rather than bent. Attempting to bend the support wires to mount the two elements in the same plane at probe centerline may have caused unacceptable stress concentrations and inadvertently aided probe failure. Fabrication and use of a probe retraction mechanism would also alleviate effects of particulates which occur during transients".

Thus, it was felt that a probe retraction system would be advantageous to extending probe life for the TECH977 engine testing. Recommendations regarding the probe design were also incorporated, as discussed in Section 3.9. This decision created a substantial design effort that included creation of computer aided design (CAD) models for relevant engine parts and externals, development of concepts for probe actuation, extension of the conceptual design to include a remote actuation and linkage method, and design of a method for sealing the probe when inserted into the combustor case. A number of design criteria were used to define the probe retraction solution:

1. Deploy/retract probes gently after engine start/shutdown
2. Position probes at desired depth and orientation
    - Ensure sensing wires are perpendicular to flow
3. Protect probe tip from flow when retracted
    - Incorporate recessed cavity that shields probe tip
4. Prevent binding or breaking probes
    - Address thermal growth differences between the combustor and combustor case
5. Maintain actuator temperatures below 400°F
6. Maintain temperatures at Type B/Cu-Cu junction below 400°F
7. Minimize air leakage around probe
    - Small amount is acceptable, as influence on engine performance is not critical
    - A 0.380-inch hole for a 0.375-inch probe produces about 0.02 lbm/sec/probe at 350 psi

A number of factors affected where the temperature probes could actually be placed, including accessibility around external plumbing on the engine cases, keep-away zones from flanges or critical areas, sufficient clearances from neighboring probes or other hardware, practical manufacturing constraints regarding reworked cases and fabricated bosses, and constraints on commercial available actuators. The design solution that emerged was to use commercially available actuators as follows:

- Combustor exit: 4 temperature probes with 2 actuators, where each actuator drives an upstream/downstream pair of probes via a yoke mechanism
- LPT entrance; 4 temperature probes with 2 actuators, where each actuator drives an upstream/downstream pair of probes via a yoke mechanism

- LPT exit: 2 temperature probes with 2 actuators, where each actuator drives one probe through the center of the actuator

4.4 Detailed Design

The instrumentation solution required the design and reworking of several existing engine components, the design and fabrication of several new parts, and the procurement of commercially available hardware. Detailed designs and formal drawings for the new and modified hardware were completed. New hardware included the following:

- 70642386-1 Thermocouple Probe Assembly
- 70642387-1 Actuator Adapter (mounts between actuator and combustor/turbine case)
- 70642388-1 Actuator Adapter (attaches mixer probe to actuator)
- 70642389-1 Actuator Adapter (mounts between actuator and mixer nozzle)
- 70642390-1/-2 Actuator Yoke (attaches combustor probes to actuators)
- 70642391-1/-2 Actuator Yoke (attached turbine probes to actuators)

The reworked engine hardware included the following:

- 70642392-1 Combustor Case, Rework (from R3745568-1)
- 70642393-1 Combustor, Rework (from R3745569-1)
- 70642394-1 LP Turbine Case, Rework (from 3035657-1)
- 70642395-1 LP Turbine Nozzle, Rework (from 3035658-2)
- 70642396-1 Mixer Nozzle, Rework (from N10972-1)
- 70642398-1 C-Duct Assembly, Rework (from P47G-09-0312-1)

In addition, a top level assembly drawing that defines the installation and integration of the dual thermocouple probes with the modified engine hardware was completed:

- 70642385-1 TC Probe Actuation System (Assembly)

CAD views of the modified combustor case and modified combustor are provided in Figure 19 and Figure 20, respectively. Figure 21 shows the integration of the pressure and temperature probes in the combustor region. The two temperature probes are simultaneously deployed into (and retracted out of) the flow via a commercial pneumatic actuator via a single yoke. CAD views of the modified turbine case and modified LP turbine nozzle are shown in Figure 22 and Figure 23, respectively. Figure 24 shows the integration of the pressure and temperature probes in the inter-turbine duct (ITD). The two temperature probes are simultaneously deployed into (and retracted out of) the flow via a commercial pneumatic actuator via a single yoke. A CAD view of the modified mixer is shown in Figure 25. Figure 26 shows the integration of the pressure and temperature probes in the mixer. The temperature probe is actuated through the center of the actuator. Figure 27 shows modifications to the C-Ducts to accommodate passage of the probes through the bypass flowpath and outside the engine. Note that the actual hardware deviated slightly from these pictures due to manufacturing and assembly constraints encountered during the hardware fabrication and engine assembly process.

Commercially available actuators, Bimba model Flat-1 FOD-313-HV, were chosen for this application (Figure 28). These are round cylinder, original style, double-acting, double-end rod, 2-inch bore size, 3-inch stroke, hollow rod, high temperature actuators. The maximum operating air pressure is 200 psi, and the maximum operating temperature is 400°F. The range of travel – which controlled the location of the deployed and retracted probe element – was defined as follows. For the retraction stop, the probe was adjusted to the predefined retracted probe position, and the probe was locked to the fully retracted actuator via the yoke. The insertion depth of the probes was set by collars that were positioned around the Inconel shroud and locked in place with an adjustment screw, and which would hold the probe at the desired insertion depth when the actuators were activated. The probe translation rate was controlled by metering air flow to the actuator using a needle valve. Bench testing of the system using dummy rods was performed to fine tune the system and procedure. Figure 29 shows details of the actuation system assembly setup for the combustor and turbine. Figure 30 and Figure 31 show details of the actuation system assembly setup for the mixer.

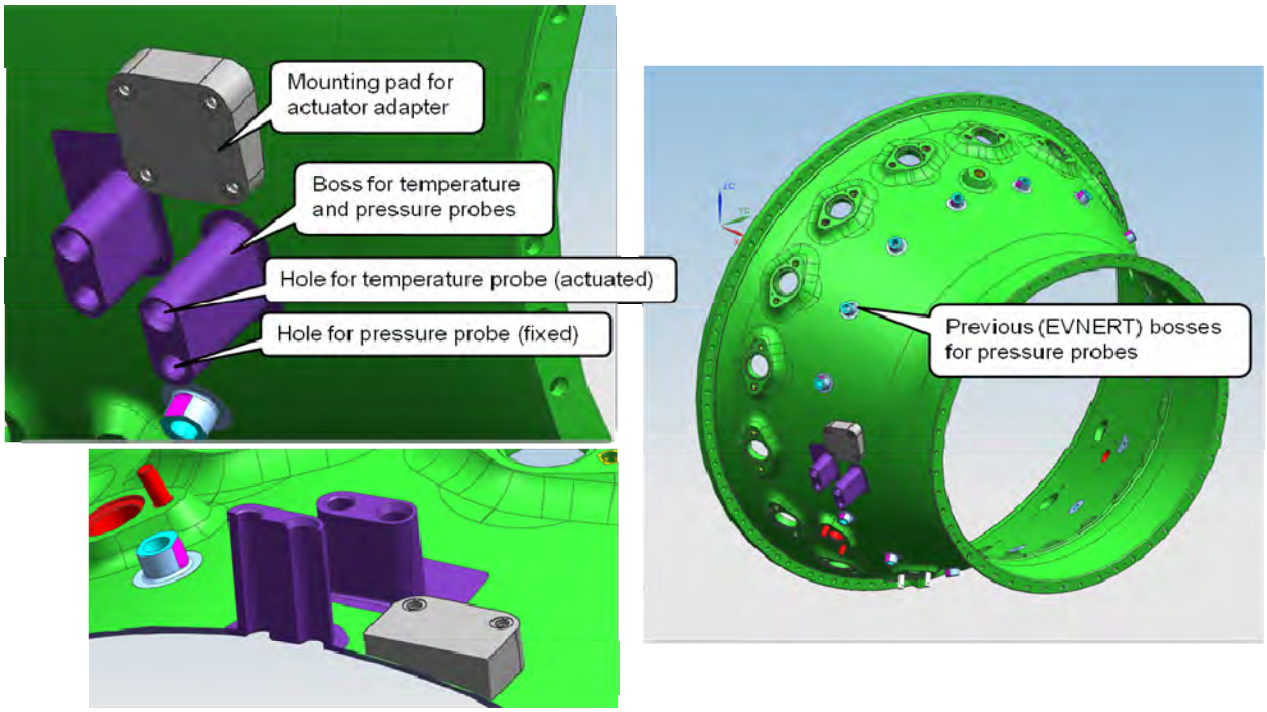

Figure 19. View of the Modifications to the Combustor Case (70642392-1).

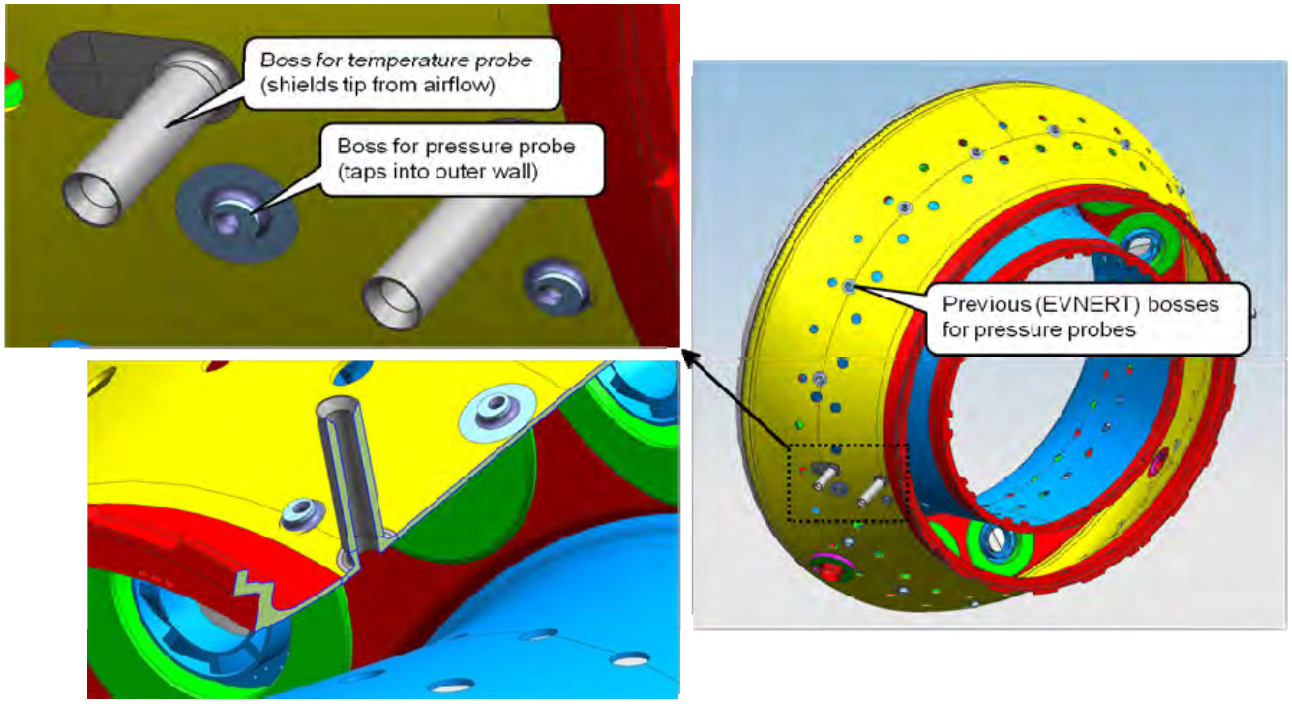

Figure 20. View of the Modifications to the Combustor (70642393-1).

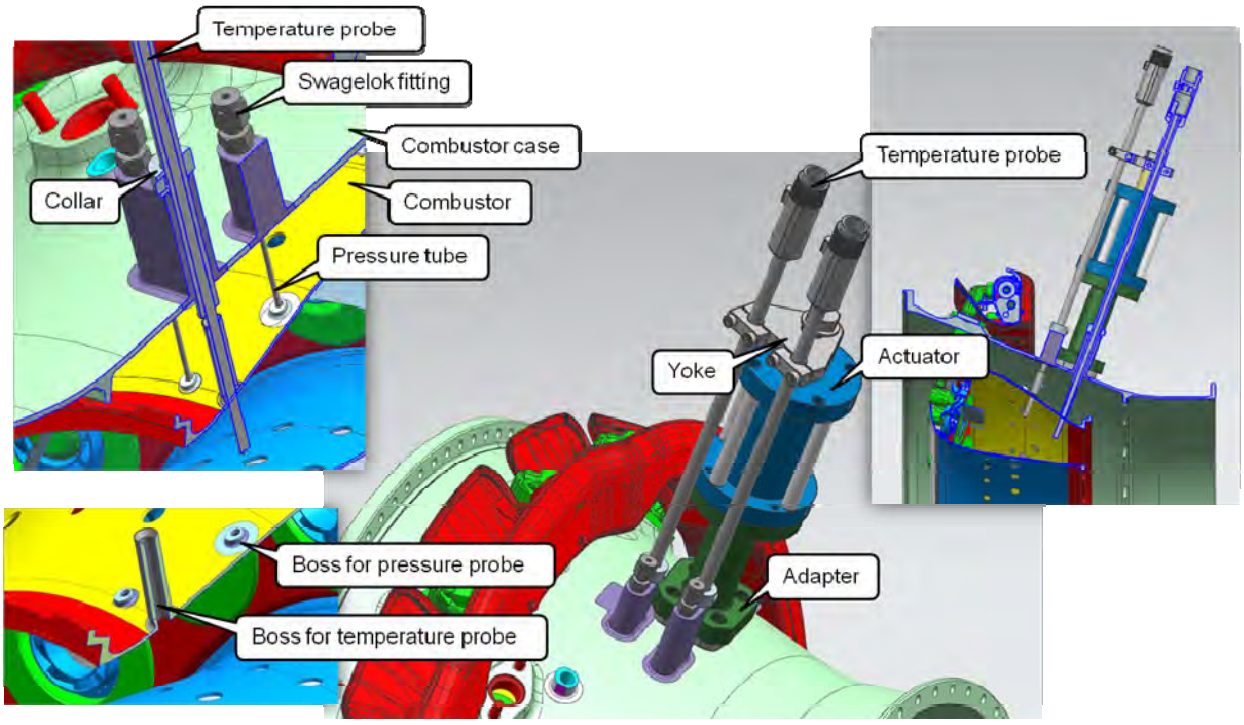

Figure 21. View of the Probe Integration and Actuation Setup for the Combustor.

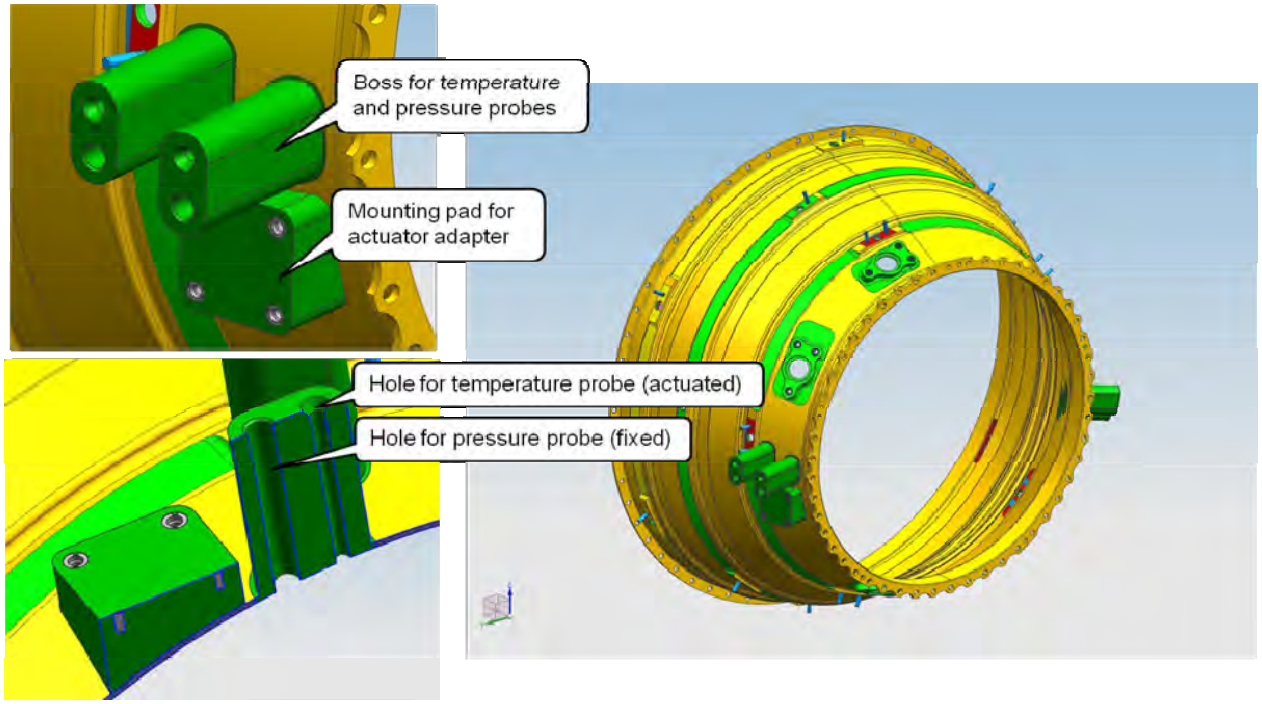

Figure 22. View of the Modifications to the Turbine Case (70642394-1).

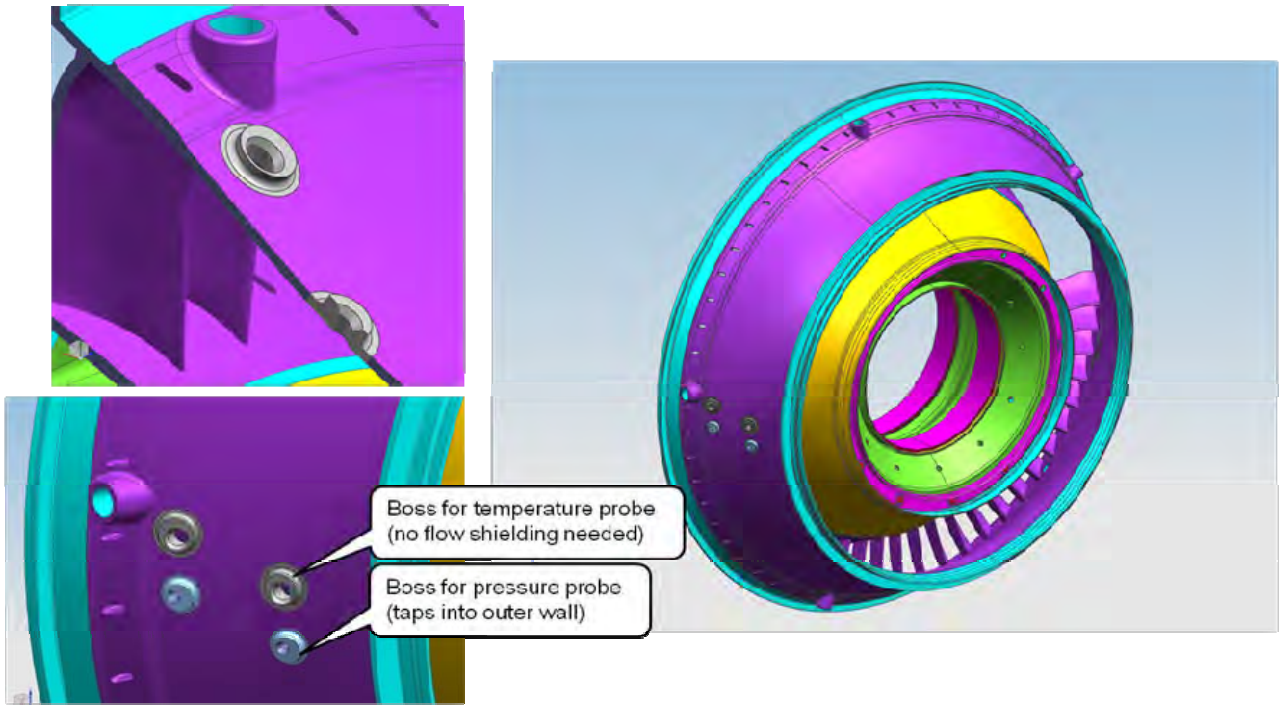

Figure 23. View of the Modifications to the LP Turbine Nozzle (70642395-1).

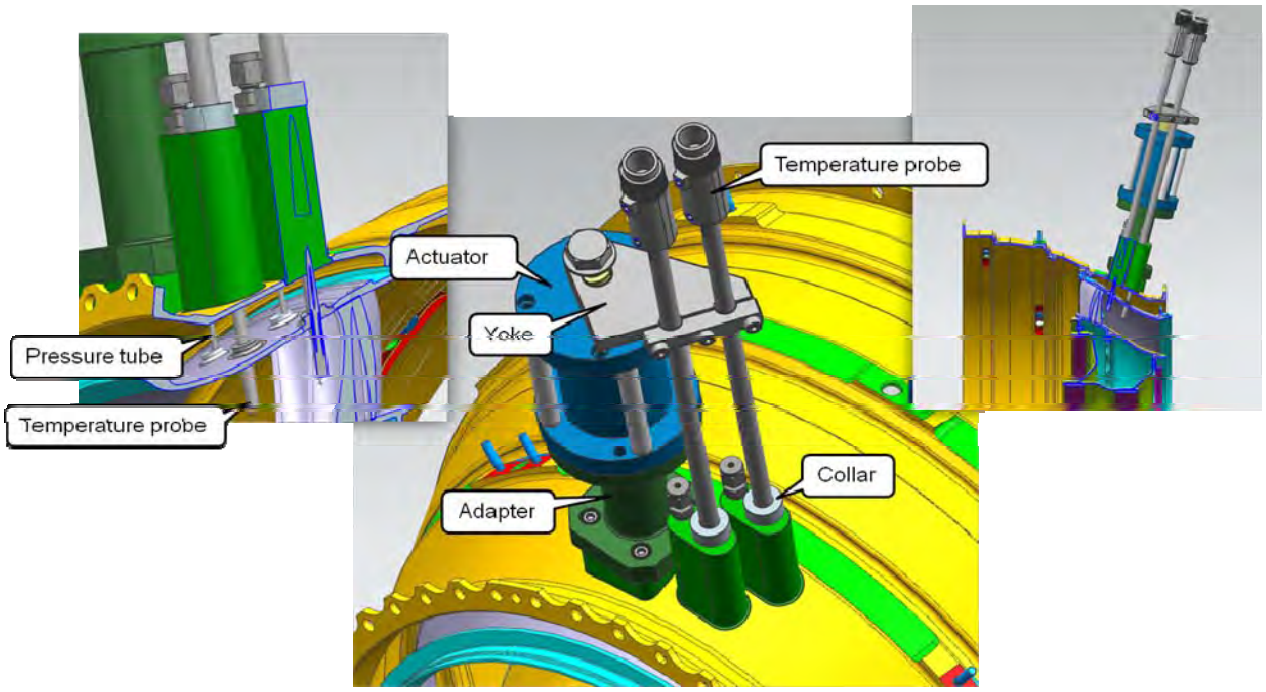

Figure 24. View of the Probe Integration and Actuation Setup for the LP Turbine.

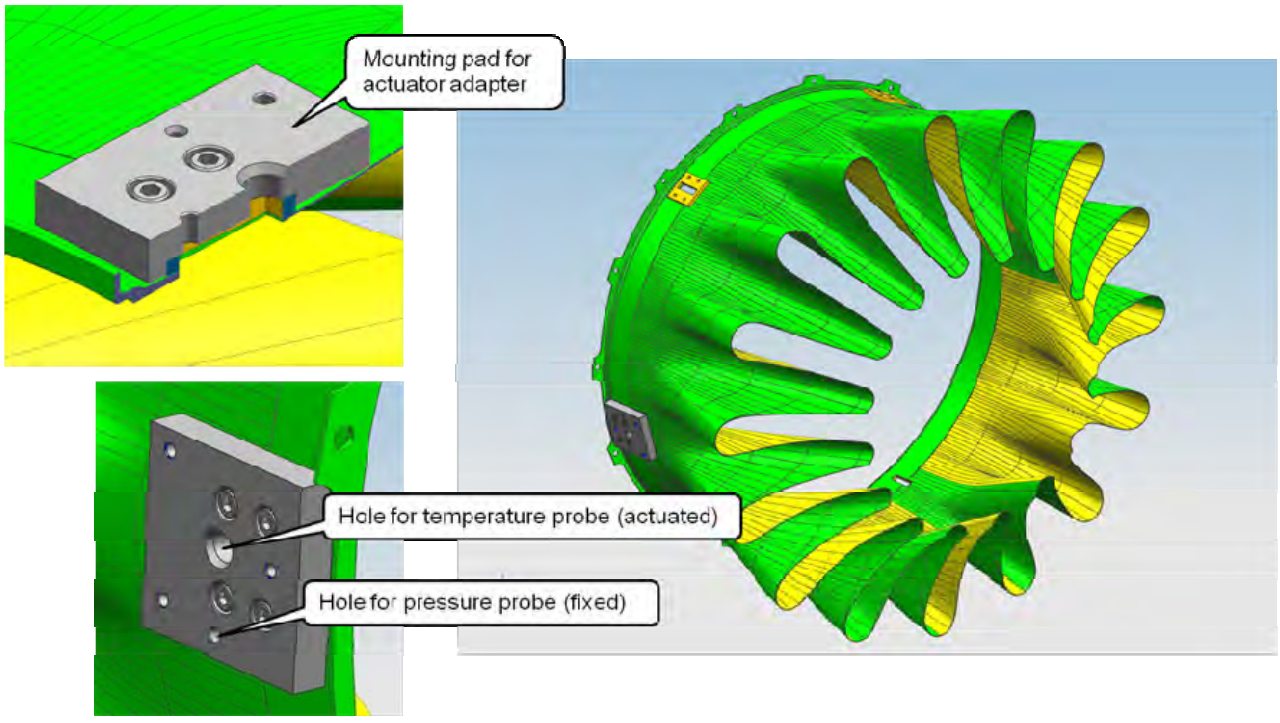

Figure 25. View of the Modifications to the Mixer Nozzle (70642396-1).

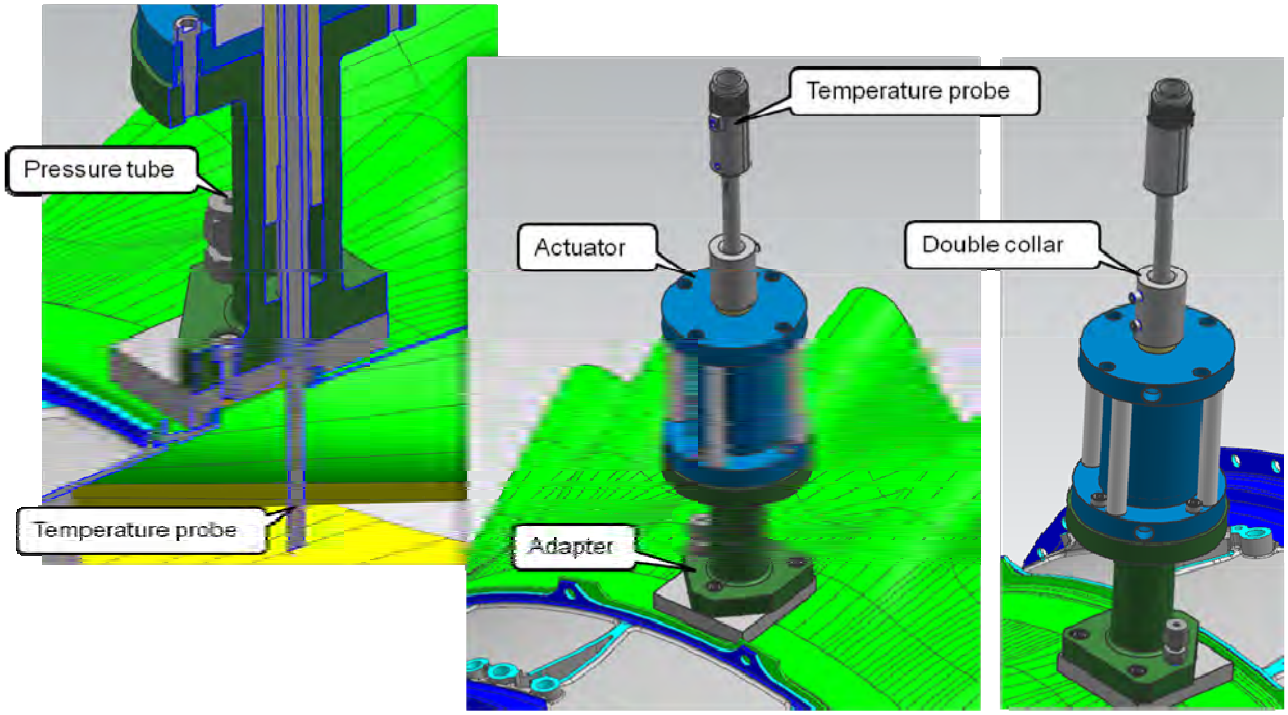

Figure 26. View of the Probe Integration and Actuation Setup for the Mixer.

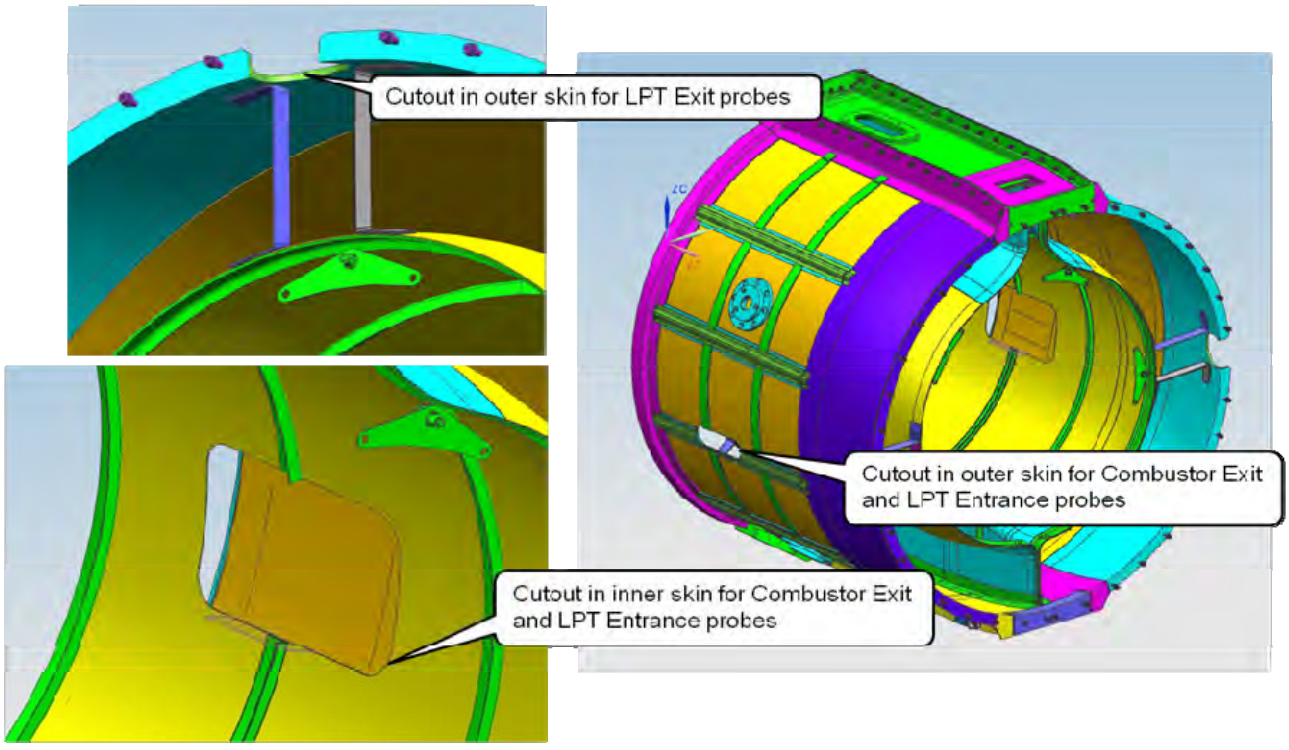

Figure 27. View of the Modifications to the C-Ducts (70642398-1).

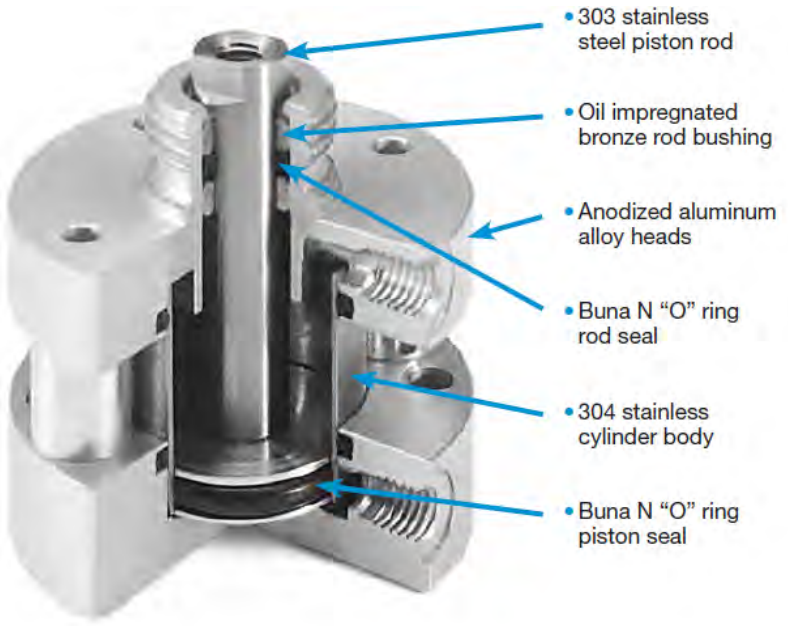

Figure 28. Bimba Flat-1 FOD-313-HV Actuators Were Used to Deploy the Probes.

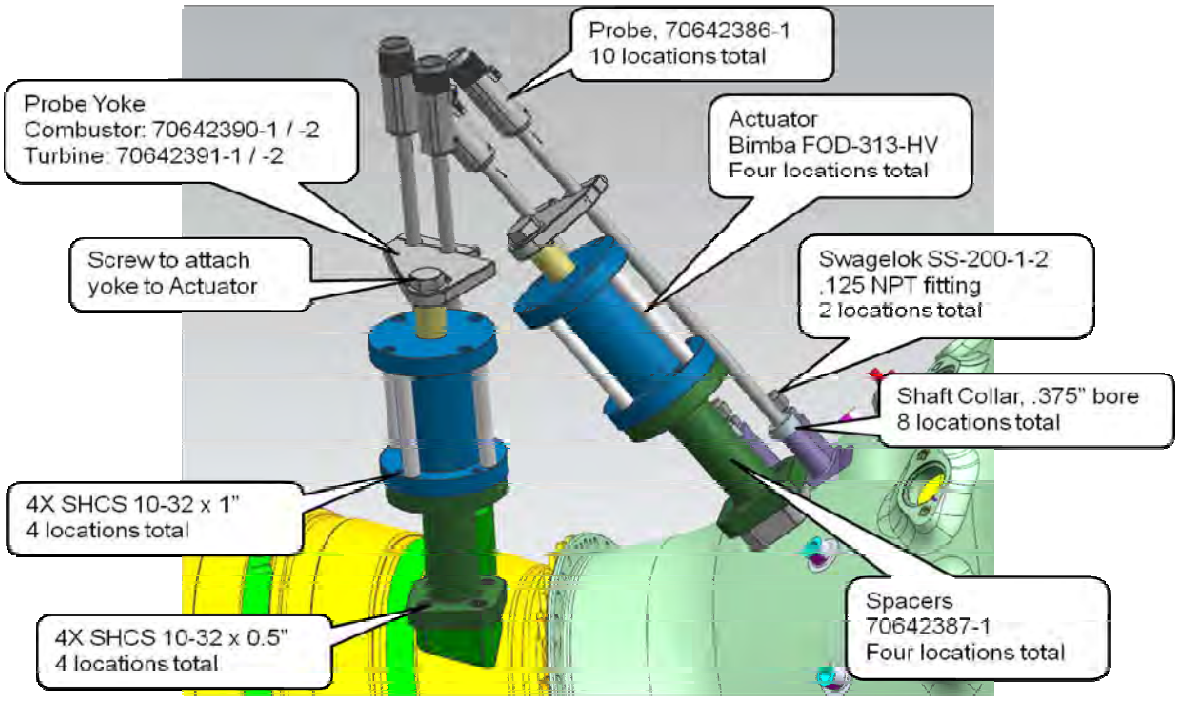

Figure 29. Actuation System Assembly for the Combustor and Turbine.

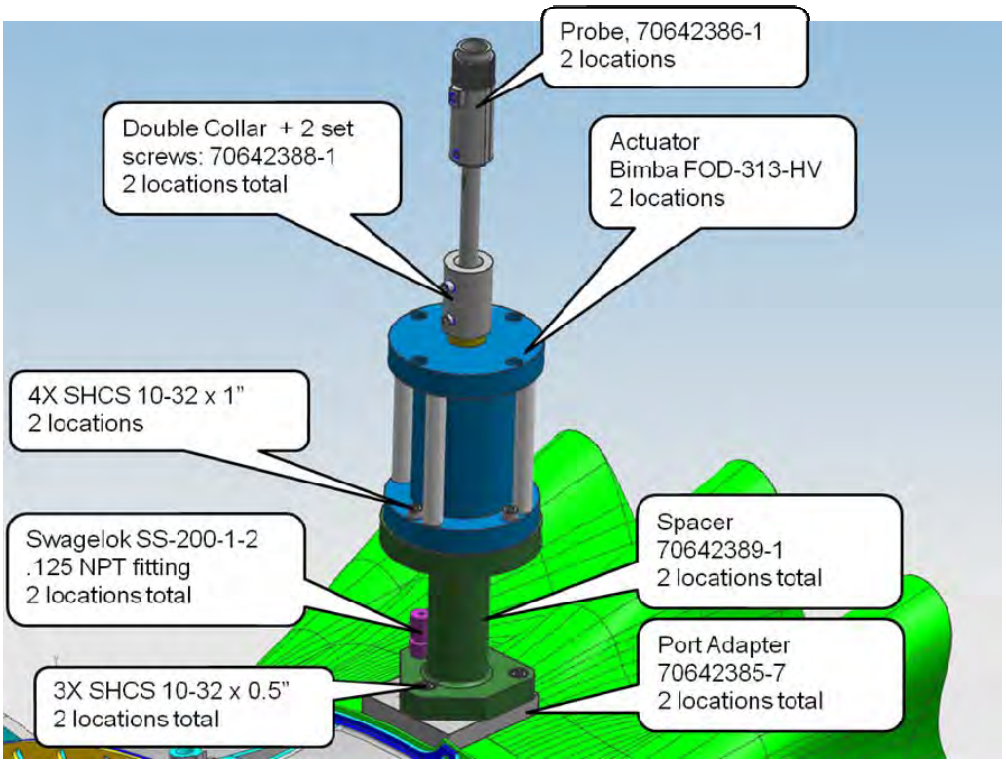

Figure 30. Actuation System Assembly for the Mixer Nozzle.

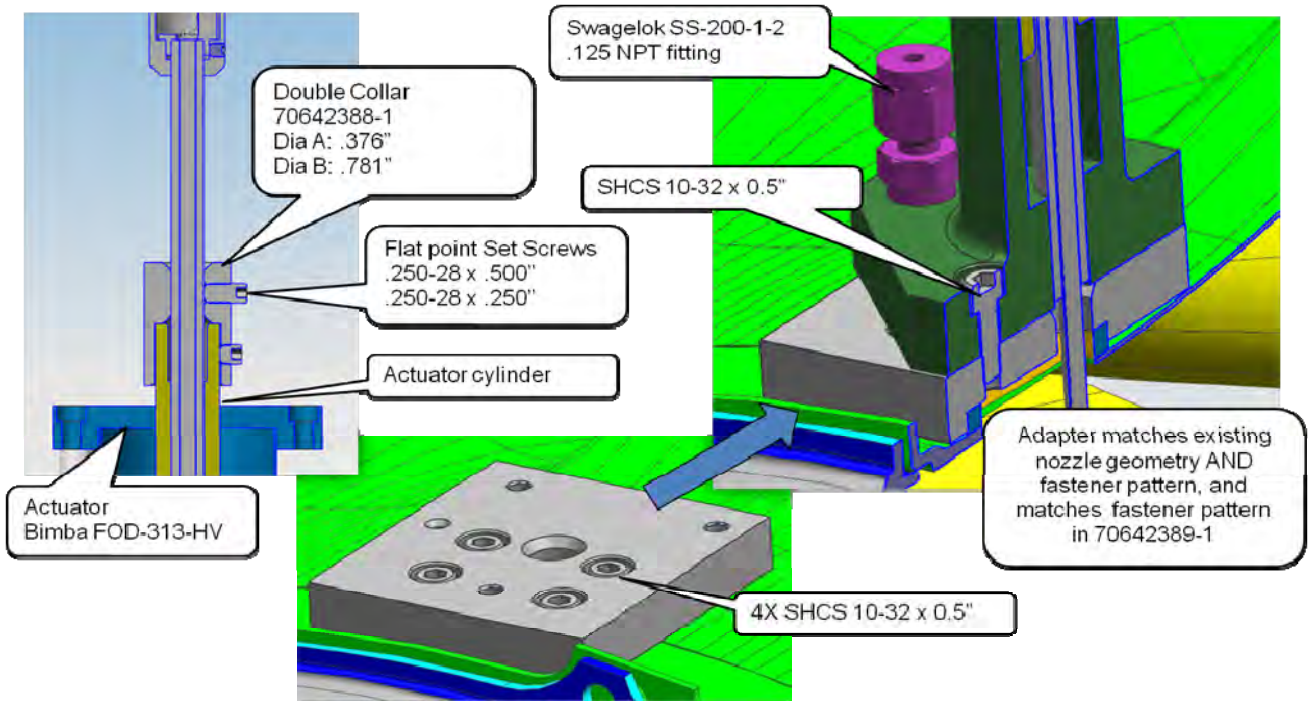

Figure 31. Details of the Actuation System for the Mixer Nozzle.

In February 2013, design reviews were held with Honeywell staff at Phoenix and NASA staff at GRC to review the approach to acquiring the dynamic temperature measurements on the TECH977 engine. During these reviews, the program objectives, prior experience, design criteria, measurement locations, probe design, engine/probe integration, engine modifications, engine operation, and risk and mitigation approaches were discussed. An agreement on the suitability of the measurement approach was obtained during these reviews. Several actions were taken, related to ensuring the structural integrity of critical hardware, validating the engine hardware and instrumentation assembly sequences, and conducting pretest instrumentation checkouts and engine check runs. The thermal differential growth of the combustor and combustor case was identified as a risk that could lead to binding and breakage of the temperature probes and potential subsequent damage to the engine. This risk was addressed during the hardware modification stage by enlarging the clearances in the combustor bosses. During engine assembly, the clearances were checked using dummy probes to ensure that the ceramic stick of the real probe would not contact the combustor boss (and exert a load on the stick that could cause it to snap) at the maximum predicted differential thermal growth.

The draft engine test plan was updated to include the latest descriptions of the modified hardware and part numbers, a revised description of the probe design, and CAD views of the instrumentation. In addition, the pretest checkouts of the actuator and engine were updated, the engine test points were re-sequenced to avoid back-to-back repeats at the same condition, and the list of dynamic data channels was updated. A final test plan was released after all the drawings were completed, and provided details of the final engine and instrumentation configuration. The final plan included additional descriptions of the pneumatic actuation system, the dynamic pressure instrumentation, and the purge flow system, along with a discussion on measurement priorities and contingencies.

5.0 TASK 3: DATA ANALYSIS METHODOLOGY

5.1 Review of Analysis Techniques

The data analysis methodology task focused on the signal processing and analysis methods needed to characterize the dynamic pressure and temperature fluctuations. This effort required consideration of the dynamic response of the sensors and sensor installations, and consideration of the subsequent processing of the dynamic signals from multiple sensors. The first question is concerned with measuring the dynamic properties of the gas at specific locations and involves identifying procedures to convert raw voltage signals into physical units that provide the best estimate of the “true” dynamic fluid properties of the system. The second question is concerned with gleaning additional information about the system, such as acoustic mode content or temperature fluctuation convection speeds, by examining relationships between signals at different locations. As with all dynamic measurements, it is important to consider the frequency responses of the transducers, the mounting configuration, the signal conditioning, the data acquisition system, and the subsequent signal processing.

After down-selecting the dual thermocouple approach as the preferred technique for measuring dynamic temperature, previous NASA reports on the subject were reviewed to understand the technique and the processing methodology employed (References 1, 2, 3, 4, 5, 6, and 7). These reports document the development and validation of the technique, review measurements and analysis on combustor rig and engine tests, and describe the theoretical and computational procedures for compensating measured data to obtain the fluctuating temperature of the gas. The compensation procedure involves modeling both the convective heat transfer from the gas stream to the wires, and the heat conduction within the thermocouple

wire and supports. The measured magnitude of the frequency response between large and small diameter wires, in conjunction with an analytical model of the frequency response ratio, enables the determination of the in-situ convective heat transfer coefficient, and subsequently a frequency response correction that is applied to the small diameter wire to obtain the local dynamic temperature. In this test program, the goal was to obtain compensated dynamic temperature measurements up to a maximum frequency range of 1 kHz. The software that performs this compensation was obtained from NASA and reviewed.

Since both dynamic temperature and dynamic pressure fluctuations were being measured simultaneously in this program, an important consideration was to account for the phase delay in the pressure due to the propagation of acoustic waves in the semi-infinite tube from the probe opening to the transducer location, which requires knowledge of the temperature within the tube. This is of interest when computing cross-spectra between pressure measurements at different locations or between pressure and temperature signals.

5.2 Dynamic Gas Temperature Measurement System (DGTMS) Software

NASA provided a set of Fortran subroutines that comprise the DGTMS software for dual thermocouple probes. These routines were reviewed and compiled using the open source MinGW GNU Fortran compiler. Due to advances in data acquisition hardware and improvements in data processing methodologies, the software had evolved somewhat from its original implementation. This evolution is well documented in a series of published reports. However, the overall process flow remains largely the same. The original development and implementation of the DGTMS code is described in References 4 and 5. In that development program, the instrumentation approach and the data compensation methodology for measuring the fluctuating gas temperature using a DTP were defined and developed. The compensation procedure requires accounting for the dynamic conductive and convective heat transfer effects in the two thermocouples and their support wires. Laboratory burner and full-scale engine tests were conducted in which fluctuating temperature time history data were recorded on magnetic tape, and compensated spectra and time history data were computed using algorithms implemented on a HP5451C Fourier analyzer. In a follow-on program, documented in References 6 and 7, further development and testing of the DTP and DGTMS code were performed. The data processing algorithms were ported to Fortran IV and analog thermocouple time history data were acquired during various bench tests and processed on an IBM mainframe. More recently, as documented in Reference 3, enhancements were made to the DGTMS code to improve the speed of the fast Fourier transform (FFT) computations, implement an analytical solution for the probe frequency response in place of the original finite difference heat transfer model, port the software to a personal computer, and acquire the data digitally. This latter version of the software was used in this test effort.

The overall process flow for the DGTMS is shown in Figure 32. The software reads a fixed format input file containing general information that includes: probe geometric parameters; operating point parameters such as fuel/air ratio, mean gas temperature, Mach number and mean gas pressure; analysis parameters; and plotting and output parameters. The software then reads a fixed format data file containing the digitized time history data from the DTP, specifically the AC voltage from the small diameter thermocouple, the AC voltage from the large diameter thermocouple, and the DC voltage from the large diameter thermocouple. The software then executes the data compensation procedure. Gas stream and thermocouple parameters are computed and an analytical estimate of the thermocouple-to-gas transfer function, as a function of an aerodynamic parameter gamma, is generated. The measured transfer function between the large and small thermocouples is computed, enabling a measured

value of gamma to be interpolated from the analytical estimates. Subsequently, an appropriate transfer function can then be defined that relates the measured thermocouple temperature spectra to the gas temperature spectra. Application of this transfer function provides the compensated temperature spectra (i.e. gas temperature spectra), and Fourier inversion provides compensated time histories.

The subroutines obtained from NASA were inspected to ensure that the methodology and procedures were consistent with the published documentation. The aforementioned reports describe a number of improvements and corrections that have been made to the software. It was verified that these modifications were in fact present in the version of the DGTMS software that was obtained from NASA. It was desired to check out and gain some experience with the software using laboratory or full-scale engine measurements acquired during the previous test programs. However, raw digital time history data and corresponding compensated spectra were not available from the previous test programs. A thorough test run of the software was conducted using data from the Honeywell burner rig testing.

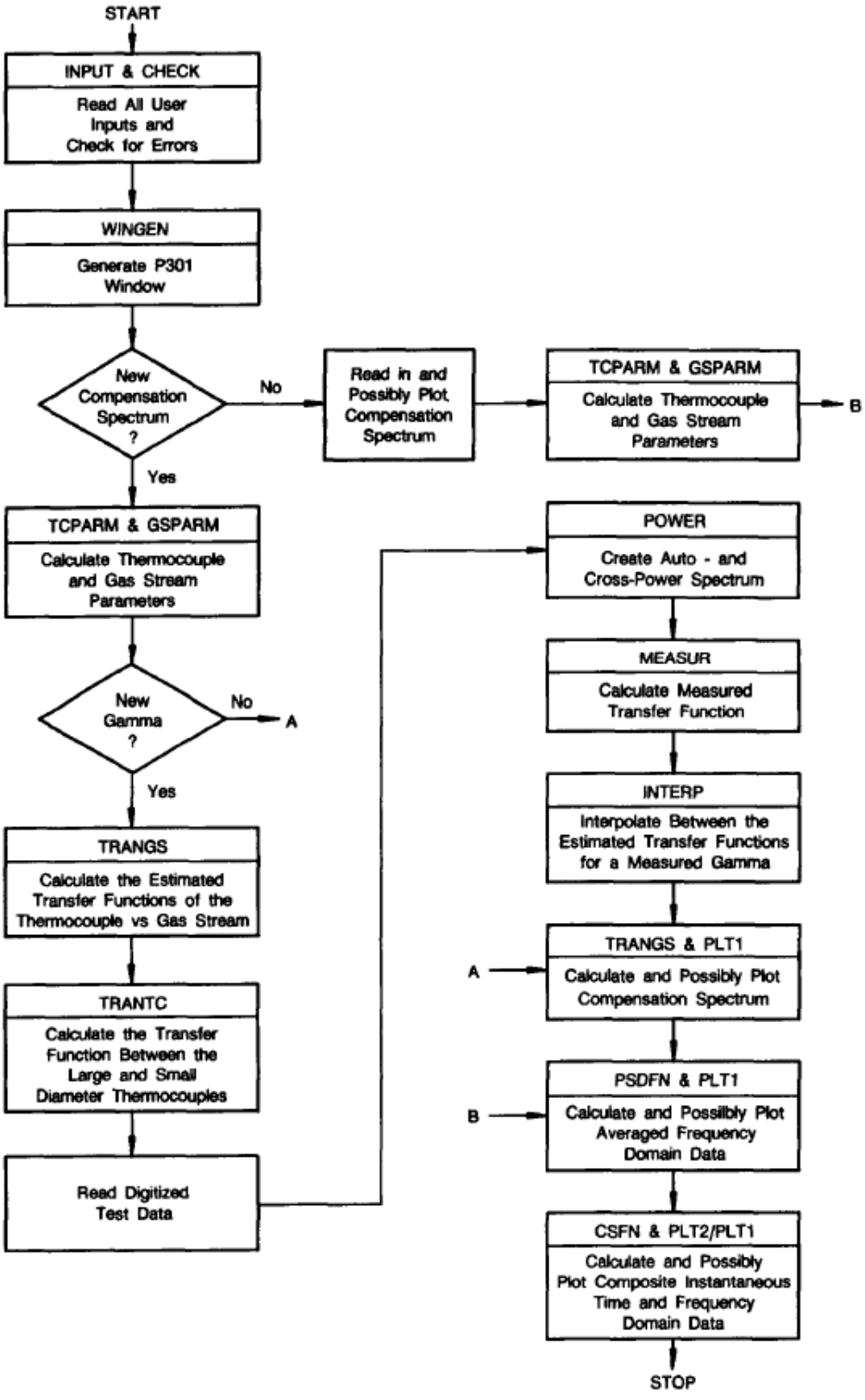

Figure 32. Typical Data DTP Data Reduction Process (Figure 8 of CR-179513).

5.3 Circumferential Mode Decomposition

Options for the arrangement of dynamic pressure probe array and associated modal decomposition were investigated. The simplest arrangement for decomposing the circumferential mode content is an azimuthal array of equally spaced transducers. The circumferential mode content at the axial location of the array can be determined using a straightforward space-time FFT of the dynamic pressure time history data. In the NASA EVNERT program, a single circumferential array of 16 equally spaced semi-infinite Kulite probes was used to measure modes in the through-flow annular combustor of the TECH977 engine (Reference 9). With this array, the circumferential mode content could be resolved to a frequency well beyond 3 kHz without any spatial aliasing, as shown in Figure 33. In order to allow more dynamic pressure probes to be used in other locations, a smaller array of 4 equally spaced probes was chosen for this program. The measurement serves as a validation that there are no dramatic changes in the circumferential mode content within the combustor. The reduced probe count results in the spatial aliasing of modes at a much lower frequency than occurred in the NASA EVNERT test. However, this effect is entirely predictable from the previous measurements. As shown in the right side of Figure 6, mode aliasing will occur above about 1000 Hz (e.g. there is an aliasing of the m = 2 and m = -2 modes near 1200 Hz). And as indicated by the arrows in the diagram, the aliased signals will cause the modes to appear within the measured modal analysis band.

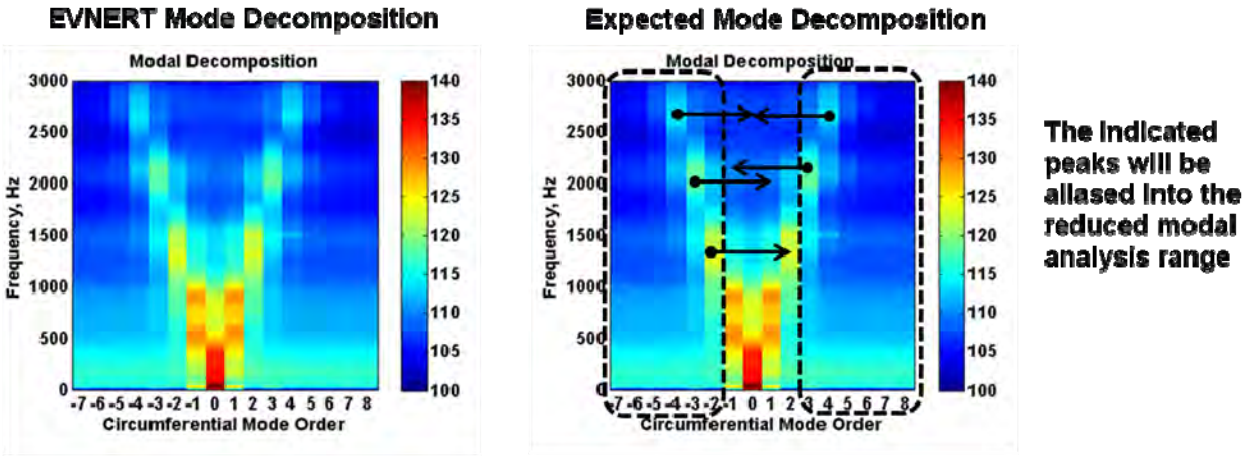

Figure 33. Aliasing of Circumferential Modes Is Predictable From Previous NASA EVNERT Array Measurements.

Semi-infinite Kulite coils have been successfully used on several recent programs at Honeywell, including auxiliary power unit (APU) combustor noise measurements during the NASA RASER program and propulsion engine combustor noise measurements during the NASA EVNERT program. An example of the semi-infinite Kulite probe, and the purge flow system used to cool the probes, is shown in Figure 34. Recent work on semi-infinite coils was reviewed. Reference 10 provides a useful comparison of flush mounted and semi-infinite probe measurements acquired using an impedance tube, a flow duct, and a micro-turbine engine, in the absence of any purge flow. Reference 11 provides an interesting computational assessment of the impact of temperature distributions on combustor probes that are cooled with nitrogen purge flow. The impact of using a cooled semi-infinite probe on the measured noise spectra, relative to a flush mounted microphone, is expected to be small, especially at the low frequencies that are of

interest in this program. These references generally confirm this expectation, but the authors do provide a better quantification, or at least an approach to quantifying, the errors associated with the semi-infinite probe arrangement.

One objective of the testing is to compute pressure-temperature cross-spectra at locations where both of these quantities are measured. The dynamic temperature measurements from the DTP are corrected using the DGTMS code to obtain the local gas temperature spectra and/or time history. The dynamic pressure data needs to be corrected to account for the frequency response of the probe system, and the most significant correction required is to account for the time delay in the signal as it propagates from the sensor tip to the Kulite location. A simple time delay can be computed assuming that the sound speed in the probe tube is known. This requires measurement of the air temperature in the tube. It was proposed to make measurements within the probe tube at one or more locations in order to provide an accurate time delay correction. Figure 35 shows an example of a Kulite tee that is instrumented with a thermocouple in order to measure the purge flow temperature. This type of tee was used to quantify the sound speed within the probe tube.

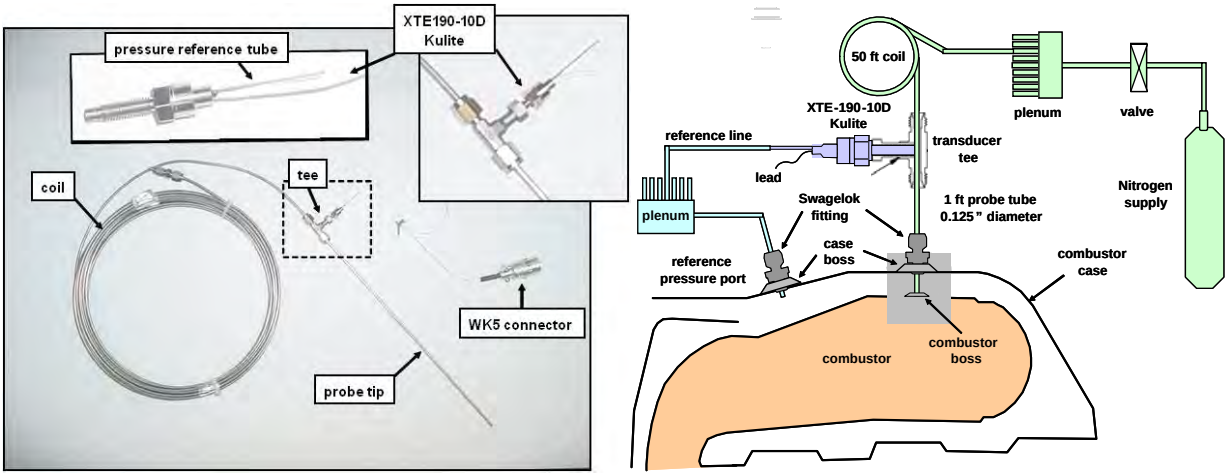

Figure 34. Semi-Infinite Probes Have Been Successfully Used on Recent Engine Test Programs.

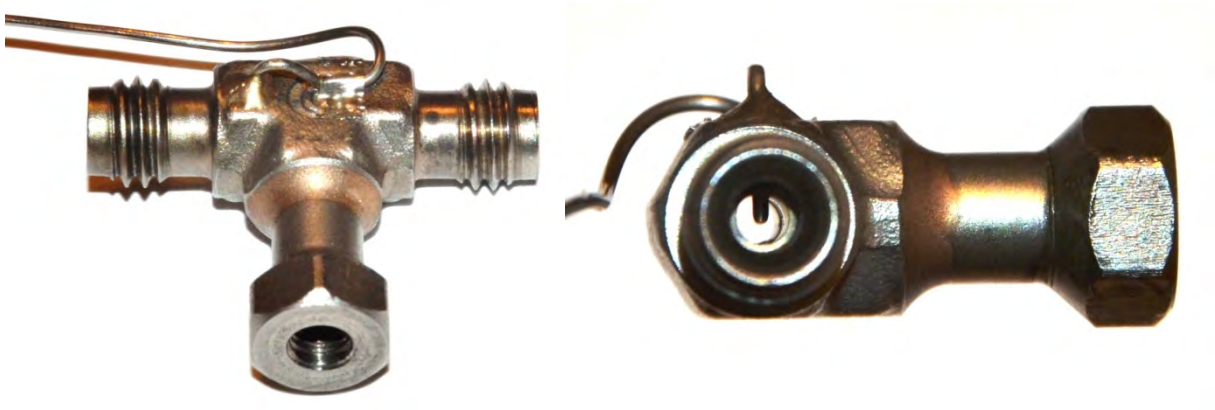

Figure 35. Example of a Kulite Tee Instrumented With a Thermocouple.

5.4 Burner Rig Test Data Analysis

As described in Section 3.7, two general types of burner rig tests were conducted using the first two DTPs procured from CEL. The first was a rotating carousel test for use with the Honeywell probes which had the intent of generating "large temperature fluctuations" at a known fixed frequency (Figure 9). This test would explore the frequency response capability of the Honeywell probes. The second was a stationary probe test with the intent of creating "small temperature fluctuations" through the natural unsteady burning and turbulent mixing of the gas (Figure 10). This test would allow a comparison of the Honeywell and NASA probes when they were exposed to a comparable unsteady temperature environment. Time history data were acquired by both a Bruel & Kjaer Pulse system and a Dewetron system. The time history data from the B&K Pulse system were exported to Universal File Format (UFF) files for subsequent processing. The data were acquired at a fixed sample rate of 8192 S/s, and for a record length of 70 seconds. Table 2 summarizes the test points that were acquired in the burner rig test.

Table 2. Summary of Test Points from the Burner Rig Test.

DGTMS Probe(s)	Test Point Type	Date & Time	Carousel Rotational Speed [rpm]	Expected Tone Frequency [Hz]	Probe 1 Small T/C Mean Temp Channel 1 [°F]	Probe 1 Large T/C Mean Temp Channel 2 [°F]	Probe 2 Small T/C Mean Temp Channel 3 [°F]	Probe 2 Large T/C Mean Temp Channel 4 [°F]	Pulse UFF Filename
HON B	Carousel On	5/31/2012 11:38	1000						Test1_HonProbe1_1.uff
HON B	Carousel On	5/31/2012 13:34	1000	200	1513	1508	n/a	n/a	1500_1KRPM_HonProbe2_1.uff
HON B	Carousel On	5/31/2012 13:41	2000	400	1568	1565	n/a	n/a	1500_2KRPM_HonProbe2_1.uff
HON B	Carousel On	5/31/2012 13:52	500	100	1526	1520	n/a	n/a	1500_500RPM_HonProbe2_1.uff
HON B	Carousel On	5/31/2012 14:00	1500	300	1523	1518	n/a	n/a	1500_1500RPM_HonProbe2_1.uff
HON B	Carousel On	5/31/2012 14:10	2000	400	1552	1545	n/a	n/a	1500_2KRpm_HonProb2_B_1.uff
HON B	Probe Behind Rod	5/31/2012 14:20	0	n/a	1536	1528	n/a	n/a	1500_0RPM_HonProbe2_Blocked_1.uff
HON B	Probe Between Rods	5/31/2012 14:26	0	n/a	1511	1503	n/a	n/a	1500_0RPM_HonProbe2_NotBlocked_1.uff
HON B	Ambient Noise, Burner Off	5/31/2012 14:32	0	n/a	room temp	room temp	n/a	n/a	Ambient_1.uff
HON B	Ambient Noise, Burner Off	5/31/2012 14:35	1000	n/a	room temp	room temp	n/a	n/a	Amb_1KRpm_1.uff
HON B	Carousel On	5/31/2012 15:16	2000	400	1464	1454	n/a	n/a	1500_2KRpm_HonProb2_C_1.uff
HON B	Carousel On	5/31/2012 15:22	2815	563	1508	1485	n/a	n/a	1500_2KRpm_HonProb2_C1_1.uff
HON A	Carousel On	6/1/2012 8:21	500	100	1425	1418	n/a	n/a	HP1_1500F_500Rpm_1.uff
HON A	Carousel On	6/1/2012 8:33	500	100	1489	1480	n/a	n/a	HP1_1500F_500Rpm_A_1.uff
HON A	Carousel On	6/1/2012 8:40	1000	200	1582	1567	n/a	n/a	HP1_1500F_1000Rpm_1.uff
HON A	Carousel On	6/1/2012 8:44	1500	300	1539	1522	n/a	n/a	HP1_1500F_1500Rpm_1.uff
HON A	Carousel On	6/1/2012 8:49	2000	400	1565	1547	n/a	n/a	HP1_1500F_2000Rpm_1.uff
HON A	Carousel On	6/1/2012 8:53	2800	560	1465	1518	n/a	n/a	HP1_1500F_2800Rpm_1.uff
HON A	Carousel On	6/1/2012 9:03	2800	560	1555	1539	n/a	n/a	HP1_1500F_2800Rpm_A_1.uff
HON A	Probe Behind Rod	6/1/2012 9:11	0	n/a	1531	1513	n/a	n/a	HP1_1500F_0Rpm_Blocked_1.uff
HON A	Removed Rod, Probe Exposed	6/1/2012 9:17	0	n/a	1009	1109	n/a	n/a	HP1_1500F_0Rpm_Not_Blocked_1.uff
HON A + HON B	Carousel On	6/1/2012 10:00	500	100	1462	1415	1289	1527	HP12_1500F_500Rpm_1.uff
HON A + HON B	Carousel On	6/1/2012 10:07	1000	200	1387	1342	1292	1569	HP12_1500F_1000Rpm_1.uff
HON A + HON B	Carousel On	6/1/2012 10:12	2000	400	1404	1359	1193	1696	HP12_1500F_2000Rpm_1.uff
HON A + NASA	Burner Edge, Fuel Press 94	6/1/2012 11:27	0	n/a	1109	1136	1144	1209	HP1NPKul_HotCore_1000_1.uff
HON A + NASA	Burner Edge, Fuel Press 155	6/1/2012 11:39	0	n/a	1439	1465	1464	1545	HP1NPKul_HotCore_1500_1.uff
HON A + NASA	Burner Core, Fuel Press 94	6/1/2012 12:16	0	n/a	1020	1036	1200	1247	HP1NPKul_Center_1000_1.uff
HON A + NASA	Burner Core, Fuel Press 155	6/1/2012 12:20	0	n/a	1398	1415	1597	1657	HP1NPKul_Center_1500_1.uff

An inspection of the time history data revealed that it was of good quality. Figure 36 shows a five second plot of the time history data from Honeywell probe #1 that was acquired by the Pulse system. The data is for the case of the probe installed in the center of the carousel rotating at 1000 rpm, at a mean gas temperature of 1580°F. The small diameter (0.004-inch) wire thermocouple clearly shows a higher response than the large diameter thermocouple wire (0.010-inch). The two wires appear to have approximately the same mean value, and the voltage fluctuations about the mean appear to be well synchronized. In this particular example, the small wire thermocouple has temperature fluctuations on the order of ±100°F (±3σ). If the data is examined closely, the quantization of the data can be observed. Although the input signal range of the Pulse A/D converter was fixed at ±10V, and no signal amplification was

employed to maximize the A/D range, the quantization is seen to be small, since the 24-bit A/D converter has a very high dynamic range. The quantization corresponds to voltage level changes on the order of 1.4μV, which corresponds to about 0.3°F at a mean gas temperature of 1500°F.

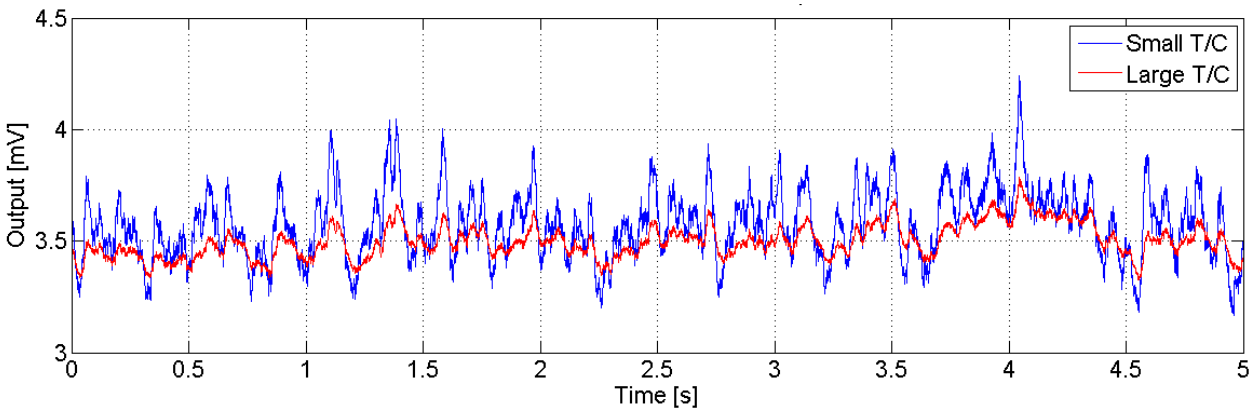

Figure 36. Representative Time History Voltage Output from the Burner Rig Test.

The test data was processed using the DGTMS software. The Fortran-based DGTMS software was obtained from NASA and compiled using the freely available GNU Fortran compiler. One code modification was made to the software. The subroutine TRFEM computes the analytical solution for the transfer function between the thermocouple wire and the gas stream (replacing the previous finite difference module). This subroutine was changed to increase the computational accuracy by using double precision in order to avoid numerical overflow. Although no test case was supplied with the code, processing of data from the burner rig test indicated that the software was operational and worked as described in the referenced reports.

Input files were created containing the design specified probe dimensions, the approximate mean flow properties of the gas, and user-selectable program control options. The time history data files were converted into a format compatible with the DGTMS software. The DGTMS format consisted of a series of 280 blocks, with each block containing 2048 data points of the small thermocouple AC signal, 2048 data points of the large thermocouple AC signal, and 2048 data points of the large thermocouple DC signal. In order to prepare these data files, the time history recordings from the large and small diameter thermocouples were each split into “mean” (DC) and “dynamic” (AC) components as follows. The DC component was generated by passing the data through a fourth order low pass Butterworth filter with a cutoff frequency of 1 Hz. The AC component was generated by passing the data through a fourth order high pass Butterworth filter with a cutoff frequency of 1 Hz. The cut-off frequency is somewhat arbitrary, but a 1 Hz cutoff was chosen to be consistent with the analog filtering characteristics that were used on the previous NASA program (e.g. Figure 8 of Reference 4). The filters were designed in Matlab using the *butter.m* function and the *filtfilt.m* function in order to obtain zero phase distortion and to minimize the starting and ending transients. An example of the splitting of the time history files is shown in Figure 37. The phase preserving characteristics of the filtering process can be seen in the overlay of the raw and reconstructed time histories.

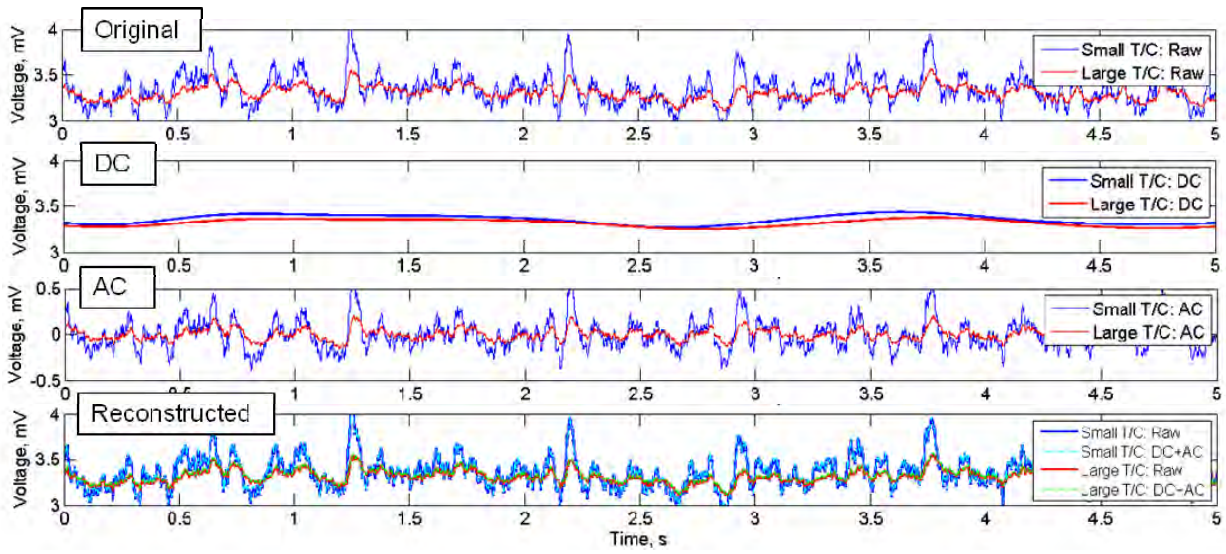

Figure 37. An Example of the Splitting of a Time History Data Into "Mean" (DC) and "Dynamic" (AC) Components.

The data analysis was performed using a frequency resolution of 4 Hz, which was chosen to have sufficient resolution and to allow convenient data manipulation. A total of 280 independent averages are available with the 70 seconds of data. A Matlab wrapper script was used to run the data files through the DGTMS software in a batch mode. The DGTMS software requires an input file that contains the probe dimensions, mean flow properties, and program control options. There can be some uncertainty in the probe dimensions and the mean flow properties. Regarding the probe dimensions, the DGTMS software employs a simplified physical model of the probe to compute the theoretical convective heat transfer between the gas stream and the probe wires, and the conductive heat transfer along the sensing and support wires. The actual physical construction is usually different from this idealized model. For example, there is often an overlap of the small sensing wires with their support wires to facilitate the welding of the two wires. In addition, there are often some differences between the design intent dimensions and the as-fabricated dimensions.

Figure 38 shows a schematic of the ideal probe design (theoretical model), the Honeywell development probe design intent, the Honeywell development probe as-fabricated design, and the NASA probe configuration. To explore the impact of the different lengths of the thermocouple junction elements, selected data points were processed using input files with different dimensional inputs. An example of the impact of variation in the dimensional inputs is shown in Figure 39, for Honeywell Probe A in the carousel spinning at 1000 rpm. The difference in the compensated frequency spectra is on the order of a few tenths of a decibel absolute error over the frequency range of interest. Another example is shown in Figure 40, for a stationary Honeywell Probe A positioned at the edge of the burner rig flame, at a fuel pressure of 155 psi. The differences are more pronounced in this case. The addition of the measured small wire extensions to the DTGMS inputs increases the compensated spectrum amplitude by about 1.5 dB. Overall, the impact of using different dimensional assumptions for the lengths of the sensing elements did have a noticeable effect on the compensated spectra, but the magnitude of the differences were not substantial, and were dependent upon the operating point analyzed. Furthermore, the relative error between different points in the spectrum is small. Thus, the errors introduced due to these variations in as-fabricated probe dimension are not

critical to the analysis. Careful attention to the fabrication of the probe sensing elements, and accurate measurement of the fabricated dimensions, help to minimize any errors associated with dimensional uncertainties.

There is also some uncertainty in the Mach number, mean pressure and mean temperature of the flow in which the probes were immersed. A sensitivity study was also conducted to explore the impact of variations in assumed mean flow parameters on the compensated spectra. The compensated spectra were found to be insensitive to the mean flow inputs. These inputs are used to establish an initial theoretical estimate of an aerodynamic parameter Γ, which is then used to construct a family of theoretical frequency response function curves. The measured frequency response functions are interpolated using this family of curves to generate a measured in-situ value of Γ. Reasonable estimates of these parameters (within 25 percent) at the test operating conditions were found to be sufficient for the code to successfully compute this in-situ value of Γ. The resulting compensated temperature spectra are not affected by these mean flow inputs.

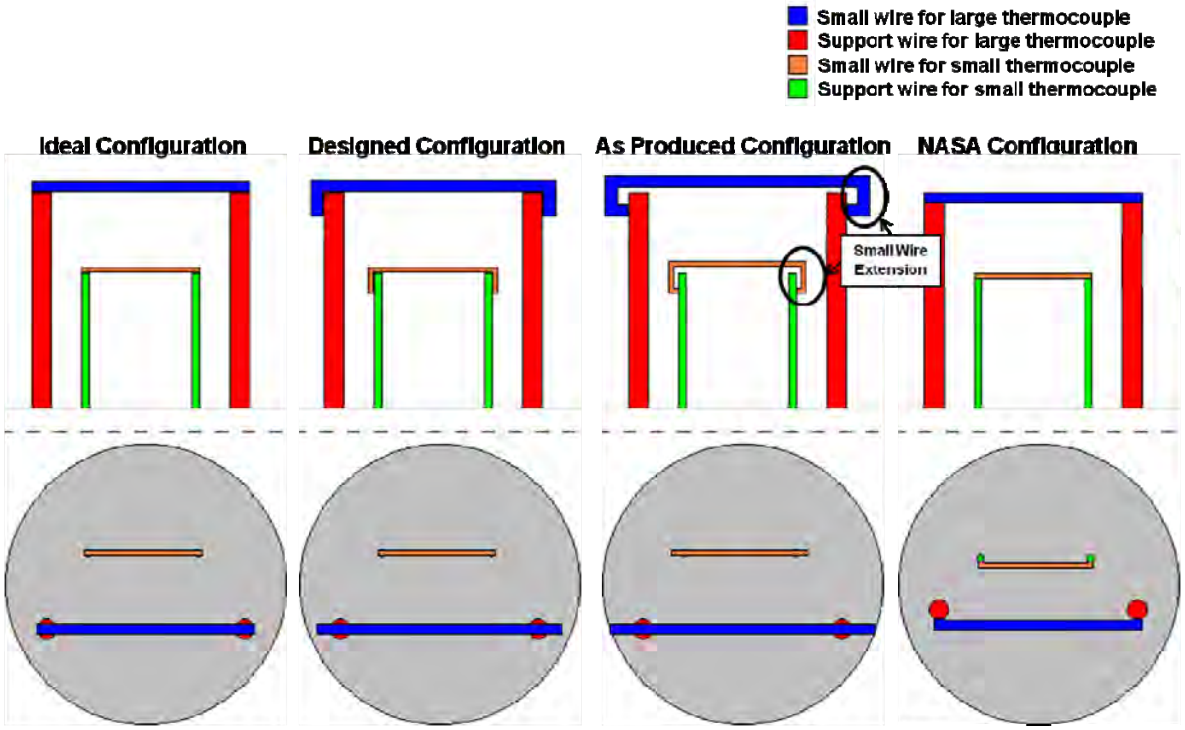

Figure 38. Schematic of Ideal, As-Designed, and As-Manufactured Probes.

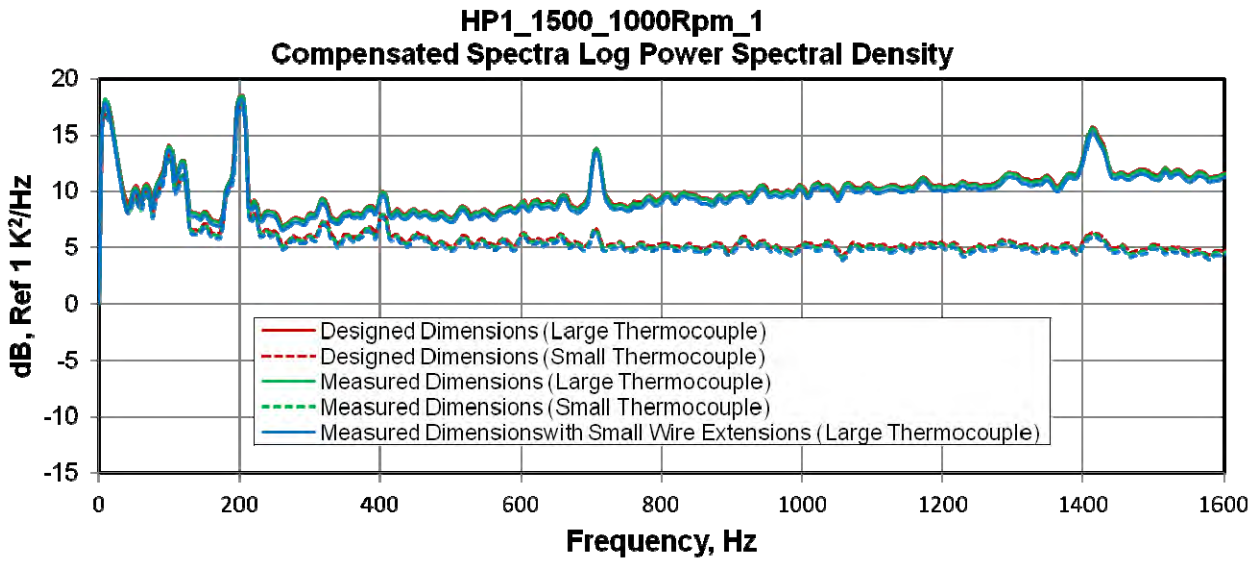

Figure 39. Sample Comparison From the Dimensional Sensitivity Analysis, for Honeywell Probe A in the Carousel Spinning at 1000 rpm.

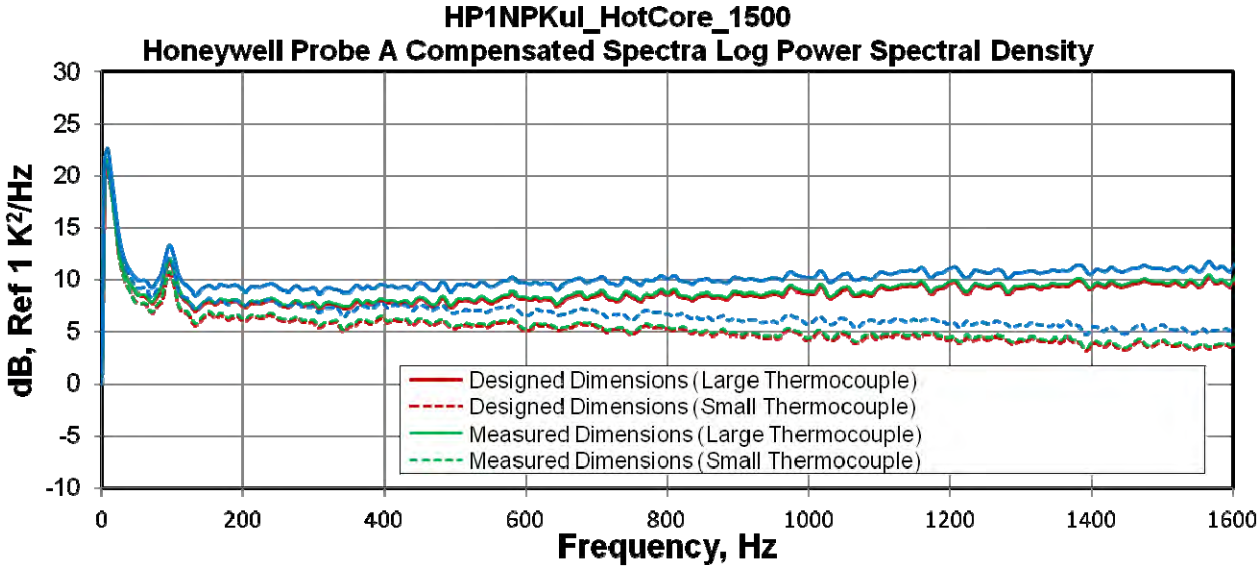

Figure 40. Sample Comparison From the Dimensional Sensitivity Analysis, for Stationary Honeywell Probe A at the Burner Flame Edge, Fuel Pressure of 155 psi.

Table 3. Measured Probe Dimensions (cm).

	Dimension	NASA Probe	Honeywell Probe A	Honeywell Probe B
Large Thermocouple	Length of Support Wire	0.4064	0.4216	0.4864
	Length of the Small Wire	0.3277	0.2769	0.3480
	Diameter of Support Wire	0.0508	0.0508	0.0508
	Diameter of Small Wire	0.0254	0.0254	0.0254
Small Thermocouple	Length of Support Wire	0.2540	0.2921	0.3353
	Length of the Small Wire	0.2160	0.2768	0.3352
	Diameter of Support Wire	0.0457	0.0508	0.0508
	Diameter of Small Wire	0.00762	0.01016	0.01016

The test data summarized in Table 2 were processed with the DGTMS software, using the measured probe dimensions in Table 3. Results from selected test points are presented here. First, a series of test points from the "large temperature fluctuation" carousel test of Honeywell Probe A are examined, for the carousel rotating at different speeds, and for the carousel stationary with the probe either blocked or not blocked by a rod (see Figure 9). Next, a series of test points from the "small temperature fluctuation" stationary test of Honeywell Probe A and the NASA probe (in close proximity) are examined, for the probes positioned at two locations in the burner flame, and for two fuel pressures (see Figure 10).

Figure 41 shows the results of the carousel test of Honeywell probe A with the carousel rotating at 500 rpm. In this and subsequent figures, several items are shown. The DC and AC portions of the time histories for the small (blue) and large (red) thermocouples are shown in the top of the figure. Ideally, the DC signals of the large and small thermocouples would be identical, assuming that the two wires are located at essentially the same point in the flow and measuring the same mean gas temperature. In reality there is a small axial and vertical separation between the small and large thermocouple wires, so slight differences are expected. Furthermore, it can be expected that the AC signal from the small wire (0.004-inch) should look similar to the AC signal from the large wire (0.010-inch), but should have greater fluctuating amplitudes due to its greater responsiveness to temperature fluctuations. In the lower left of each figure, the power spectral density of the AC portion of the small and large wire thermocouple signals are plotted on a logarithmic scale, with a 0 dB reference of 1 K^2/Hz. These power spectra densities (PSDs) correspond to the spectra of the *wire* (not gas) temperatures. In the figures bottom left there is also an enlargement of a portion of the AC time history data. In the lower right of each figure, the compensated power spectral density is plotted, which is obtained by running the DGTMS software on the measured data. This compensated power spectral density represents the estimated temperature spectrum of the actual gas, and is determined by computing a small wire compensation spectrum using data from both thermocouples, and applying the compensation spectrum to the PSD from the small wire thermocouple.

In Figure 41, the DC signals of the small and large wires are in good agreement, with some slight drift downwards with time due to a slight shift in the operating condition. The AC signals of the small and large wires oscillate in unison, with the small wire having higher responsiveness to temperature fluctuations as expected. The PSD of the small wire and large

wires have similar shapes, with the amplitudes of the small wire being 5 to 10 dB above those of the large wire over most of frequency range. The compensated PSD reveals a peak at 100 Hz, which is equal to the rod passing frequency (500/60 rev/s*12 rods/rev), indicating that large amplitude temperature fluctuations are successfully being generated at the desired frequency. The broadband portion of the spectrum is quite flat with amplitude that is generally 10 dB below the 100 Hz peak.

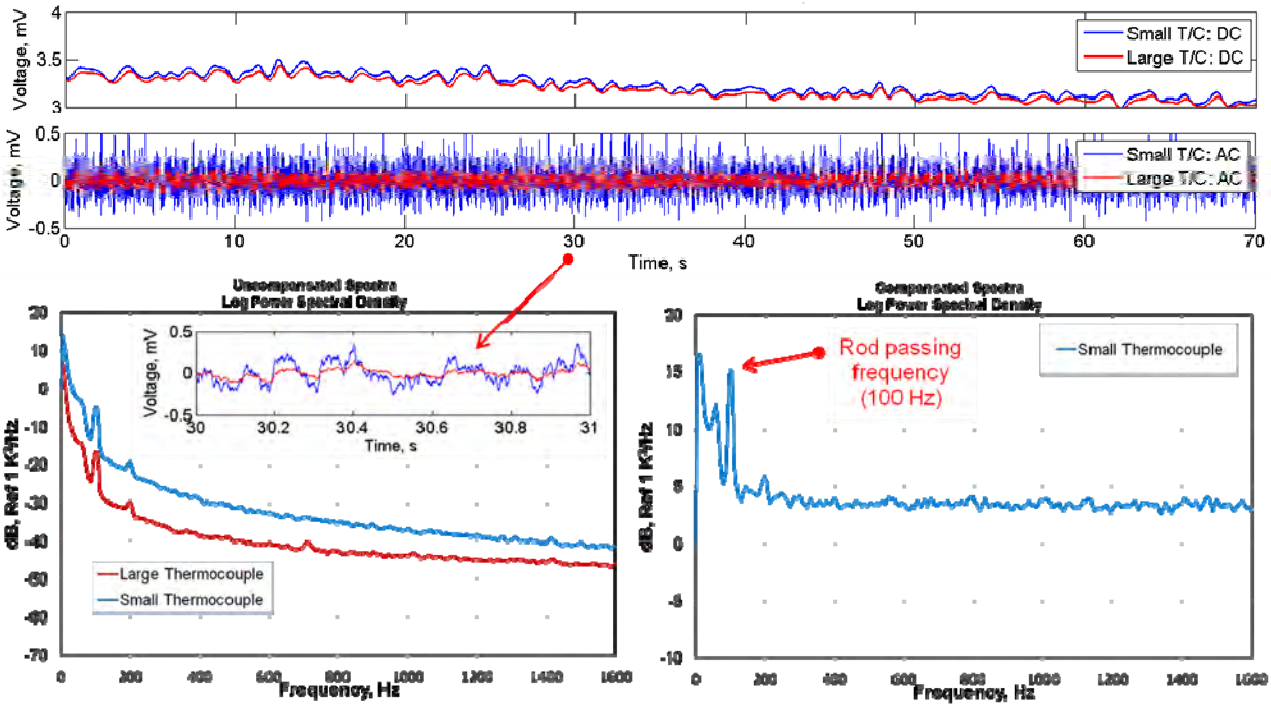

Figure 41. Results From the Carousel Testing of Honeywell Probe A at 500 rpm.

Figure 42 shows the results of the carousel test of Honeywell probe A with the carousel rotating at 1000 rpm. The results are similar to the 500 rpm case, except for the expected shift in the rod passing peak to 200 Hz. Figure 43 shows the results for the carousel rotating at 2000 rpm. Again the results are similar, except for the shift in the rod passing frequency to 400 Hz. The broadband levels do not change significantly and remain flat over most of the frequency range. Figure 44 shows the results for the carousel rotating at its maximum speed of 2800 rpm. The compensated spectrum is more interesting in this case. In addition to the rod passing frequency at 560 Hz, there is a family of peaks at multiples of the carousel 1-per-rev frequency of 47 Hz, indicating that there are rod-to-rod temperature non-uniformities in the flow impinging on the probe. This could be due to the fact that there were physical differences between the rods (e.g. surface roughness and vertical alignment, see Figure 9) that are affecting the flow. The rotating carousel test confirmed the ability of the probes to measure temperature fluctuations to frequencies of at least 600 Hz, which encompasses the main expected combustion noise range.

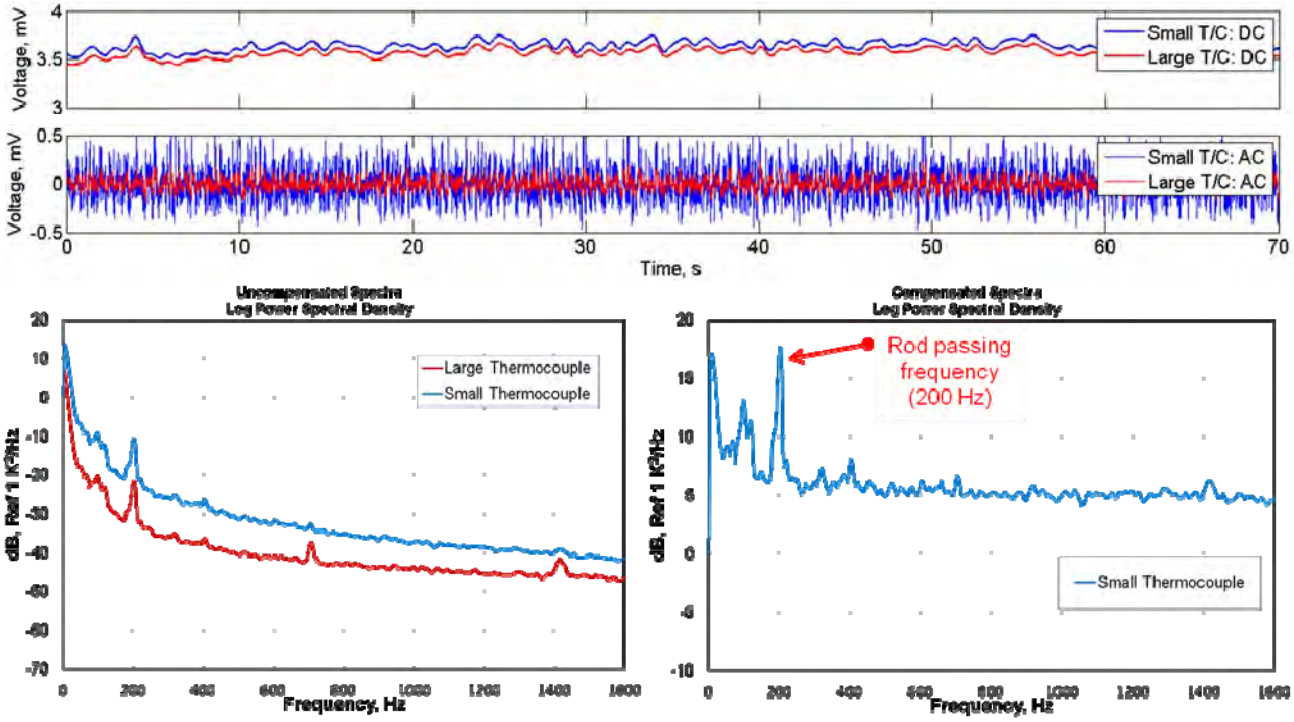

Figure 42. Results From the Carousel Testing of Honeywell Probe A at 1000 rpm.

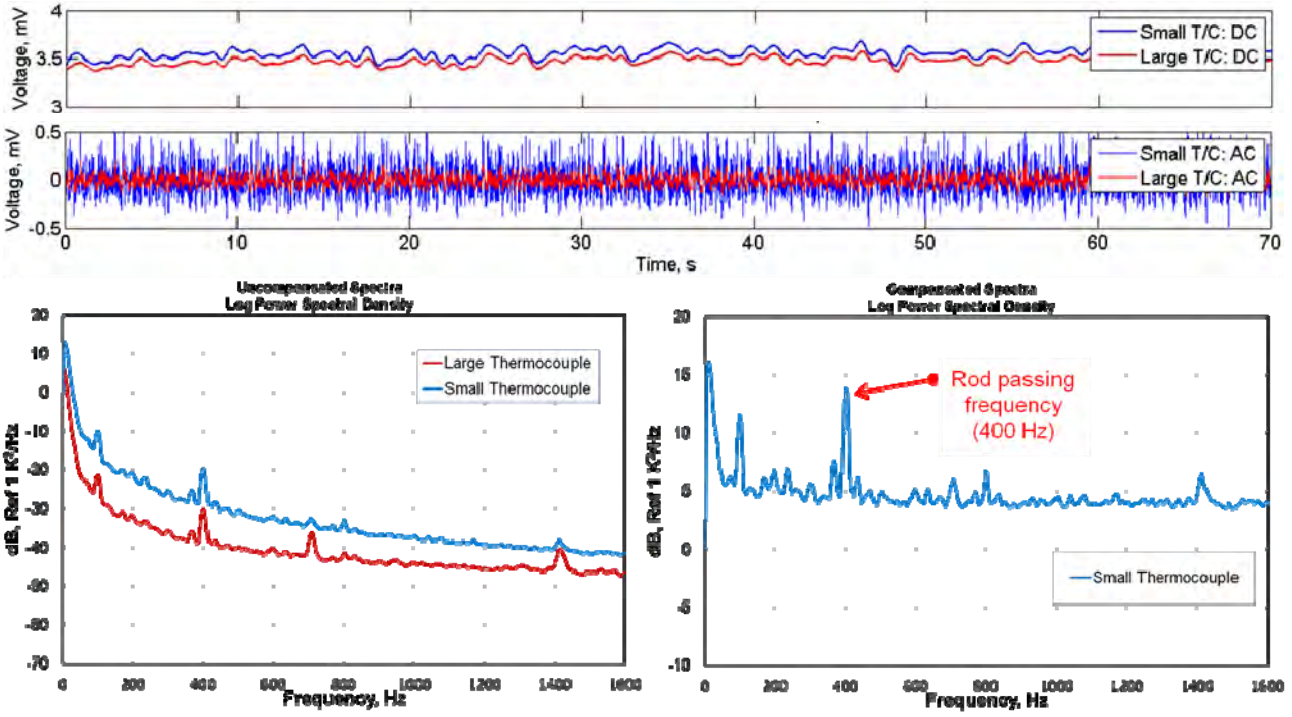

Figure 43. Results From the Carousel Testing of Honeywell Probe A at 2000 rpm.

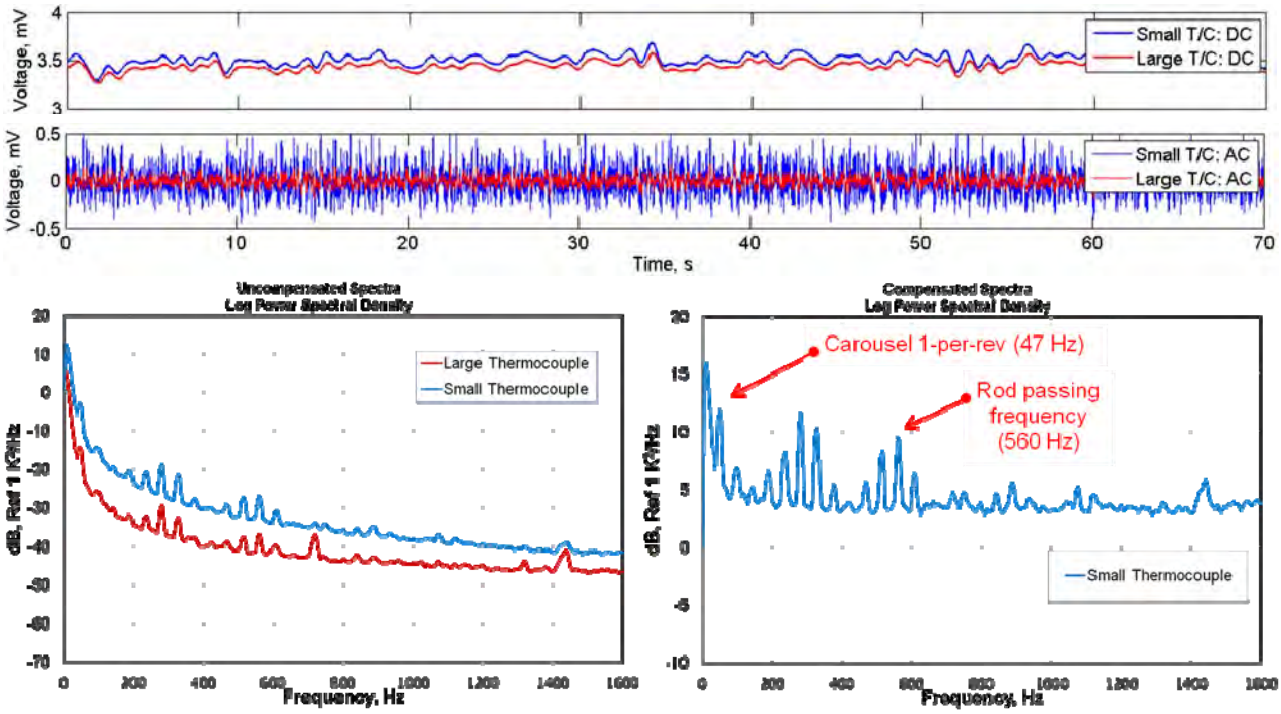

Figure 44. Results From the Carousel Testing of Honeywell Probe A at 2800 rpm.

Figure 45 shows the results from the carousel testing of Honeywell Probe A at 0 rpm and with the probe positioned directly behind a rod. The DC signals from the small and large wires are in good agreement. The AC signals from the small and large wires, however, shows some anomalies starting at about 7 seconds into the time record and lasting for 38 seconds. As seen in the zoomed-in view, there appears to be some excess high frequency noise that appears suddenly. The PSDs of the AC signals are also suspicious, in that the spectra of the two wires quickly flatten out and merge together, calling into question the quality of the data. The source of the excess noise is unknown but it was noted that the potting material on the back of the probe was beginning to break off, perhaps allowing the wires to touch. The desired outcome for this test was to observe higher frequency temperature oscillation than could be obtained by the spinning carousel due to vortex shedding of the gas flow. It was expected that a half-inch rod immersed in the 1500°F flow with a typical Mach number of 0.3 to 0.4 would have a vortex shedding frequency well above 1000 Hz. Measurement of the vortex shedding phenomenon would provide confirmation of the upper frequency range capability of the probes. Unfortunately, due to the extraneous noise, the data above a few hundred Hertz is suspicious. The broadband levels of the compensated data are observed to increase strongly with frequency, which is questionable. Interestingly, there are some peaks at low frequencies, but their source is currently unknown.

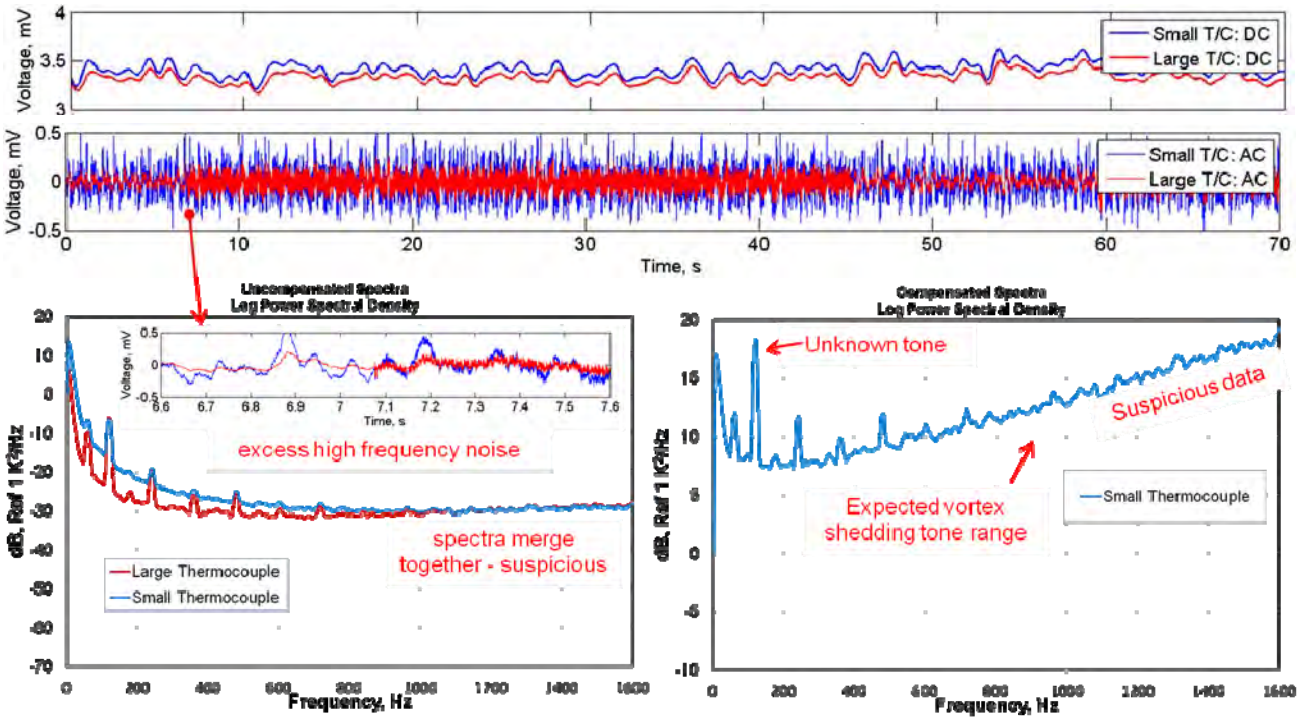

Figure 45. Results From the Carousel Testing of Honeywell Probe A at 0 rpm and With the Probe Positioned Directly Behind a Rod.

Figure 46 shows the results from the carousel testing of Honeywell Probe A at 0 rpm and with the probe directly exposed to the flow. In this case a smooth, purely broadband spectrum was expected. The mean temperature was only around 1060°F, as opposed to about 1500°F on the previous test points. There is a larger discrepancy between the small and large DC signals, suggesting that the operating point or relative positioning of the probe in the flame changed. The broadband levels of the compensated spectrum are about the same amplitude as the rotating carousel test points. Interestingly, there is a tone near 700 Hz, and its harmonic at 1400 Hz is also visible. This tone is also observable in many of the previous rotating carousel spectra. The origin of the tone is unknown, but it is hypothesized that it is related to the fuel delivery pump or system.

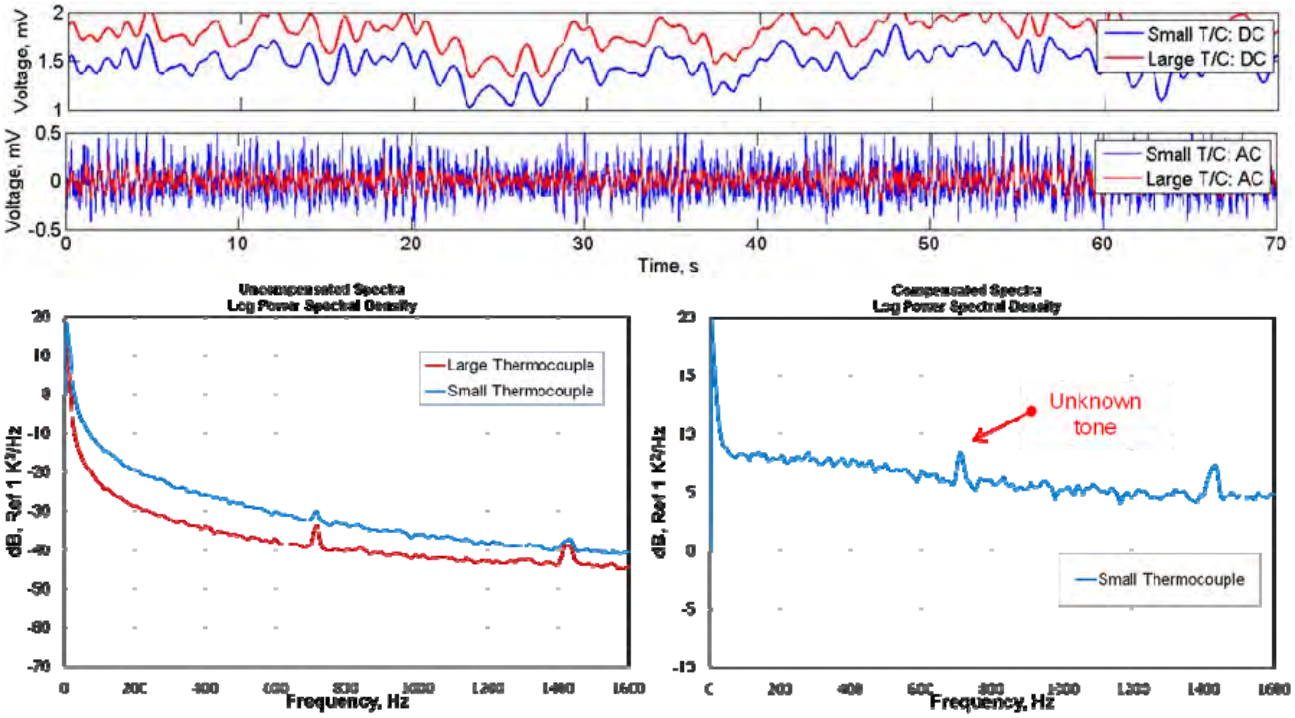

Figure 46. Results From the Carousel Testing of Honeywell Probe A at 0 rpm and With the Probe Directly Exposed to the Flow.

Of particular interest in this test series is how the Honeywell probe compares to the NASA probe when the two are exposed to the same fluctuating temperature environment (Figure 10). In particular, since the diameter of the small wire of the NASA probe (0.003-inch) is less than the diameter of the small wire on the initial prototype Honeywell probes (0.004-inch), it was of interest to examine any differences in the uncompensated and compensated small-wire spectra between the two probes. Note that the final design for the DTP used 0.003-inch and 0.010-inch diameter wires for the small and large sensing elements, respectively. Figure 47 shows a comparison of the data from the two probes, with the probes located near the burner flame edge, and with a fuel pressure of 94 psi. The mean temperature is about 1150°F. The DC signals from the four wires are in pretty good agreement and trend together, although the large wire thermocouple on the NASA probe appears to run a little high. The AC signals from the four wires also show the expected trends. The signals generally trend up and down together. The signals from the large wires on both probes match fairly well. And the signals from the small wires are similar, but with the small NASA wire having higher amplitude, as would be expected due to its smaller diameter.

Comparing the uncompensated PSDs, the data is very encouraging. The spectra of the large thermocouples from the Honeywell and NASA probes (which both have wire diameters of 0.010-inch) are almost identical, as would be expected if the probes are exposed to the same fluctuating gas temperature. The spectra of the small wire on the NASA probe has the same general shape, but higher amplitude, than the spectra from the small wire on the Honeywell probe, which is also expected due to the smaller diameter of the wire on the NASA probe. Comparing the compensated spectra, i.e. the estimated gas temperature spectra, one would ideally like to see the NASA and Honeywell probes to be in agreement if the probes are in the same point in the flow, or at least match well up to some high frequency limit, beyond which the

two might be expected to deviate due to their different frequency response limits associated with the small wire thermocouple. The compensated spectra from the two probes are observed to be in fairly good agreement, with the Honeywell probe being about 2-3 dB higher than the NASA probe. It is difficult to conclude whether the small difference is a result of differences in the probes themselves or differences in the environment in which they are immersed.

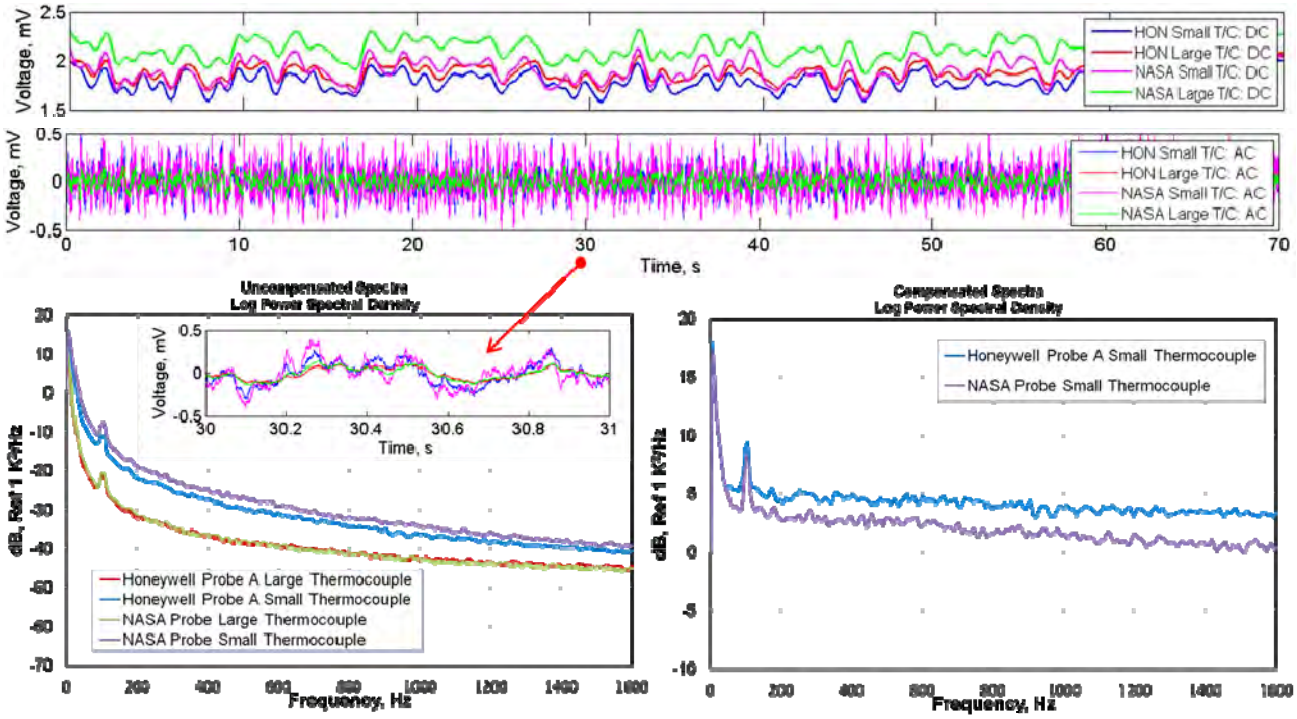

Figure 47. Results From the Stationary Testing of Honeywell Probe A and the NASA Probe, Positioned at the Burner Flame Edge, at a Fuel Pressure of 94 psi.

Figure 48 shows a comparison of the data from the two probes, with the probes located near the burner flame edge, and with a fuel pressure of 155 psi. The mean temperature is close to 1500°F. The conclusions are very similar to the previous comparison at 94 psi. The compensated spectra from the NASA and Honeywell probes are in even better agreement, with the Honeywell probe reading about 1-2 dB higher than the NASA probe. Also, the amplitudes of the compensated spectra are slightly higher than those at 94 psi, perhaps due to the higher mean operating temperature.

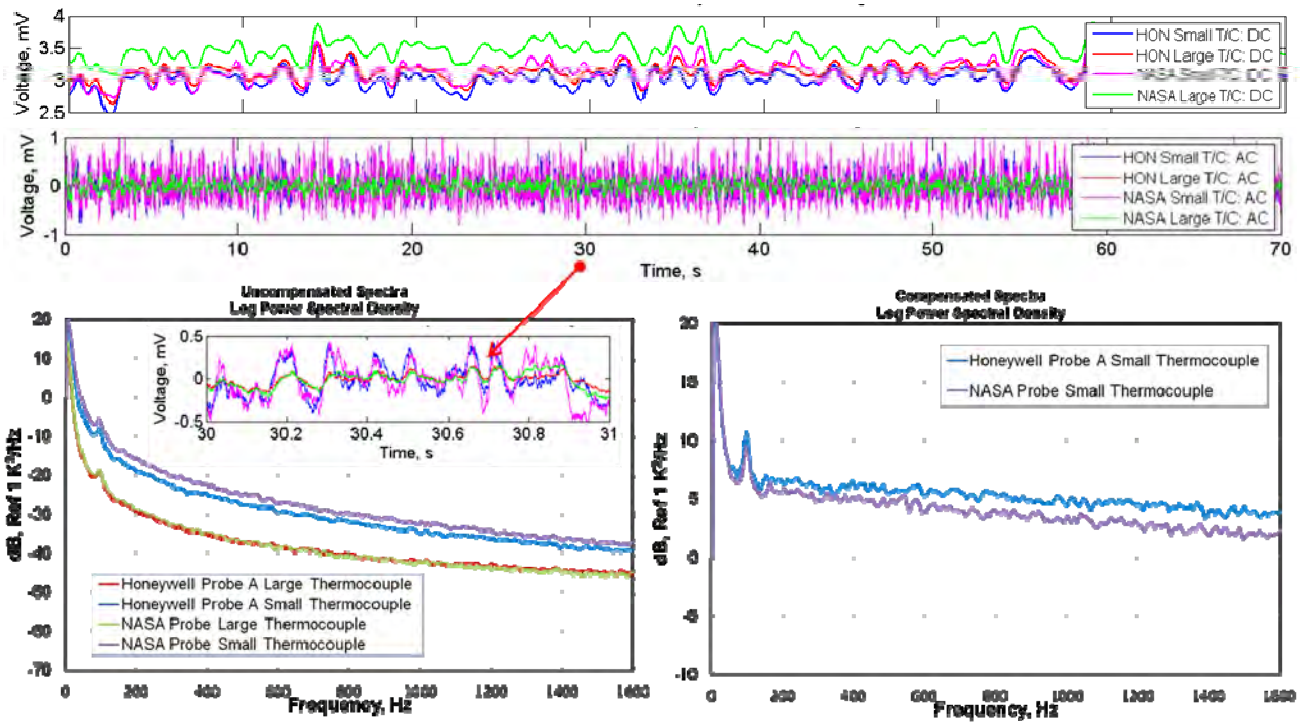

Figure 48. Results From the Stationary Testing of Honeywell Probe A and the NASA Probe, Positioned at the Burner Flame Edge, at a Fuel Pressure of 155 psi.

One might expect to see different levels of turbulent mixing, and thus different amplitudes of temperature fluctuations, when making measurements at different locations in the burner flame. Figure 49 shows a comparison of the data from the NASA and Honeywell probes, with the probes located near the burner core, and with a fuel pressure of 94 psi. The DC levels from the two probes show some significant differences, with the NASA probe reading higher (average temperature near 1200°F) than the Honeywell probe (average temperature near 1000°F), suggesting that there were significant differences in flow conditions for the two probes, despite their close physical proximity. But the AC signals for the two probes appear to oscillate in a similar fashion most of the time, indicating that there is still considerable similarity in the fluctuating temperatures that the probes are exposed to. Looking at the uncompensated frequency spectra, the large wire spectra for the two probes deviate slightly, whereas the small wire spectra are closer than was observed at the flame edge. This suggests that there is a discrepancy between the probes, or a difference in the environment in which they are placed, or both. The compensated spectra show large differences, on the order of 5 dB, with the Honeywell probe reading higher than the NASA probe.

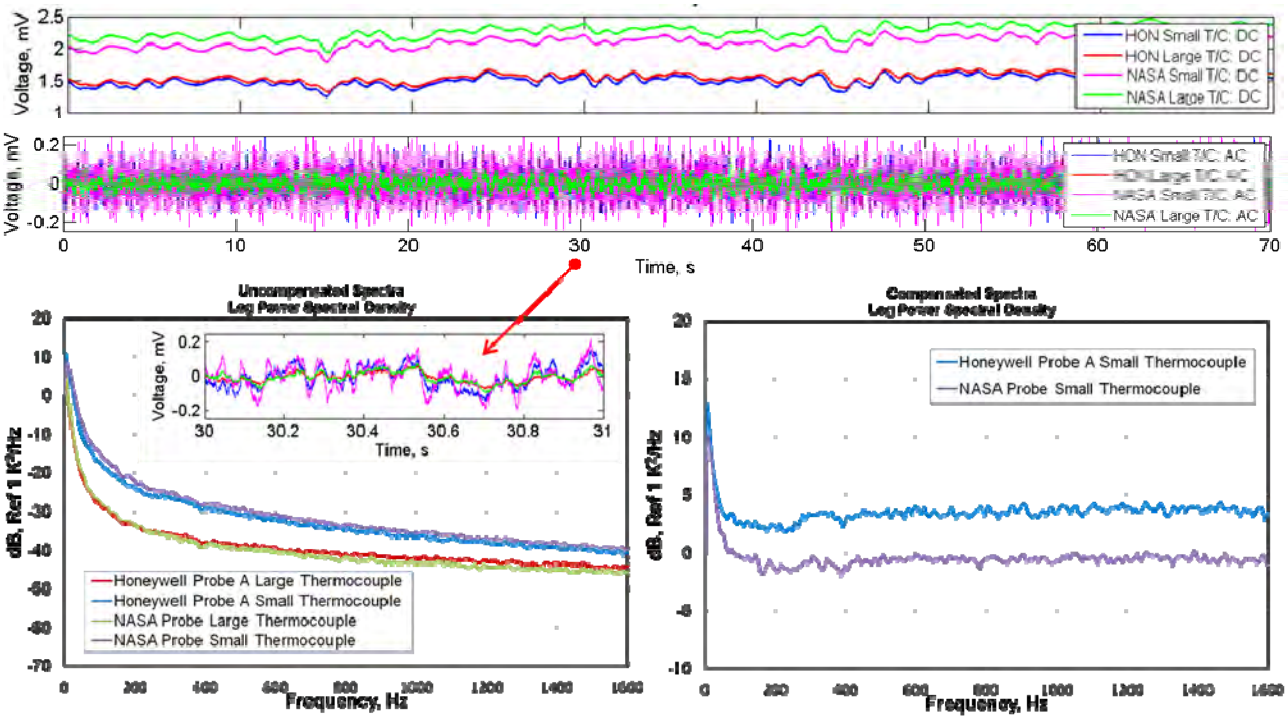

Figure 49. Results From the Stationary Testing of Honeywell Probe A and the NASA Probe, Positioned at the Burner Flame Core, at a Fuel Pressure of 94 psi.

Figure 50 shows a comparison of the data from the NASA and Honeywell probes, with the probes located near the burner core, and with a fuel pressure of 155 psi. The results are very similar to the 94 psi core flame case. The higher fuel pressure translates to higher temperatures, with the NASA probe reading an average temperature near 1600°F compared to the Honeywell probe reading near 1400°F.

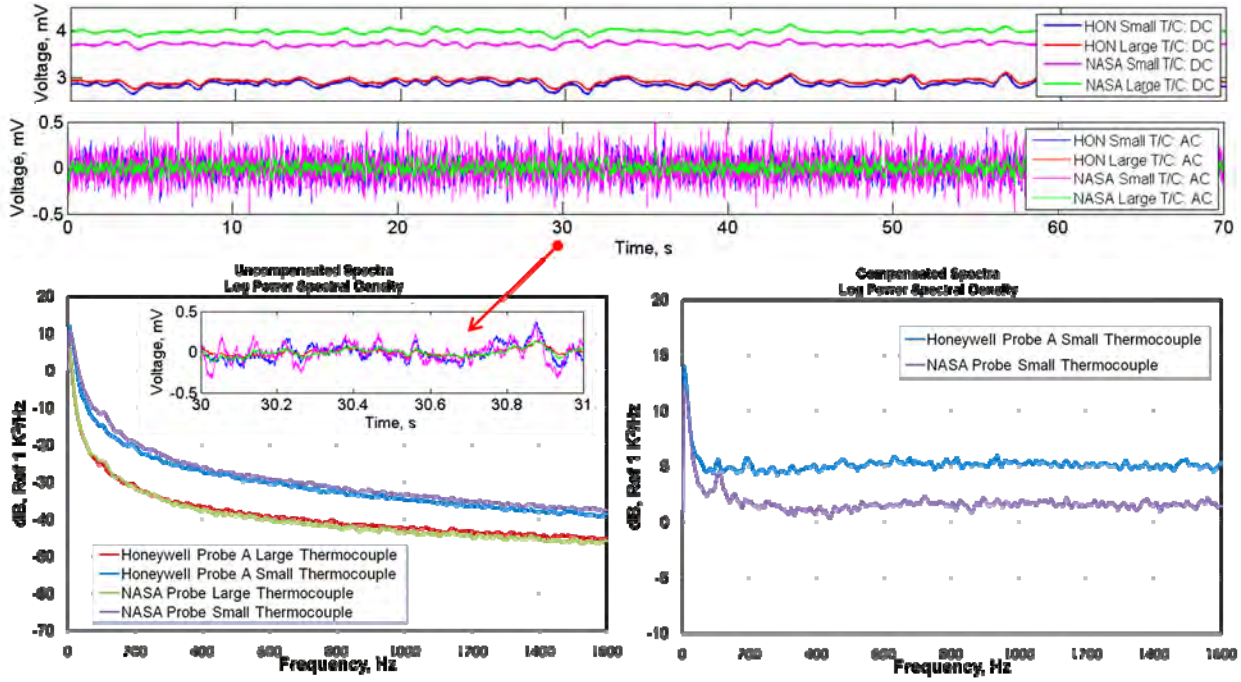

Figure 50. Results From the Stationary Testing of Honeywell Probe A and the NASA Probe, Positioned at the Burner Flame Core, at a Fuel Pressure of 155 psi.

Not all of the test data that was collected could be processed using the DGTMS software. There were some cases where there was a clear issue with the data itself. Figure 51 shows such an example, for the carousel test of Honeywell Probe A at the maximum rotational speed of 2800 rpm. The time history data for the small diameter wire was suspiciously noisy. The test setup was inspected, and it was found that the wires on the back side of the probe might have been touching due to the potting material falling off. The test point was repeated after the inspection of the setup, and good quality data was obtained that was successfully processed with the DGTMS software.

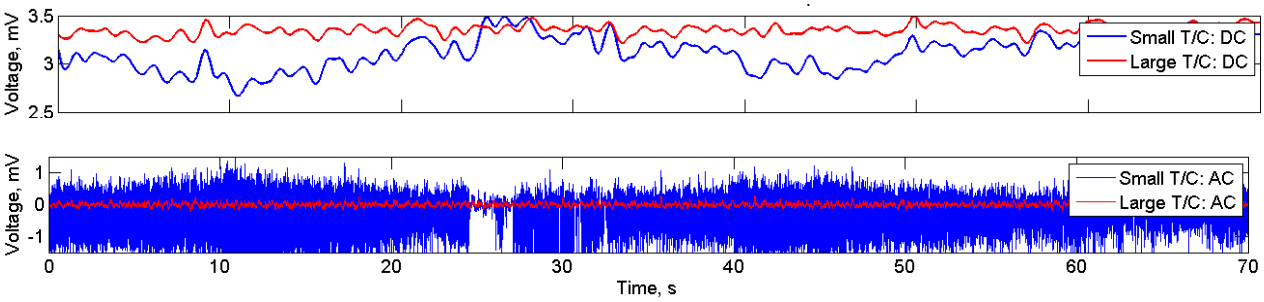

Figure 51. Example of Problematic Data From the Carousel Test of Honeywell Probe A at 2800 rpm (First Attempt).

As a second example, the data from Honeywell Probe B that was acquired when both Probe A and Probe B were in the carousel together, could not be processed, at either 500, 1000, or 2000 rpm. Figure 52 shows the time history data for the 2000 rpm test point. The mean output from the small and large thermocouple wires on Probe B showed a very large split. The mean output from the small and large thermocouple wires on Probe A were in close agreement. This

suggested that there was an issue with Probe B. An explanation for the problem is lacking. But data was acquired on the previous day for Probe B in isolation in the carousel, and the data did not show this behavior and was successfully processed. Figure 53 shows the time history data for Probe B in the carousel spinning at 2000 rpm, showing that the small and large wire DC data was in excellent agreement.

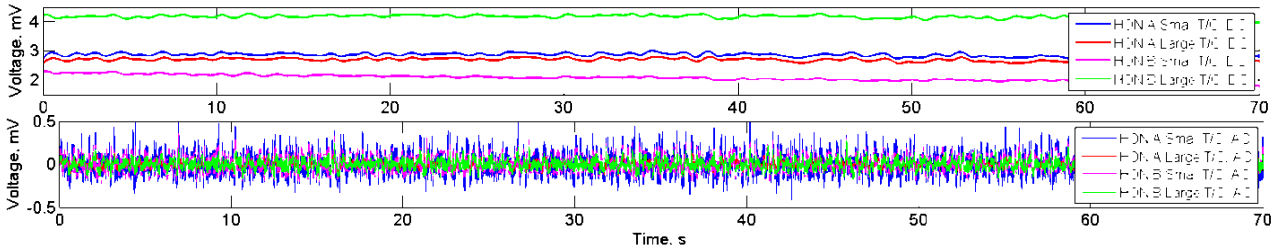

Figure 52. Example of Problematic Data From Honeywell Probe B From the Carousel Test of Probes A & B Together at 2000 rpm.

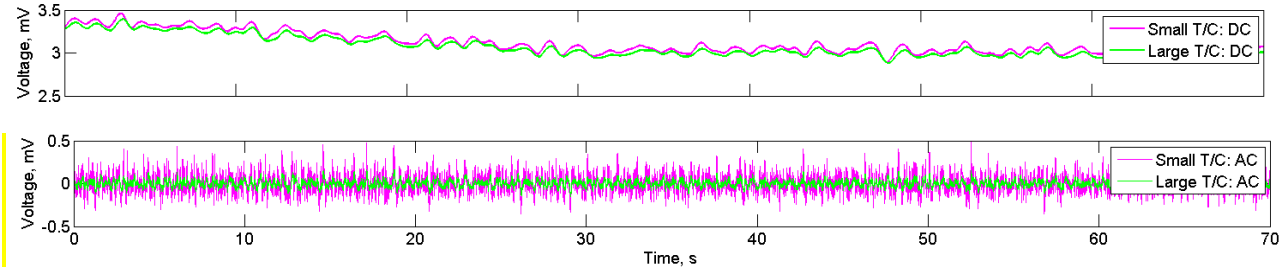

Figure 53. Example of Good Data From Honeywell Probe B From the Carousel Test of Probes B By Itself at 2000 rpm.

Overall, the burner rig test provided a good exercise of the data acquisition systems and the DGTMS data reduction software. Data at a variety of test points were acquired, and the fluctuating voltages from the NASA and Honeywell probes were successfully processed with the DGTMS software. The software was robust and efficient, and well conditioned in that a failure to converge on a compensated spectrum often indicated that there was a fundamental problem with the data (e.g. noise on the signals, improper probe placement) or the input files (e.g. incorrect user inputs). The data showed the expected overall trends: the voltages of the small and large diameter thermocouple wires move in unison, and the small diameter wire is more responsive and has greater fluctuating amplitudes. Large fluctuating temperatures were produced at the expected frequencies in the carousel tests, both at the rod passing frequency, and to a lesser degree, at the one-per-rev frequency. Broadband temperature fluctuations were produced in both the carousel and stationary probe tests.

In addition, the Honeywell and NASA probes, which had different designs and had different diameters for the small thermocouple wires, compared well. The spectra from the large diameter wires were generally in excellent agreement, as was expected since the wire diameter was the same for both, namely 0.010-inch. The spectra from the small diameter wire on the NASA probe (0.003-inch) was higher than that from the small diameter wire on the Honeywell probe (0.004-inch), which was also expected due to the higher responsiveness of the smaller

diameter wire. The compensated spectra for the Honeywell and NASA probes were in close agreement, but not identical. The differences could be caused by different thermal environments to which the probes were exposed, despite being in close proximity. Overall, the results of the burner rig testing were very encouraging, providing a good check of the system capability, and providing experience and insight to ensure quality acquisition of fluctuating temperature data on an engine test.

6.0 TASK 4: TECH977 ENGINE TEST

6.1 Engine Build with Modified Hardware

The TECH977 test engine, SN 119123, was moved from engineering stores to a development engine assembly area, and the engine was partially disassembled to gain access to the core engine hardware components requiring modification. Figure 54 shows a photo of the engine prior to disassembly. The C-ducts, which form the inner and outer flowpath of the bypass duct, are removed from the engine, so that the combustor and turbine cases are visible. This engine is the same serial number that was extensively tested during the NASA EVNERT program. Some of the pressure probe tubes (16 equally spaced Kulites) that were used to measure the dynamic pressure in the combustor are visible in the photo.

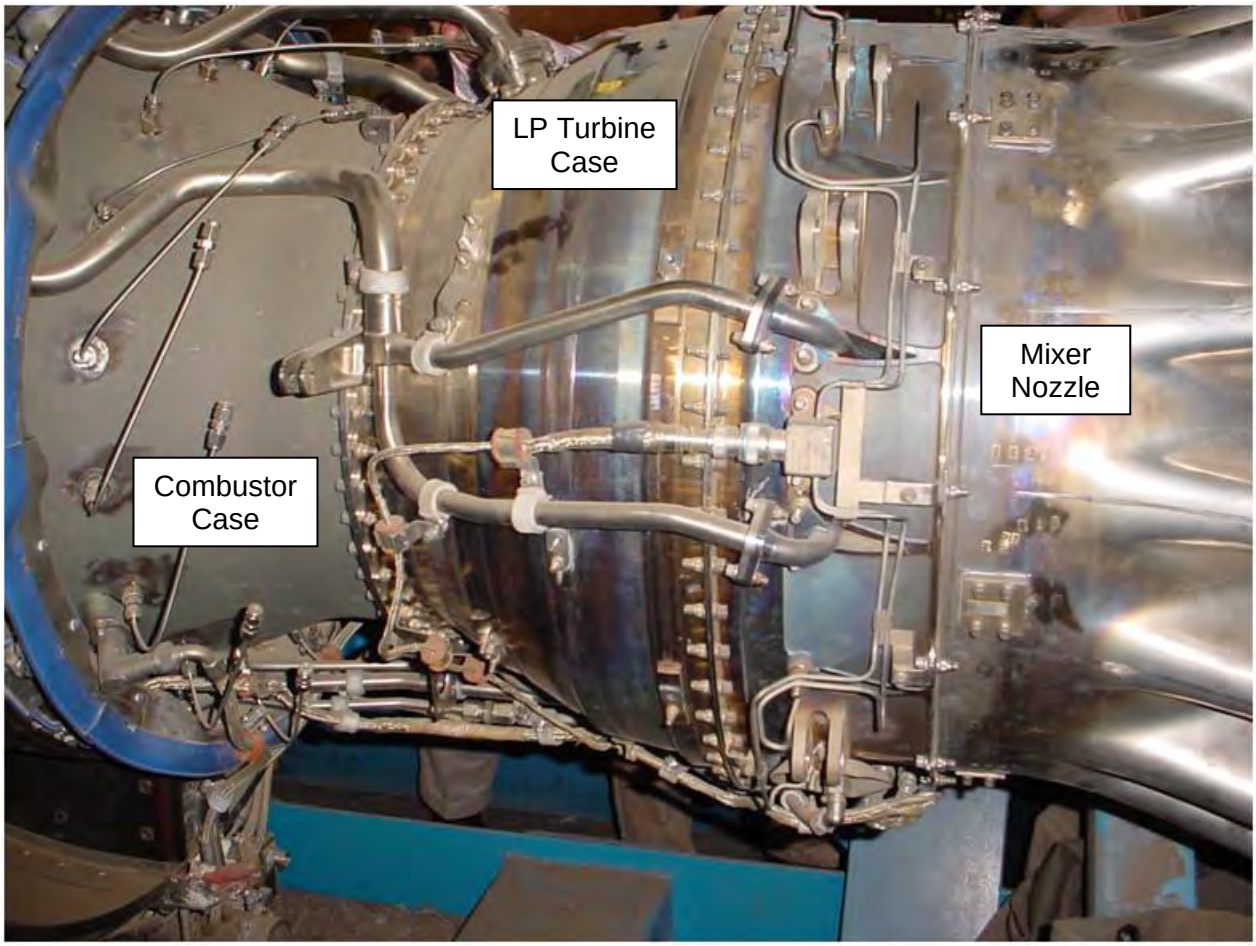

Figure 54. Photo of the TECH977 Engine Prior to Relocation for Disassembly.

The combustor case was removed from the engine and modified to incorporate the guide bosses for the temperature and pressure probes in the combustor and turbine. The combustor development shop fabricated the adaptive hardware bosses (Figure 55) and modified the case by welding the adaptors and bosses in place. Figure 56 shows the combustor case being laser cut using an industrial Nd:YAG laser and the resulting access hole. Figure 57 shows the combustor case after the bosses had been welded on.

Figure 55. Fabricated Combustor Case Wedges and Bosses.

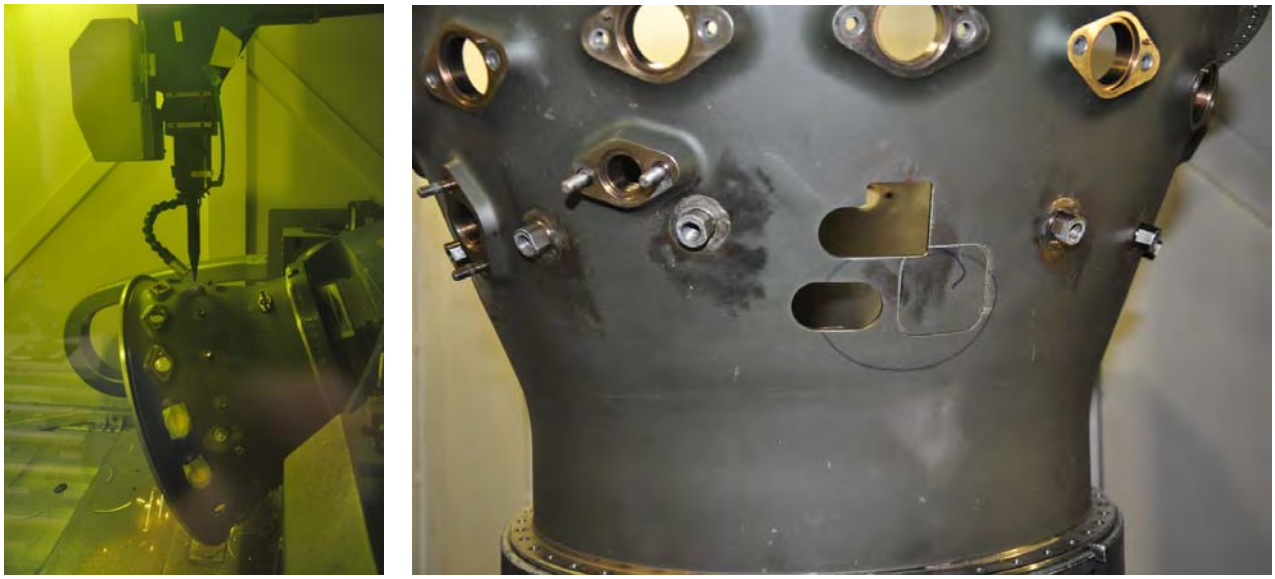

Figure 56. TECH977 Combustor Case Being Laser Cut.

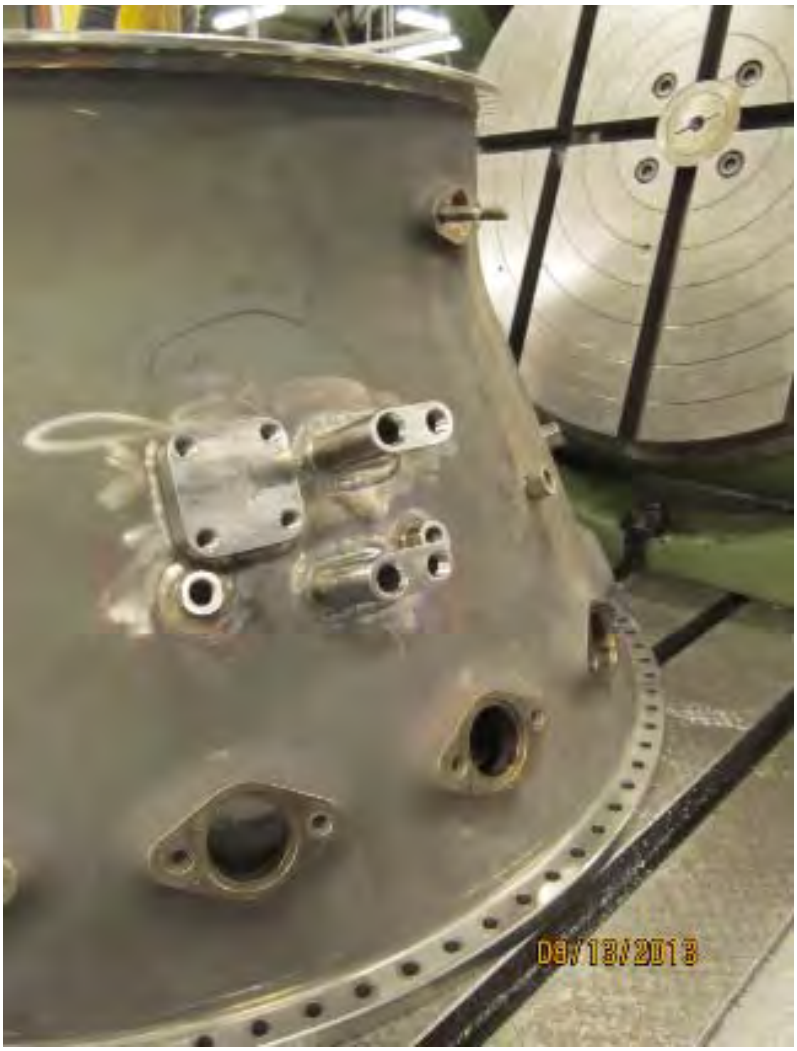

Figure 57. Modified Combustor Case Showing Bosses and Wedges Welded in Place.

Significant amounts of rework were required to address issues discovered during fitting tests and during engine assembly. The modified combustor and combustor case were reworked in order to provide additional clearance for the thermal probes. Figure 58 shows how inaccurate engine modifications led to a misalignment of the thermal probes with the combustor case boss. This misalignment would have resulted in unacceptable interference between the ceramic shaft of the DTP and the boss clearance hole potentially resulting in probe fracture during use. Hence the bosses were reworked to extend the clearance hole. Figure 59 shows the relationship between the assembled and installed actuators and the extended bodies of the dummy probes. Notice that probes extending from the inter turbine duct assembly are not collinear due to the orientation of the underlying bosses that define the path of the probe. In order to avoid binding during actuation the drive yokes required modified to accommodate the differential travel between the two probe axes. Figure 60 and Figure 61 show how the yokes on either side of the engine were modified to accommodate this non collinear orientation of the probes. Slots were machined into the fixture brackets and locking knuckles were used on the probe bodies to carry the actuation load while accommodating motion in the plane of the yokes.

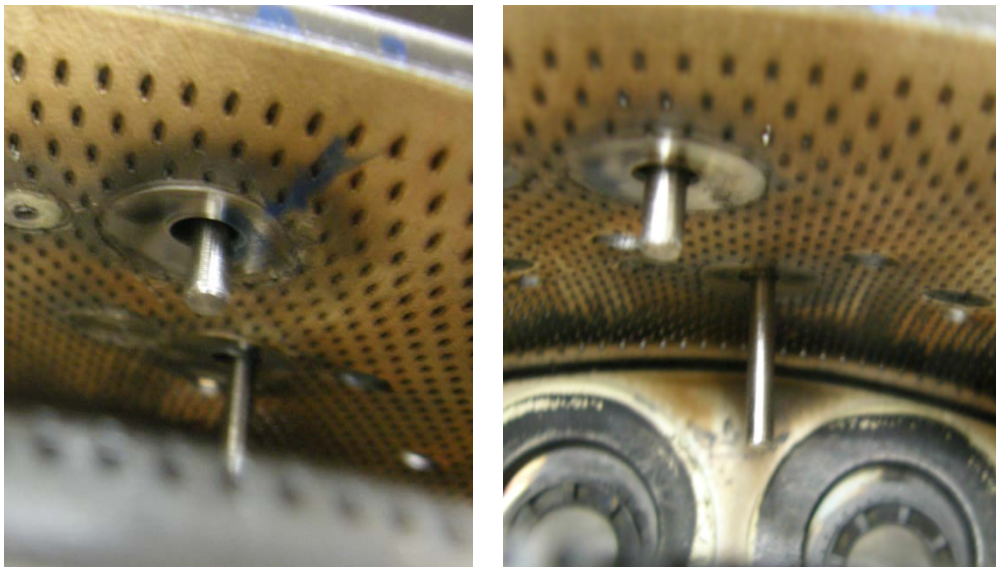

Figure 58. Sensor End of the Three O'clock and Nine O'clock Orientations of the Dummy Probes Protruding Into the Combustor Case.

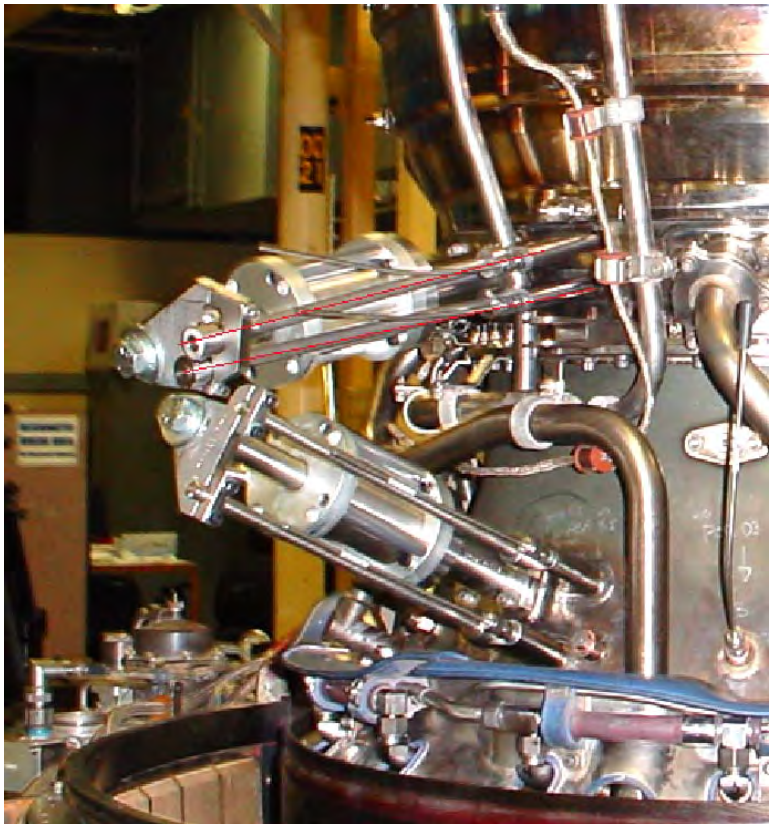

Figure 59. Assembled Actuators With Dummy Probes Installed.

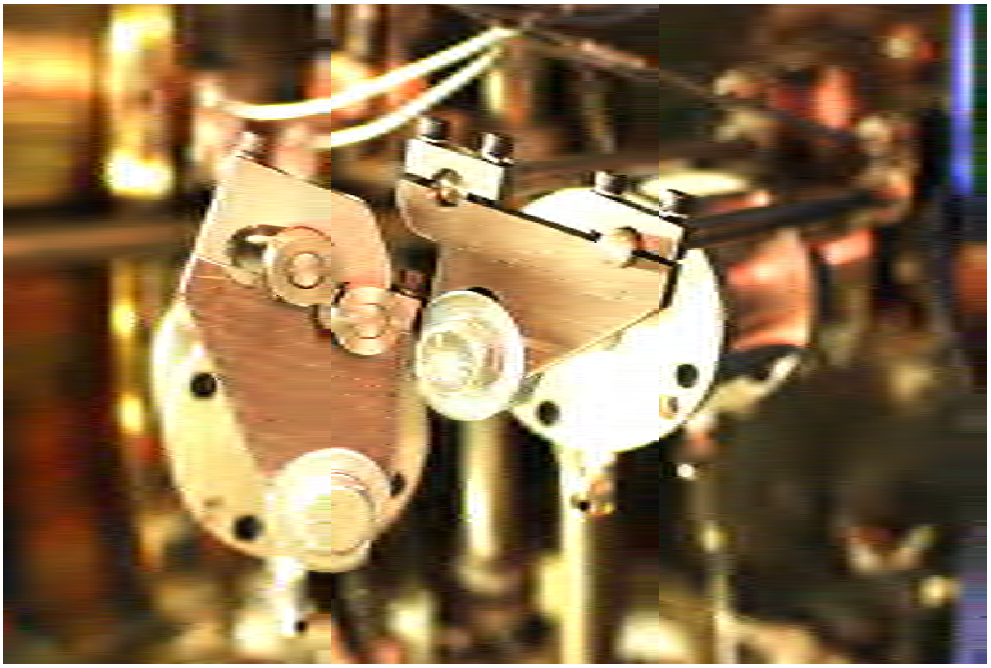

Figure 60. End View Showing Modification of the Drive Yoke Used to Actuate Inter Turbine Duct Thermal Probes at the Three O'clock Orientation.

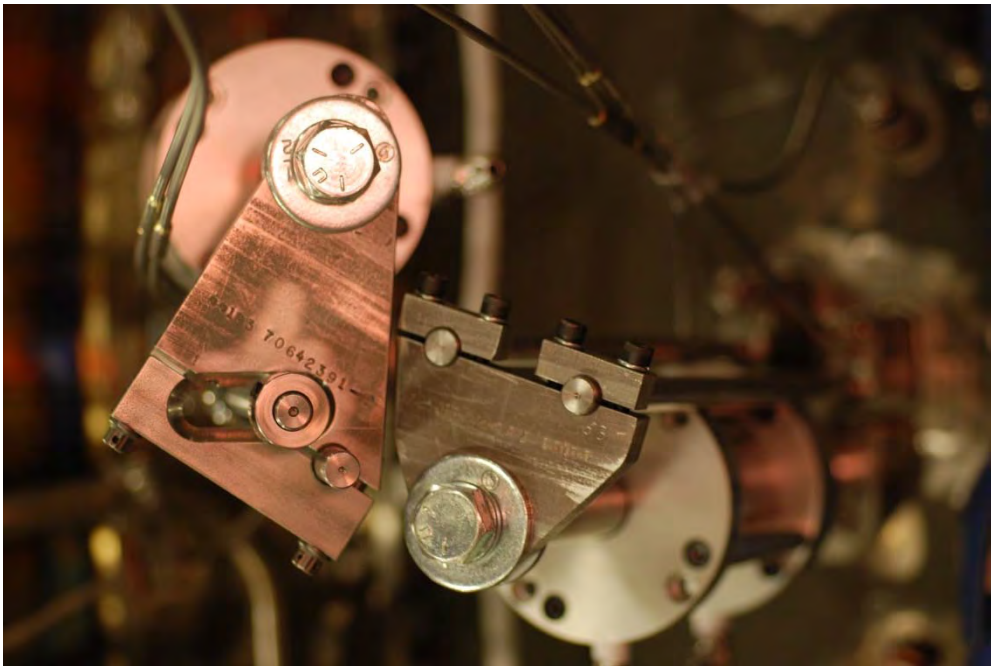

Figure 61. End View Showing Modification of the Drive Yoke Used to Actuate Inter Turbine Duct Thermal Probes at the Nine O'clock Orientation.

In addition to the initial two DTP probes manufactured by CEL, a total of eleven probes were manufactured by Aerodyne Engineering of Indianapolis, IN. When initially received from the supplier these probes did not pass Honeywell's quality standards. Figure 62 shows a typical example of their original as-received condition. Evidence can clearly be seen of welding blobs, uneven posts and wire lengths, excess ceramic coverage, thermocouple necking and overall poor quality fabrication. As a result, the probes were returned to the supplier for rework and remanufacture. Figure 63 shows that the subsequently delivered remanufactured probes were significantly improved. The complete collection of the assembled DGTMS probes ready for assembly into the modified engine is presented in Figure 64.

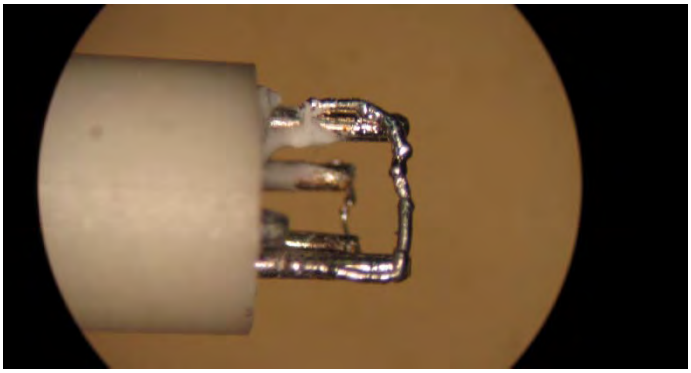

Figure 62. Example Temperature Probe Originally Received From The Supplier.

Figure 63. Temperature Probes Fabricated for the TECH977 Engine Test.

Figure 64. Completed Temperature Probes.

6.2 Engine Installation

We had originally planned to run the engine in an indoor test cell, but when an outdoor cell became available, i.e. Honeywell's San Tan Cell 965, we elected to use this cell since it provided better access around the engine. In addition this outdoor cell did not suffer from the reverberant environment effects of an indoor cell. The one change that was made to the acoustic measurement setup was to locate the two external microphones on inverted ground plane stands, rather than on poles. Figure 65 and Figure 66 show photos of the overall engine installation at Cell 965. The engine was configured with a laboratory bellmouth and screen, and a laboratory exhaust nozzle.

Figure 65. View of the TECH977 Installed at San Tan Cell 965 (Right Side, ALF).

Figure 66. View of the TECH977 Installed at San Tan Cell 965 (Left Side, ALF).

The nitrogen purge flow systems for the combustor and the turbine Kulite instrumentation are shown in Figure 67 and Figure 68. The systems were installed according the purge flow schematic in the engine test plan. Figure 69 shows the installation of the temperature probes in the combustor, ITD, and mixer. Figure 70 shows a close-up of the installed combustor and turbine probes at the right hand side (ALF). Figure 71 shows the locations of the two external microphones.

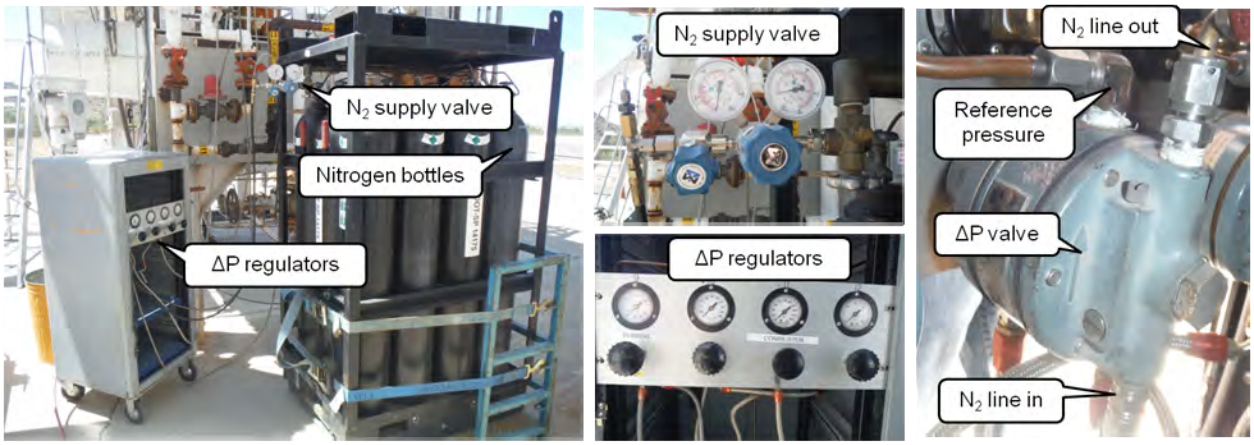

Figure 67. View of the Nitrogen Purge Flow Supply System.

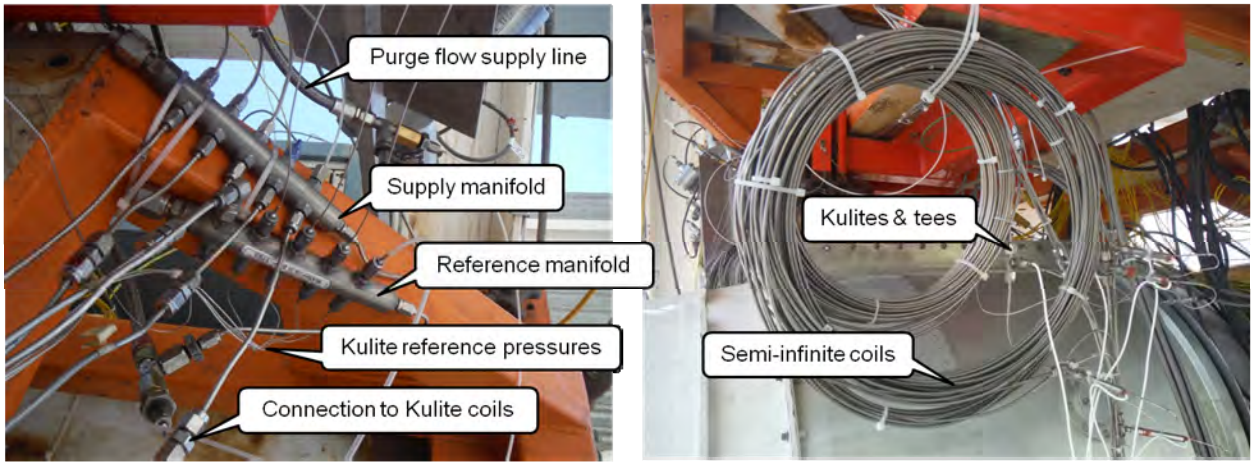

Figure 68. View of the Purge Flow Manifolds, Kulite Coils, and Kulites.

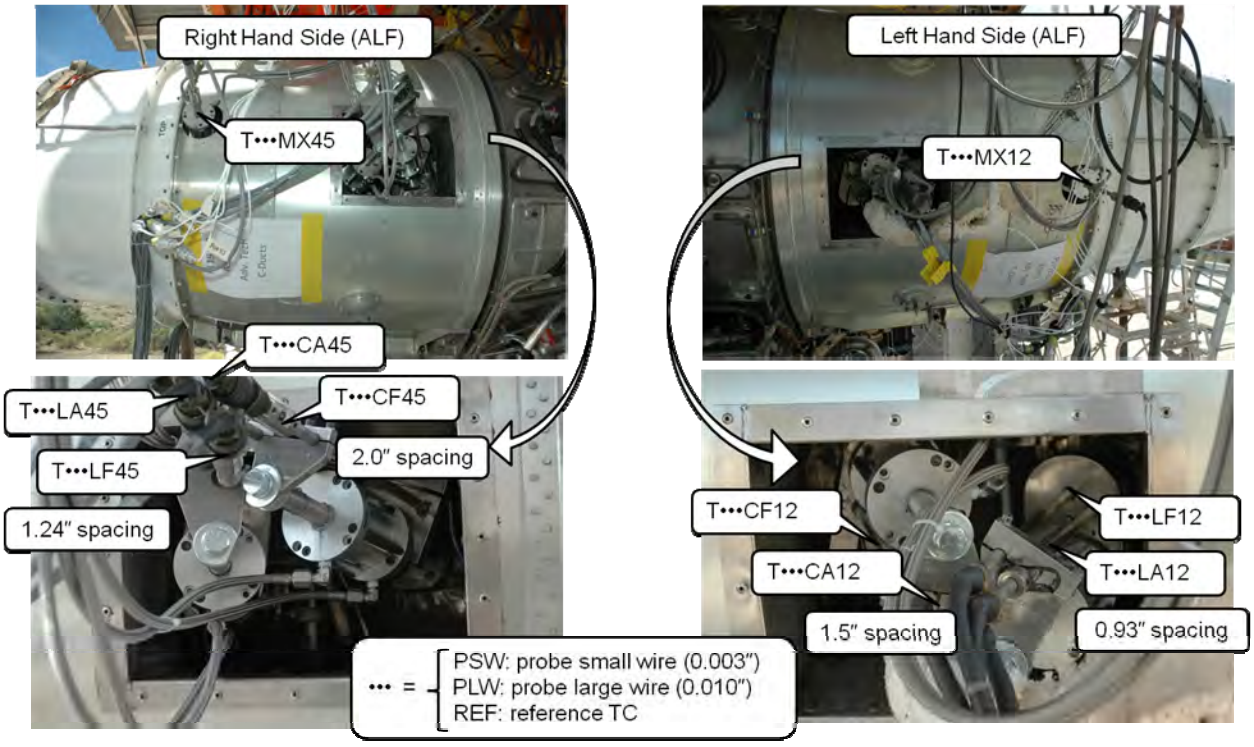

Figure 69. View of the Installed Temperature Probe Hardware.

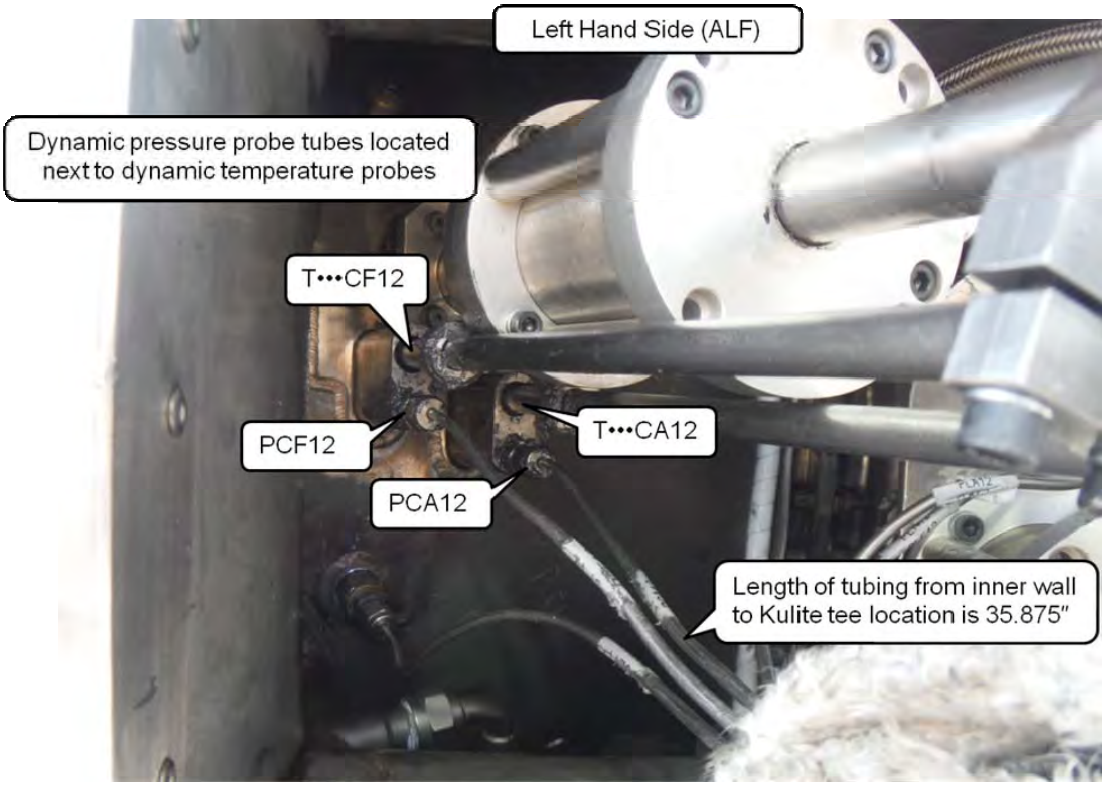

Figure 70. Closeup of the Pressure Tubes and Temperature Probes.

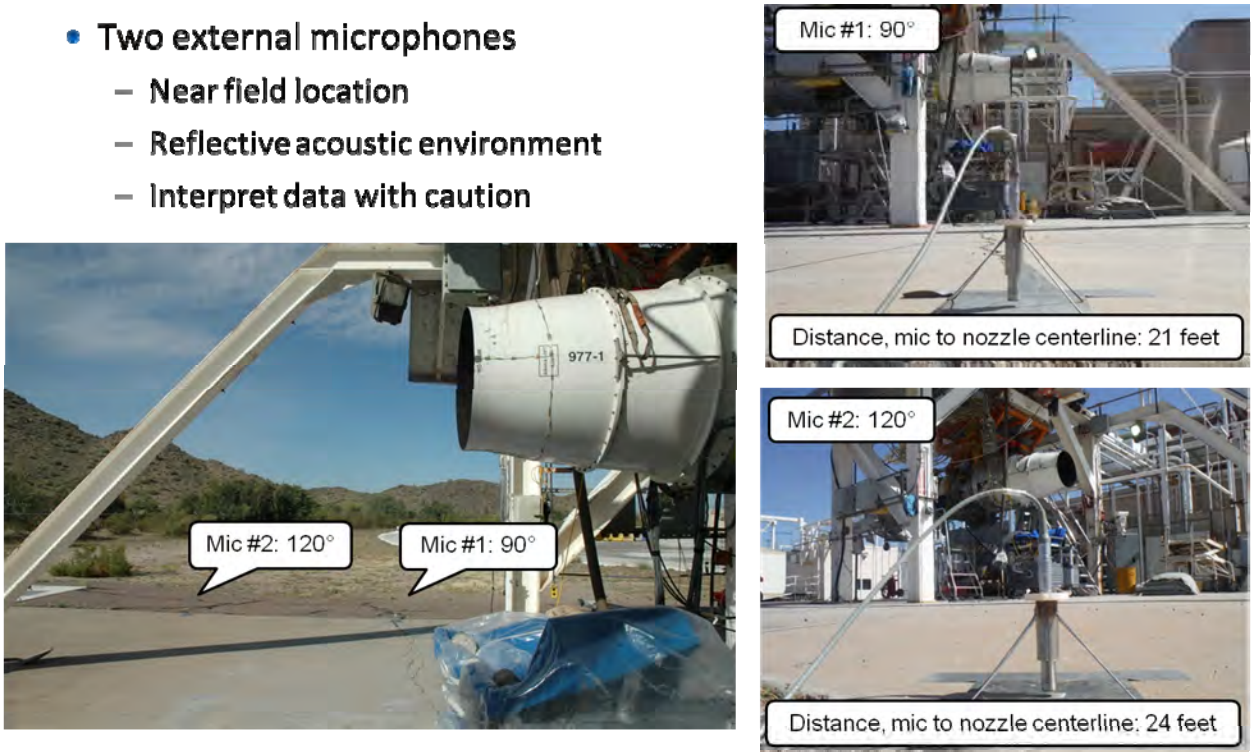

Figure 71. Location of the Two External Microphones.

6.3 Instrumentation Setup

As described in Section 3.2, a Dewetron system, Model 801, configured with 64 channels of dynamic differential amplifiers, series MDAQ-SUB-ACC, and 24-bit delta-sigma analog-to-digital cards, model Orion 1624, was used as the primary data acquisition system. A Brüel & Kjær Pulse system, configured with 48 channels of 24-bit analog-to-digital modules, using eight 6-channel LAN-XI Type 3050-A-060 cards, and driven with Pulse Labshop software (Version 18.0.1.1) was used as a backup system. The voltages from the temperature probes were recorded directly without amplification and without the use of a reference junction, using the system connectivity described in Section 3.7, Figure 5. In order to minimize signal losses and electrical interference, the cable lengths for the temperature probes were kept as short as possible. Each of the ten temperature probes were connected to the Dewetron data acquisition system using a 10.5-foot long cable. Each cable contained three wire pairs: one pair for the small wire thermocouple, one pair for the large wire thermocouple, and one pair for the reference thermocouple. The wires were shielded to minimize electrical interference. A set of 4-foot long patch cables of similar construction were used to tee the voltages from the Dewetron system to the Pulse system. Figure 72 shows the connection of the temperature probe cables to the Dewetron system, and the cables that tee the signals over to the Pulse system. Figure 73 shows the connection of the tee cables to the Pulse system.

Figure 72. View of the Cable Connections to the 64-Channel Dewetron Recorder.

Figure 73. View of the Cable Connections to the 48-Channel Pulse Recorder.

The signals from the thirteen Kulites and the two external microphones were recorded simultaneously with the temperature signals. A rack of Sonoran Microsystems amplifiers was used to provide the signal conditioning (voltage supply, filtering, and amplification) for the Kulites, as shown in Figure 74. The amplified signal outputs were connected to both the Dewetron and Pulse data recorders. Figure 75 shows the cable connections on the Sonoran

Microsystems unit; the gray cables provide the power supply to and the signal response from the Kulites, and the white cables are for the amplified output signals. The Kulite transducers were calibrated as follows. On the Dewetron system, each Kulite channel was calibrated by entering the factory calibrated sensitivity from the vendor supplied data sheets. The factory sensitivities were very close to the nominal transducer sensitivity of 10.0 mV/psi for the XTE190-10D model Kulite. On the Pulse system, each Kulite channel was calibrated by applying a pistonphone signal with the use of a special adapter. The resulting calibration was nearly the same as the nominal sensitivity, so there was very little difference between the two systems.

Due to the short cable lengths of the temperature probes, the Dewetron and Pulse data acquisition front ends needed to be placed close to the engine. Each data system was placed on a cart located beneath the exhaust nozzle. Each data system was operated remotely from the console room using a dedicated laptop connected to the front end via an Ethernet cable. Pretest checkouts of the data systems were conducted after the probes were installed to verify that the data systems were operating properly and that there were no sources of electrical noise from the test facility that would contaminate the data.

The Kulite measurements were made using semi-infinite probes. The length of the sensing end of the tube was selected to position all of the Kulites outside of the engine bypass duct. This was done to enable access to the Kulite sensors should any fail during the test and need to be replaced. This also ensured access to the Kulite tees and fittings in case any leaks were discovered during the checkout of the purge flow systems. The overall length of the sensing tube, from the sensing end, located flush with the outer wall of the core flowpath, to the Kulite location in the tee, was 35.875-inch for all of the Kulite sensors. The sensing line was constructed by brazing a one foot section and a two foot section together using an outer sleeve (to avoid internal discontinuities in the flowpath), to produce a 36-inch line. A 0.5-inch length of the sensing line was cut off during installation of the Kulite tees (the ends of the tubes had been previously brazed shut during the checkout of the purge flow system). When the sensing line is installed onto the tee, the distance from the end of the sensing line to the center of the tee where the Kulite sensor sits is 3/8-inch. Thus, the overall length from the sensing end of the tube to the sensor face is 35.875-inch. This length was made identical for all 13 Kulites to simplify the subsequent data corrections.

Figure 74. View of the Front of the Sonoran Microsystems Signal Conditioning Rack Used With the Kulites.

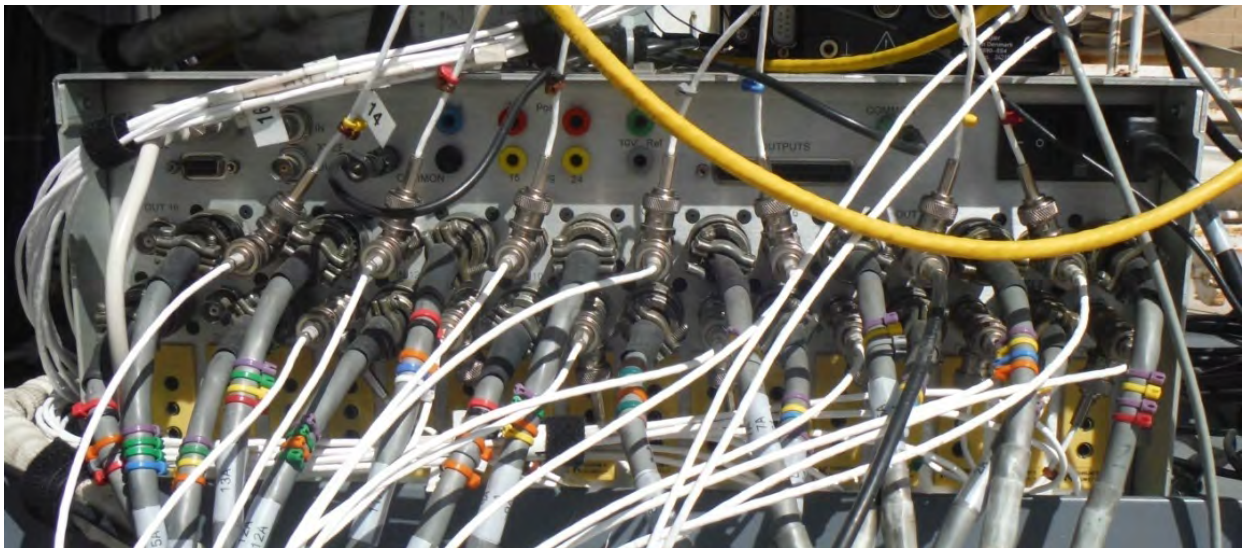

Figure 75. View of the Cable Connections on the Sonoran Microsystems Signal Conditioning Rack Used with the Kulites.

6.4 Pretest Checkouts

Pretest checks of the data acquisition system, the purge flow system, and the probe actuation system were conducted prior to the actual test to ensure that all systems were functioning as desired. A checkout of the data acquisition system was conducted to ensure that there were no new sources of electrical interference introduced at the test cell, relative to the testing that was performed in the laboratory. The background electronic noise floor associated with the temperature probes and cabling was consistent with levels measured in the bench testing. A checkout of the purge flow system was performed prior to installation of the Kulites to ensure that the purge flow supply pressure tracked the reference pressure in the combustor and turbine sections of the engine. The delta-p pressure regulators were adjusted to provide an initial pressure (prior to engine start) of a few psi above the (ambient) reference pressure. During engine operation, the regulators adjust the supply pressure in unison with changes in the reference pressure. However, there was a tendency of the delta-p to drop slightly as the engine speed (and core pressure) increased. The delta-p pressure regulators were adjusted to both (1) maintain a positive delta-p to ensure that purge flow is supplied through the Kulite tubes at all speeds and (2) minimize the delta-p so that the purge flow does not create excessive hydrodynamic noise over the Kulites or disrupt the temperature measurements.

A checkout of the probe actuation system was performed to ensure that the system was operational and to make final adjustments to the amount of manifold pressure. The desire was to provide enough pressure to ensure full deployment, but low enough to provide a gentle insertion so as not to jar the delicate thermocouple elements. The initial checkout was accomplished using a set of dummy probes of the same dimensions as the actual probes. The dummy and actual probes were scribed to ensure that the correct insertion depths were obtained at the deployed condition. The checkout indicated that at some locations, a chamfer was required on the Inconel housing to enable the probe to be installed into the guide boss. After the initial checkouts with the dummy probes, the sheaths of the temperature probes were coated with a nickel-based anti-seize compound and the real probes were installed. The probes were installed with the sensing elements aligned normal to the flow (engine axis). A final test of

the actuation system was performed prior to starting the engine using the actual probes. Video cameras were placed to observe the actuation of the probes during engine operation.

6.5 Test Data Planned

The test plan called for collection of data at the operating conditions defined in Table 4 where NFC is the corrected fan speed and N1C is the corrected low pressure spool speed. The operating conditions consisted of ambient noise with and without purge flow, ground idle, and four low power operating speeds. These engine speeds cover the range of interest for an aircraft approach condition. Since jet noise is relatively low on approach, this is the regime where combustion noise would be of practical importance to aircraft noise. The four speeds were to be repeated to provide an indication of data repeatability. The objective was to systematically step through the test matrix and record 70 seconds of data at each condition. The data would be acquired by both the Dewetron and Pulse systems at roughly the same time, although the two data systems were not precisely synchronized in time with one another. The data would be acquired at a sample rate of 10 kHz on the Dewetron system and at 65.536 kHz on the Pulse system. The temperature probes were to be deployed and retracted before and after each engine speed point to preserve probe life while the next operating point was established. Engine operational and performance data would also be collected during testing at a sample rate of 10 Hz.

Table 4. Planned Operating Conditions for Data Collection.

Test Code	NFC [N1C] Percent	Kulite Purge Flow	Temperature Probe
977CNAMNP	Engine Off	OFF	Retracted
977CNAMWP	Engine Off	ON	Retracted
977CNAMGI	Ground Idle	ON	Deployed
977CNAM4801	48.0 [47.0]	ON	Deployed
977CNAM5401	54.0 [52.9]	ON	Deployed
977CNAM6001	60.0 [58.8]	ON	Deployed
977CNAM6501	65.0 [63.7]	ON	Deployed
977CNAM4802	48.0 [47.0]	ON	Deployed
977CNAM5402	54.0 [52.9]	ON	Deployed
977CNAM6002	60.0 [58.8]	ON	Deployed
977CNAM6502	65.0 [63.7]	ON	Deployed

6.6 Test Data Acquired

The desired test matrix was completed, but the test execution differed from the plan due to several challenges that emerged during testing. The initial part of the test worked exactly as desired. On 3/26/2014, after performing the ambient noise measurements, the engine was started, warmed up at idle, and then set to the first operating condition of 48 percent corrected fan speed. The data systems were turned on (both the high sample rate Dewetron and Pulse systems, and the low sample rate engine data recorder). The probe actuators were enabled and the probes were successfully deployed into the flowpath. The successful deployment and operation of the probes indicated that the thermal growth of the engine was properly accounted for in the design of the actuation system. All of the temperature probes responded to the high core temperatures, as witnessed by the calculated temperatures on the Dewetron system, and data was collected for 70 seconds. Figure 76 shows a sample readout from the Dewetron system. The ability to have real time computation of the wire temperatures with this system was extremely helpful.

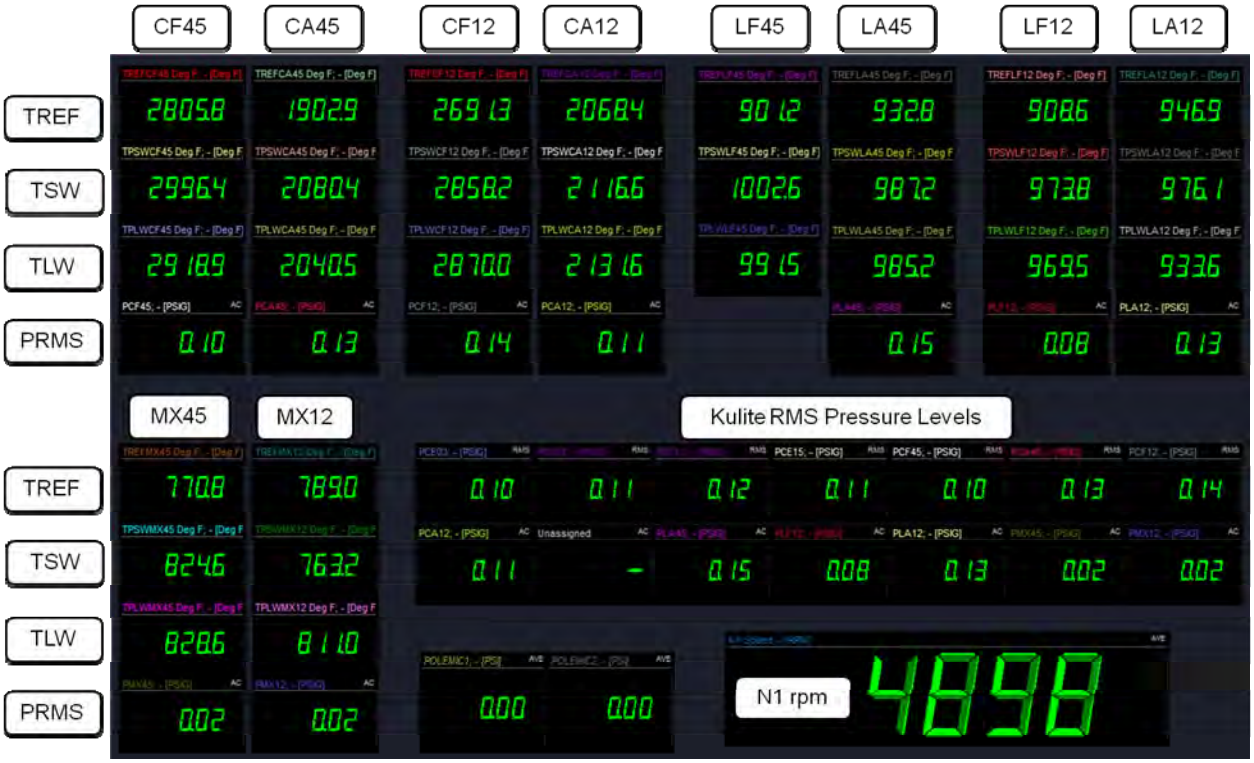

Figure 76. Sample Readout from the Dewetron System at 48 Percent Speed (3/26).

All of the probes in the combustor region survived this initial test point, which was a considerable achievement as there was significant uncertainty regarding the peak operational temperatures at the combustor probe locations. The mean temperatures measured in the combustor, particularly at the forward locations (2900°F), were substantially higher than expected based on engine cycle estimates at the combustor exit location (1800°F), but not out of line with what might be expected in the flame zone. After collecting the data, the probes were retracted and the data systems were stopped. It was noticed that the retraction of the probes was much slower than what was observed during the checkout, possibly indicating that the probes were starting to stick, which raised a concern about whether the repeated deployment and retraction of subsequent test points would be successful. The test team had a brief discussion on whether to proceed with the next planned test point at 54 percent, or skip to a higher power point first, in case any probes or actuators started to give problems. It was estimated that the 65 percent test point was likely too hot for the forward probes to survive, based on temperatures observed at 48 percent and the expected temperature increase with speed. So the 60 percent speed point was attempted. The probes were inserted and appeared to deploy, but the Dewetron data system locked up. The probes were retracted and the engine was brought to idle to reset the data system. A second attempt at the 60 percent speed point was then attempted. However, the forward and aft combustor probes at clocking location 12 (see Figure 77 for instrument clocking locations) did not appear to fully insert, and the small wire signal on the aft combustor probe at location 12 was lost (presumably due to a failure in the connector). Also, the small wire thermocouple signal on the combustor aft probe at location 4.5

was lost shortly after insertion, even though the temperatures at this location were modest. The probes were retracted to diagnose why the combustor probes at location 12 did not insert fully. During retraction, the aft combustor probe at location 4.5 would not retract fully. The engine was brought to idle to try to free the stuck probes, and an attempt at the 54 percent speed point was made. The probes were deployed and data was collected, but the combustor probes on both sides did not insert fully. The engine was shutdown to diagnose the probe actuation system lockups and the data system lockups.

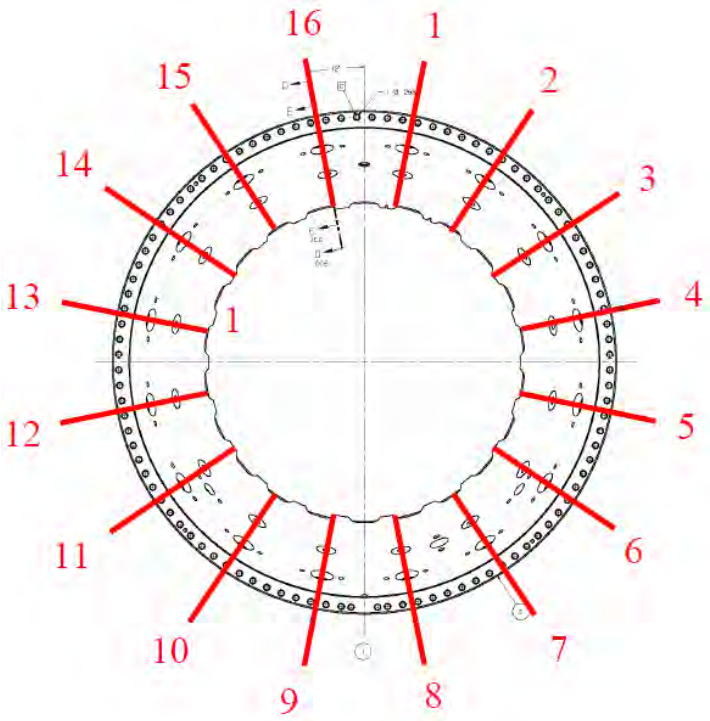

Figure 77 Instrumentation Clocking Locations, Aft Looking Forward.

On 3/27/2014, repairs were made to the installation. The aft probe at combustor location 4.5 was completely frozen and could not be removed from the engine, even with significant force. It was disconnected from the actuator. The combustor probes at location 12 were not operational after shutdown. The spare probe was installed in the aft combustor position, and the mixer probe at location 4.5 was moved to the forward combustor position. This was done to provide a full complement of operational probes on the left side of the engine (ALF). Anti-seize lubricant was applied to all of the probes. Checkouts of the data systems were also performed but did not reveal any anomalies that would explain the lockups. The Dewetron data file at 60 percent speed was found to be corrupted. The sample rate on the Dewetron recorder was increased from 10 kHz to 20 kHz, since fewer channels were being recorded and the data system could process the remaining channels at a higher rate.

Data collection continued on 3/28/2014. Because of the difficulties with the actuation system, it was decided to actuate the probes after reaching the first operating point, and leave them deployed until the last test point. Data was collected at 48 percent and 54 percent, and these points were repeated. During these test points, the Dewetron and Pulse systems again experienced intermittent lockups. On the Dewetron system, the displays showing the real time data would briefly freeze up. Subsequent inspection of the data file showed warning flags

stating that data records were dropped, but this appeared to be a rare event. On the Pulse system, the software would also occasionally lock up. Data was next collected at 60 percent speed. The forward combustor probe at location 4.5 was lost due to excessive temperatures (>3100°F). After data collection, the probes were retracted and the engine was shut down to again diagnose the data system lockups.

Subsequent troubleshooting identified that a potential cause of the data system lockups was high sound levels near the engine might have induced excessive vibration of the hard drives, causing problems with streaming the data to disk. The acquisition systems could not be relocated due to the short cable lengths used with the temperature probes, so instead they were covered with heavy Kaowool acoustic blankets to shield them from the engine noise. After this was done, no further problems were encountered.

The probes were recoated with anti-seize compound and the engine was started and stabilized at the 54 percent speed point. The probes were deployed, and data was collected. Data was then collected at 60 percent and 65 percent corrected fan speed (NFC). At the 65 percent speed point, the forward combustor probe at location 12 was lost due to excessive temperatures (>3100°F). After collecting repeat data at 65 percent, the probes were retracted and the engine was shut down. This completed the test matrix. No problems were ever encountered with the turbine or mixer temperature probes, and no problems were ever encountered with the Kulite probes or microphones.
Because of the issues encountered with the combustor probe actuator lockups and the data system lockups, the collection of the test data was not in the order or the format originally planned. On the Pulse system, individual recordings were made for each of the test point, and binary universal file format (UFF) files were created from each of these separate recordings. On the Dewetron system, the recordings generally contained multiple test points, and so the data for a particular test point needed to be exported to a Matlab file in a post-processing step. Table 5 summarizes the test data that was acquired on the Dewetron and Pulse systems.

Table 5. Matrix of Test Data Acquired.

Test Date	Test Code	NFC Percent	Kulite Purge Flow Status	Temperature Probes	Dewetron Data	Pulse Data
03/26/2014	977CNAMNP	Engine Off	OFF	Retracted	Y	Y
03/26/2014	977CNAMWP	Engine Off	ON	Retracted	Y	Y
03/26/2014	977CN4801	48.6	ON	Deployed	Y	Y
03/26/2014	977CN6001	60.1	ON	Deployed	N	Y
03/26/2014	977CN6002	60.0	ON	Deployed	Y	Y
03/26/2014	977CN5401	54.0	ON	Deployed	Y	Y
03/28/2014	977CNNP	Engine Off	OFF	Retracted	Y	Y
03/28/2014	977CNWP	Engine Off	ON	Retracted	Y	Y
03/28/2014	977CN48RT	48.0	ON	Retracted	Y	Y
03/28/2014	977CN4801	48.0	ON	Deployed	Y	Y
03/28/2014	977CN5401	54.0	ON	Deployed	N	Y
03/28/2014	977CN5402	54.0	ON	Deployed	Y	Y
03/28/2014	977CNGI01	23.2	ON	Deployed	Y	N
03/28/2014	977CN4802	48.4	ON	Deployed	Y	Y
03/28/2014	977CN5403	53.9	ON	Deployed	Y	Y
03/28/2014	977CN6001	60.2	ON	Deployed	Y	Y
03/28/2014	977CNGI02	23.1	ON	Deployed	Y	N
03/28/2014	977CNGI03	23.0	ON	Deployed	Y	N
03/28/2014	977CN5404	54.1	ON	Deployed	Y	Y
03/28/2014	977CN6002	60.1	ON	Deployed	Y	Y
03/28/2014	977CN6501	64.9	ON	Deployed	Y	Y
03/28/2014	977CNGI04	23.1	ON	Deployed	Y	N
03/28/2014	977CN6502	65.1	ON	Deployed	Y	Y
03/28/2014	977CNGI06	23.1	ON	Deployed	Y	N

The temperature probes that were operational during the Dewetron recordings are provided in Table 6. It is easy to tell by inspection of the data files which temperature probes are operational. Table 7 and Table 8 provide the serial numbers and location of the temperature probes used for the testing on March 26 and 28, respectively.

Table 6. Operational Temperature Probes for Dewetron Data Files.

		CB FWD 4.5			CB AFT 4.5			CB FWD 12			CB AFT 12			IT FWD 4.5			IT AFT 4.5			IT FWD 12			IT AFT 12			Mixer 4.5			Mixer 12		
Date	% NFC	REF	SW	LW	REF	SW	LW	REF	SW	LW	REF	SW	LW	REF	SW	LW	REF	SW	LW	REF	SW	LW	REF	SW	LW	REF	SW	LW	REF	SW	LW
3/26/2014	48																														
3/26/2014	60					1a		0	0	0	0	1b	0																		
3/26/2014	54	0	0	0	0		0	0	0	0	0		0																		
3/28/2014	48				2	2	2				3	3	3													4	4	4			
3/28/2014	54				2	2	2				3	3	3													4	4	4			
3/28/2014	48				2	2	2				3	3	3													4	4	4			
3/28/2014	54				2	2	2				3	3	3													4	4	4			
3/28/2014	60	5	5	5	2	2	2				3	3	3													4	4	4			
3/28/2014	23				2	2	2				3	3	3													4	4	4			
3/28/2014	23				2	2	2				3	3	3													4	4	4			
3/28/2014	54				2	2	2				3	3	3													4	4	4			
3/28/2014	60				2	2	2				3	3	3													4	4	4			
3/28/2014	65				2	2	2	5	5		3	3	3													4	4	4			
3/28/2014	65				2	2	2			5	3	3	3													4	4	4			

	Probe Operating, Data Presumed to be Good
	Probe Operating, Data is Questionable
	Probe Not Operating
	Probe Not In Use
0	Data unusable, probe was not properly inserted
1	(a) element died during insertion, temp < 2300F, (b) element dead before probe was inserted
2	This probe was stuck in an uninserted position and could not be removed/replaced; Removed from data collection
3	Spare probe was used in this location
4	Dummy probe inserted, removed from data collection; The mixer probe from this location was moved to the CF12 location
5	Probe elements destroyed by excessive temperatures, > 3100F

Table 7. Location of Temperature Probes for the Testing on 3/26.

Left Hand Side (ALF)	
Location	**Probe Number**
Combustor FWD	8
Combustor AFT	3
LP Turbine FWD	7
LP Turbine AFT	1
Mixer	11

Right Hand Side (ALF)	
Location	**Probe Number**
Combustor FWD	6
Combustor AFT	4
LP Turbine FWD	10
LP Turbine AFT	9
Mixer	5

Table 8. Location of Temperature Probes for the Testing on 3/28.

Left Hand Side (ALF)	
Location	**Probe Number**
Combustor FWD	5
Combustor AFT	2
LP Turbine FWD	7
LP Turbine AFT	1
Mixer	11

Right Hand Side (ALF)	
Location	**Probe Number**
Combustor FWD	6
Combustor AFT	4 (dead)
LP Turbine FWD	10
LP Turbine AFT	9
Mixer	Dummy

6.7 Test Data Export

On the Dewetron system, recordings were made throughout several test points due to issues encountered with software lockups. After the test, separate data files were exported from the Dewetron system to Matlab binary format using the DEWESoft X program. The software is freely available for posttest analysis and can be downloaded from www.dewetron.com. The software can be used in the "Analysis" mode without a license to manipulate existing data files. The data file of interest was opened up by navigating to the file using the folder browser and double clicking the file. Data was exported to MATLAB format by zooming in on the region of interest in the time history, selecting the "export" tab, selecting "absolute time" for the time units, selecting the channels of interest, clicking "File export" and selecting *.mat format with the "MATLAB 7.3 MAT file (> 2 GB)" option, and clicking "Export." The test data from the Pulse system was exported to a binary UFF for ease of subsequent analysis. This format is readable into Matlab using a special-purpose script.

7.0 TASK 5: DATA PROCESSING AND DISTRIBUTION

7.1 Task 5.1 Process Unsteady Temperature and Pressure Data

The purpose of this subtask was to perform initial data processing on the temperature and pressure data. The statement of work for this subtask consisted of the following elements:

1. Process the unsteady temperature data (10 probes) for all test points
    - Perform initial data review and quality assessment
    - Define DGTMS software process for compensated spectra
    - Create compensated time histories of the fluctuating temperature at each probe location for each operating condition
2. Process the unsteady pressure data (13 probes) for all test points
    - Perform initial data review and quality assessment
    - Process power spectral density spectra
    - Create phase-corrected pressure time histories that correspond to the dynamic pressure at the tip of the pressure probe
3. Process engine external acoustic data (2 microphones) for all test points
    - Perform initial data review and quality assessment
    - Process power spectral density spectra

The results from these subtasks are discussed in the following subsections.

7.1.1 Unsteady Temperature Data

7.1.1.1 Data Review and Quality Assessment

There are several aspects of data quality that are of interest to the temperature data. These include an initial inspection of the data, an assessment of data quantization, an evaluation of the electronic noise floor, and statistical characterization of the time history data. The electronic noise floor of the data systems is of critical interest. As previously mentioned, the voltage signals from the data systems were recorded directly without amplification.

An initial inspection of the data is provided in Figure 78 through Figure 81 for the test points 48, 54 and 60 percent respectively. In these figures, dynamic portion of the small wire and large wire thermocouple time histories are examined for the four tested engine speeds. For these plots, the time history data was converted from millivolts to degrees Fahrenheit using the NIST coefficients for Type B thermocouples. The signal was then split into DC and AC components using a cut-off frequency of 1 Hz, using a process that is described in the next section. Figure 78 shows the AC components of the small and large wire thermocouples for the five probes on the left hand side of the engine (aft looking forward) at the 48 percent speed point. Visual inspection of these plots reveals several features. First, it provides an indication of the magnitude of temperature fluctuations of the wire elements (note: this is not the fluctuating gas temperature). In the combustor, the small wire temperature typically fluctuates between -200°F and 200°F, and the large wire temperature typically fluctuates between -50°F and 50°F. In the ITD, the fluctuating wire temperatures are one order of magnitude smaller than those observed in the combustor. And in the mixer, they are about 50 percent smaller than those observed in the turbine. And the fluctuations of the small and large wires in the mixer region are roughly in unison. There appears to be a slight degree of coherence between the upstream and downstream probes in the combustor. There appears to be a very high degree of coherence between the upstream and downstream probes in the ITD. These characteristics are similar at the higher engine speeds.

A first look at the spectral content on these signals is shown in Figure 82 and Figure 83, where the power spectral density of the small wire and large wire temperature signals is presented for the 48 percent and 60 percent speeds. The spectra show a smooth, wideband content, with amplitude decreasing with frequency. The overall shape is similar to that observed in the burner rig test and previous contractor reports. The spectral levels in the combustor are much higher than those in the ITD or mixer. The amplitudes of the inter-turbine and mixer probe elements are seen to flatten out at high frequency, which is a result of reaching the electronic noise floor, as discussed later. The changes in the spectral content due to changes in the engine speed is not dramatic.

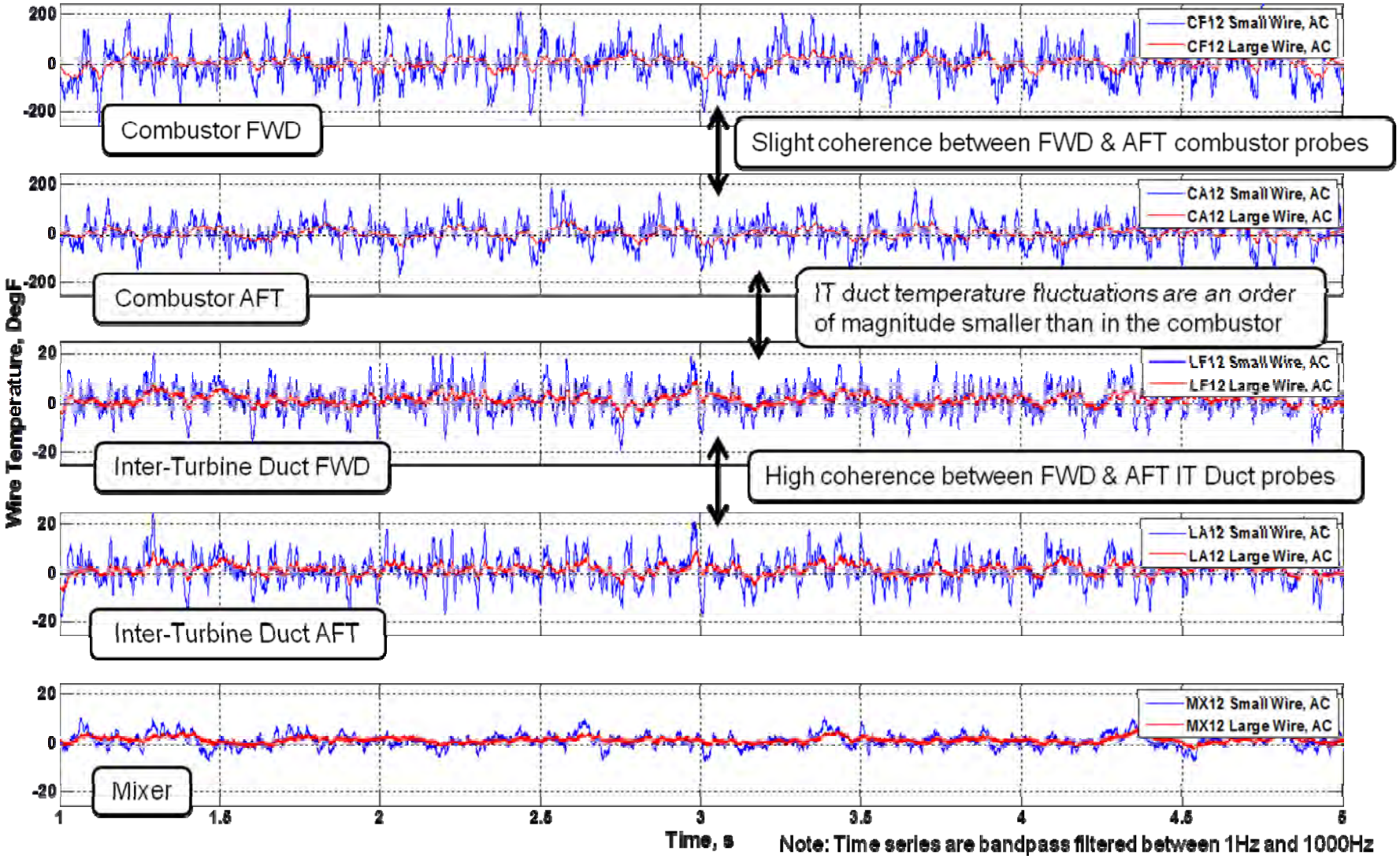

Figure 78. Fluctuating Temperatures of the Small and Large Wires at 48 Percent Speed.

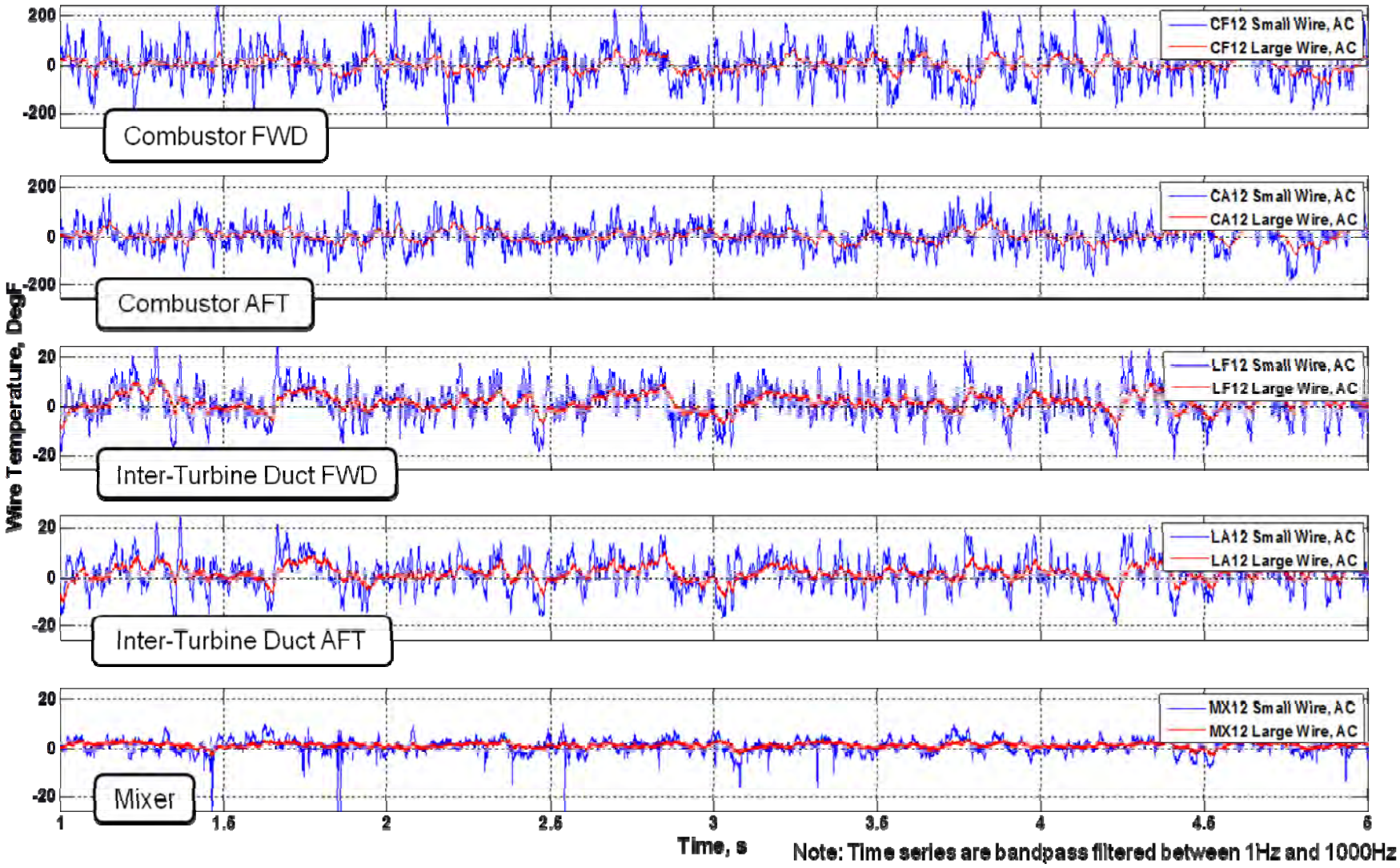

Figure 79. Fluctuating Temperatures of the Small and Large Wires at 54 Percent Speed.

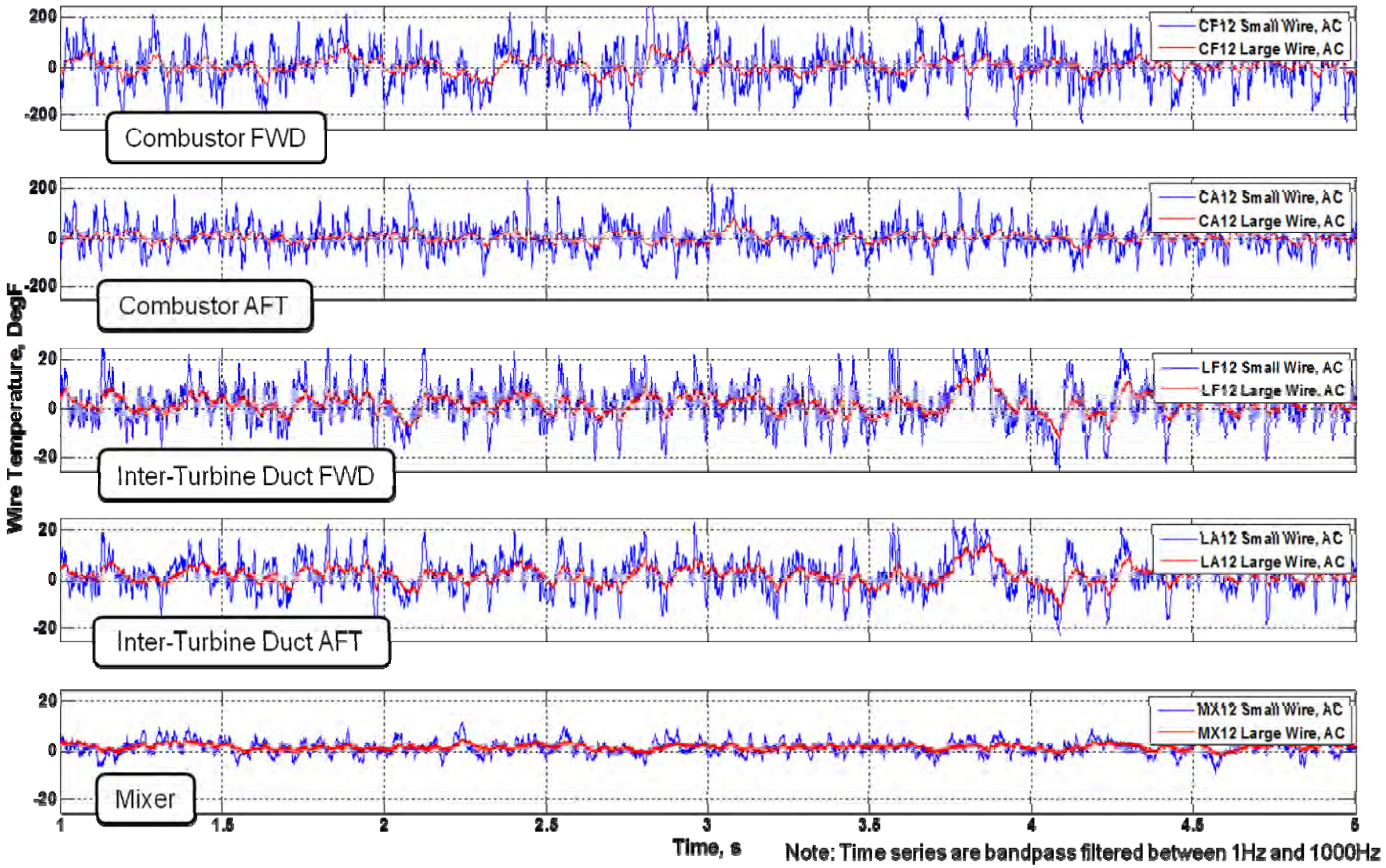

Figure 80. Fluctuating Temperatures of the Small and Large Wires at 60 Percent Speed.

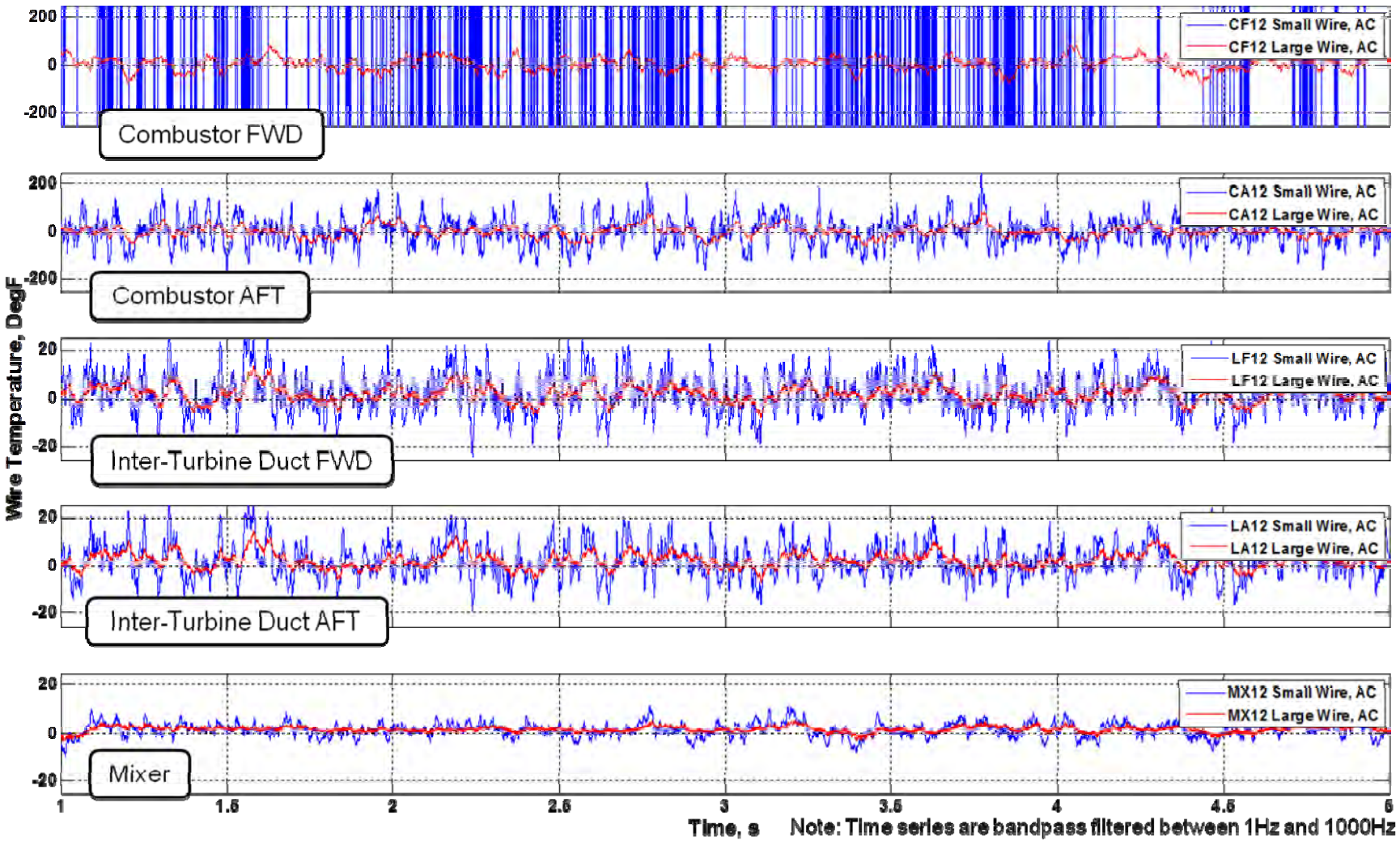

Figure 81. Fluctuating Temperatures of the Small and Large Wires at 65 Percent Speed.

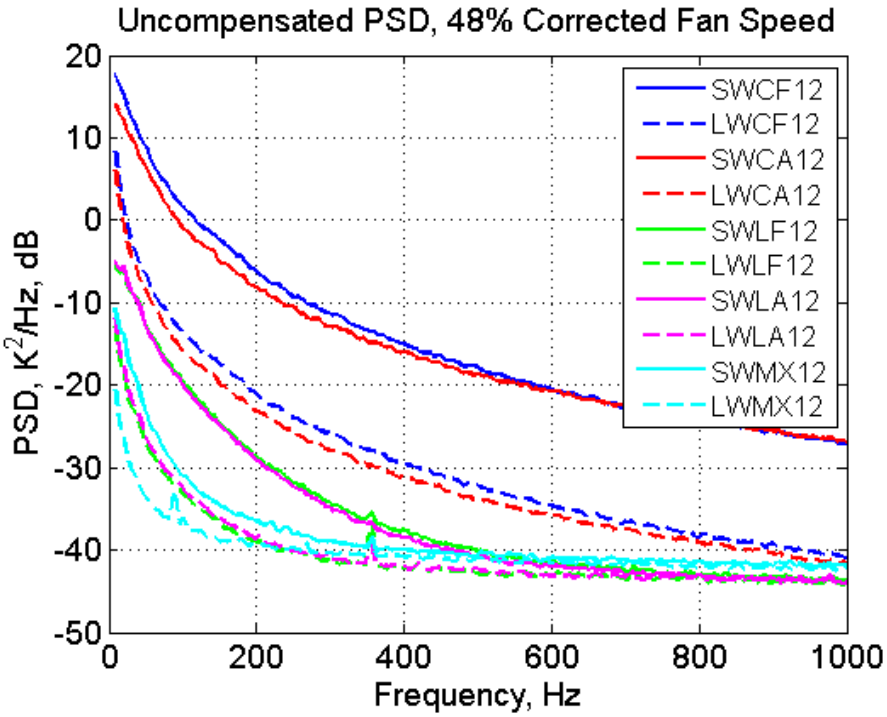

Figure 82. Representative Spectra of the Raw Temperature Signals at 48 Percent Speed.

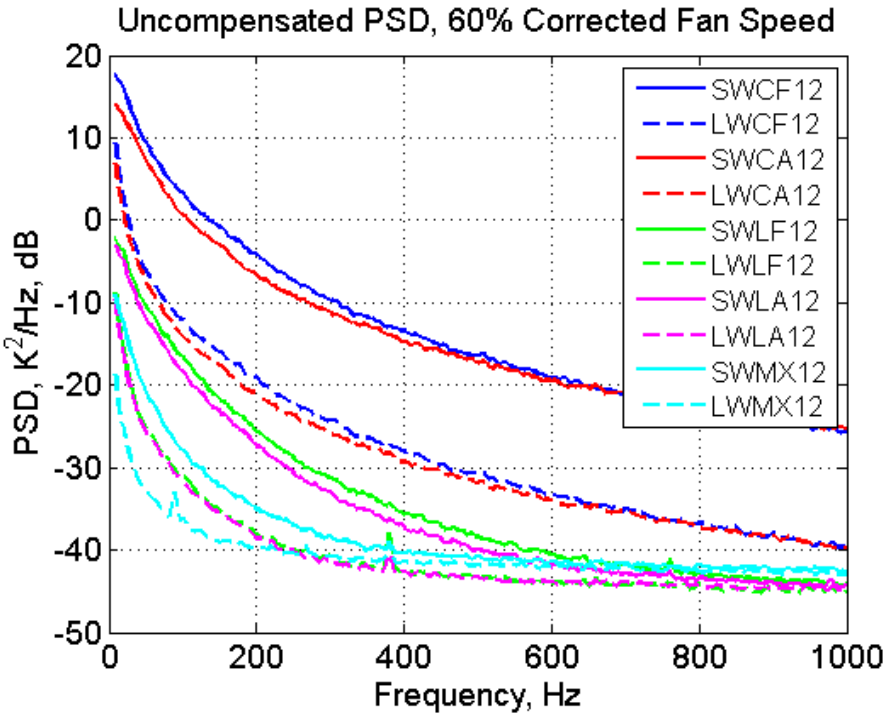

Figure 83. Representative Spectra of the Raw Temperature Signals at 60 Percent Speed.

Data quantization is another important consideration. Since the thermocouple voltage signals were recorded without amplification, the signals could not be arbitrarily gained to optimize the fixed input range of the analog-to-digital converters on the data systems. The nominal input range of the DEWETRON ORION 1624 series analog-to-digital cards is ±10 V. This is also the nominal input range of the Brüel & Kjær LAN-XI 3050-A-060 analog-to-digital modules. Both systems provide 24-bit digital conversion, so the dynamic range is large enough to accurately measure very small voltages. There is the added consideration of the data type and precision used in outputting the measured data (e.g. whether raw A/D counts are considered, or floating point values). In order to get a sense for the practical impact of quantization on the measured data that is subsequently analyzed with these data systems measured data were inspected. The small wire thermocouple voltages from the forward combustor probe at the 4.5 location were examined.

Figure 84 shows a snippet of data from the Pulse system, taken directly from the binary UFF file (sample rate of 65536 Hz). The oscillation in the voltage caused by the temperature fluctuations is evident in the top part of the figure. The bottom part of the figure shows the difference in voltage between neighboring data points, and is useful for spotting quantization effects. There is a clear horizontal banding of these voltage increments, indicating quantization of the data. The increment between bands is 1.417 μV, which is an extremely small voltage change. The temperature increments corresponding to this voltage quantization, for the range of temperatures of interest in this test, are shown in Table 9, where the conversion from voltage to temperature was performed using the NIST curves for Type B thermocouples. The temperature increments range from 0.7°F at mean temperatures near 700°F (e.g. the mixer location) to 0.2°F at mean temperatures near 3000°F (e.g. at the combustor forward location). From the standpoint of indirect noise generation, being able to resolve the temperature fluctuations to this level of resolution (note that these are uncompensated) is considered adequate.

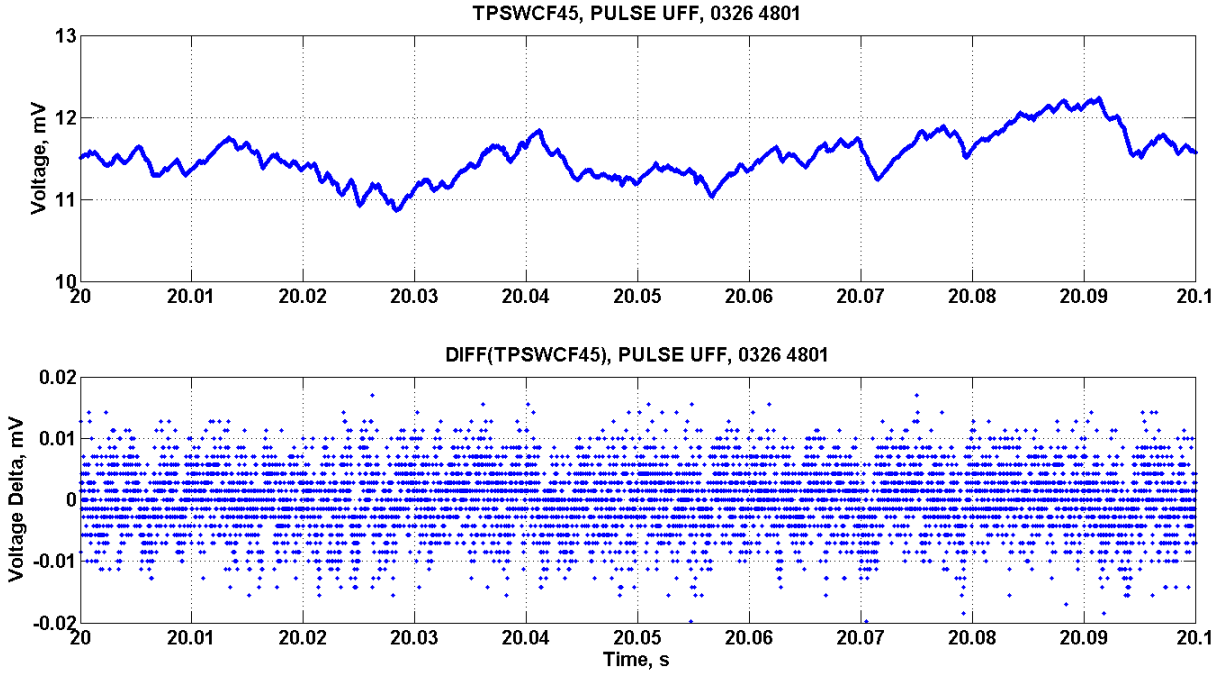

Figure 84. Example of Quantization of Raw Temperature Signals Recorded by the Pulse System.

Table 9. Temperature Increments Corresponding to 1.42 µV Quantization.

mV	T (°F)	mV	T (°F)	mV	T (°F)	mV	T (°F)
11.845	3000.0	5.7115	2000.0	1.4300	1000.0	0.6812	700.0
11.8464	3000.2	5.7129	2000.3	1.4314	1000.5	0.6826	700.7

Figure 85 shows a snippet of data from the Dewetron system, taken from the Matlab data file that was exported from the Dewetron system (sample rate of 10000 Hz). The time corresponds to the same snippet of data from the Pulse system in Figure 84. The oscillation in the voltage caused by the temperature fluctuations is evident in the top part of the figure. The bottom part of the figure shows the difference in voltage between subsequent data points, and is useful for spotting quantization effects. There is no clear banding of these voltage increments, suggesting that the quantization of the data is substantially smaller than is observed with the Pulse system. The banding can only be observed by zooming in much more closely. The increment between bands appears to be about 0.03 µV. The temperature increments corresponding to this voltage quantization are more than an order of magnitude smaller than the Pulse system, or less than 0.1°F at mean temperatures of 700°F and above. Thus, quantization of the temperature data acquired by the Dewetron system (the primary data system) is likely of no consequence. There is one caveat, in that the compensation gain can be quite large at high frequencies (20 to 30 dB at 500 Hz) so evaluating the impact of quantization more carefully needs to consider the frequency content of the measured signals and the amplitudes of those frequency components at which indirect combustion noise becomes important.

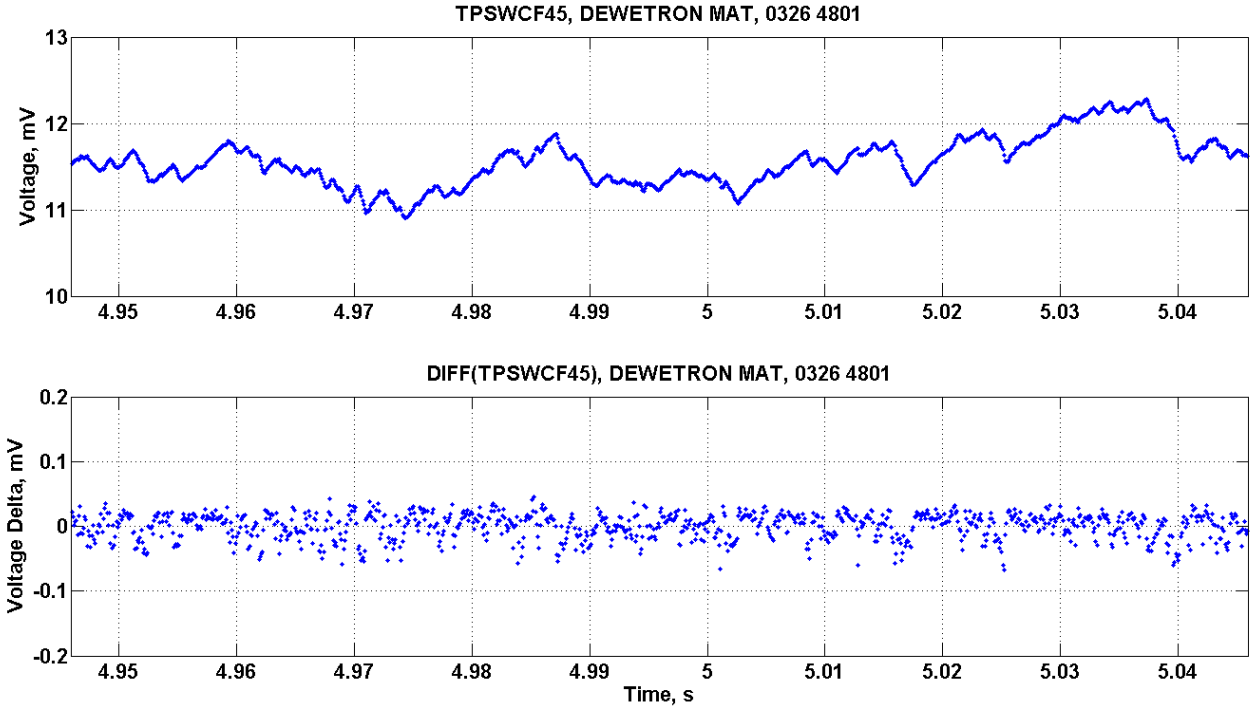

Figure 85. Example of Quantization of Raw Temperature Signals Recorded By the Dewetron System.

The background electronic noise floor is also an important consideration. The extremely small voltage fluctuations of interest are riding on top of a small DC voltage level corresponding to the mean temperature of the environment in which the thermocouples are immersed. If the background electronic noise of the recording system is too high, the mean voltage and/or the fluctuating component could be lost in the noise. Figure 86 shows the power spectral density of the electronic noise floor of the small wire (SW in the figure key) and large wire (LW in the figure key) thermocouples measured prior to engine start, compared to the levels measured at the 48 percent speed test point. The measurements made prior to engine start are shown as dotted lines in the figure ('AWB Purge On' in the figure key) and the measurement made at 48 percent are shown with solid lines ('0326 4801' in the figure key). The background electrical noise of all of the thermocouples is essentially the same. The noise floor ranges from -20 dB at 20 Hz down to about -30 dB at 1000 Hz, with 0 dB corresponding to 1 μV. This data was processed with a Hanning window, 50 percent overlap, and a frequency resolution of 4 Hz. The noise floor corresponds to extremely low temperature fluctuations. For example, a 500 Hz sinusoidal signal with a root-mean-square amplitude of 0.1 μV would just barely protrude above the noise floor. This corresponds to measured temperature fluctuations below 0.1°F.

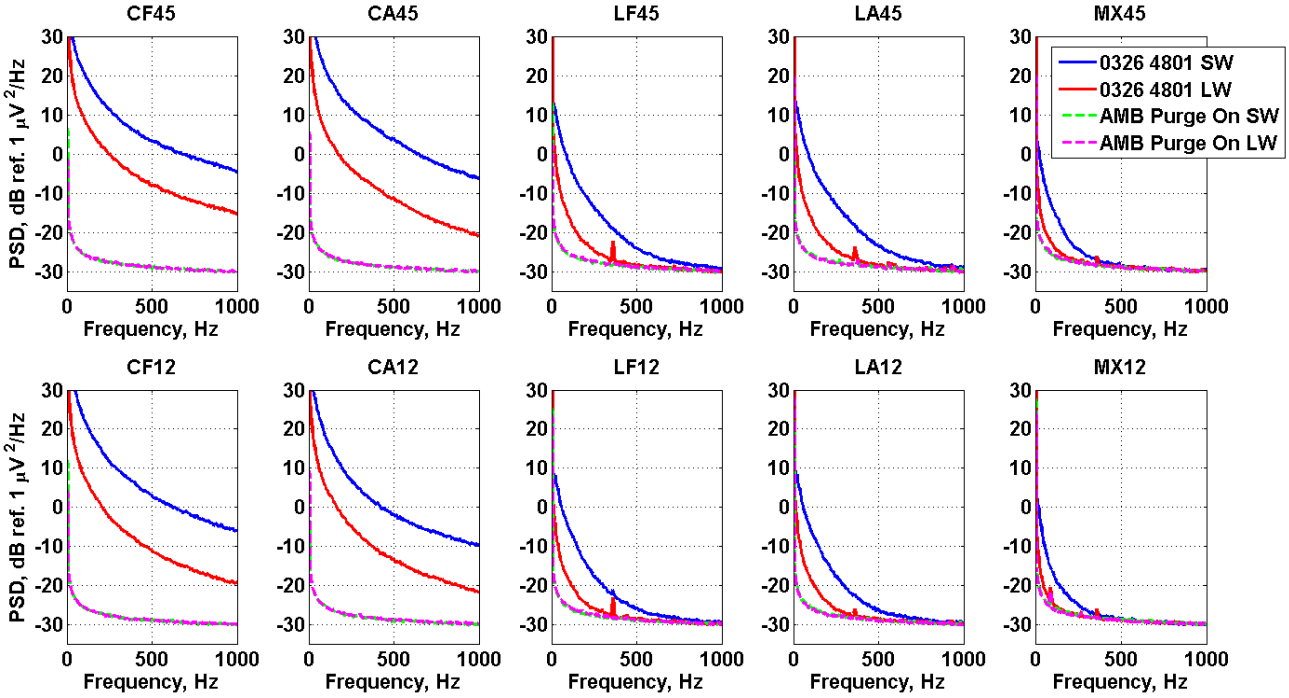

Figure 86. Dewetron System Electronic Noise Floor for Temperature Probes.

The electronic noise floor is clearly acceptable for raw measurement of temperature using an ideal temperature probe that requires no compensation. However, the physical size and limited frequency response of the probes used here have compensation factors on the order of 20 to 30 dB, which dictates that the measurement system should be capable of resolving much smaller fluctuations. For example, if it is deemed necessary to resolve fluctuating temperatures on the order of 10°F at 1000 Hz, then the measurement system must have a noise floor that is one or two orders of magnitude smaller than those corresponding voltages to accommodate the compensation process. A fundamental question is, "what amplitude of fluctuating temperatures need to be resolved, and over what frequencies?" To answer this, one needs to know how the magnitude of these temperature fluctuations relates to the magnitude of the pressure

fluctuations that are generated upon convection of these entropy waves through the turbine, and how these pressure fluctuations compare to the other noise sources of the engine. At the present time, the answer to this question is not known. It is not currently known even what order of magnitude of temperature fluctuations is important. In addition, the conversion from temperature to pressure might be highly dependent on the specifics of the engine.

Figure 86 indicates that the voltage signals from the combustor probes i.e. CF45, CA45, CF12 and CA12 in the figure, are well above the noise floor to at least 1000 Hz, so that no limitation is imposed on the compensation process. The ITD probes i.e. LF45, LA45, LF12 and LA12 in the figure, should only be compensated to about 500 Hz if the small wire is used for compensation, or 250 Hz if the large wire is used for compensation. Applying compensation beyond these frequencies will only result in the amplification of signal noise. The mixer probes i.e., MX45 and Mx12 in the figure should only be compensated to about 250 Hz if the small wire is used for compensation. Considering that the noise floor roughly corresponds to fluctuations on the order of 0.1°F, fluctuations on the order of 1°F or less cannot be resolved at the higher frequencies. From the standpoint of the indirect noise generation, this currently does not appear to impose any limitation. The fluctuations in the ITD and the mixer beyond these frequency limits are, from a practical perspective, probably too small to be of any interest. Thus the electronic noise floor of the Dewetron system appears to be acceptable for practical purposes.

7.1.1.2 DGTMS Software Process for Compensated Spectra

The DGTMS software was used to determine the compensation spectra and compute the compensated temperature spectra. No major modifications were made to the program, and the code worked well in the form received from NASA. The various subroutines of the code are well documented in previous contractor reports (References 1, 6, 7). The process for using the DGTMS software to compensate the data is similar to that used during the burner rig test. Because of the large number of probe/test point combinations, a semi-automated process was used. A Matlab script was written to perform the following steps:

1. Create the DGTMS input file. This file contains the probe dimensions, mean flow properties, and various program control options.

2. Create the DGTMS time history data file.
   - Resample the data from its acquired sample rate to 8192 Hz.
   - Split the time histories into AC and DC components using fourth order Butterworth filters with a cut-off frequency of 4 Hz.
   - Export the data to a fixed format text file.

3. Run the DGTMS program.

4. Read the compensation spectra and the compensated temperature spectra from the DGTMS output files and export these to Excel.

5. Create compensated time histories using an interpolated compensation spectrum and save these out as Matlab binary files for additional post-processing.

Pertinent details of these steps are now described in more detail, with reference to the data set acquired at 48 percent corrected fan speed collected on March 26. To run the DGTMS

software, the user must supply an input file and a data file. Both files are in ASCII text format. The input file contains information regarding the thermocouple probe geometry and the mean flow properties, along with parameters that specify various aspects of the data processing, program control, and output. The input file is described in Table 6 of Reference 7.

The input file requires the thermocouple probe dimensions to use in the convective and conductive heat transfer model. The dimensions of the individual probe elements were not measured, so the nominal dimensions from the engineering drawing, shown in Figure 87, were used with one modification. The diameter of the support wires is nominally 0.020-inch. However, there is an overlap region where the smaller diameter sensing wires are welded on top of the support wires. As a result, the actual construction deviates from the ideal theoretical model that is used in the DGTMS code. To approximately account for this difference, an effective diameter was defined, given by the diameter of a cylindrical wire that has the same combined volume (mass) as the 0.020-inch support wire and the overlapped portion of the 0.10-inch or 0.003-inch sensing wire. Table 10 provides the nominal values of the probe elements along with the computed "effective diameter" of the support wires. These values were used in the DGTMS input file.

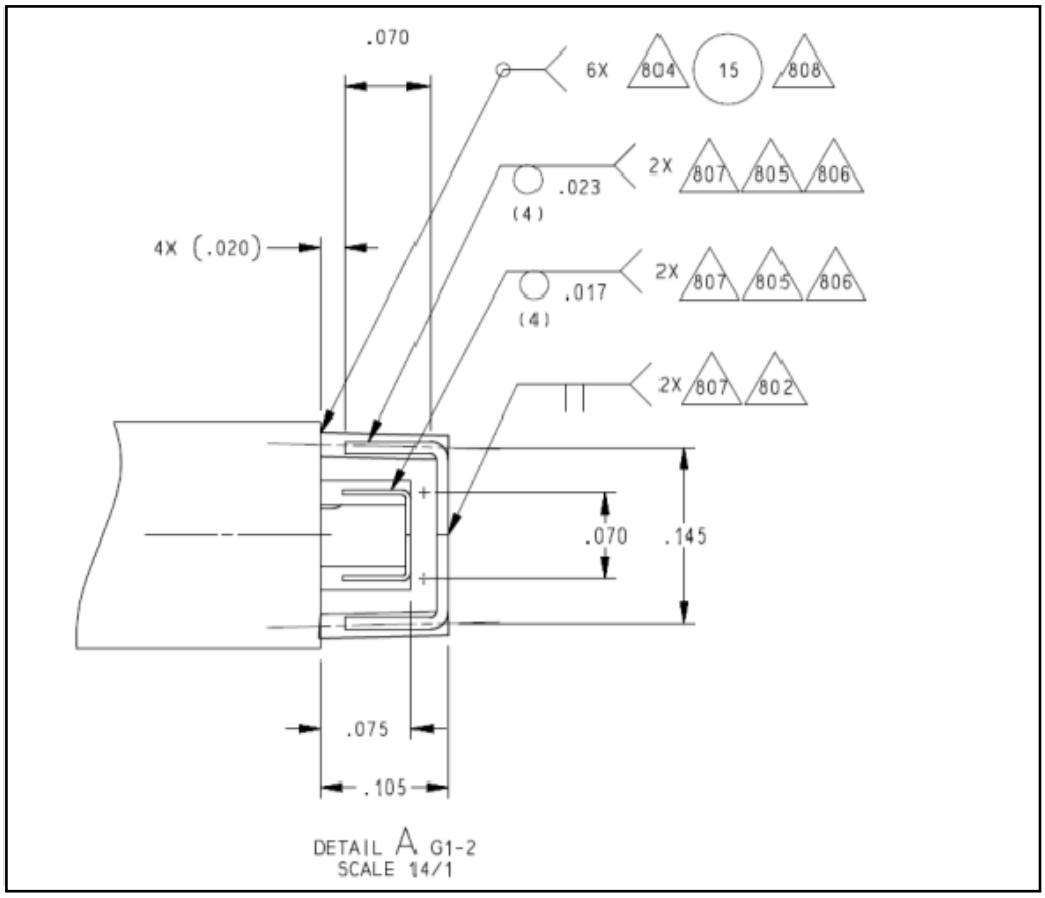

Figure 87. Nominal Dimensions of the Thermocouple Probe Elements.

Table 10. Thermocouple Probe Dimensions Used in the DGTMS Input File.

Feature	Thermocouple	Value	Adjusted
Length of support wire	Large Diameter	0.105-inch (0.267 cm)	-
Half of total length of the smaller wire	Large Diameter	0.073-inch (0.184 cm)	-
Diameter of support wire	Large Diameter	0.020-inch (0.0508 cm)	0.0557 cm
Diameter of smaller wire	Large Diameter	0.010-inch (0.0254 cm)	-
Length of support wire	Small Diameter	0.075-inch (0.191 cm)	-
Half of total length of the smaller wire	Small Diameter	0.035-inch (0.0889 cm)	-
Diameter of support wire	Small Diameter	0.020-inch (0.0508 cm)	0.0512 cm
Diameter of smaller wire	Small Diameter	0.003-inch (0.00762 cm)	-

Next, the DGTMS time history data file was created. The first step is to resample the data from the acquired sample rate (namely 10 kHz or 20 kHz for the Dewetron data acquired on March 26 or 28, respectively) to a more modest sample rate. A sample rate of 8192 Hz was chosen for this purpose, which significantly over samples the frequency range of interest. The data was resampled in Matlab using the *resample* function. The initial and final $1/8^{th}$ second of the time history was clipped off to remove portions of the signal that might have been distorted by starting and ending transient artifacts. The time histories for the large and small wire thermocouples were then split into AC and DC components. Low-pass and high-pass fourth order Butterwoth filters with a cutoff frequency of 4 Hz were defined using the Matlab *butter* function and applied to the data using the *filtfilt* function so that the filtered time history has zero phase distortion. The cut-off frequency is somewhat arbitrary, and a value between 1 Hz and 20 Hz would probably be appropriate. The 4 Hz cut-off was chosen to coincide with the 4 Hz analysis bandwidth used later in the processing.

Figure 88 through Figure 92 plot the time history data for the 10 temperature probes after resampling and splitting into DC and AC components. Inspection of the DC signals for the small wire and large wire thermocouples shows that DC amplitudes are very similar (ideally, they would be identical) and that the low frequency undulations are the same for both sensing elements. This provides confidence that both sensing elements are operating correctly. The reason for the small difference in DC levels in some cases is unknown. The small and large thermocouple junctions are not at the exact same point in space (the two junctions are displaced 0.030-inch in the radial direction and 0.056-inch in the axial direction), so some of the difference might be due to actual differences in flow temperatures, but further investigation is required. Inspection of the AC signals shows that the small wire thermocouple has much greater amplitude than the large wire thermocouple, as expected, and that the fluctuations are in unison. Inspection of the full time history plots for the various test conditions is helpful, as there are occasionally anomalies in the data that are readily apparent. For example, the small wire AC time history for the CA12 probe in Figure 89 indicates an unexplained anomalous behavior near 30 seconds. The data in this region is suspect.

The data file for the DGTMS code is a formatted file containing the small wire thermocouple AC data, the large wire thermocouple AC data, and the DC data from either the small or large wire (which is usually very similar). For this report, the DC data from the large wire was used. The data is arranged in blocks, as described on page 16 of Reference 7, in units of millivolts. Once the input file and the data file have been created, the DGTMS software can be executed.

In order for the DGTMS code to be able to successfully compute the in-situ heat transfer coefficient for a particular probe at a given operating point, there must be sufficient coherence (greater than 0.8) between the small and large thermocouple wires at low frequencies (say

below 50 Hz). Thus it is of interest to examine the coherence between the small and large thermocouple wires. An example is presented in Figure 93, which plots the coherence for the ten probes at the March 26 48 percent speed point. In the combustor, there is substantial coherence over a wide range of frequencies. The aforementioned anomaly in the small wire time history data for the CA12 probe results in a loss of coherence relative to the other combustor probes. This probe was replaced for the second day of testing, and the coherence improved in the repeat of the test point. The coherence in the ITD and mixer are sufficiently high at low frequencies, but drops off very rapidly with frequency. This is a result of the temperature fluctuations at frequency becoming extremely small and the corresponding voltage fluctuations reaching the electronic noise floor of the data acquisition system. The Matlab function *mscohere* was used to compute coherence in these analyses.

The DGTMS software was run for all functioning temperature probes at all operating conditions. For each probe, at each condition, an input file and a time history data file was created. The DGTMS software was executed from the Matlab script. Program control options in the input file were set to compute the compensation spectrum and the compensated temperature spectrum for the small wire thermocouple (IFLAGS(3)=1). For comparison purposes, a second input file was created with the program control options set to compute the compensation spectrum and the compensated temperature spectrum for the large wire thermocouple (IFLAGS(3)=2). The computed small wire compensation spectra for the combustor, ITD, and mixer probes at the March 26 48 percent speed operating point are shown in Figure 94, Figure 95, and Figure 96, respectively. The amplitude and phase of the compensation spectra are smooth, well behaved, and have magnitudes and shapes that are similar to previous results.

Within the DGTMS code, the compensation spectrum for the small (or large) wire thermocouple is applied to the measured spectrum of the small (or large) wire thermocouple to produce the compensated temperature spectrum, which is the estimated spectrum of the fluctuating temperature of the gas stream. Figure 97 shows a representative result for the CA45 probe at 48 percent speed. This location is of particular interest, since the temperature fluctuations at the aft end of the combustor convect into the high pressure (HP) turbine and are hypothesized to create pressure fluctuations via the indirect noise generating mechanism. The figure shows the results for both the small wire and large wire compensation. In this case, the results are similar regardless of which wire is chosen for the compensation process, lending confidence regarding the consistency of the compensation process. The compensated temperature spectra are smooth and wideband. On a linear frequency scale, there are no significant peaks in the spectrum. The PSD amplitude (in dB) decreases with frequency in a nearly linear fashion.

As one point of comparison, in Figure 98, the compensation spectra for the combustor probes at 48 percent speed are compared to the compensation spectra that were computed during the P&W F100 testing (Reference 4). Caution needs to be exercised here, because the probe design, probe placement, engine characteristics, and operating condition are different between the two test programs. However, there are enough similarities to make the comparison worthwhile. The combustor compensation spectra in the TECH977 test are seen to be quite similar to the turbine nozzle compensation spectrum in the F100 test, lending confidence that the DGTMS measurement and software analysis processes are producing results that are consistent with previous testing.

The compensated spectra for the four combustor probes at 48 percent speed are shown in Figure 99. There is very little difference in the compensated spectra for the two aft probes, indicating that the temperature fluctuations on either side of the engine have similar magnitude near the exit of the combustor. This is an encouraging result, since the aft combustor probe at

location 4.5 became inoperative early in the test series. There is also not a dramatic difference in the compensated amplitude between the forward probes and aft probes. For the CF45 probe, there is a difference of about 5 dB between the small wire and large wire compensated spectra. The reason for the discrepancy is not currently known.

The compensated spectra for the four ITD probes at 48 percent speed are shown in Figure 100. Here, because of the electronic noise floor, the compensated spectra are not reliable above a certain frequency. For the large wire thermocouple, the compensated spectra are only reliable below about 200 Hz. For the small wire thermocouple, the compensated spectra are only reliable below about 500 Hz. There is no dramatic difference in compensated amplitude between the upstream and downstream probes at the location 4.5, or between the upstream and downstream probes at location 12, indicating that the temperature fluctuations are not changing with axial distance. There is slight difference between the probes on the two sides of the engine, with the probes on location 4.5 reading about 3 dB higher than those on the opposite side. At 200 Hz, where both the large and small compensated spectra should be valid, there is a 5 dB difference between the compensated spectra. Presumably, the small wire compensated spectra would be more reliable due to the higher signal-to-noise ratio. Although the small wire compensated spectra can only be computed up to 500 Hz, this does not appear to impose any practical limitation, because the temperature fluctuations, even at low frequencies, are so small that convection through the LP turbine nozzle is unlikely to create any significant indirect noise. However, this presumption requires validation, which is outside the scope of this work effort.

The compensated spectra for the two mixer probes at 48 percent speed are shown in Figure 101. Because of the electronic noise floor, the compensated spectra are not reliable above a certain frequency. For the large wire thermocouple, the compensated spectra are only reliable below about 50 Hz. For the small wire thermocouple, the compensated spectra are only reliable below about 250 Hz. There is no dramatic difference in compensated amplitude between the probes on the two sides of the engine. Although the small wire compensated spectra can only be computed up to 250 Hz, this does not appear to impose any practical limitation, because the temperature fluctuations are so small that convection through the remainder of the nozzle is unlikely to create any significant indirect noise.

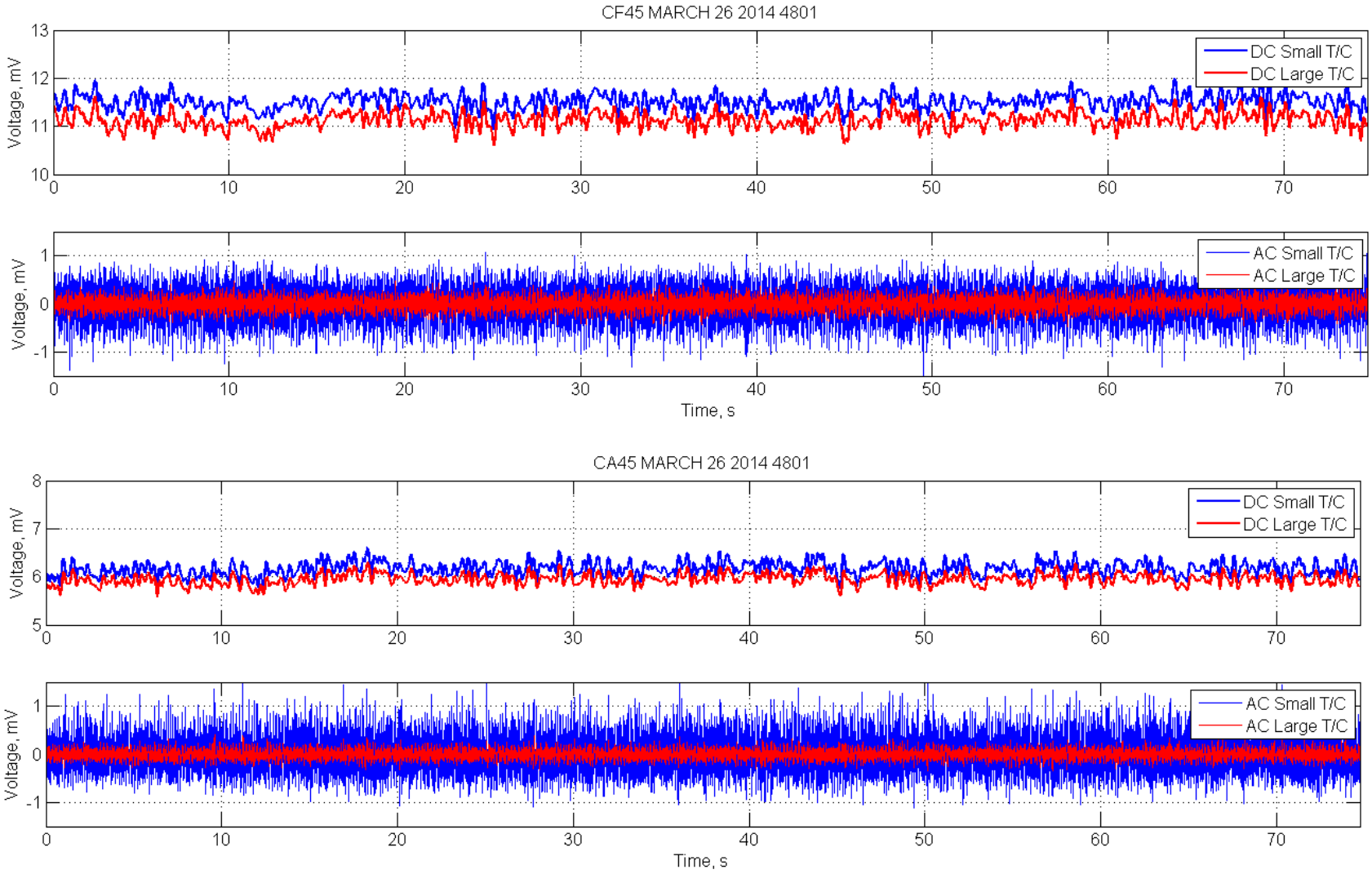

Figure 88. DC and AC Time Histories for the CF45 and CA45 Probes at the March 26 48 Percent Speed Point.

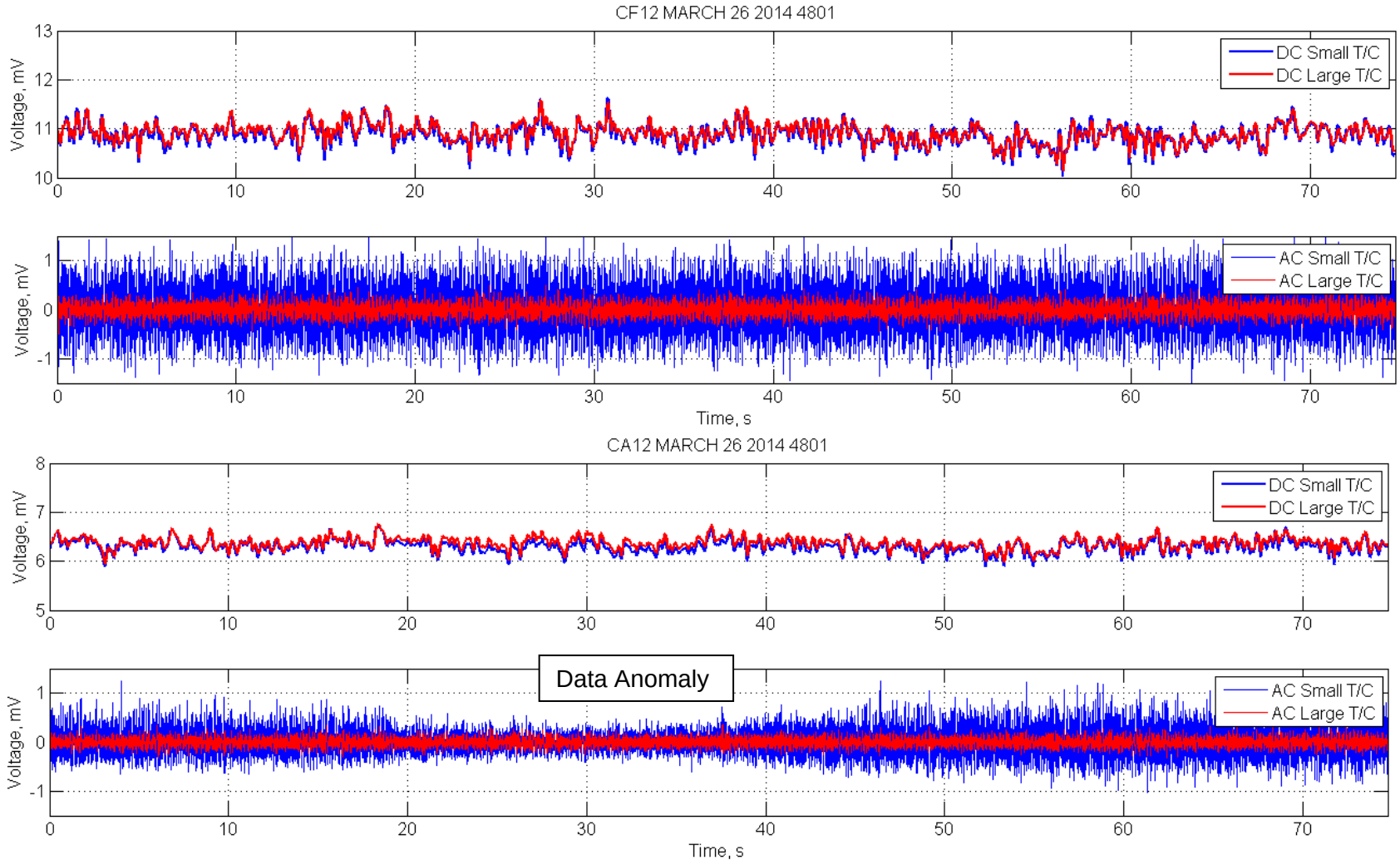

Figure 89. DC and AC Time Histories for the CF12 and CA12 Probes at the March 26 48 Percent Speed Point.

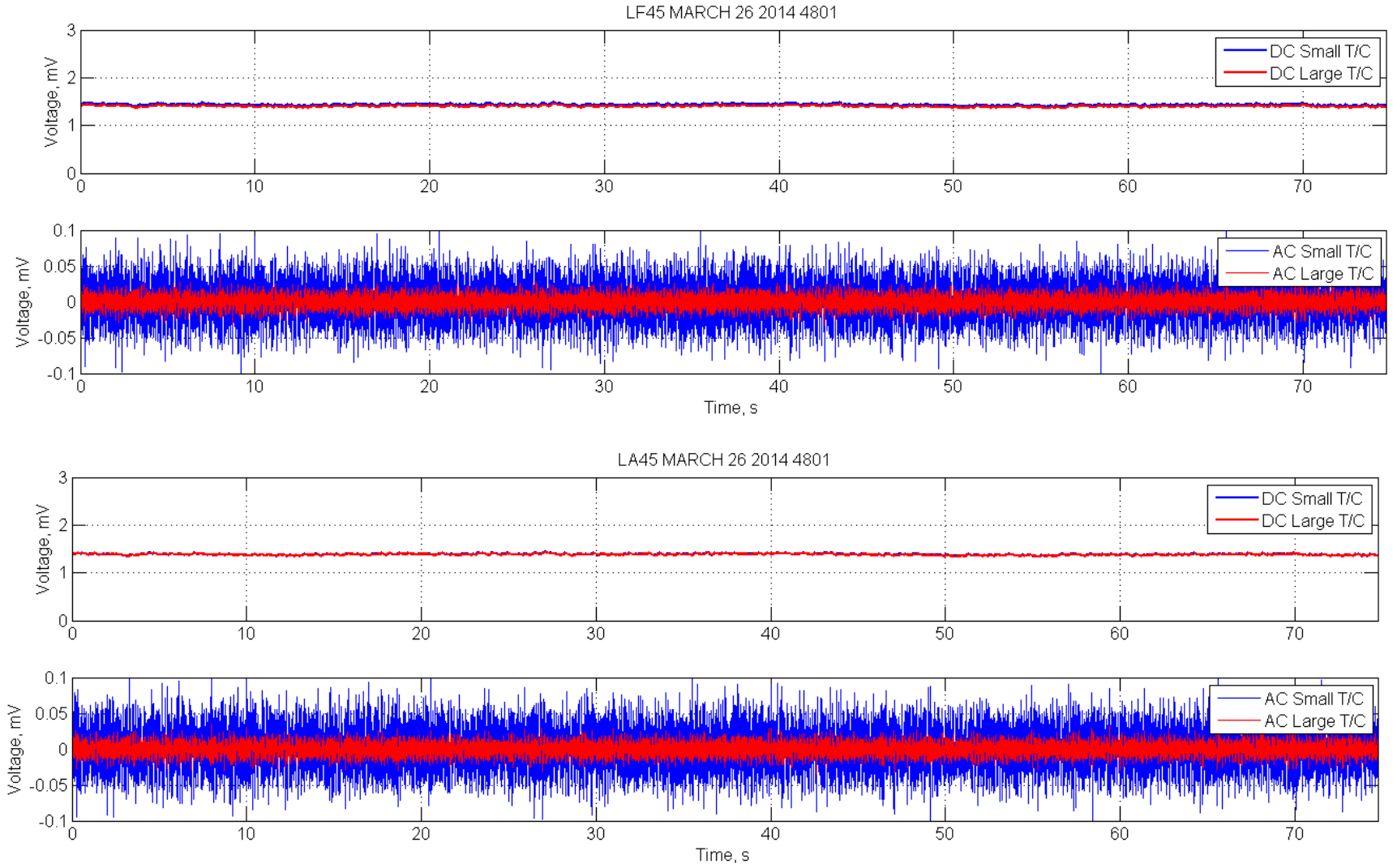

Figure 90. DC and AC Time Histories for the LF45 and LA45 Probes at the March 26 48 Percent Speed Point.

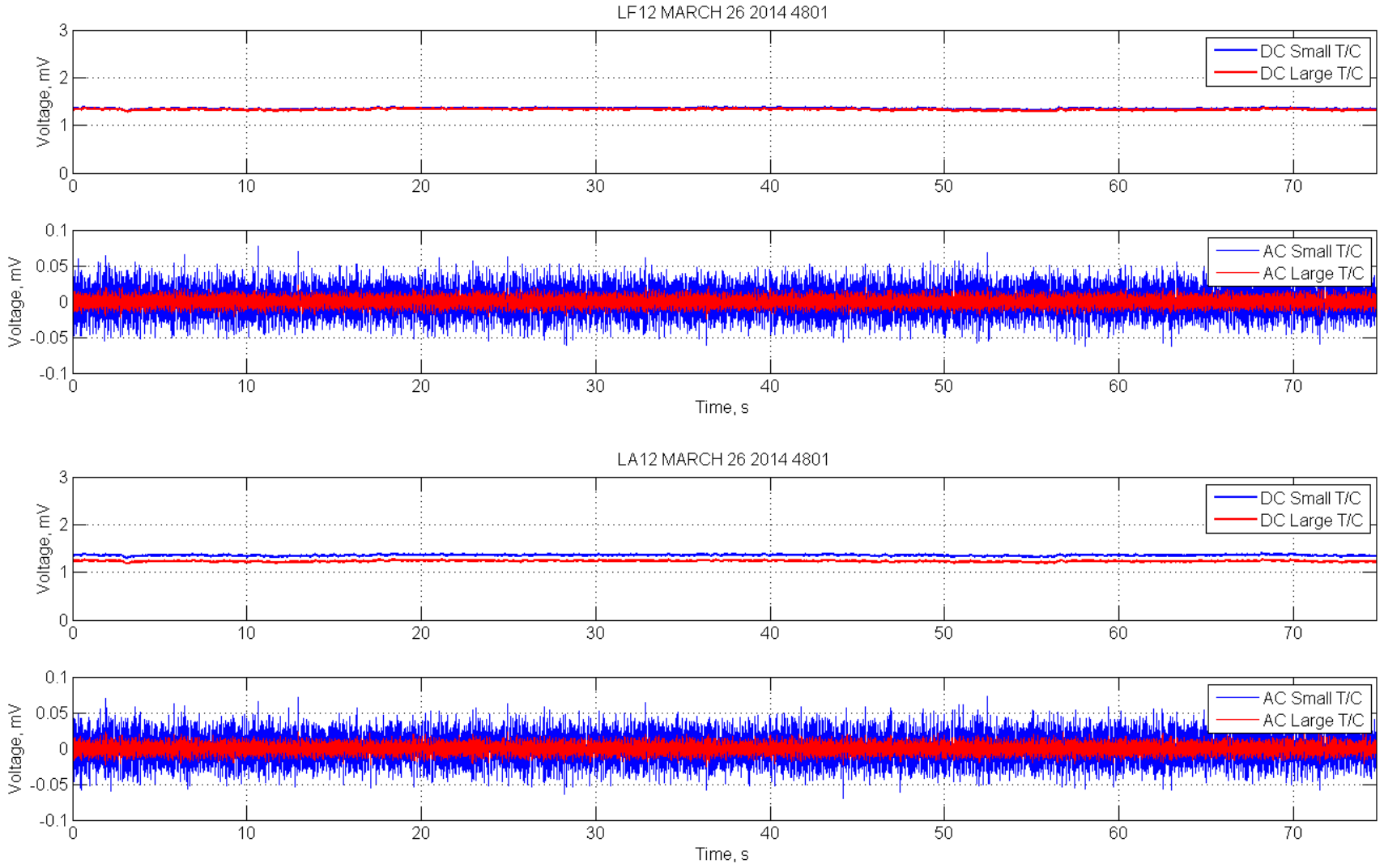

Figure 91. DC and AC Time Histories for the LF12 and LA12 Probes at the March 26 48 Percent Speed Point.

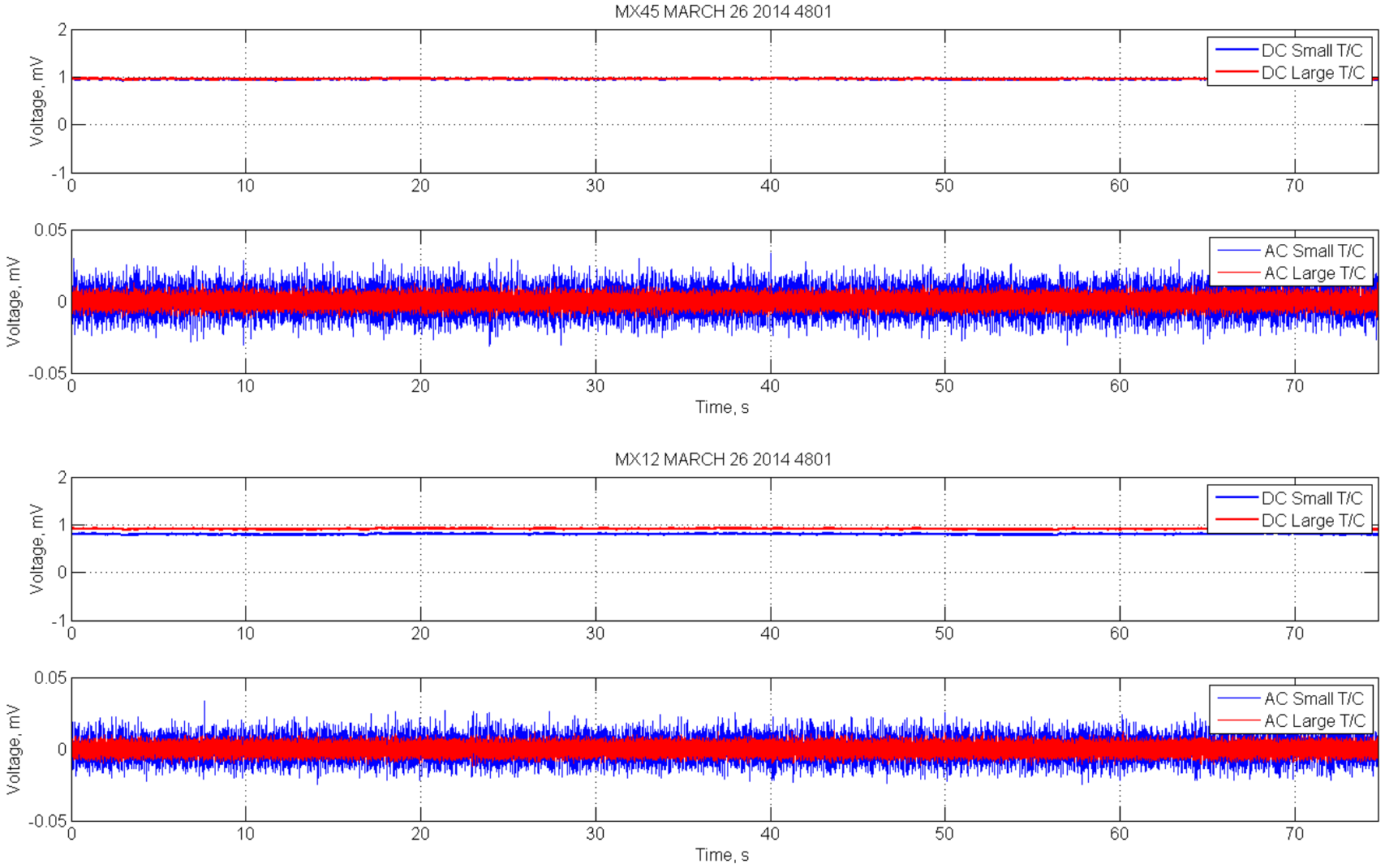

Figure 92. DC and AC Time Histories for the MX45 and MX12 Probes at the March 26 48 Percent Speed Point.

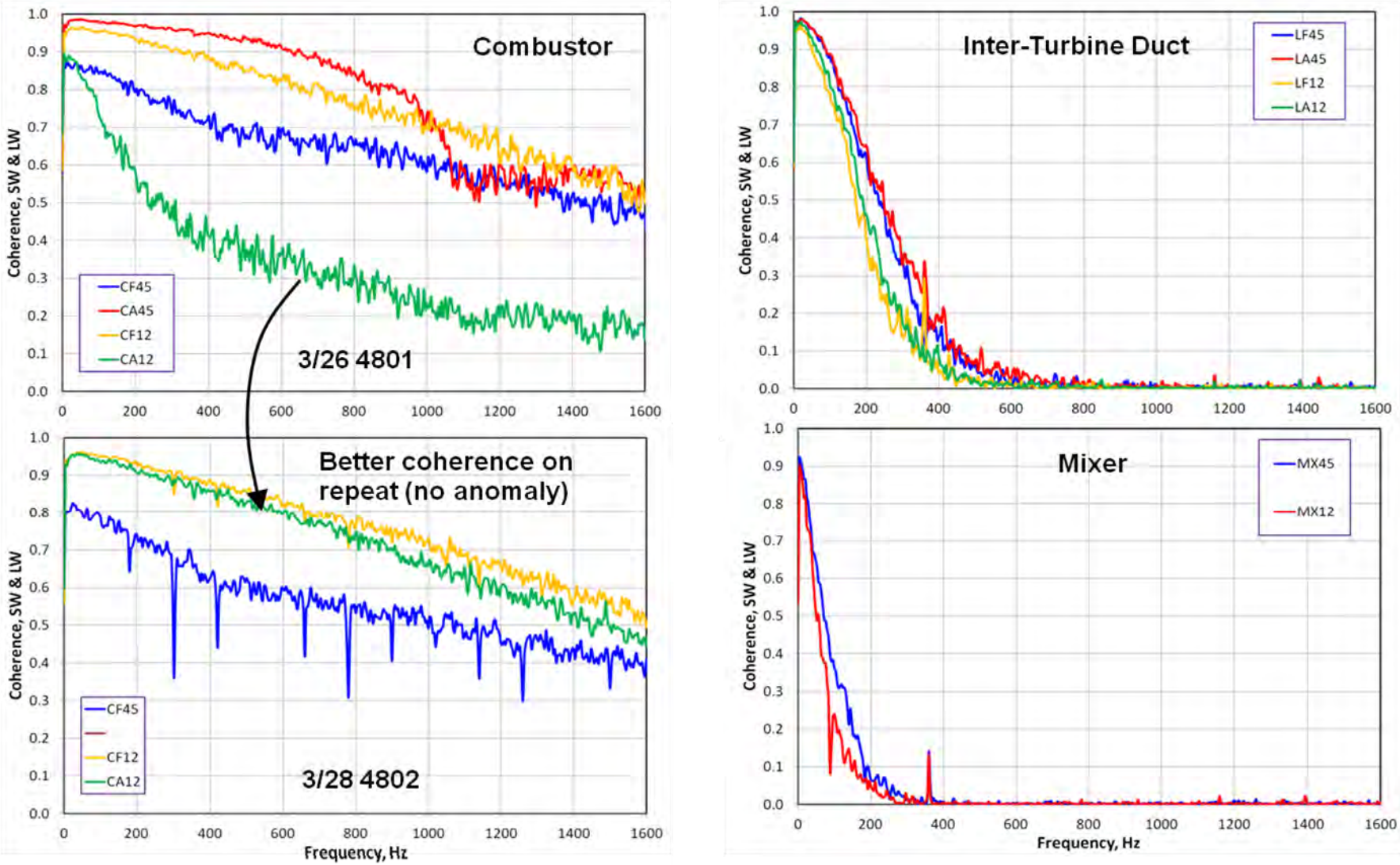

Figure 93. An Example of the Coherence Between the Small Wire and Large Wire Thermocouple (T/C) Raw Time Histories.

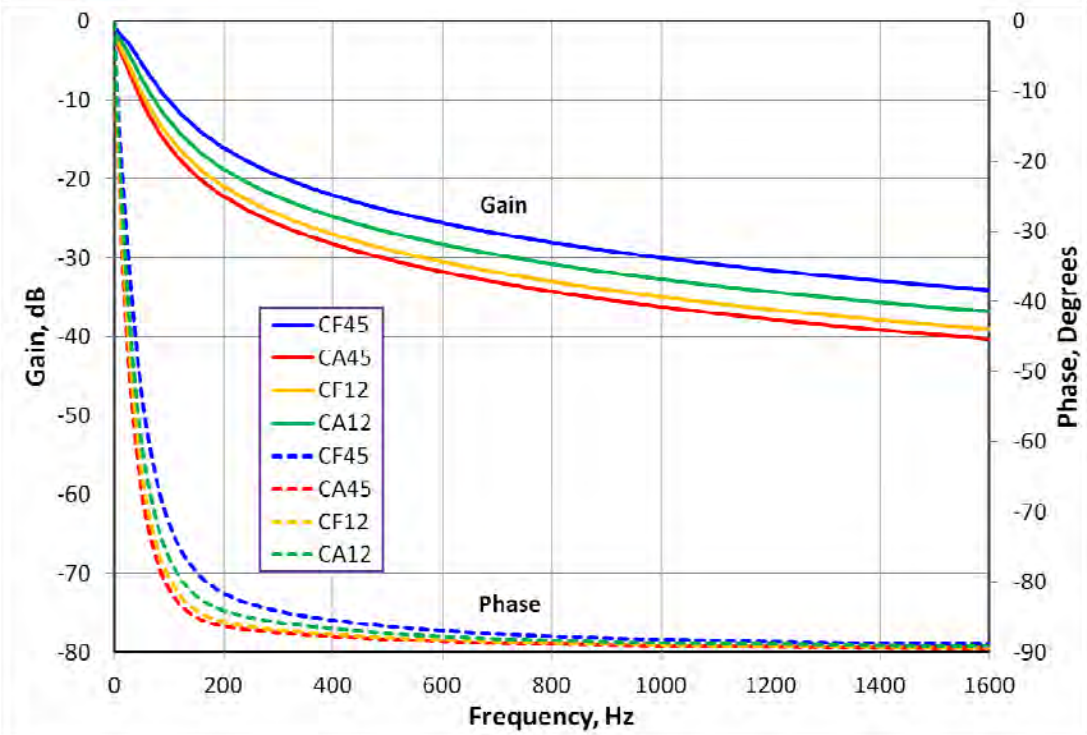

Figure 94. Small Wire Compensation Spectra for the Combustor Probes at 48 Percent.

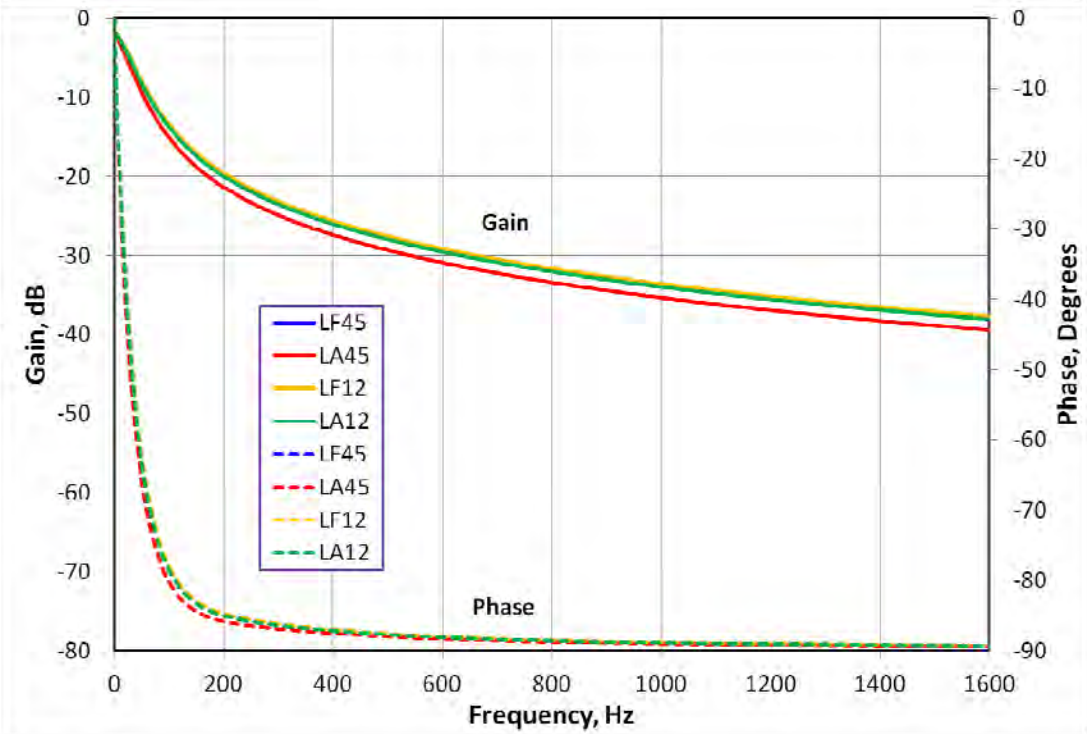

Figure 95. Small Wire Compensation Spectra for the Turbine Duct Probes at 48 Percent.

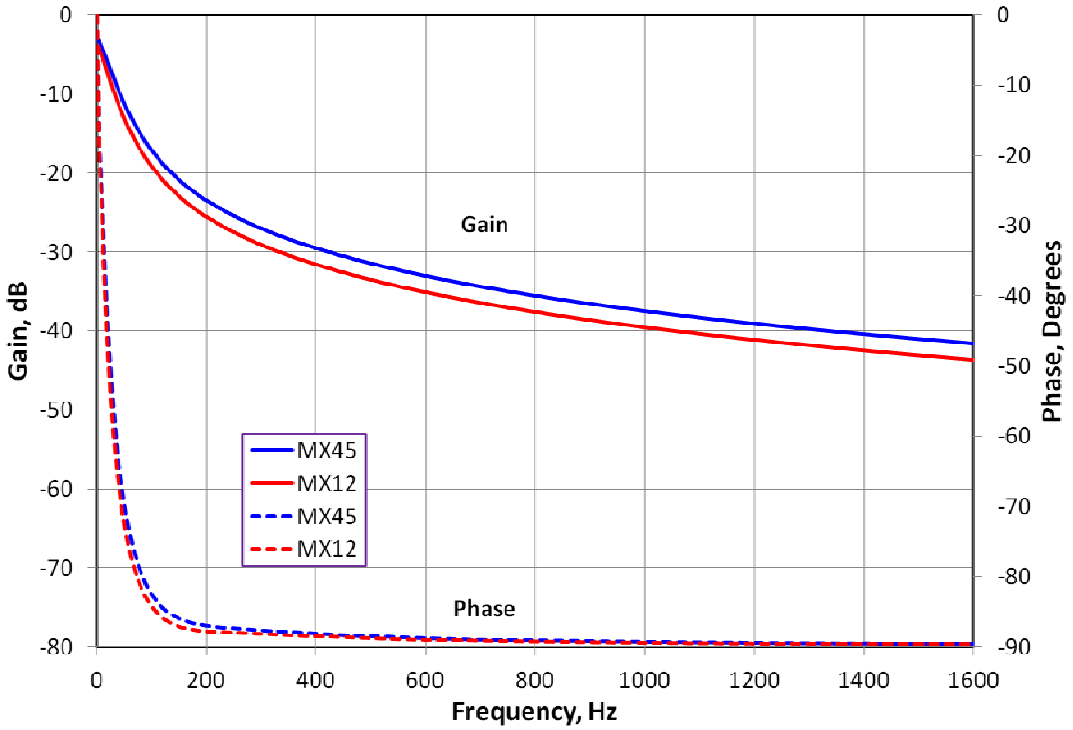

Figure 96. Small Wire Compensation Spectra for the Mixer Probes at 48 Percent.

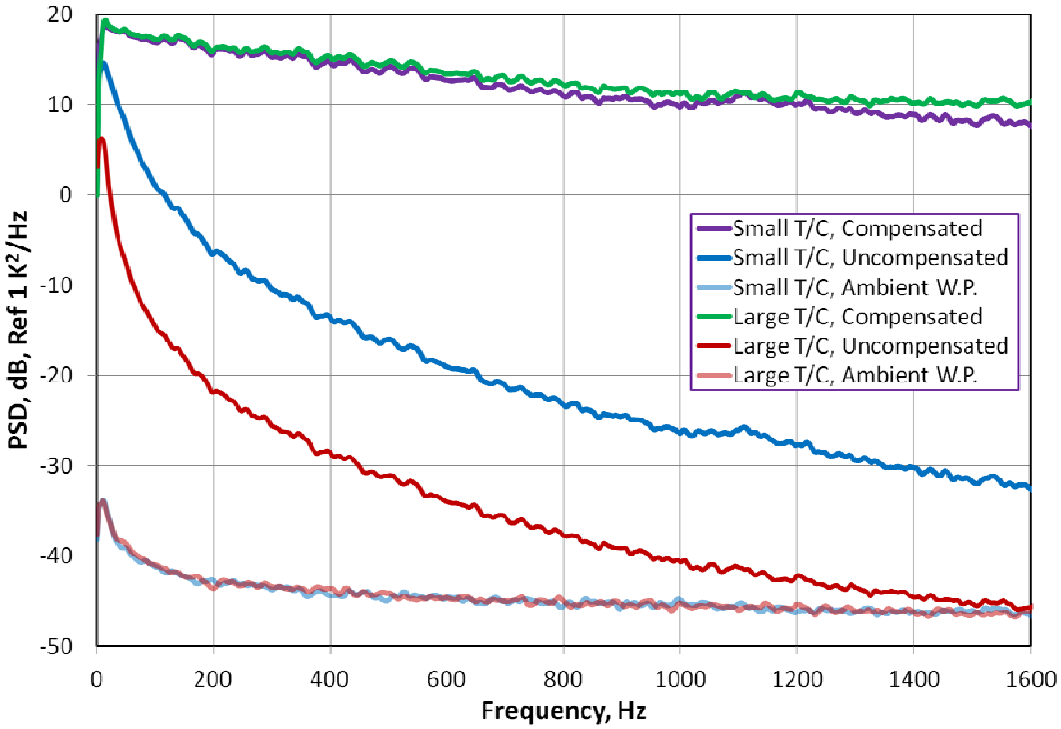

Figure 97. Small and Large Wire Compensated Spectra for the CA45 Probe at 48 Percent.

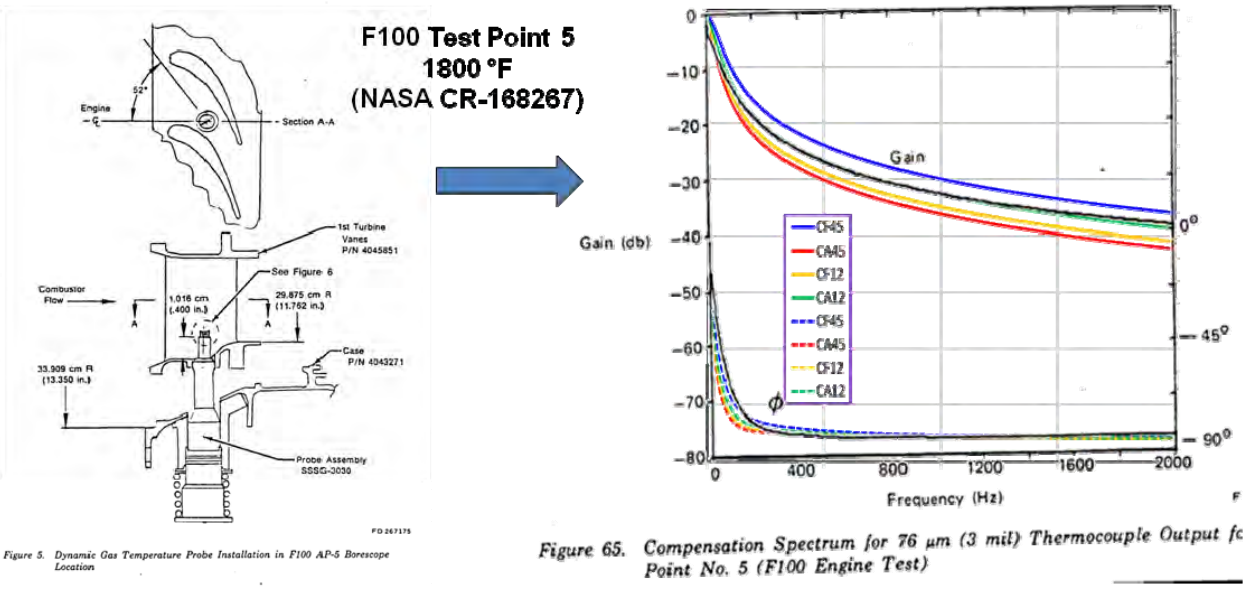

Figure 5. Dynamic Gas Temperature Probe Installation in F100 AP-5 Borescope Location

Figure 65. Compensation Spectrum for 76 μm (3 mil) Thermocouple Output fc Point No. 5 (F100 Engine Test)

Figure 98. Comparison of TECH977 and F100 Compensation Spectra.

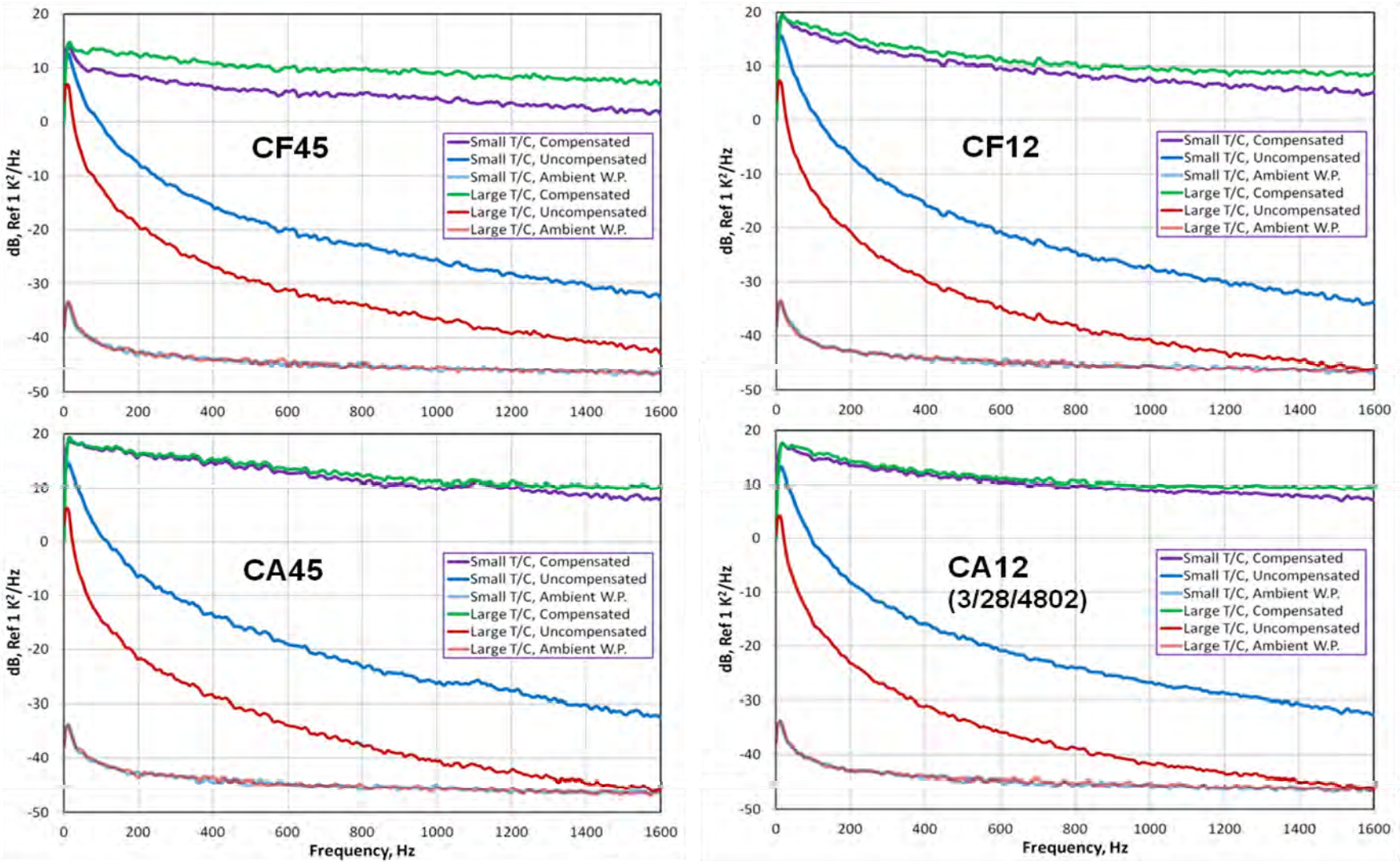

Figure 99. Small and Large Wire Compensated Spectra for the Combustor Probes at 48 Percent.

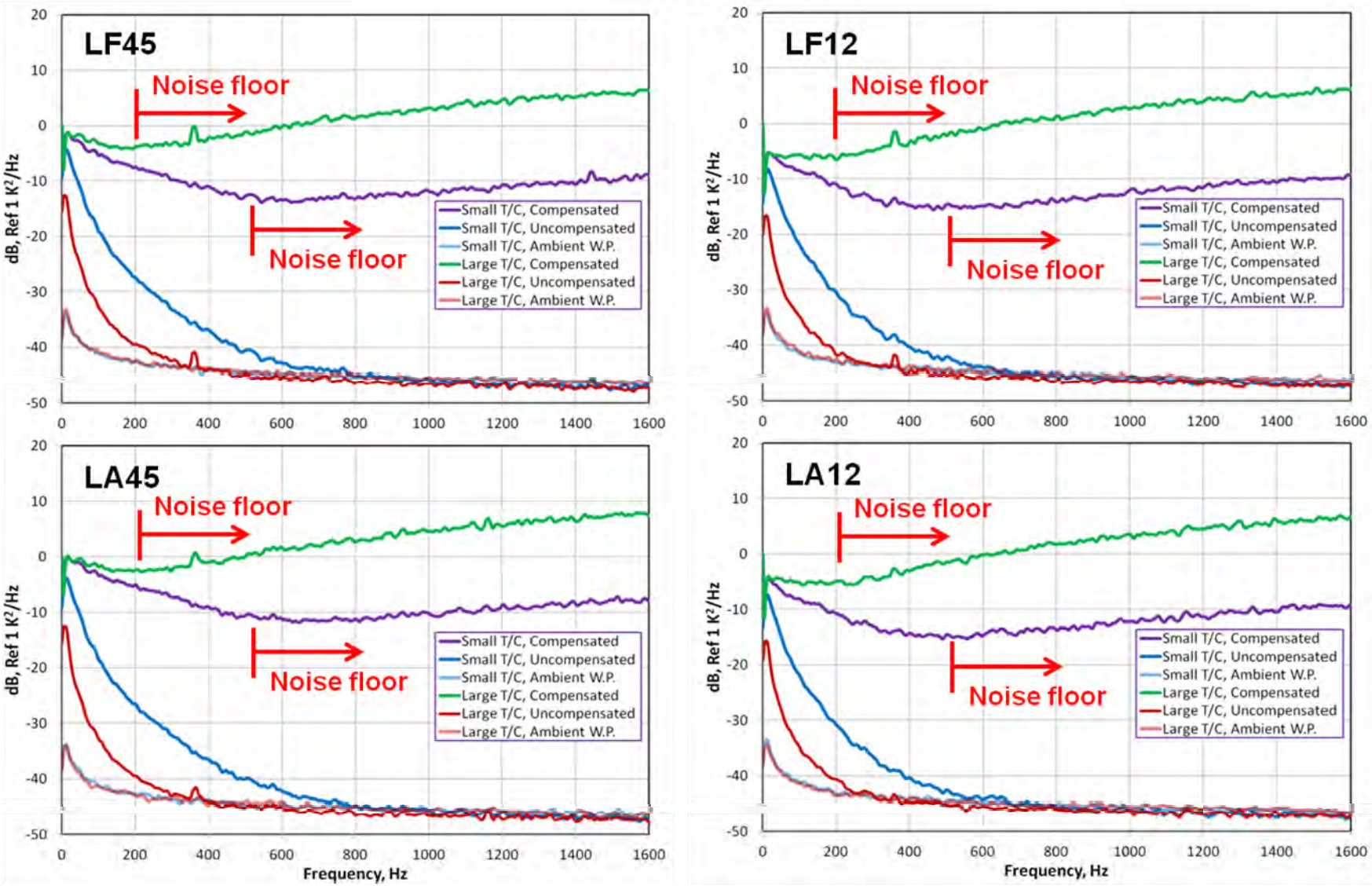

Figure 100. Small and Large Wire Compensated Spectra for the Inter-Turbine Duct Probes at 48 Percent.

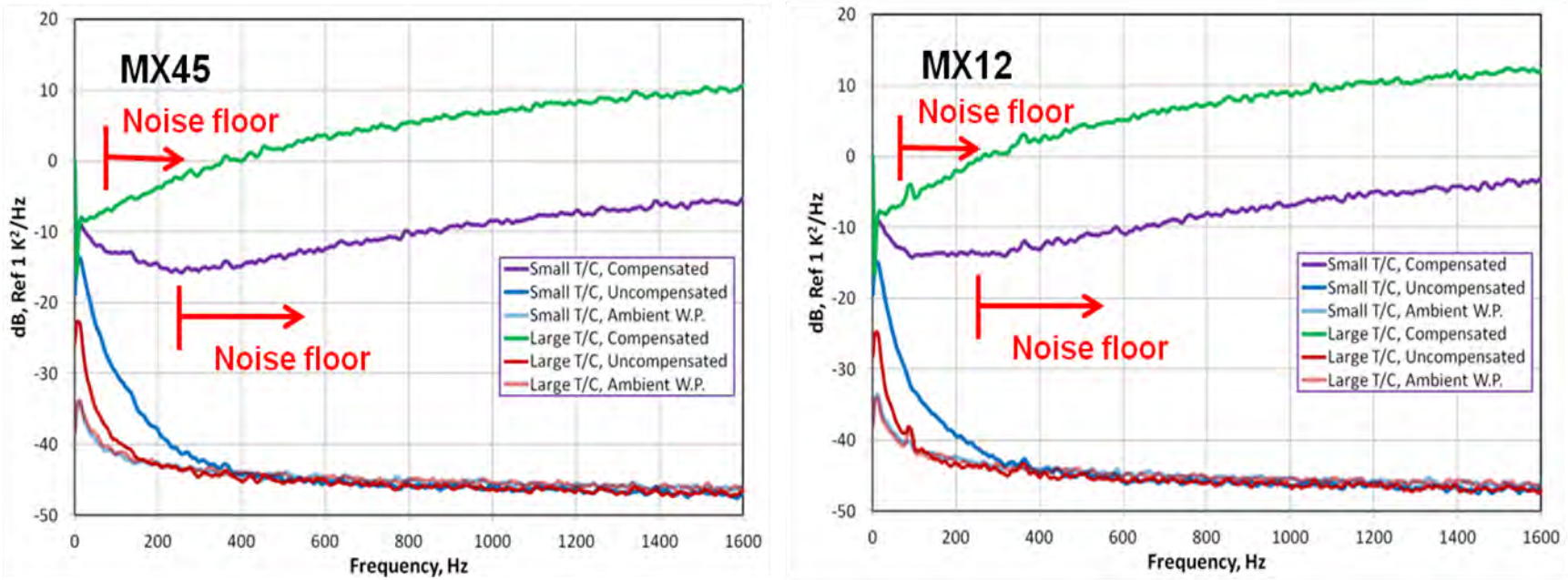

Figure 101. Small and Large Wire Compensated Spectra for the Mixer Probes at 48 Percent.

7.1.1.3 Compensated Time Histories

Compensated time histories – providing the estimate of the fluctuating temperature of the gas stream (up to the frequency range limits) – can be generated by applying the compensation spectra to the measured time history data in the frequency domain via complex division. The DGTMS code has some built-in functionality to create compensated time histories. Because of computer hardware limitations at the time the code was written, the compensated time histories are only generated one FFT block at a time. A full compensated time history could be generated by connecting the individual blocks, but it is time consuming and prone to discontinuities at the block boundaries.

An alternative approach is to compute a compensated time history in one shot by interpolating the compensation spectrum. Such a scheme works well because the compensation spectra are smooth and well behaved functions. The steps of the process are as follows:

1. Compute the FFT of the entire SW time history (one single block).

2. Interpolate the compensation spectrum to the same number of points in the FFT.

3. Apply the compensation spectrum via complex division in the frequency domain.

4. Take the inverse FFT to get back to the time domain.

Unlike the block-by-block process used in the DGTMS software, this approach does not apply a Hanning window to the data prior to taking the Fourier transform. Because the data sequence is very long, typically 0.5 million data points, the errors introduced by the discontinuity between the beginning and ending sample is negligible. The FFT assumes the sequence to be periodic over that time interval, and the Fourier components of the step discontinuity are smeared into the spectrum. However, with a long data sequence, the amplitude of these contributions is small compared to the frequency content in the (random) signal.

An important consideration when generating the time histories is that the compensation should not be applied to portions of the raw time history that are dominated by electrical noise. In the DGTMS code, the ITHRSH parameter is a user-selected relative threshold level that specifies the compensation limit. If there are frequency components with amplitudes below the threshold level, then the compensation is not applied and the amplitude of these frequency components is zeroed out. This parameter can be determined by comparing the uncompensated spectrum with the noise floor. An alternative approach is to only compensate the time history up to a certain frequency, so that the result becomes a band-limited compensated time history. Because it is pretty clear at what frequency the electronic noise floor is reached, this alternative approach was used.

The compensation process was applied in Matlab. The interpolation of the compensation spectrum was performed using the Matlab *interp1* function, and the forward and inverse discrete Fourier transforms were performed using the Matlab *fft* and *ifft* functions. As an example of the generation of the compensated time history, consider the time history data from the aft combustor probe at location 12 (CA12) for the 48 percent speed point, using the March 28 4802 test point data. The raw time histories of the probe are shown in Figure 102 after splitting into DC and AC components. The time history data appear to be of good quality (compare this to Figure 89, which had a data anomaly). Figure 103 compares the entire compensated time histories generated in two ways, (1) by applying the interpolated small wire compensation

spectrum to the small wire time history data, and (2) by applying the interpolated large wire compensation spectrum to the large wire time history data. It is apparent that the temperature fluctuations of the compensated time histories, which represent the fluctuating gas temperature, are substantially larger than the measured fluctuating wire temperatures. Fluctuations on the order of ±750°F are common. Furthermore, the small wire and large wire compensated time histories are very similar. Figure 104 shows this more clearly by plotting a close-up of the time histories over a short time span of 0.1 second.

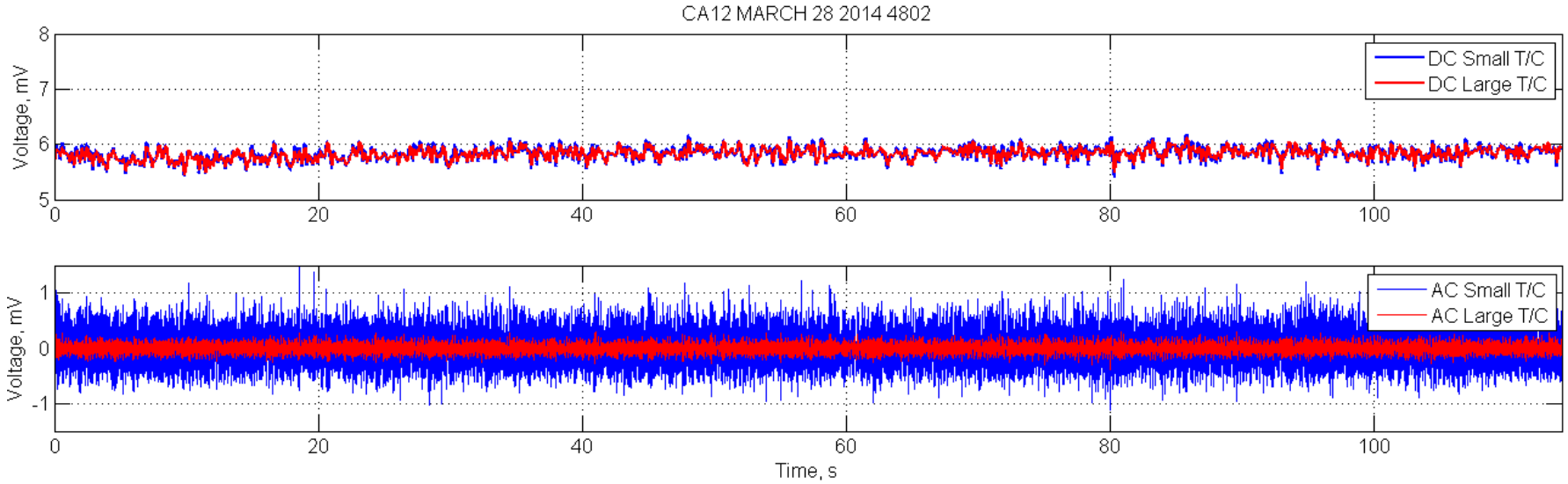

Figure 102. Uncompensated DC (Top) and AC (Bottom) Time History Data for Combustor Probe CA12 at 48 Percent.

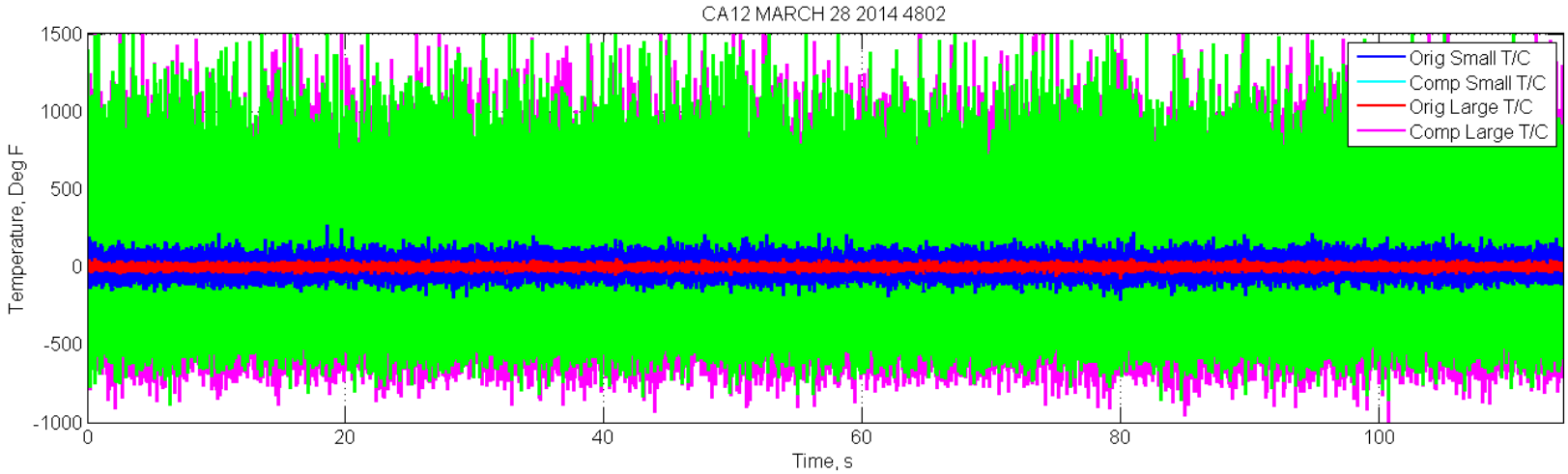

Figure 103. Small Wire and Large Wire Compensated Time Histories for Combustor Probe CA12 at 48 Percent.

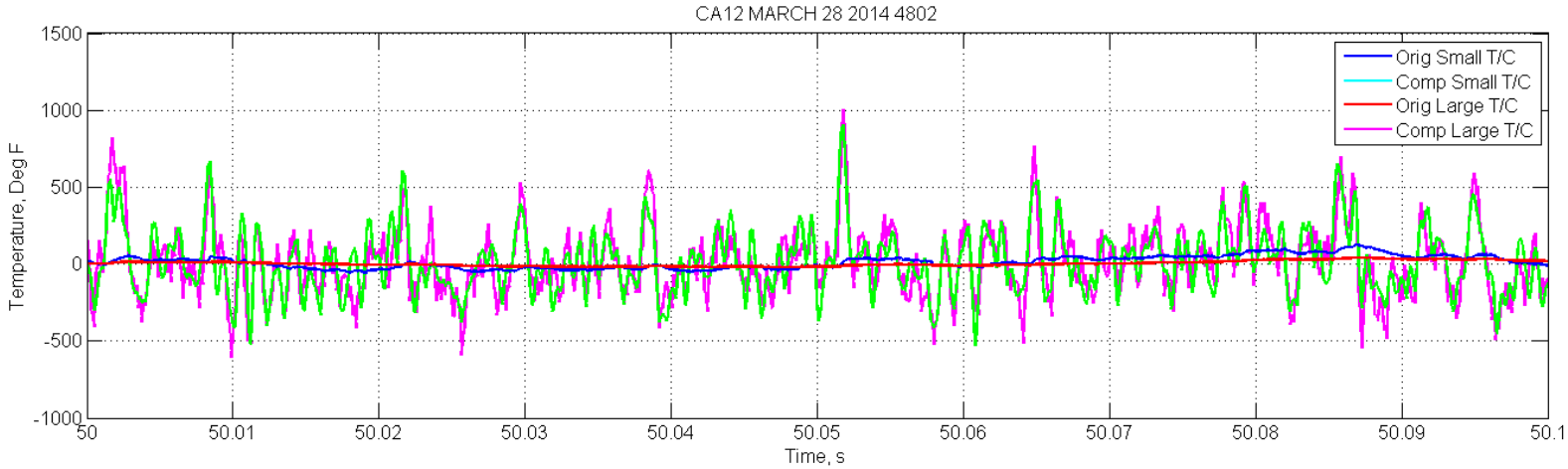

Figure 104. Close-Up of Small and Large Wire Compensated Time History Data for Combustor Probe CA12 at 48 Percent.

7.1.2 Unsteady Pressure Data Processing

7.1.2.1 Data Review and Quality Assessment

The internal dynamic pressure data was acquired using Kulite model XTE190-10D transducers. These are 10 psi differential piezoresistive transducers with a nominal sensitivity of 10.0 mV/psi. They have been extensively used at Honeywell for measuring internal engine dynamic pressures. The differential style provides excellent signal-to-noise characteristics, but requires that the sensors be supplied with a mean reference pressure that is close to the pressure in the environment being measured. As previously mentioned, the transducers were installed into tees and used with semi-infinite coils due to the high temperatures in the measurement environment. A very small nitrogen purge flow was also blown through the coils to keep the transducers cool, even though they are located outside of the engine compartments in this particular test. Signal conditioning was provided by a rack of Sonoran Microsystems amplifier modules.

Two important data quality assessments are signal-to-noise ratio and the impact of purge flow. The plots within the figure are labeled using a naming convention where P is pressure, E is EVNERT, C is combustor, A is aft, F is forward, L is inter-turbine duct, MX is mixer and the numbers refer to the clocking pattern defined through Figure 77. Figure 105 shows a comparison of the electronic noise floor with the engine off, the noise floor when the engine is off and the purge flow is on, and the noise levels measured at the 48 percent speed point, for the 13 Kulites and 2 external microphones. The electronic noise floor is at least 20 dB below the measured noise levels when the engine is running. When the purge flow is turned on, there is an increase in ambient noise, particularly for the Kulites in the combustor (which may have had a higher velocity purge flow), but the ambient noise is still at least 20 dB below the measured noise levels when the engine is running. Thus, there is no concern regarding either electronic noise or noise associated with the purge flow. It should be mentioned that the purge flow does change somewhat over the range of tested engine speeds, but the delta-pressure between the supply manifold and the reference manifold tends to decrease with speed, so that the noise associated with the purge flow system should also decrease slightly with increasing engine speed.

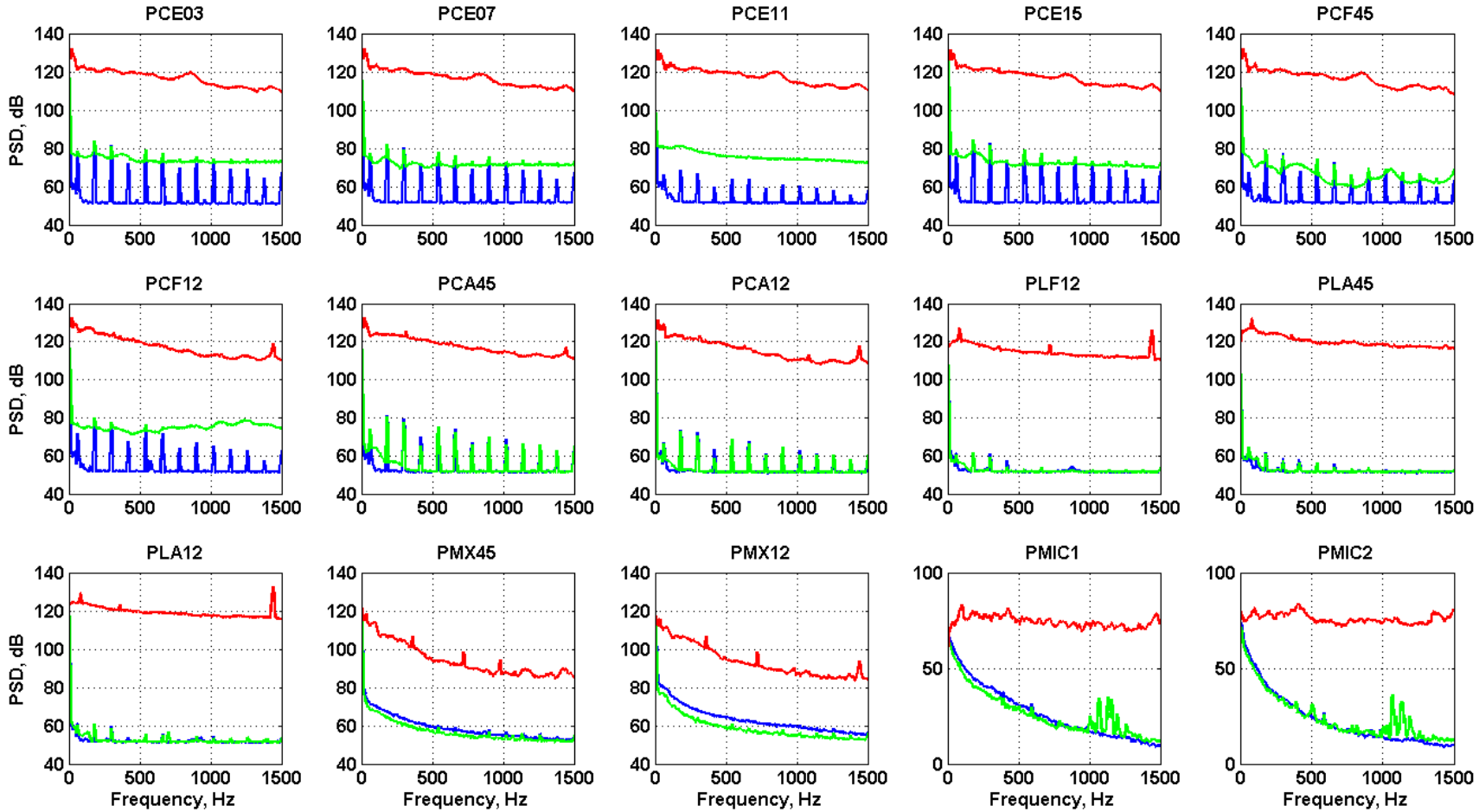

Figure 105. A Comparison of the Noise Floor of the Dynamic Pressure Transducers, With and Without Purge Flow.

7.1.2.2 Power Spectral Density Spectra

Power spectral density spectra were created from the dynamic pressure time histories for all of the 13 Kulite sensors and the two external microphones, for all engine operating conditions. PSD spectra for the 48 percent, 54 percent, 60 percent, and 65 percent operating speeds are shown in Figure 106, Figure 107, Figure 108, and Figure 109, respectively. The spectra for PCE03, PCE07, PCE11, and PCE15 are tightly grouped and nearly overlay one another. This is not surprising, as these sensors, which comprise the four-sensor sub-array from the 2007 NASA EVNERT test, are all located at the same axial position on the combustor. In the EVNERT test, the dynamic pressure spectra in the combustor array were very similar.

The spectrum for PCF45 is very similar to the four sub-array sensors. This is also not surprising, as this sensor is located nearly at the same axial location (recall the PCF45 temperature probe – and it accompanying pressure probe – is the most forward temperature probe in the combustor). The PCA45 and PCA12 pressure spectra have similar spectral shapes, and the amplitudes are fairly close, but they don't overlay each other as well as one might expect for sensors that are at the same axial station. The PCA12 pressure spectrum often has the lowest amplitude of all the combustor sensors at high frequency (1000 Hz). The PCF12 pressure spectrum is most similar to the PCA45 and PCA12 spectra.

The PLA12 and PLA45 pressure probes have fairly similar spectra, and have the highest amplitudes at high frequency. Interestingly, the PLF12 pressure probe has a similar spectral shape but is a good 5 dB lower in amplitude than the PLA12 and PLA45 probes. The reason for this difference in amplitude is not known. There is no probe in a corresponding forward location at the opposite side, since the PLF45 pressure line was used as a reference pressure tap for the turbine purge flow system (a separate reference pressure tap had not been incorporated on the turbine case). Furthermore, the PLF12 spectrum often has a lower amplitude at 400 Hz than any of the combustor probes.

The spectra of the two mixer probes, PMX45 and PMX12, are very similar to one another but have substantially lower amplitudes than the combustor and turbine sensors. Comparing the spectra across different engine speeds, these conclusions generally persist, with some exceptions. The most notable change with higher engine speed is a gradual increase in spectral amplitudes for all of the sensors.

Comparing the combustor and turbine spectra, it is difficult to make an argument for the presence of indirect noise. For example, there is not a frequency range where the turbine pressure spectra all show a large increase over the combustor pressure spectra, as one might expect if substantial indirect noise was generated downstream of the high pressure turbine. However, this viewpoint might be overly simplistic. A portion of the indirect combustion noise could propagate forward into the combustor, confusing the picture. A solid argument for the presence or absence of indirect combustion noise will need to rely on more sophisticated analyses.

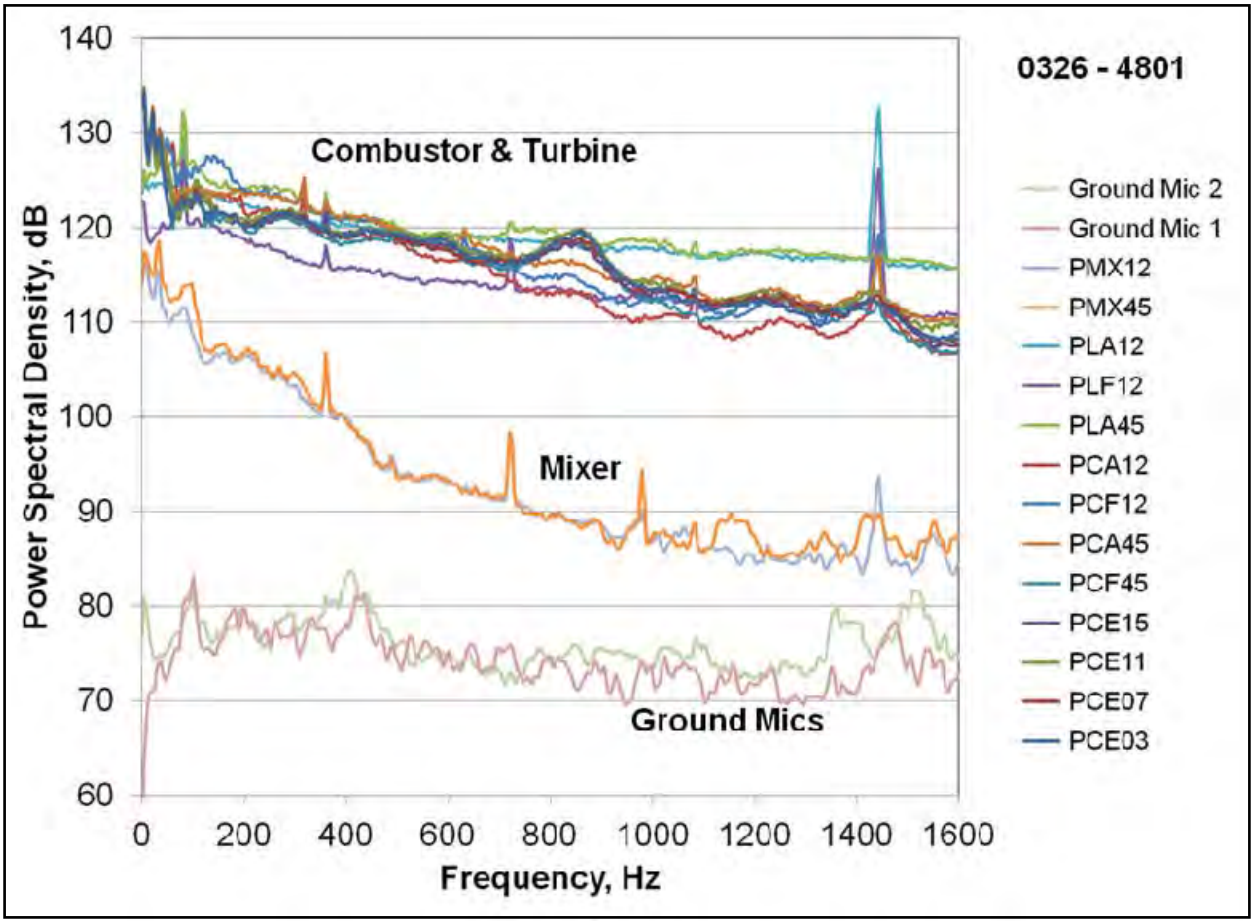

Figure 106. Dynamic Pressure Spectra at 48 Percent Speed From Data Collected March 26.

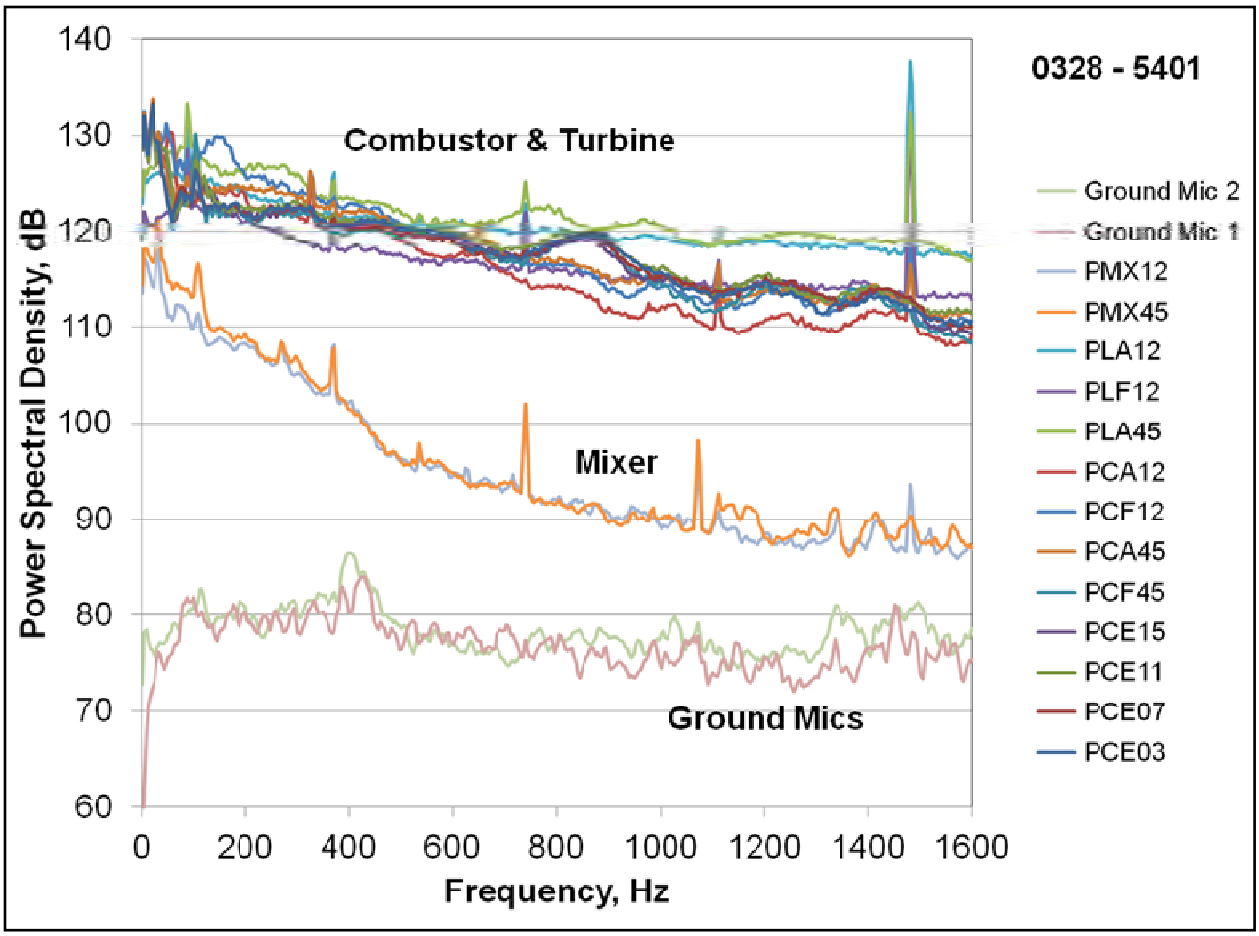

Figure 107. Dynamic Pressure Spectra at 54 Percent Speed From Data Collected March 28.

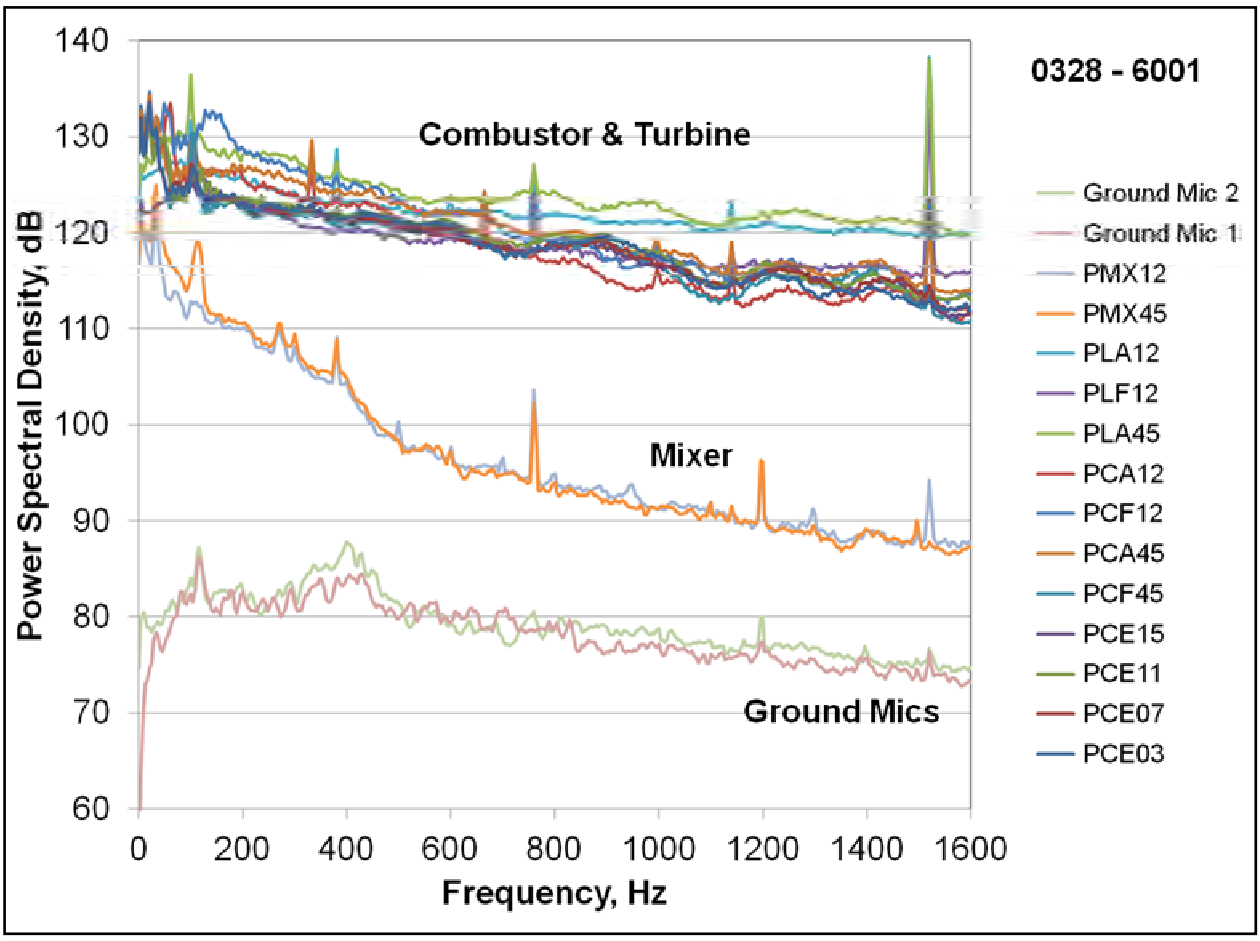

Figure 108. Dynamic Pressure Spectra at 60 Percent Speed From Data Collected March 26.

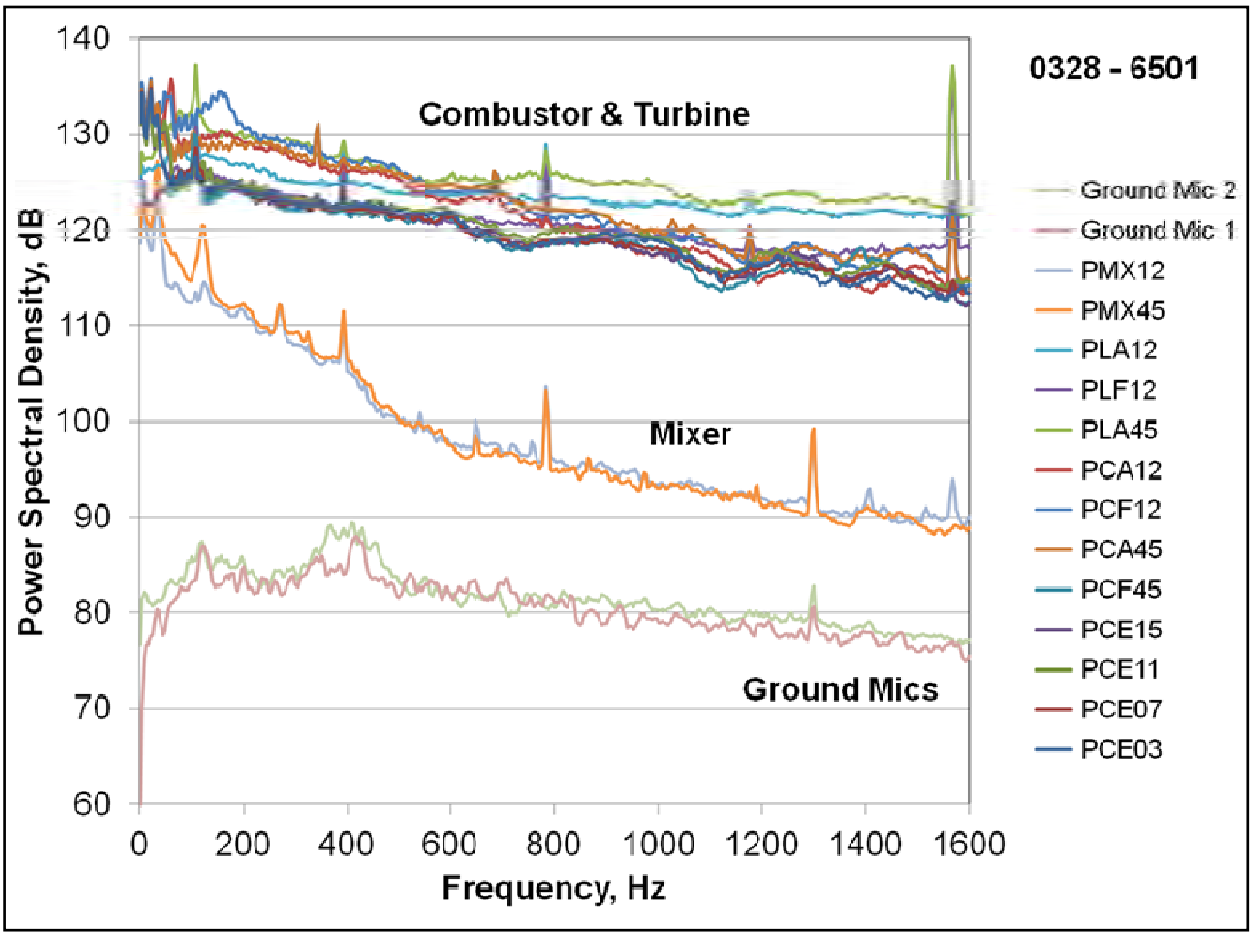

Figure 109. Dynamic Pressure Spectra at 65 Percent Speed From Data Collected March 28.

7.1.2.3 Phase-Corrected Pressure Time Histories

Phase-corrected pressure time histories were generated which correspond to the dynamic pressure that would have been measured at the tip of the sensing tube. That is, when using semi-infinite probes, there is a propagation delay due to the time that it takes the pressure signal to propagate up the length of tubing, from the engine duct wall to the Kulite location in the tee. To compute the time delay, the length of the sensing line tube and the sound speed in the tube must be known. The length of the sensing line was a constant 35.875-inch for all of the Kulite probes (the semi-infinite coils where the sound is attenuated were 40 feet long). Nitrogen purge flow was used in the combustor and turbine pressure probes to prevent hot gases from being compressed into the tubes during engine operation. As a result, the temperature and thus sound speed in those sensing lines is expected to be quite uniform. Purge flow was not required for the mixer probes, since the mean pressures and temperatures were much lower. Half of the Kulite tees were instrumented with thermocouples to measure the temperature of the gas in sensing tubes. The thermocouples were positioned just slightly beyond the Kulite tap location, on the semi-infinite coil side of the tee.

Figure 110 shows the Kulite tee temperatures measured during the testing on March 26. Most of the thermocouples registered nearly the same temperature. Furthermore, the temperatures

were not very sensitive to changes in engine operating condition. On this particular day, the temperatures were typically 76°F. The temperatures were only measured at a single point, so the temperature distribution throughout the three foot length of the sensing tubes as they snaked around the engine case and into the engine core is not known. For this analysis, it was assumed that the temperature in the tube was uniform over its entire length. At a temperature of 76°F, the sound speed in the sensing line is 1134 ft/s and there will be a time delay of 2.64 ms for the acoustic wave to propagate from the end of the sensing line (tapped flush to the outer wall of the engine core duct) to the Kulite location. Figure 111 and Figure 112 show the Kulite tee temperatures measured during the testing on March 28. Aside from the CE15 probe, all of the tee temperatures were nearly the same. The temperature was around 62°F for the first engine run and 72°F for the second engine run, corresponding to time delays of approximately 2.67 ms and 2.65 ms, respectively. These propagation time delays are summarized in Table 11.

Table 11. Propagation Time Delays Assumed for Kulite Pressure Signals.

Test Date	Assumed Time Delay, ms
03/26/2014	2.64
03/28/2014 First Engine Run	2.67
03/28/2014 Second Engine Run	2.65

The purge flow temperature measured in the CE15 tee (labeled TKCE15 in the figures) appears to be an outlier. It is not known why the thermocouple in the CE15 tee was reading higher than the others, but this tee was close to the engine, near the cutout in the bypass duct, where warm secondary flow (used for cooling the engine core) was escaping from the seals around the cutout and impinging on the tee. It is possible that the tee housing was simply heated by this impinging air, and that the thermocouple was in turn heated via conduction, leading to an erroneous reading. On the other hand, it is possible that the purge flow in the tube was also heated and that the reading is accurate. In order to decide whether special treatment is needed for this sensing line, the following analysis procedure was considered.

Since the CE15 pressure probe is part of the sub-array in the forward part of the combustor, it is possible to inspect the cross-spectral phase between the probes in this sub-array and infer whether there are substantial differences in the temperatures (sound speeds) of the purge flow inside the sensing tubes. The sensing tubes in this array are equally spaced and have equal length. As will be shown in the next section, certain acoustic modes are dominant in the combustor over certain frequency ranges, and as a result there is a well defined phase relationship between the signals measured at different locations. For example, the plane wave is dominant below 500 Hz. So if the purge flow temperatures (sound speeds) inside the sensing lines are all the same, then the signals measured by the Kulites will all be in phase and the cross-spectral phase will be zero for all pairs of Kulites. On the other hand, if the temperatures inside these tubes are substantially different, then the cross spectral phase will be non-zero, with a difference that increases linearly with frequency.

Consider the data from March 26 at the 60 percent speed point, where the CE15 Kulite tee temperature read 120°F, corresponding to a time delay of 2.53 ms, and the CE11 Kulite tee temperature read 78°F, corresponding to a time delay of 2.63 ms. If the probes are sensing the same plane wave pressure field (dominant up to 500 Hz), and if the temperature readings are accurate, then there should be a time delay difference of 0.1 ms between the CE11 and CE15 signals, corresponding to a phase difference of 18 degrees at 500 Hz (the phase difference being a linear function of frequency).

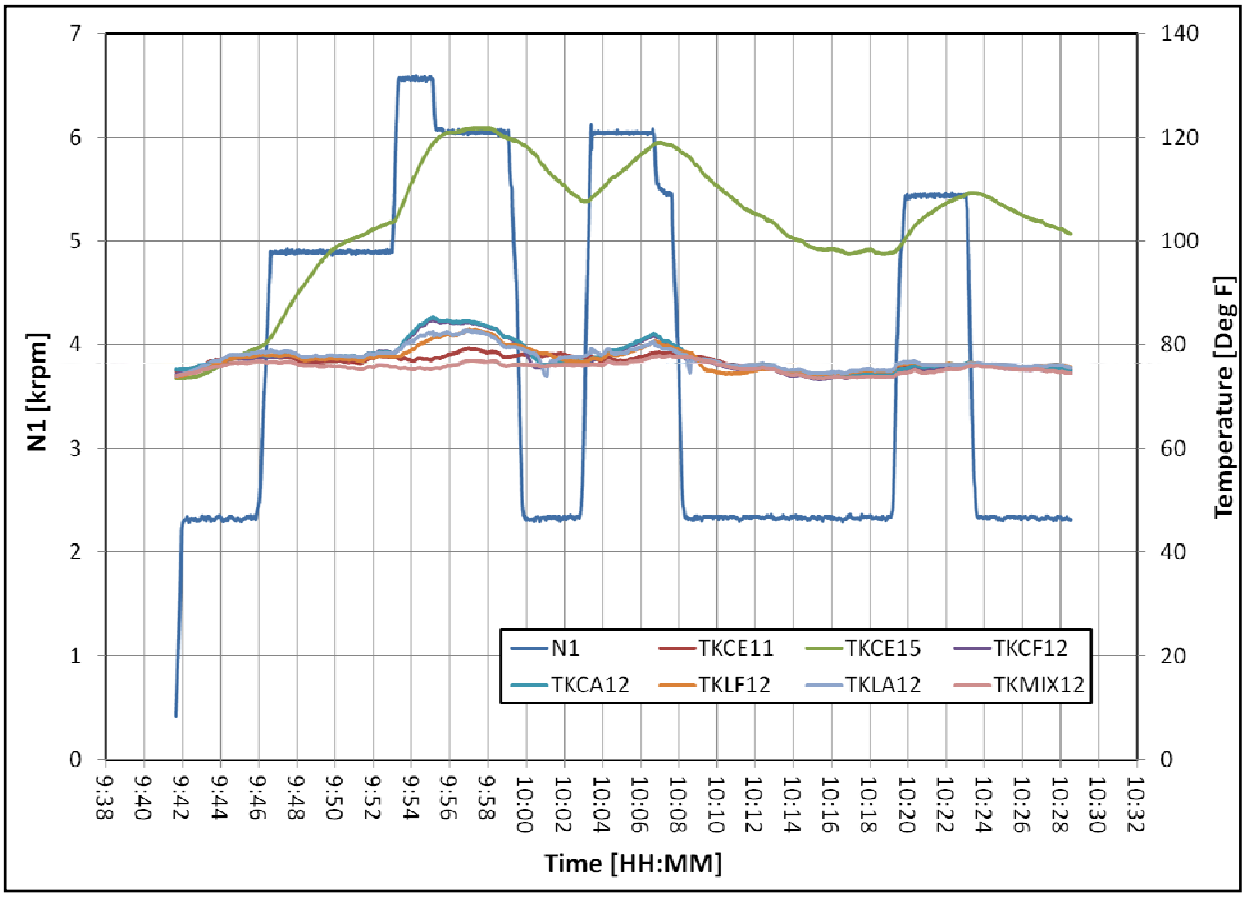

Figure 110. Purge Flow Temperatures Measured During the March 26 Test.

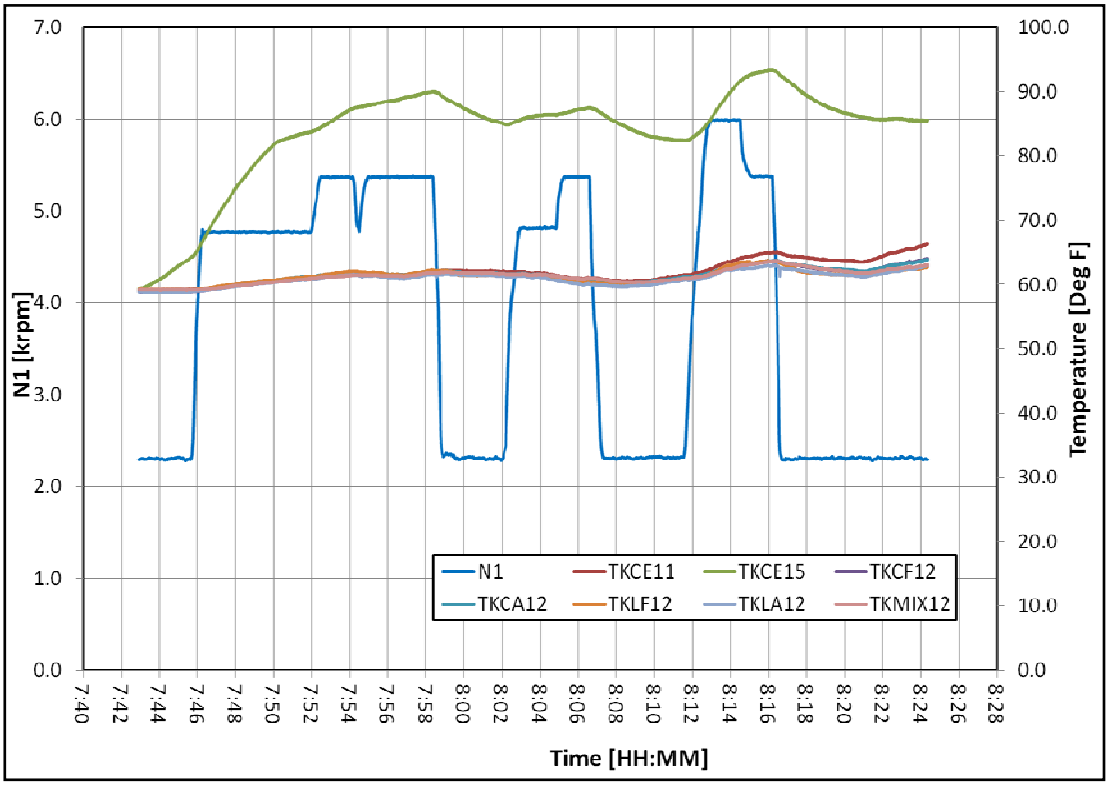

Figure 111. Purge Flow Temperatures Measured During the March 28 Test.

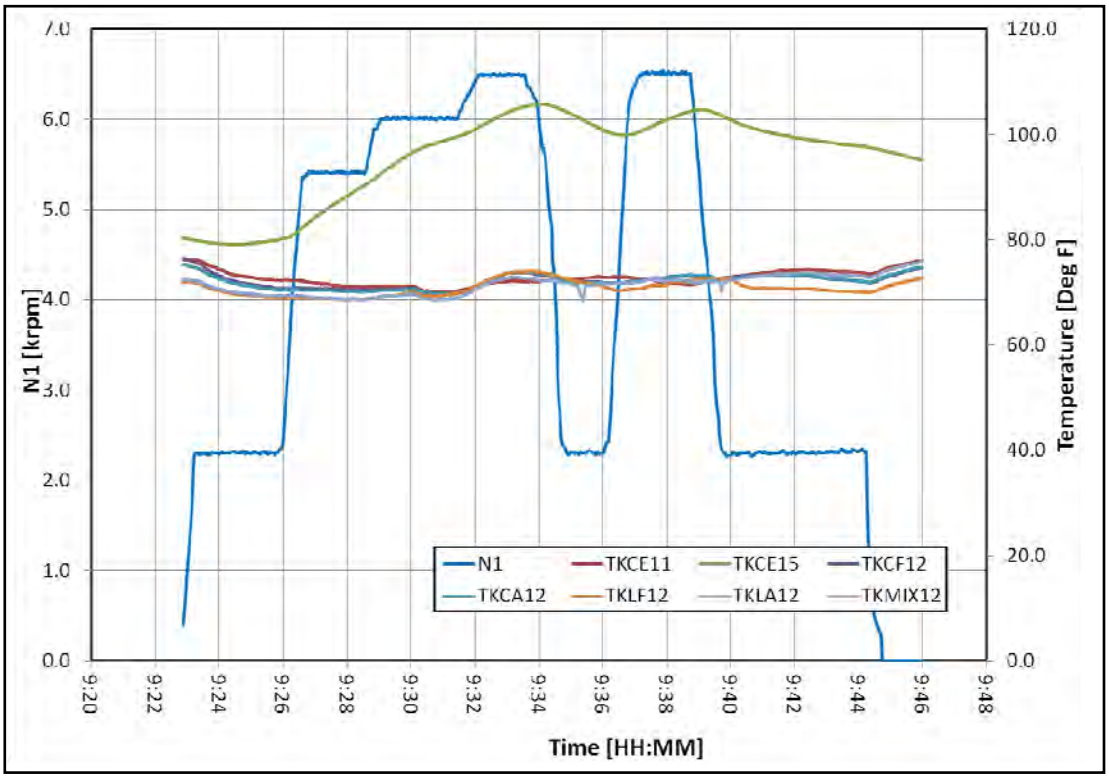

Figure 112. Purge Flow Temperatures Measured During the March 28 Test (Continued).

Figure 113 shows the phase of the cross spectrum for different combinations of probes in the combustor sub-array. The phase has been plotted only for those frequencies where the coherence between the same two channels, shown in Figure 114, is greater than 0.05. There does appear to be a very slight phase shift associated with the CE15 signal, as indicated by the slight negative slope of the phase involving the CE15 signals. However, the slope of approximately -0.02°/Hz is about half of that associated with a 0.1 ms time delay (-0.04°/Hz). Therefore, it is concluded that there may have been some heating of the CE15 purge flow, but not as much as indicated by the measured temperature. The CE15 signal appears to have, at worst, a 0.05 ms shorter time delay than the other probes in the sub-array. For the analyses considered here, and for the frequency range of interest (< 1000 Hz), there appears to be little error in assuming a constant time delay for all of the probes in the combustor, and further, all of the pressure probes in the engine. Therefore, a common time delay correction was used for all of the Kulite probes, differing slightly by test time, as summarized in Table 11.

As a point of comparison, Figure 115 shows the cross-spectral phase for the same combinations of sensors from the EVNERT program, References 8 and 9, Run Without Fan test, for coherence values above 0.05. It appears that in the EVNERT test there may have been slightly larger tube-to-tube variations in purge flow temperature, even though all of the sensing tube lengths in that combustor array were only 12 inches long.

There are additional effects related to the propagation of acoustic waves in the tube that have not been accounted for. There is a frequency dependent attenuation that occurs in the sensing line due to viscous dissipation. The reduction in amplitude has not been quantified, but is considered to be small over the frequency range of interest in this program (<1000 Hz). Also, in order to route the sensing tubes outside the engine, there are numerous bends in the tubes. These bends were made to be as gradual as possible so as not to create an impedance discontinuity. There impact of these bends is considered to be small over the frequency range of interest, but a precise quantification of the effects has not been made.

Phase-corrected pressure time histories were generated to be consistent with the compensated temperature time histories. These pressure time histories were created as follows. First, the time delays were determined using the measured tee temperatures and known length of tubing, as summarized in Table 11. Next, a sequence of “delayed” times was constructed at the same sample rate as the original pressure data. The pressure data was then interpolated to these new delay times using the Matlab *interp1* function. The first sample of interpolated pressure data corresponds to the same physical time as the first sample of temperature data, as if the pressure measurement had been made directly at the wall. The interpolated pressure signals were then resampled at a frequency of 8192 Hz using the Matlab *resample* function, and then high pass filtered using the Matlab *filtfilt* function, with the first and last $1/8^{th}$ second clipped off to be consistent with the processing of the dynamic temperature data. The net result of the correction is that the pressure time histories which are resampled to 8192 Hz are shifted by about 22 samples in order to align the pressure data with the temperature data. For some analyses, this time delay does not have a substantial impact. For example, the time delay results in a loss of coherence between pressure and temperature, but with a 4 Hz analysis bandwidth, the reduction in coherence is quite small.

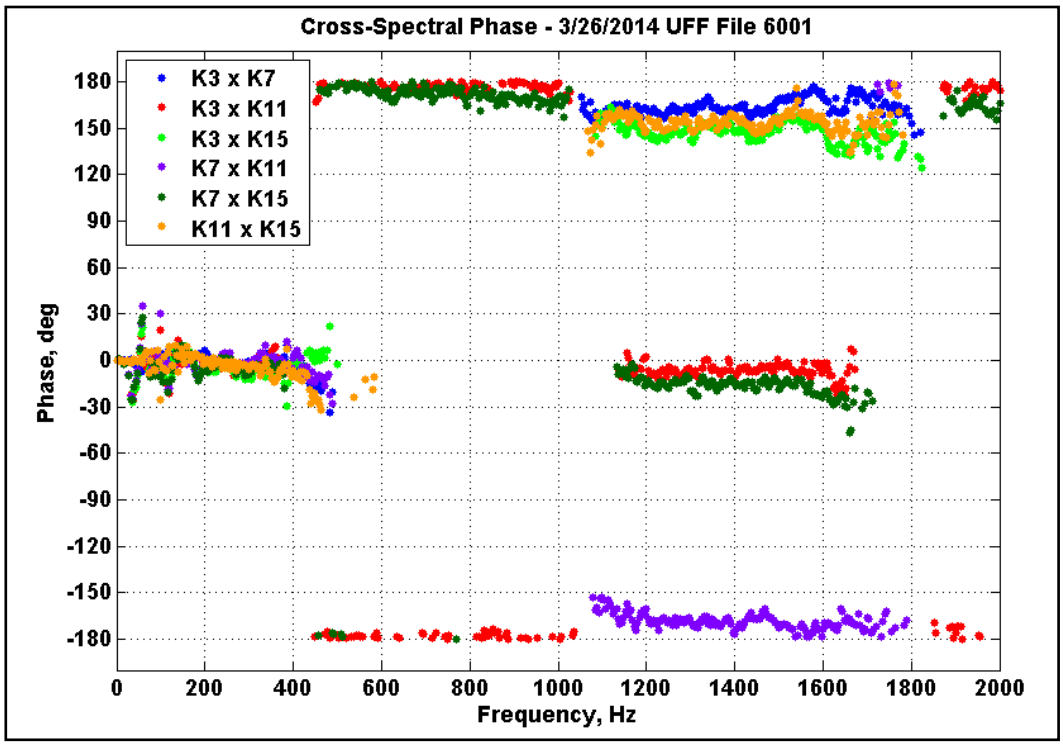

Figure 113. Cross-Spectral Phase Between Pressure Probes in the Combustor Sub-Array, at 60 Percent Speed, for Coherence Values above 0.05.

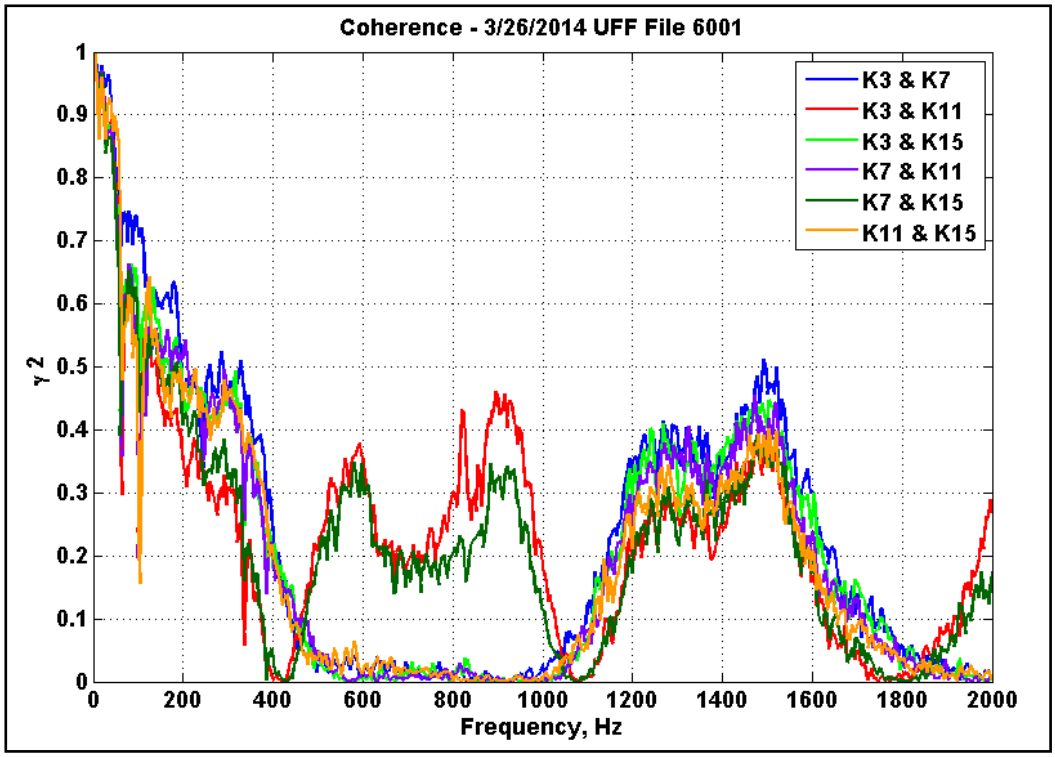

Figure 114. Coherence Between Pressure Probes in the Combustor Sub-Array at 60 Percent Speed.

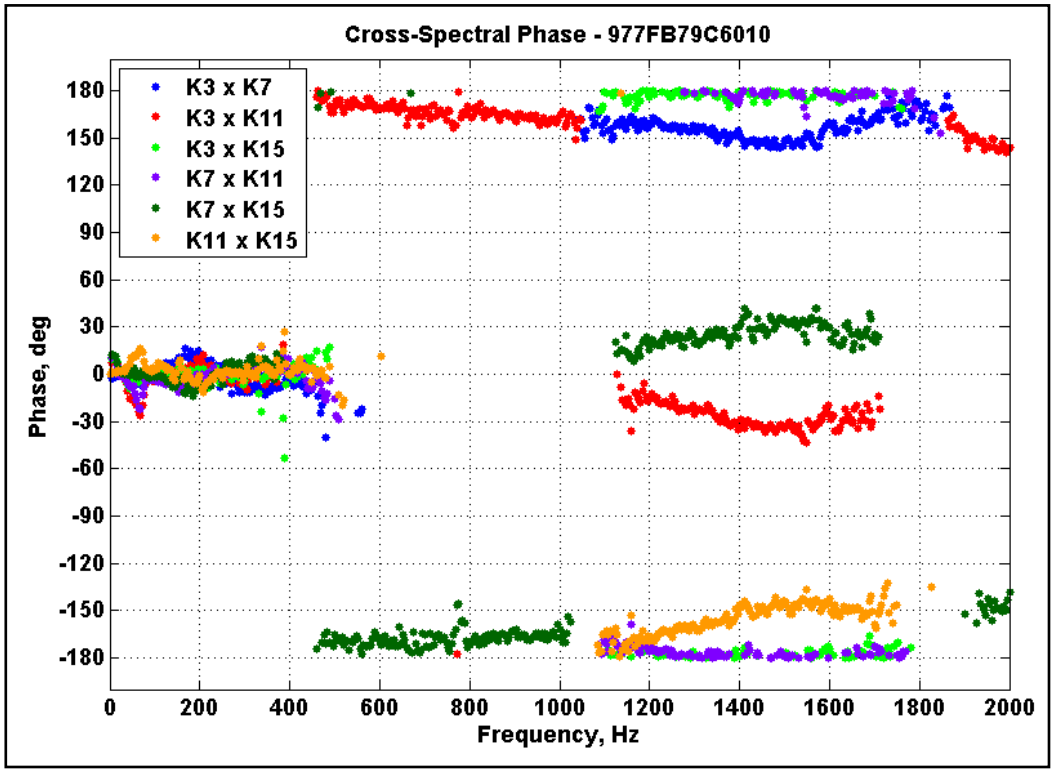

Figure 115. Cross-Spectral Phase for Combinations of Pressure Signals in the Combustor Sub-Array, at 60 Percent Speed, from the EVNERT Run Without Fan Test.

7.2 Task 5.2: Acoustic Modal Analysis

7.2.1 Combustor Circumferential Mode Decomposition

A circumferential mode decomposition of the upstream 4-microphone combustor array was performed. As a background, during the Run Without Fan work element of the 2007 NASA EVNERT program, the TECH977 was instrumented with an array of 16 equally-spaced dynamic pressure sensors, in the form a semi-infinite coils using a 12-inch sensing line. The ends of the pressure sensing lines were flush with the outer wall of the combustor, and were oriented azimuthally at the same angular positions as the 16 fuel nozzles. Details of the testing and analysis results can be found in References 8 and 9. For the DGMTS test, measurements were made using a subset of this array to provide a comparative reference to the previous dataset. An array of four equally spaced sensors was used. Figure 116 shows a comparison between the locations of the probes that were used in the 2007 EVNERT test and the 2014 DGTMS test. The biggest difference in the instrumentation setup between the two tests was that the sensing lines used in the DGTMS test were three times longer than the EVNERT test. Figure 117 compares the noise spectra at the four common locations for the two tests, at the 48 percent speed condition. Figure 118 compares the noise spectra at the four common locations at 60 percent speed. Overall, there is a good match in the shapes and amplitudes of the noise spectra measured in the two tests.

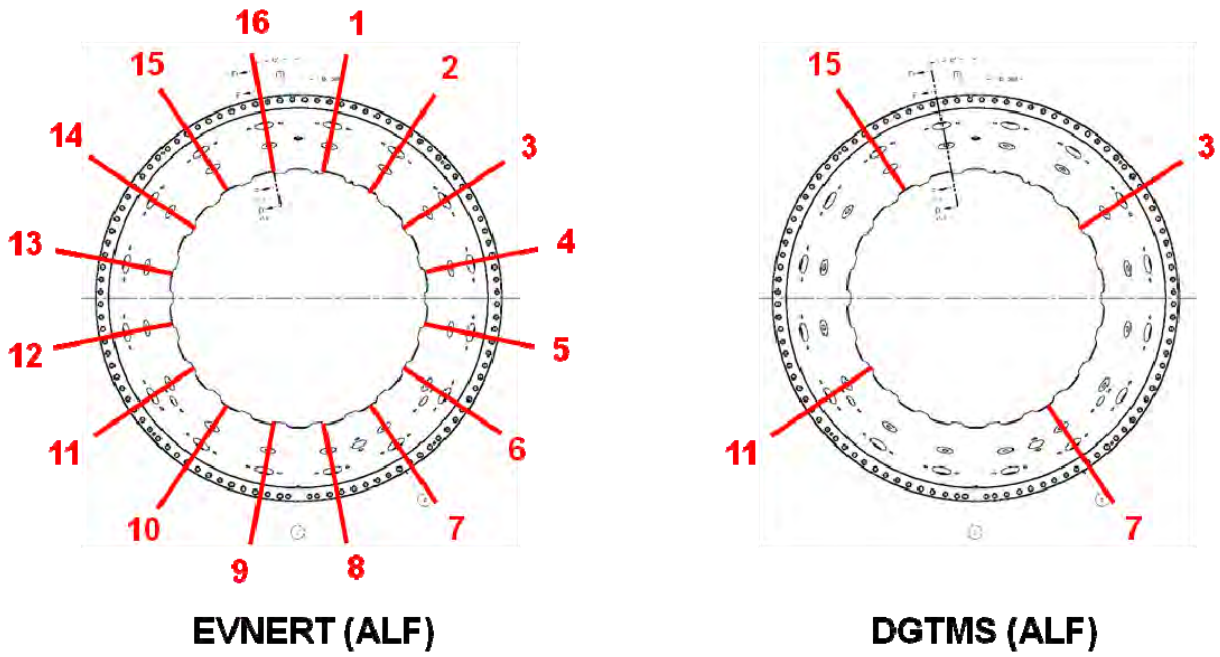

Figure 116. Kulite Probe Locations for the Combustor Circumferential Mode Array.

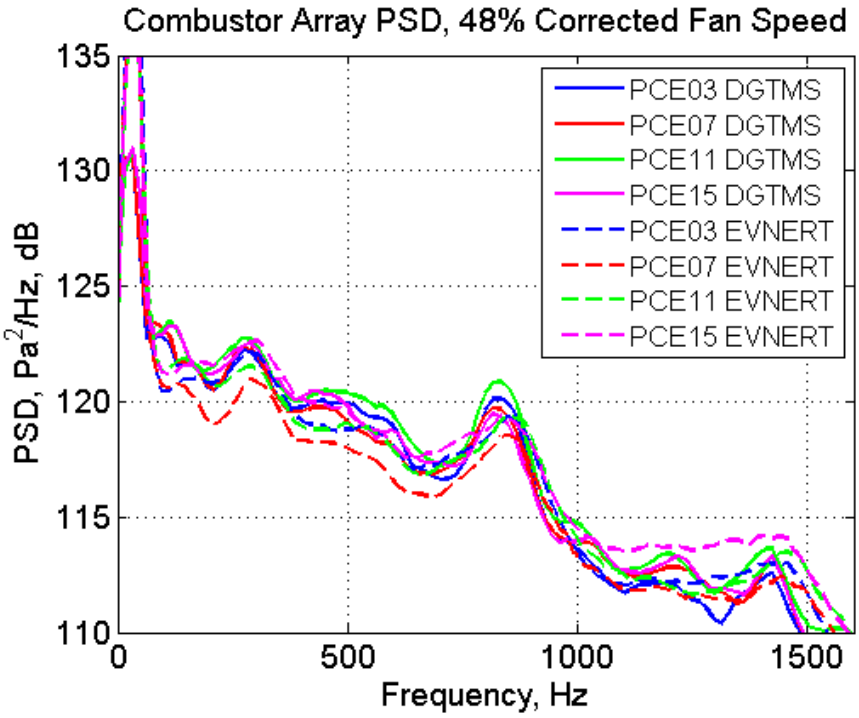

Figure 117. Comparison of Combustor Noise Spectra With Previous Measurements at 48 Percent Speed.

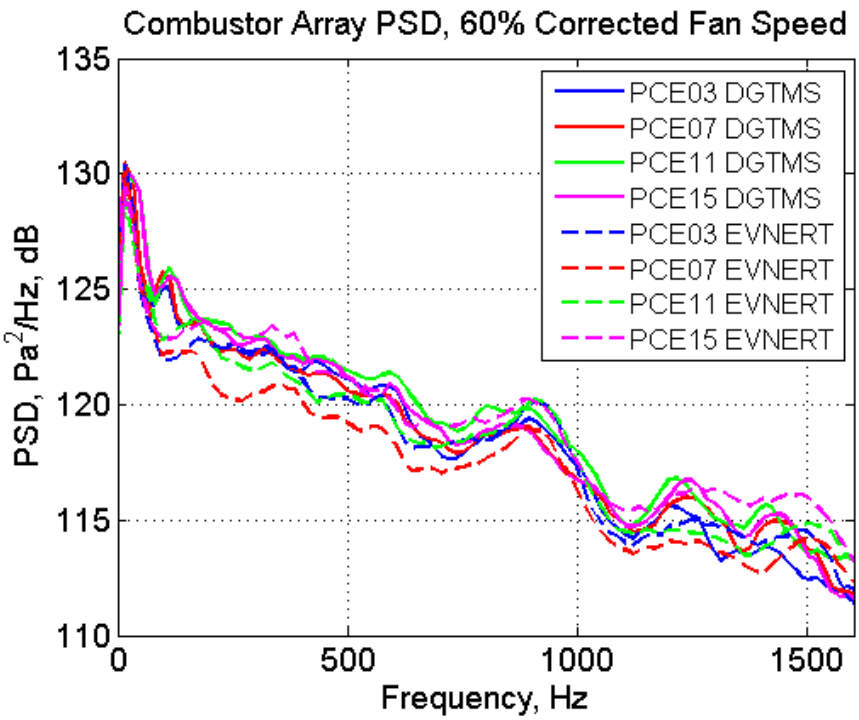

Figure 118. Comparison of Combustor Noise Spectra With Previous Measurements at 60 Percent Speed.

The modal structure of the sound field in the combustor was explored in References 8 and 9. When using a finite number of transducers, there is a limit to the number of modes that can be uniquely identified. Mode aliasing will occur if the number of sensors is too small. Figure 119 shows what happens to the mode decomposition when the 4-sensor array is used instead of the full 16-sensor array, using the NASA EVNERT measurements at 48 percent speed. With an array of 16 sensors, the modes can be fully distinguished to a frequency well beyond 3 kHz. However, when only four sensors are used, mode aliasing occurs. Above 1000 Hz, the 16-sensor analysis shows the m=-2 and m=2 modes are present with roughly equal amplitude. With a 4-sensor array, these two modes are aliased to the same mode analysis bin, and cannot be distinguished. Above 2000 Hz, the 16-sensor analysis shows that the m=-3 and m=3 modes are present with roughly equal amplitude. In the 4-sensor analysis, the m=-3 mode is aliased to the m=+1 bin, and the m=+3 mode is aliased to the m=-1 bin. Although the two modes are distinguished from one another, the mode orders have been aliased. Figure 120 and Figure 121 shows the same comparison at 54 percent speed and 60 percent speed (the 65 percent speed point was not tested in the EVNERT Run Without Fan test). The modal plots and conclusions are nearly the same. One can conclude that below 1000 Hz, the m=0 mode, m=-1, and m=1 modes can be resolved without aliasing.

Next, a comparison is made between the EVNERT test data and the DGTMS test data. A side-by-side comparison of the 4-sensor modal decomposition results at 48 percent speed is presented in Figure 122. A similar comparison at 54 percent and 60 percent speed are presented in Figure 123 and Figure 124, respectively. Visually, the results for the two tests are extremely similar, both in terms of the modal content and the amplitudes of the modes. This is to be expected, since the same engine core was used in both tests (although the rest of the engine setups were quite different).

A closer inspection of the comparison at these three speeds is presented in Figure 125 through Figure 127, where the modal decomposition results have been rotated at an angle to highlight subtle differences. Comparing the two, the DGTMS modal amplitudes appear to be nearly the same as the EVNERT modal amplitudes, but with an additional amplitude modulation. The frequency of this amplitude modulation appears to be near 200 Hz. The reason for this difference is not known, but the combustor in the DGTMS test has additional holes to accommodate the extra temperature and pressure instrumentation. It can be determined that the undulation is not due to the presence of the temperature probes in the combustor. Figure 128 shows a comparison at 48 percent speed with the temperature probes retracted and deployed, and no difference is seen in the modal decomposition.

The individual pressure spectra for the four probes for 48 percent, 54 percent, and 60 percent speed are compared in Figure 129 through Figure 131. There is very good agreement in the individual spectral amplitudes between the two tests, with the exception that the DGTMS data shows additional undulations. Also noteworthy is that the Kulite tees for the PCE11 and PCE15 sensors were instrumented with thermocouples (which protrude slightly into the flowpath), whereas the PCE03 and PCE07 sensors did not. There is no noticeable qualitative difference in the spectra between tubes that have thermocouples and the tubes that don't. This suggests that the thermocouples installed into the Kulite tees have a negligible influence on the noise propagation in the tube.

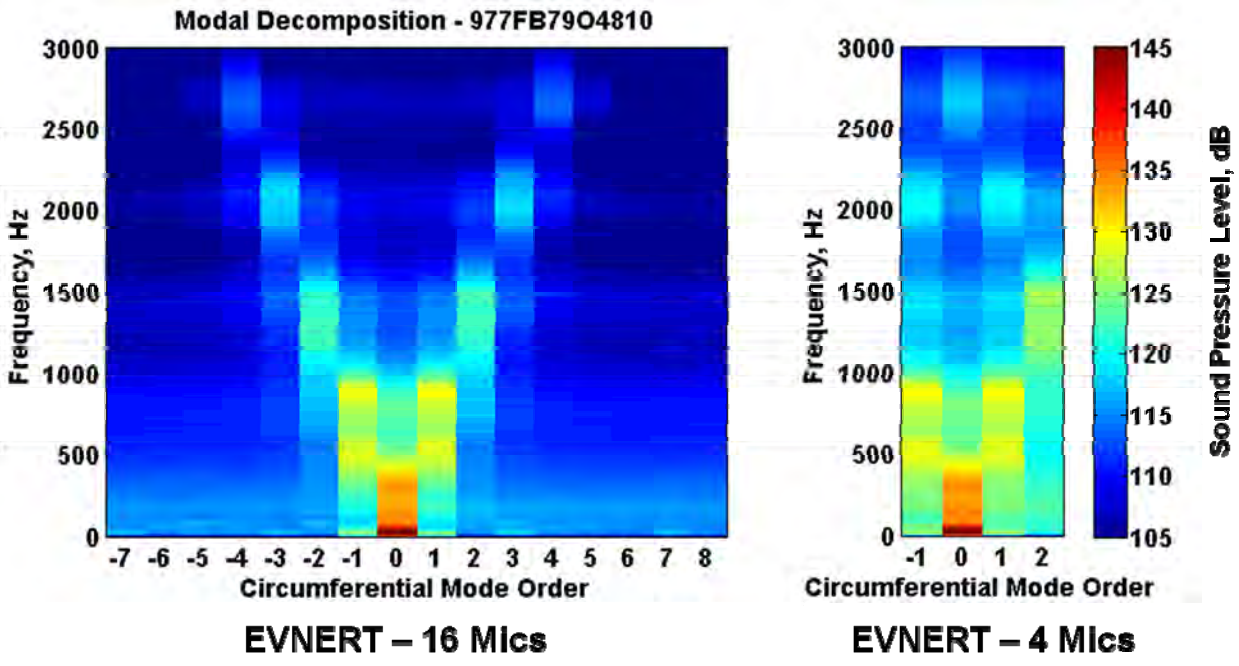

Figure 119. Mode Aliasing With a Reduced Number of Sensors at 48 Percent.

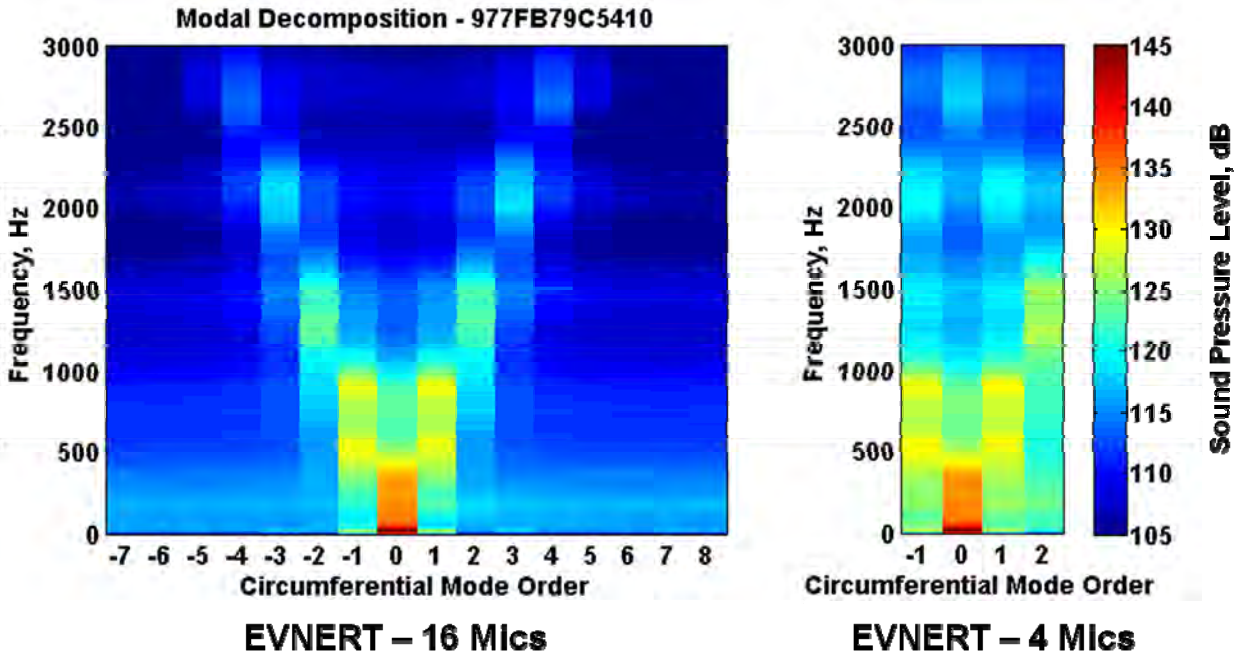

Figure 120. Mode Aliasing With a Reduced Number of Sensors at 54 Percent.

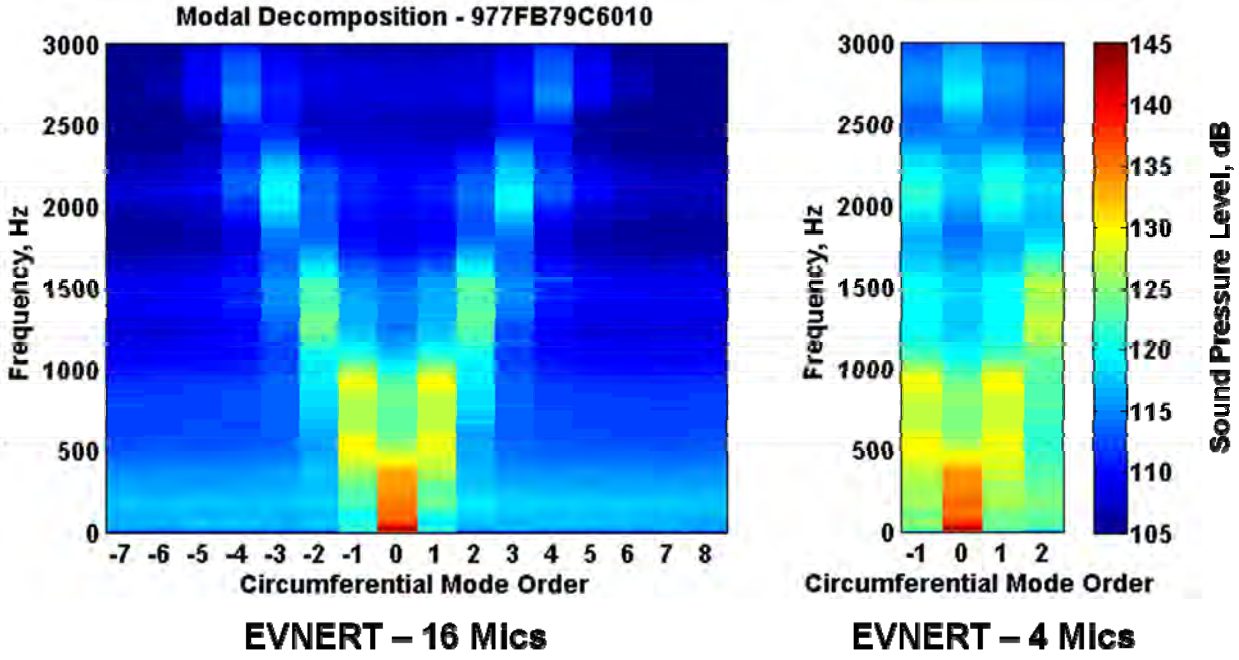

Figure 121. Mode Aliasing With a Reduced Number of Sensors at 60 Percent.

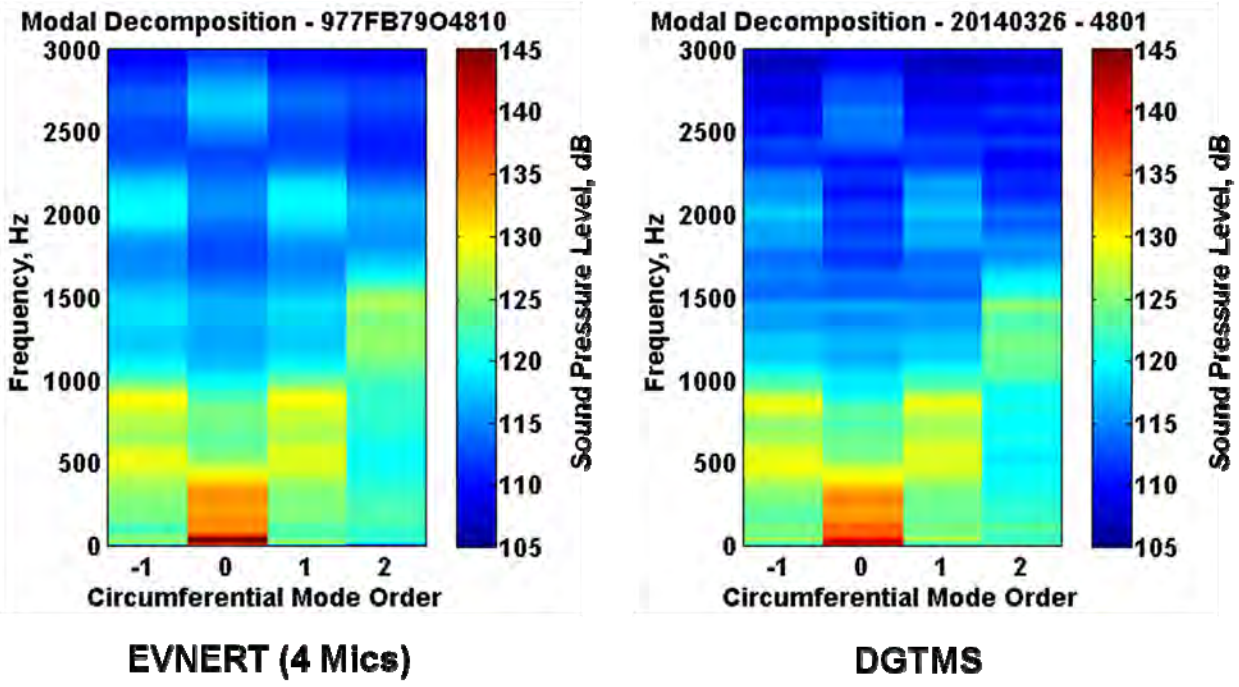

Figure 122. Comparison of Modal Decomposition Results at 48 Percent Speed.

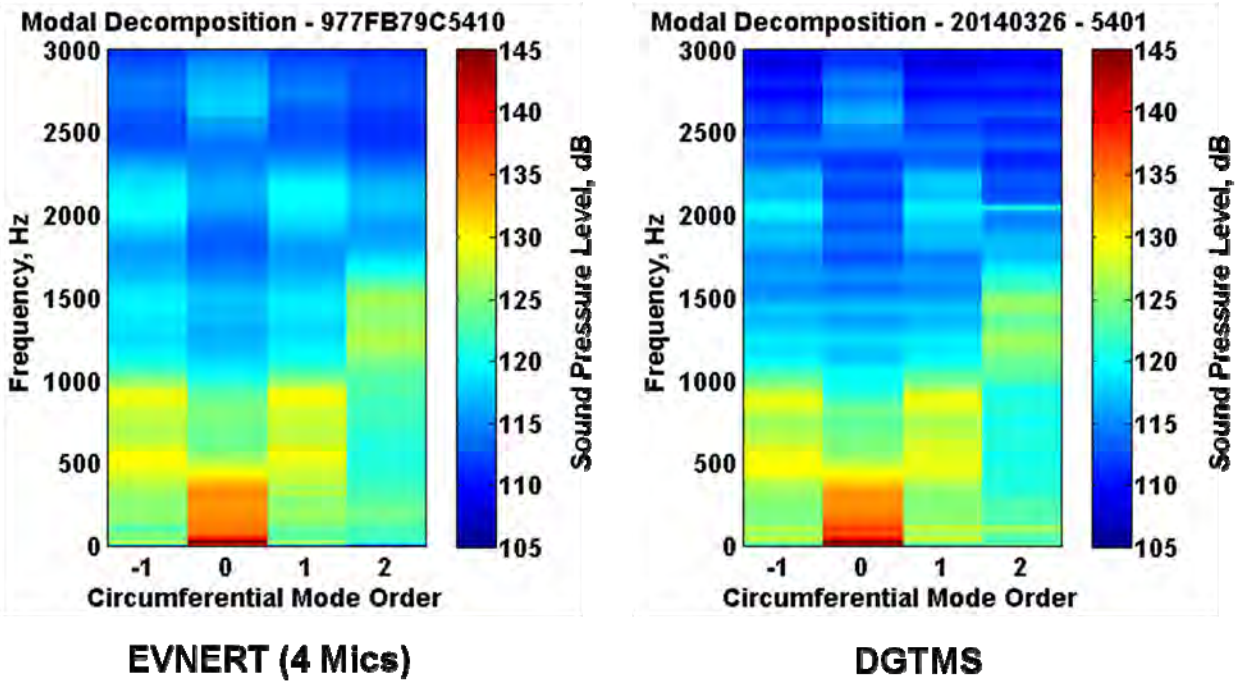

Figure 123. Comparison of Modal Decomposition Results at 54 Percent Speed.

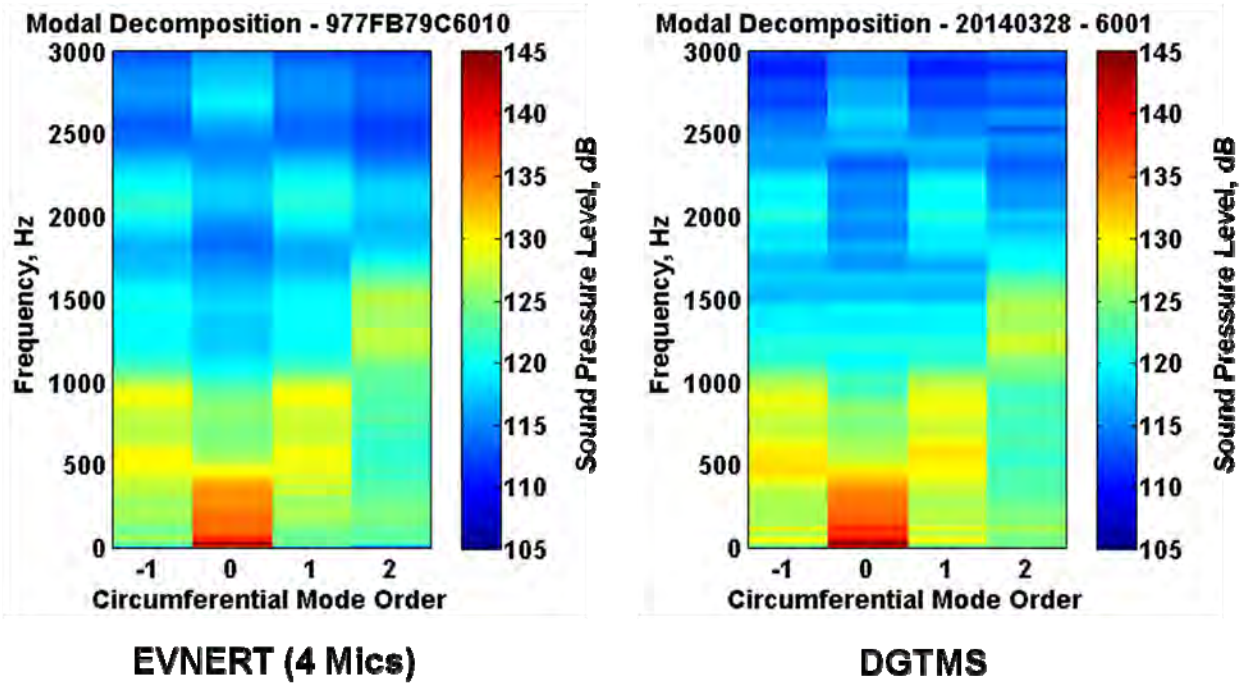

Figure 124. Comparison of Modal Decomposition Results at 60 Percent Speed.

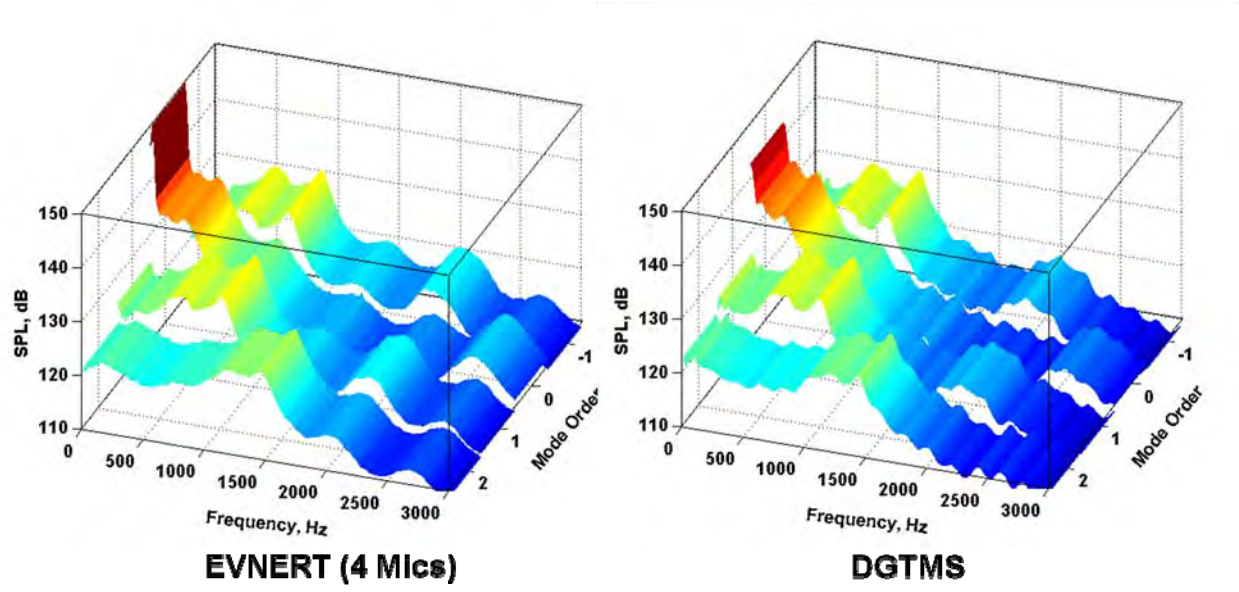

Figure 125. Comparison of Modal Decomposition Results at 48 Percent Speed.

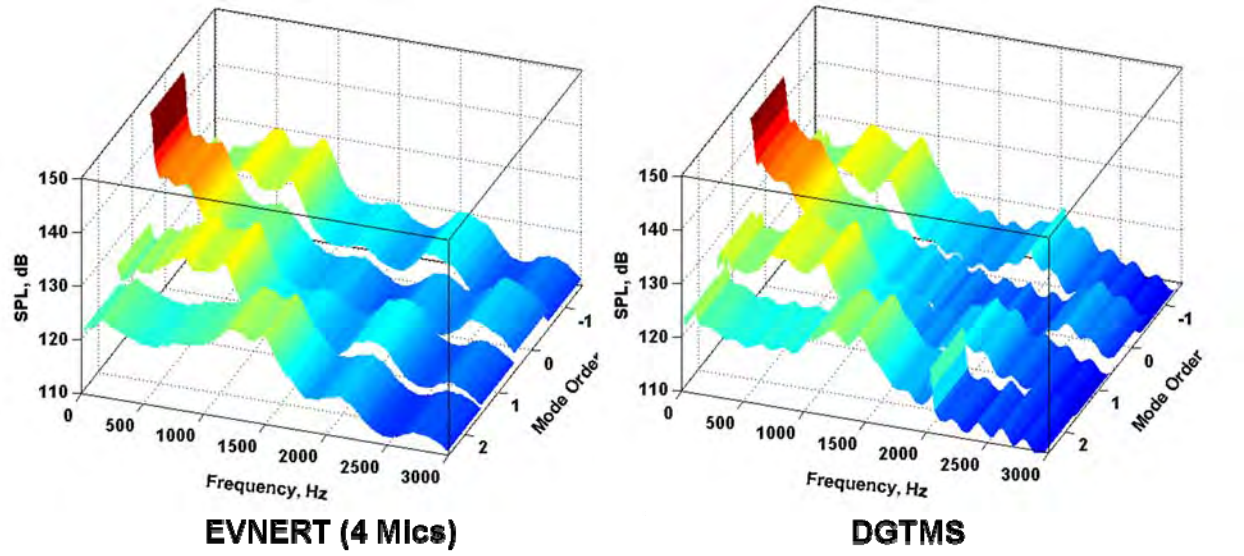

Figure 126. Comparison of Modal Decomposition Results at 54 Percent Speed.

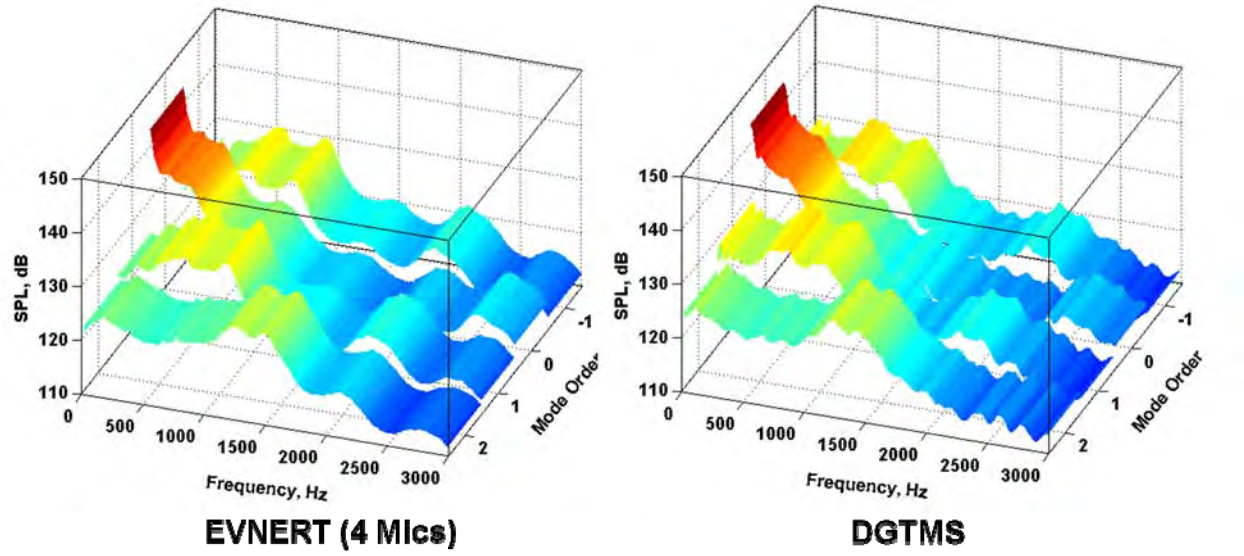

Figure 127. Comparison of Modal Decomposition Results at 60 Percent Speed.

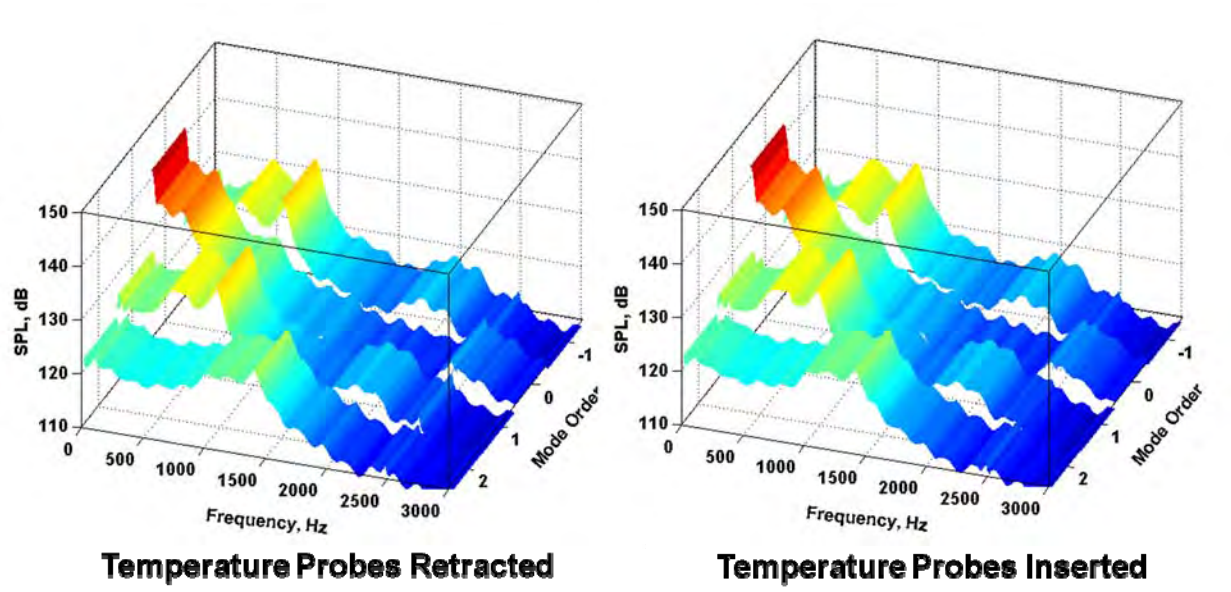

Figure 128. Comparison of DGTMS Modal Decomposition at 48 Percent Speed, With Temperature Probes Retracted and Inserted Into the Combustor.

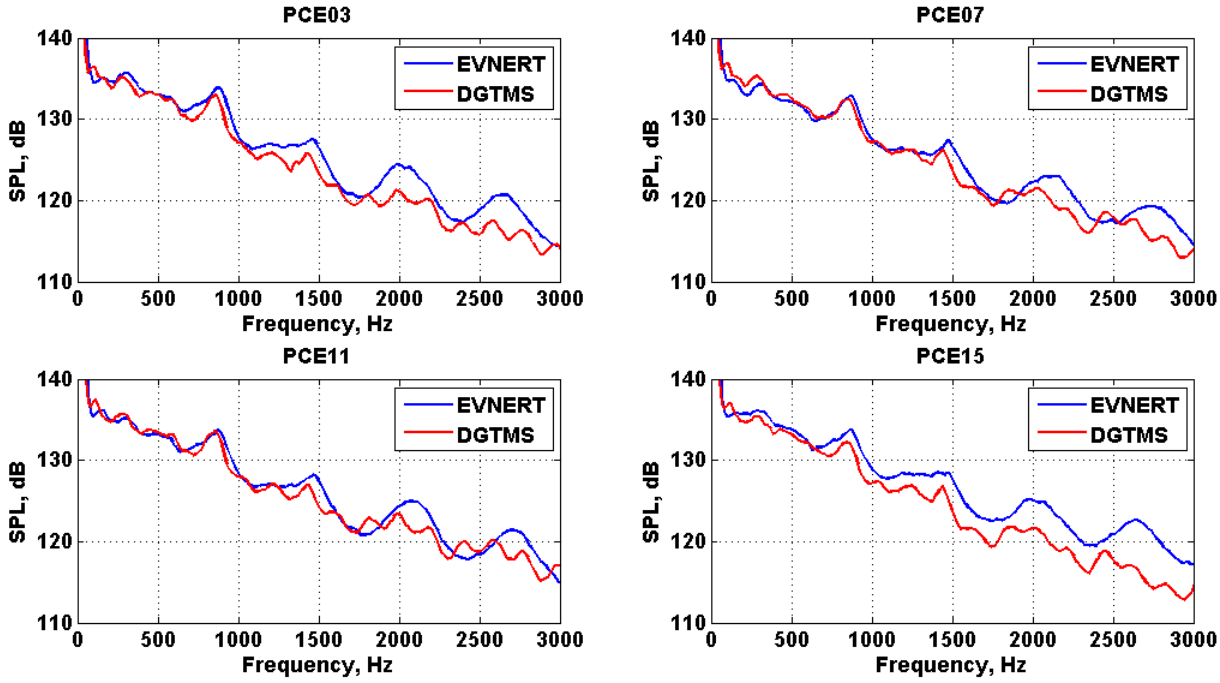

Figure 129. Comparison of DGTMS and EVNERT Spectra at 48 Percent Speed.

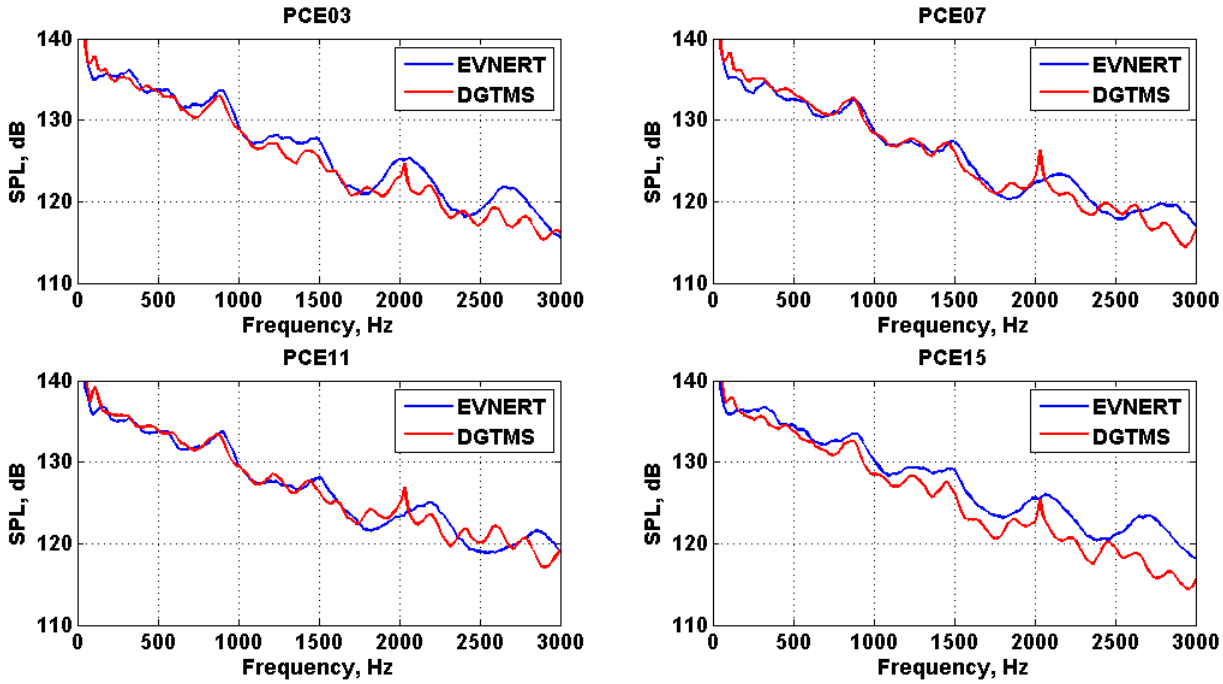

Figure 130. Comparison of DGTMS and EVNERT Spectra at 54 Percent Speed.

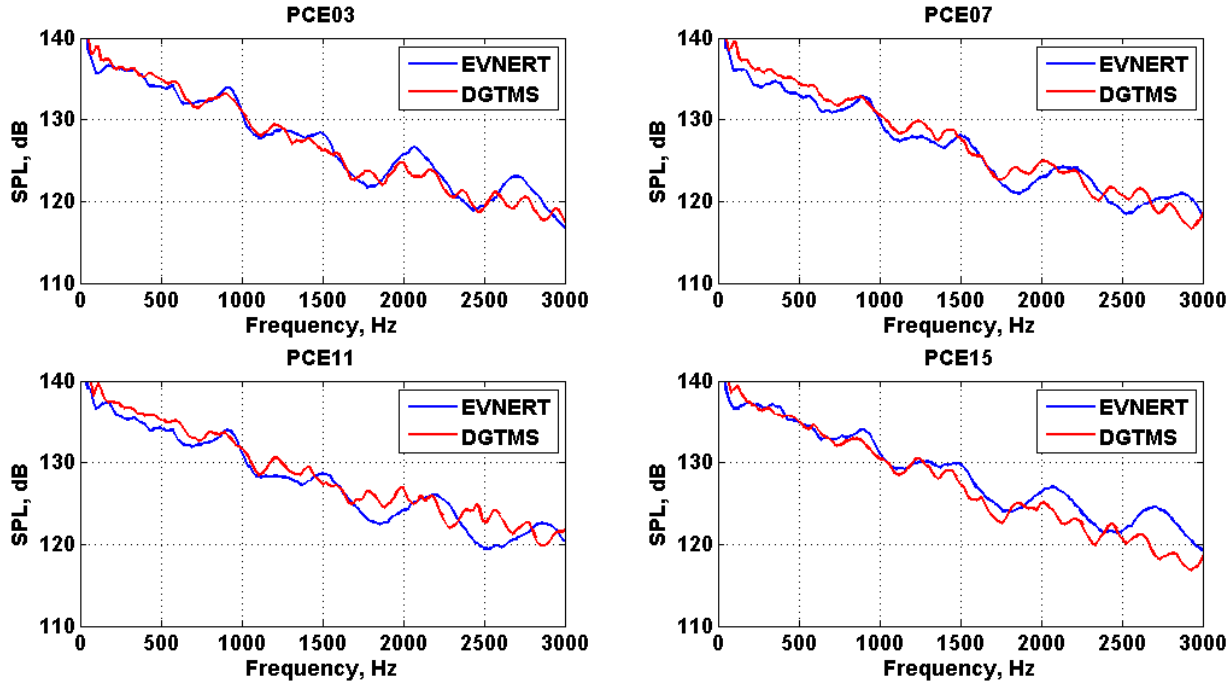

Figure 131. Comparison of DGTMS and EVNERT Spectra at 60 Percent Speed.

7.2.2 Trends in Spectra and Levels With Operating Condition

Section 7.1.2.2 provided a discussion on the trends in the dynamic pressure spectra as a function of operating condition. Figure 132 presents a comparison of the overall sound pressure level, computed over the frequency range from 50 Hz to 1000 Hz, for the internal and external pressure sensors, as a function of engine speed. There is a general increase in overall sound pressure level (OASPL) as the engine speed increases, on the order of 6-7 dB from the 48 percent speed point to the 65 percent speed point. All of the sensors exhibit the same general trend.

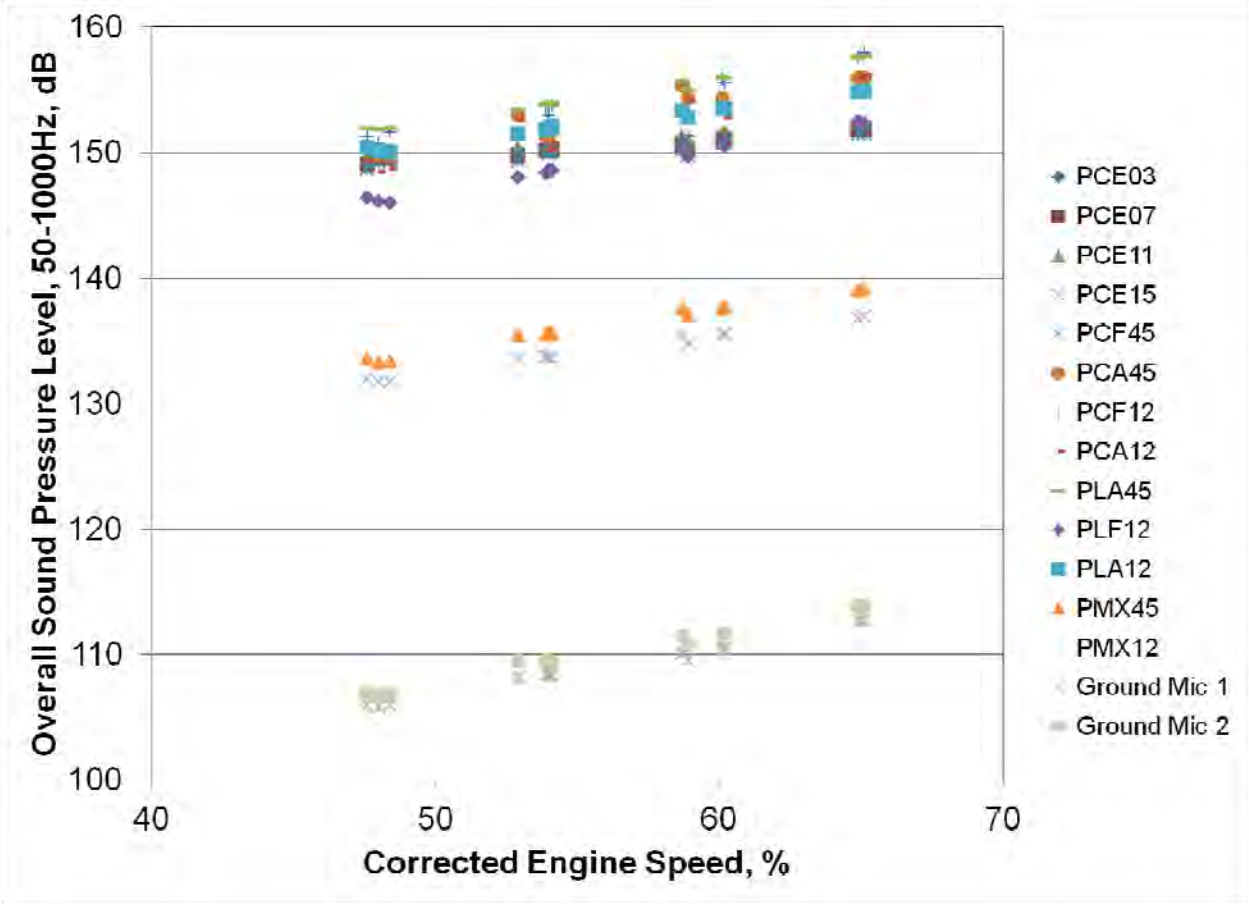

Figure 132. OASPL Variation as a Function of Engine Speed.

7.2.3 Time Delays for Matched Pairs of Kulites

Cross-spectra between pairs of dynamic pressure signals were computed to examine time delays. The transducer pairs examined were the two upstream/downstream probe pairs in the combustor, PCA45xPCF45 and PCA12xPCF12; the two aft probe combustor-to-turbine pairs on the same side of the engine, PLA45xPCA45 and PLA12xPCA12; the upstream/downstream pair in the turbine, PLA12xPLF12, and the two turbine-to-mixer pairs on the same side of the engine, PMX45xPLA45 and PMX12xPLA12. The cross-spectra were computed for all operating conditions and repeat points, in order to identify trends in the results.

Figure 133 presents the cross spectral phase between the upstream and downstream pressure probes in the combustor and ITD, at 48 percent speed (March 26). The cross-spectral phase at higher operating speeds is very similar. Figure 134 shows the cross-spectral phase at 65 percent speed (March 28). There appears to be a fairly well defined phase relationship at low frequencies (the phase is not random), but the behavior is not entirely simple. Between the CF45 and CA45 probes, the phase appears to change linearly from 0 to 100 Hz, remains fairly constant from 100 Hz to 400 Hz, and changes in a somewhat linear fashion from 400 Hz to 800 Hz. Between the CF12 and CA12 probes, there is a nonlinear relationship between 0 and 200 Hz, after which the phase remains relatively constant at 0 degrees up to 800 Hz. Between the LF12 and LA12 probes, the phase is near zero up to about 300 Hz. Overall, the phase change is not a simple linear function of frequency, and thus the interpretation of the results does not lend itself to a simple time delay analysis as one would have for a simple propagation problem, where disturbances would be expected to propagate at either at the sound speed or the flow speed.

There are several issues that contribute to this complexity. The geometry where the pressure measurements are being made is semi-enclosed, leading to the possibility of reflections of acoustic waves and acoustic resonances. Furthermore, there are changes in the flowpath geometry between the upstream and downstream probes, leading to the possibility of mean flow variation and acoustic mode evolution. In any case, one might still attempt to fit a linear curve through the low frequency portion of the data. This was attempted over a range of 50 Hz to 800 Hz for the pairs of pressure probes in the combustor, and between 20 Hz and 200 Hz for the pair of pressure probes in the ITD. The result of the fit is presented in Table 12. In some cases there is a reasonable close correspondence with the time delays for convective propagation. For example, the average fit-derived time delay of 0.13 ms between PLF12 and PLA12 corresponds fairly closely with the expected convective time delay of 0.1 ms, discussed later in Section 7.3.3. These results must be interpreted with caution however.

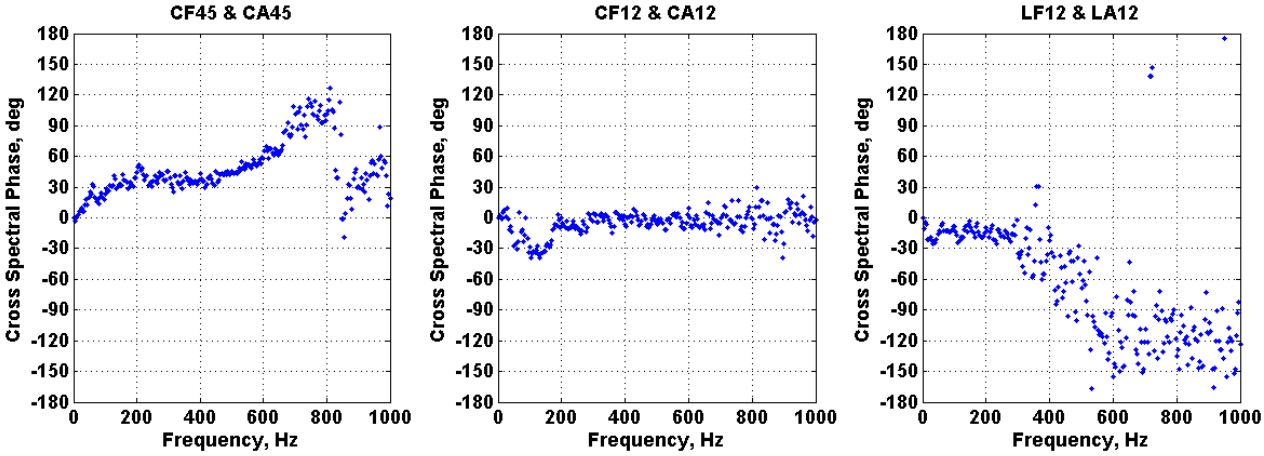

Figure 133. Cross-Spectral Phase Between the Upstream/Downstream Dynamic Pressure Probes in the Combustor and ITD, at 48 Percent (March 26).

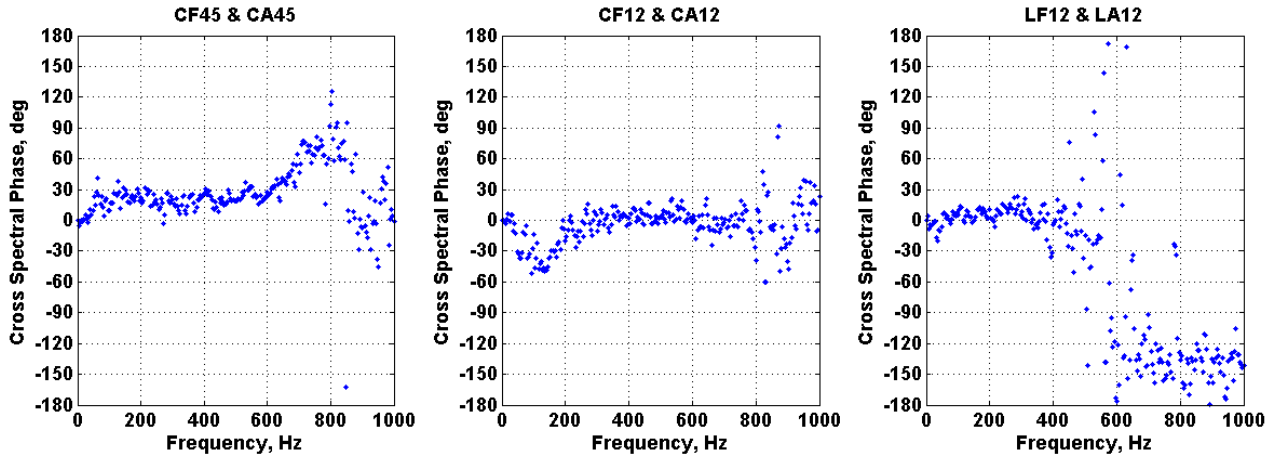

Figure 134. Cross-Spectral Phase Between the Upstream/Downstream Dynamic Pressure Probes in the Combustor and ITD, at 65 Percent (March 28).

Figure 135 presents the cross spectral phase between the aft combustor and aft ITD pressure probes (using sensors on the same sides of the engine) and between the aft ITD and mixer probes (using sensors on the same sides of the engine), at 48 percent speed (March 26). The cross-spectral phase at higher operating speeds is very similar. Figure 136 shows the cross-spectral phase at 65 percent speed (March 28). There is substantial scatter in the data, but there appears to be a region below about 200 Hz where the phase change exhibits a roughly linear change with frequency. A linear fit of the data was attempted over a frequency range from 20 to 200 Hz. The result of the fit is presented in Table 12.

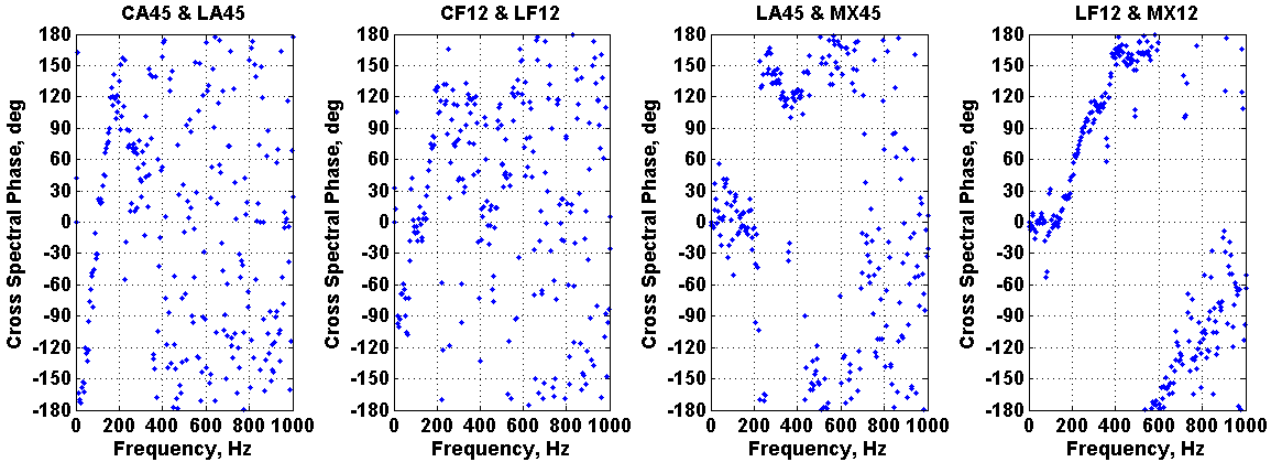

Figure 135. Cross-Spectral Phase Between the Combustor/Turbine and Turbine/Mixer Dynamic Pressure Probes, at 48 Percent (March 26).

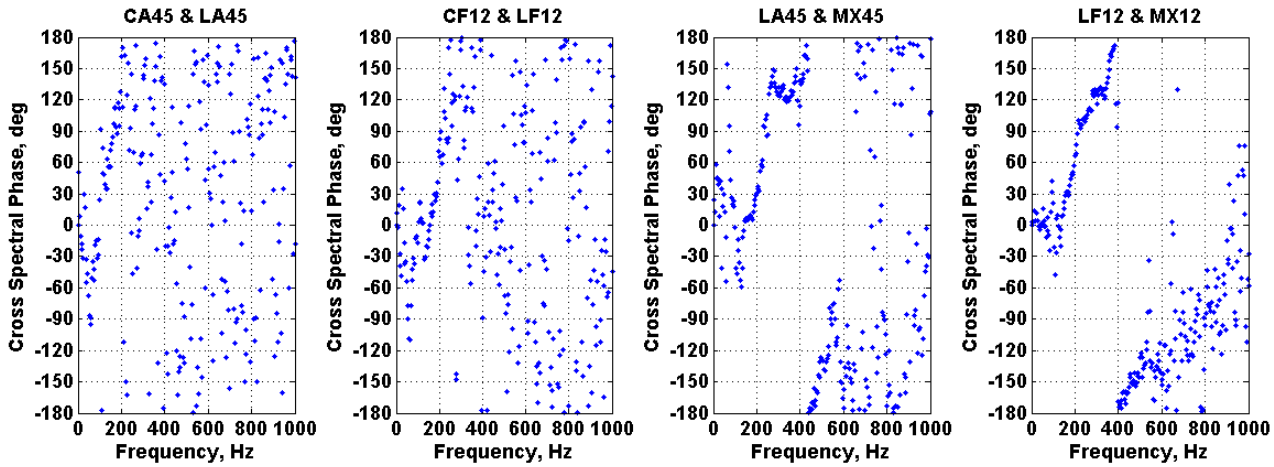

Figure 136. Cross-Spectral Phase Between the Combustor/Turbine and Turbine/Mixer Dynamic Pressure Probes, at 65 Percent (March 26).

Table 12. Propagation Time Delays (in Milliseconds) Computed From Linear Fit of Measured Pressure Cross-Spectra.

Test Date and Operating Point	PCA45 x PCF45	PCA12 X PCF12	PLA45 X PCA45	PLA12 X PLF12	PLA12 X PCA12	PMX45 X PLA45	PMX12 X PLA12
20140326_977CNAM4801_1	0.27	0.08	5.09	0.08	4.22	1.25	-0.43
20140326_977CNAM5401_1	0.22	0.10	4.84	0.10	4.01	1.12	0.66
20140326_977CNAM6001_1	0.15	0.11	4.44	0.08	3.53	1.20	0.93
20140326_977CNAM6002_1	0.14	0.12	3.89	0.09	4.07	1.24	0.81
20140328_977CNAM4801_1	0.29	0.06	5.03	0.18	4.35	1.18	0.35
20140328_977CNAM4802_1	0.29	0.05	5.04	0.15	3.84	0.56	0.26
20140328_977CNAM5401_1	0.26	0.05	5.22	0.15	3.21	0.86	0.70
20140328_977CNAM5402_1	0.26	0.07	4.76	0.07	4.10	1.56	0.75
20140328_977CNAM5403_1	0.29	0.07	5.09	0.13	3.38	0.70	0.63
20140328_977CNAM5404_1	0.25	0.07	4.96	0.24	4.19	1.12	0.50
20140328_977CNAM6001_1	0.22	0.10	4.01	0.13	3.79	1.20	0.91
20140328_977CNAM6002_1	0.20	0.12	3.87	0.03	4.03	0.92	1.19
20140328_977CNAM6501_1	0.16	0.11	2.96	0.18	2.95	1.16	0.62
20140328_977CNAM6502_1	0.16	0.13	2.99	0.17	2.51	1.11	0.64
AVERAGE	0.23	0.09	4.44	0.13	3.73	1.08	0.61

7.3 Task 5.3: Spectra and RMS Levels of Temperature and Pressure

7.3.1 Trend Evaluation of Combustor Temperature Data

It is of interest to examine trends in both the mean and fluctuating temperatures measured by the probes in the combustor, the ITD, and the mixer. Figure 144 displays the mean temperatures measured in the combustor as a function of engine speed. All of the probes show a nearly linear trend of the mean temperature increasing with engine speed. At an engine speed between 60 percent and 65 percent, the critical temperature of 3100°F is reached at the forward probe locations, at which point the platinum/rhodium thermocouple wires melt. In the test, the CF12 probe reached this critical temperature at a slightly higher speed than the CF12 probe, perhaps because the CF12 probe is not as far forward or because it is in a less active part of the flame zone (being located behind a fuel nozzle, and not between fuel nozzles like the CF45 probe). The mean temperatures at the aft combustor probes CA45 and CA12 are very similar and much smaller than the forward probe mean temperatures. There is evidently substantial mixing that occurs between the forward and aft locations, a conclusion that becomes important when considering cross-correlations between the upstream and downstream probes. There is not a significant difference between the mean temperatures of the two aft probes which are at the same axial station. The measured mean temperatures at the aft probe locations were about 300°F more than expected based on engine cycle predictions. There might be additional flow mixing that occurs downstream of the aft probes. Figure 145 displays the mean temperatures measured in the ITD and the mixer as a function of engine speed. Again, the mean temperatures increase almost linearly with engine speed. The ITD probes at the 4.5 location appear to run slightly hotter (about 80°F) than the ITD probes at the 12 location. The measured temperatures in the ITD and mixer are in good agreement with the temperatures expected from engine cycle predictions.

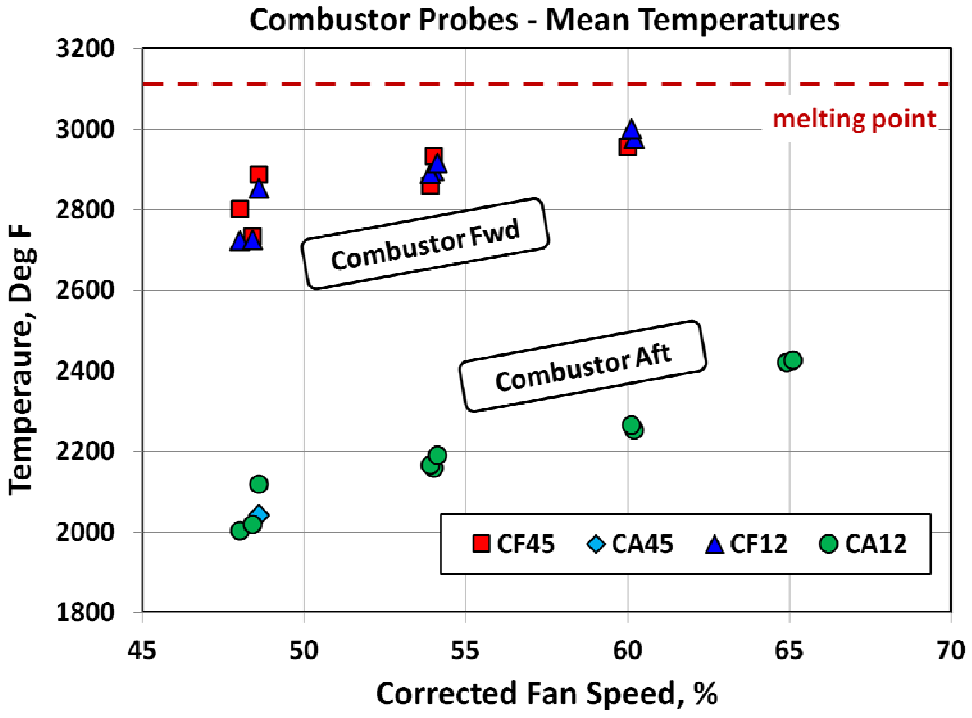

Figure 137. Mean Temperatures Measured in the Combustor.

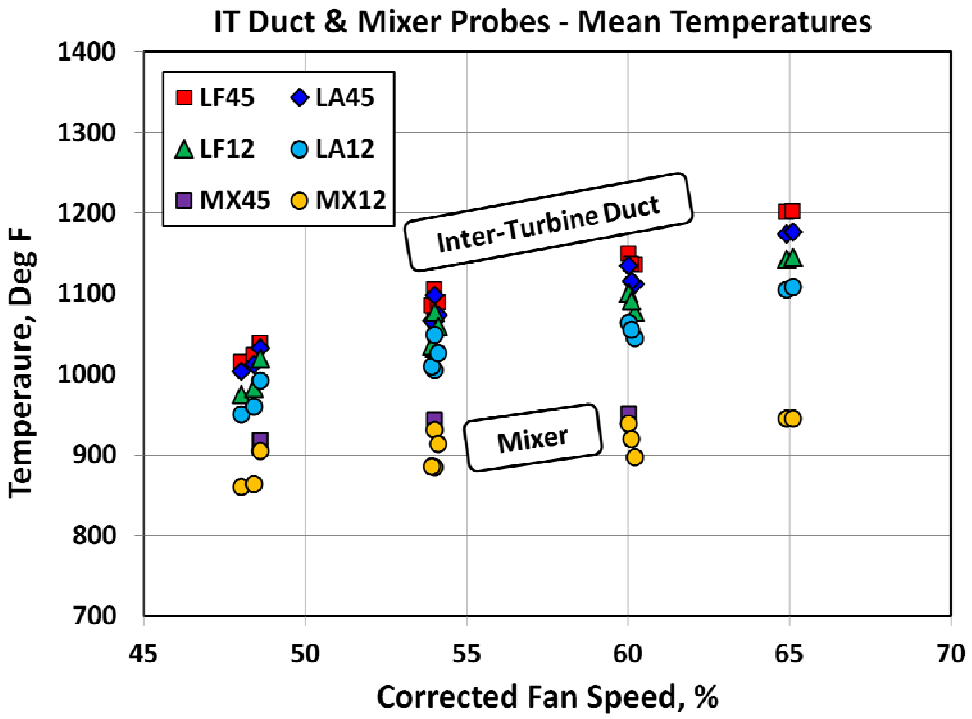

Figure 138. Mean Temperatures Measured in the ITD and Mixer.

It is of particular interest to know how the compensated temperature spectra change with operating speed, and how repeatable the measurements are. Figure 139 presents the small wire compensated temperature spectra for the forward combustor probe CF12 at speeds of 48 percent, 54 percent, and 60 percent, along with the repeat points. The repeatability of the measurements is excellent, and there is very little difference in the amplitude of the compensated spectra as the engine speed changes. Figure 140 presents the small wire compensated temperature spectra for the aft combustor probe CA12 at speeds of 48 percent, 54 percent, 60 percent, and 65 percent, along with the repeat points. The spectral amplitudes at the aft combustor probe location are about 5 dB less than those at the forward combustor probe location. The repeatability of the measurements is excellent, and again there is very little difference in the amplitude of the compensated spectra as the engine speed changes.

Figure 141 presents the small wire compensated temperature spectra for the forward ITD probe LF12 at speeds of 48 percent, 54 percent, 60 percent, and 65 percent along with the repeat points. Here, the frequency range has been truncated at 500 Hz, since the data becomes contaminated by the electronic noise floor above this frequency. The repeatability of the measurements is excellent, and there is very little difference in the amplitude of the compensated spectra as the engine speed changes. The compensated temperature spectra are 20 dB below the compensated spectra at the aft combustor location, and thus the temperature fluctuations in the ITD are an order of magnitude smaller than they are in the combustor. Figure 142 presents the small wire compensated temperature spectra for the aft ITD probe LA12 at speeds of 48 percent, 54 percent, 60 percent, and 65 percent along with the repeat points. The results are very similar to the forward probe LF12, which might be expected if the residual temperature fluctuations are simply convected by the mean flow.

Figure 143 presents the small wire compensated temperature spectra for the mixer probe MX12 at speeds of 48 percent, 54 percent, 60 percent, and 65 percent along with the repeat points. Here the repeatability is not as good. Here, the frequency range has been truncated at 250 Hz, since the data becomes contaminated by the electronic noise floor above this frequency. Even below 250 Hz, the voltages are very low and the coherence between the large and small wires is not high, and for some cases the compensation process becomes questionable. The spectra with the lower amplitudes are believed to be more correct, since these test points show higher coherence and the compensated spectral amplitudes trend downwards with increasing frequency. More careful processing of the mixer probe data is warranted, and might improve these results. This was not pursued here since these temperature fluctuations, being of such low amplitude and at the exit of the engine, are probably not of practical importance.

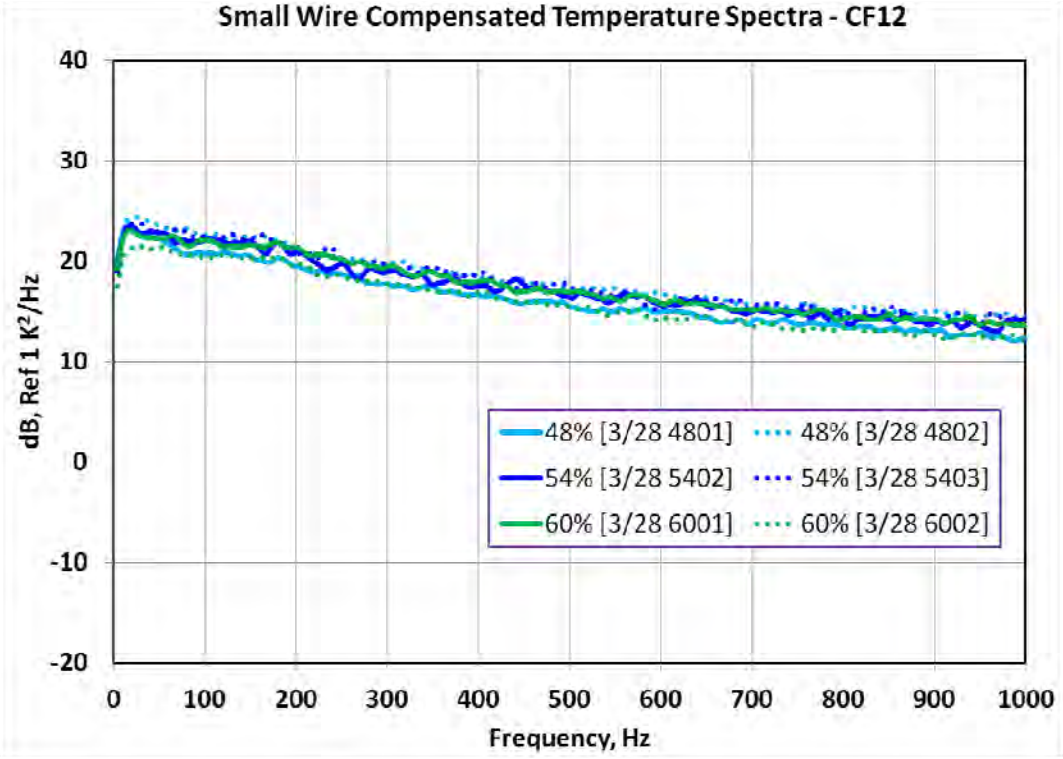

Figure 139. Speed Trend and Repeatability of the Compensated Small Wire Temperature Spectra at the Forward Combustor Location 12.

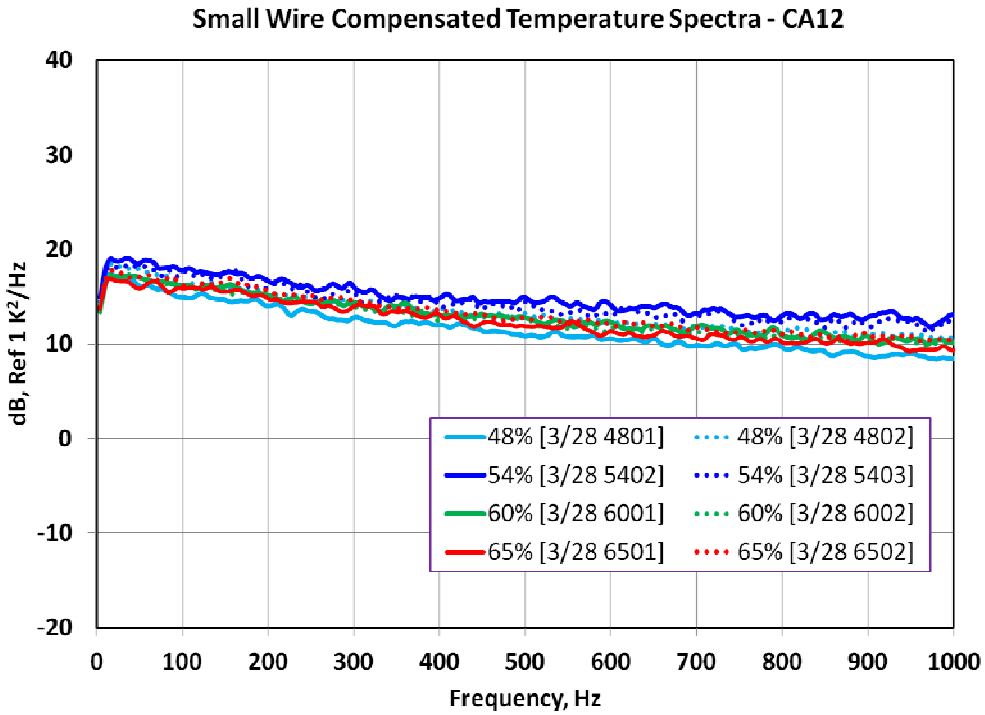

Figure 140. Speed Trend and Repeatability of the Compensated Small Wire Temperature Spectra at the Aft Combustor Location 12.

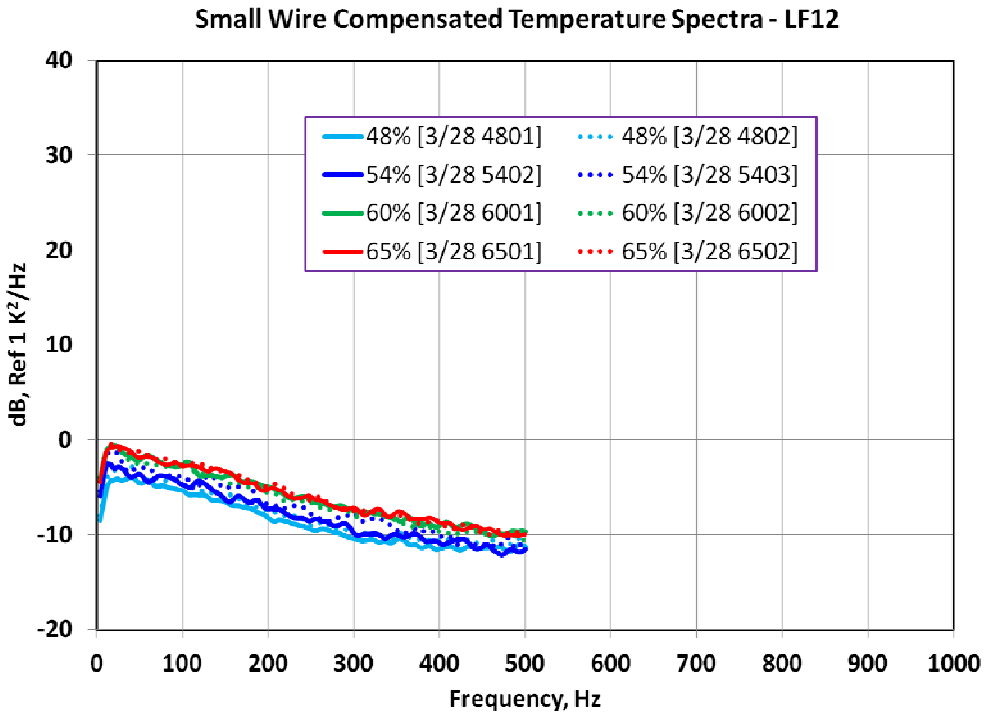

Figure 141. Speed Trend and Repeatability of the Compensated Small Wire Temperature Spectra at the Forward ITD Location 12.

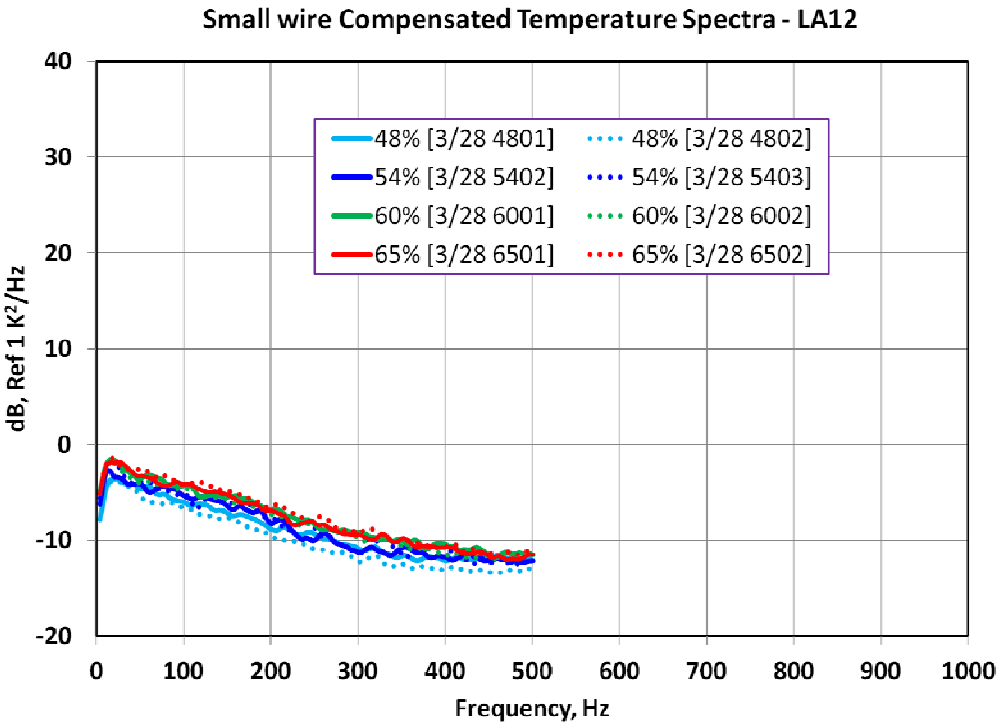

Figure 142. Speed Trend and Repeatability of the Compensated Small Wire Temperature Spectra at the Aft ITD Location 12.

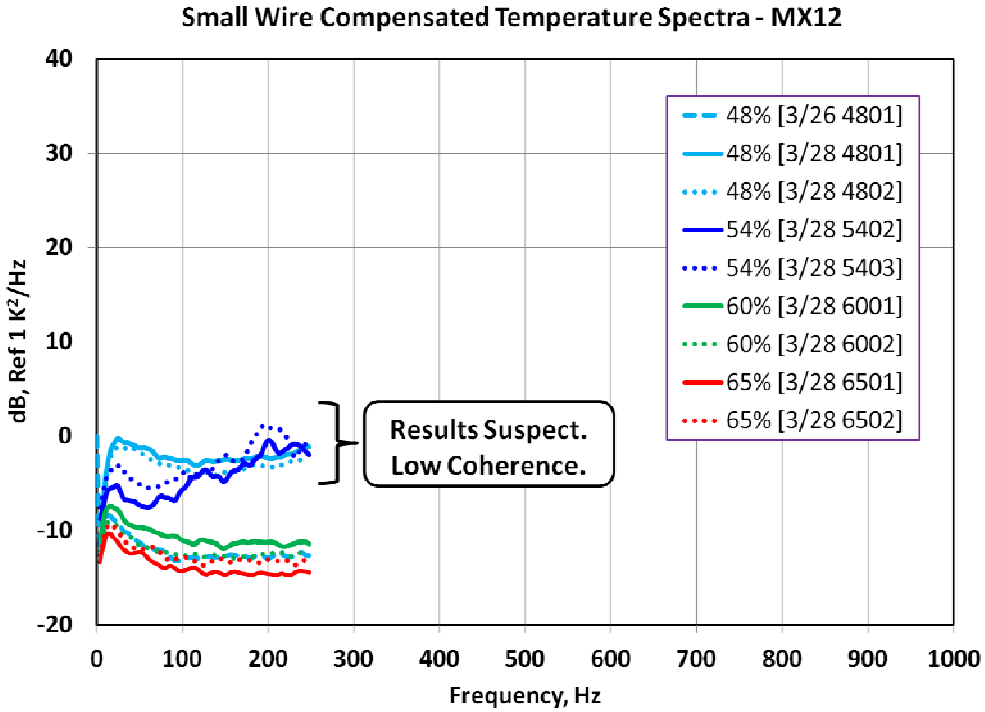

Figure 143. Speed Trend and Repeatability of the Compensated Small Wire Temperature Spectra at the Mixer Location 12.

7.3.2 Temperature Spectra at HPT and LPT Exits

Section 7.1.1.2 presented compensated temperature spectra at the combustor exit (HPT entrance), the LPT entrance, and the LPT exit (mixer). Comparing the compensated spectra, the temperature fluctuations at the LPT entrance are an order of magnitude smaller than those at the HPT entrance. If the indirect noise generation process through the HP and LP turbines are comparable (i.e. if a given fluctuating temperature produces a fluctuating pressure of the same order of magnitude through either turbine), then the indirect noise generated in the LP turbine would be an order of magnitude smaller in amplitude than the indirect noise generated in the HP turbine. The compensated temperature spectra in the LPT exit (mixer) have about half the amplitude as the compensated temperature spectra in the LPT entrance (ITD). The residual temperature fluctuations at the LPT exit convect through the mixer nozzle and into the exhaust nozzle. Since there are no rotating blade rows, the mean flow gradients are not as pronounced as those in the LPT, and one might surmise that any indirect noise generation would be weaker than the indirect noise generated in the LPT. Thus, one concludes that any further study of indirect noise generation in the TECH977 engine should focus first on the combustor temperature fluctuations convecting through the HPT. The indirect noise generated in the HPT should dominate the indirect noise generated elsewhere.

7.3.3 Time Delays for Matched Pairs of Small Wire Thermocouples

The computation of phase delays between matched pairs (upstream and downstream) of small wire thermocouples is of interest because this can shed light on the convection speed of the temperature fluctuations. It is first useful to examine the coherence between the two time history signals. The coherence between the pairs of small wire thermocouples at the 3/26 48 percent speed point is shown in Figure 144, over the frequency range from 0 to 500 Hz. For this analysis, the compensated time histories were used.

The coherence in the combustor is quite low. There appears to be some slight coherence at combustor location 12 at low frequency, but the level is only 0.1 at 50 Hz. The coherence levels at combustor location 4.5 are less than 0.05. The higher coherence at location 12 may be due to the smaller probe axial spacing of 1.5-inch at that location, versus the 2.0-inch spacing at location 4.5. Recall also that the upstream and downstream probes were intentionally offset in the azimuthal direction, so that the downstream probe would not be in the wake of the upstream probe. This offset may contribute to some loss of coherence, as the probes would be sensing slightly different temperature fields. However, it appears that continued mixing between the upstream and downstream probes is the main reason for the reduced coherence in the combustor. As shown in Section 7.3.1, there is a dramatic difference in the mean temperature of the upstream combustor probes versus the downstream combustor probes, indicating that substantial mixing of the hot and cold gases, and potentially continued burning of the fuel, is still occurring.

On the other hand, the coherence between the upstream and downstream small wire pairs in the ITD is quite high. This is to be expected, since the flow downstream of the HPT is well mixed with no residual burning. The remaining temperature fluctuations should be largely convected down the duct by the mean flow. Taylor's hypothesis, where the turbulent eddies (and temperature fluctuations) are considered to be frozen in the flow, is probably a good approximation here. The coherence levels at combustor location 4.5 are slightly higher than those at location 12. This is a bit unexpected, since the axial spacing of 1.2-inch at location 4.5 is slightly larger than axial spacing of 0.9-inch at location 12. However, the coherence at both locations is quite high regardless, being above 0.8 at low frequencies.

The cross-spectral phase between the upstream and downstream small wire thermocouples is presented in Figure 145. As expected from the low coherence, there is not an obvious trend in the combustor data. However, for the CF12 and CA12 pair, there does appear to be a slight indication of a time delay in the cross-spectral phase below 100 Hz, as suggested by a roughly constant slope in the phase. In the turbine, the results are much more dramatic, as might be expected from the high coherence levels. There is a clearly identifiable constant slope region in the cross-spectral phase from 0 to 500 Hz, suggestive of a convective time delay. The slope at location 4.5 is larger than the slope at location 12, which is consistent with a larger spacing between the probes.

To obtain an estimate of the convection speeds, a linear fit of the cross-spectral phase data is applied. For the combustor locations, a reliable linear fit could not be obtained due to the high amount of scatter in the cross-spectral phase. It appears that the residual mixing and burning is too large to derive a reliable estimate of the eddy convection speed. For the ITD locations, a linear fit is applied to the phase data between 100 and 400 Hz. This fit is expected to be very good due to the high coherence and strong linear relationship in the cross-spectral phase. An example of the linear fit through the data is shown in Figure 146. The time delays are then calculated from the measured slopes as $\tau = (d\theta/df)/360°$. Time delays for the upstream/downstream ITD pairs were calculated for all of the test points. The computed time delays are shown in Table 13. The average computed time delay is 0.15 ms for location 4.5 with the 1.24-inch probe spacing, and 0.09 ms for location 12 with the 0.93-inch probe spacing. This is very close to the expected values. The expected time delays in the ITD, computed using the engine cycle estimated flow velocity (computed from the Mach number and temperature or sound speed) and assumed sensor spacing, is 0.13 ms for location 4.5 with the 1.24-inch probe spacing and 0.1 ms for location 12 with the 0.93-inch probe spacing. The expected time delay is roughly constant over the tested engine speeds. A comparison between the measured and cycle-predicted time delays is provided in Figure 147. Considering the various uncertainties in the measurements and cycle predictions (probe spacing, mean flow direction, cycle accuracy, etc.) the agreement is quite good. This provides a convincing confirmation that the temperature fluctuations in the ITD region are simply convected by the mean flow.

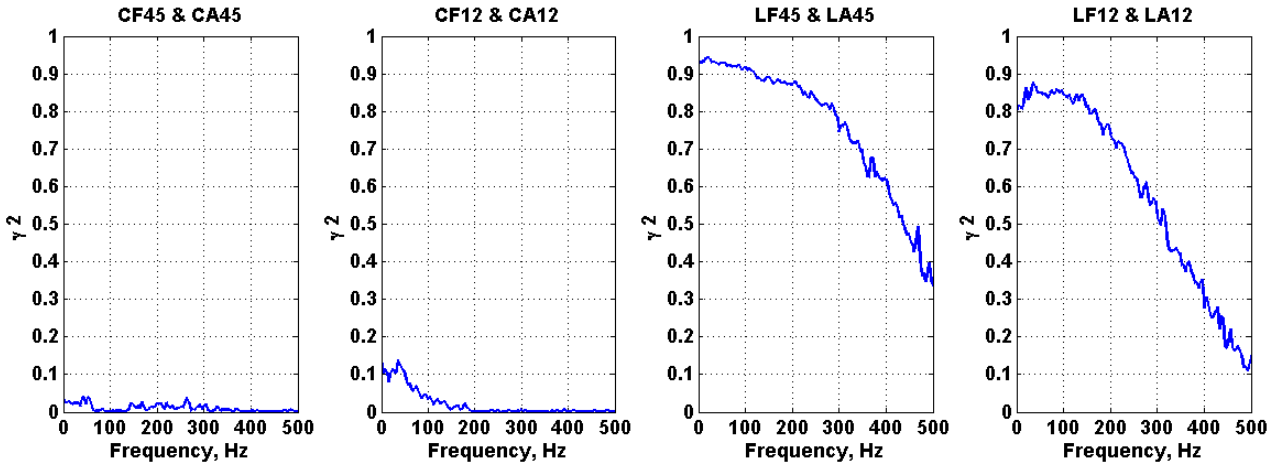

Figure 144. Coherence Between the Upstream and Downstream Small Wire Thermocouple Pairs at the March 26 48 Percent Speed Point.

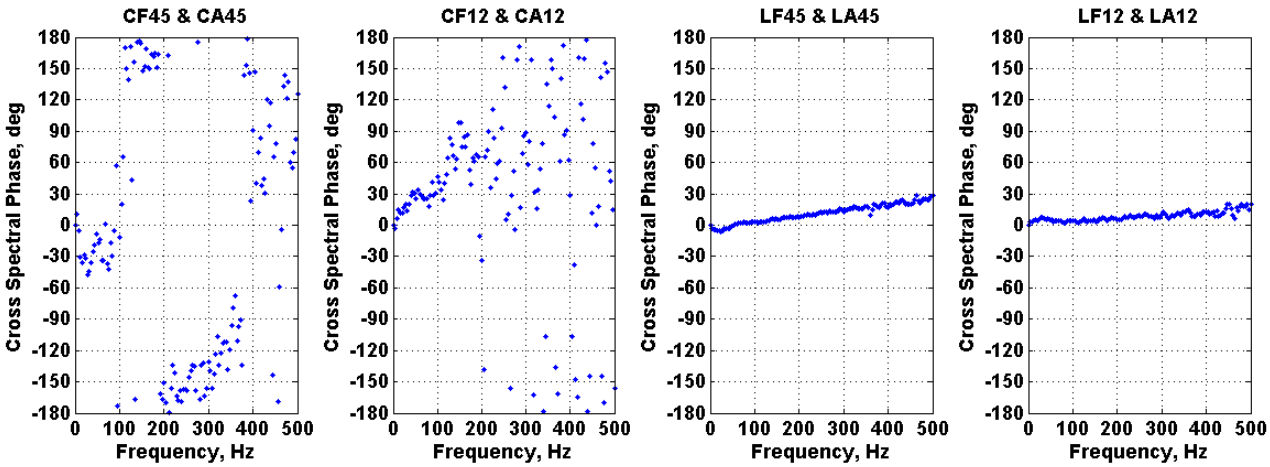

Figure 145. Cross-Spectral Phase Between the Upstream and Downstream Small Wire Thermocouple Pairs at the March 26 48 Percent Speed Point.

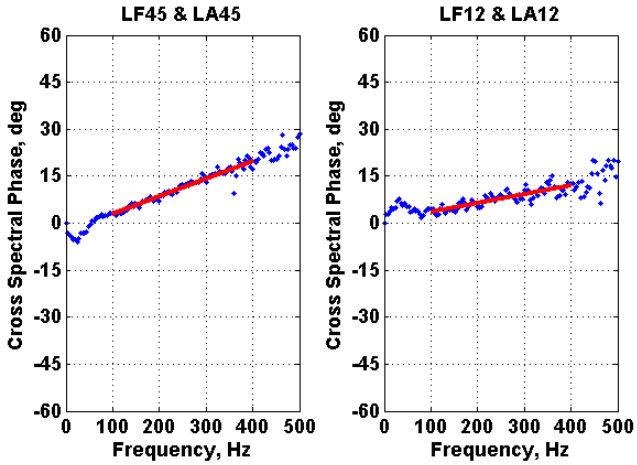

Figure 146. Example of Linear Fits of the Cross-Spectral Phase Between the Upstream and Downstream Small Wire T/C Pairs at the March 26 48 Percent Speed Point.

Table 13. Propagation Time Delays Computed for Small Wire T/C Pairs.

Test Date and Operating Point	Computed Time Delay Between LF45 and LA45, ms	Computed Time Delay Between LF12 and LA12, ms
03/26/2014 4801	0.156	0.077
03/26/2014 6001	0.148	0.096
03/26/2014 5401	0.130	0.076
03/28/2014 4801	0.144	0.064
03/28/2014 5402	0.153	0.085
03/28/2014 4802	0.159	0.061
03/28/2014 5403	0.153	0.085
03/28/2014 6001	0.146	0.105
03/28/2014 5404	0.140	0.095
03/28/2014 6002	0.144	0.123
03/28/2014 6501	0.155	0.127
03/28/2014 6502	0.149	0.128
AVERAGE	0.15	0.09

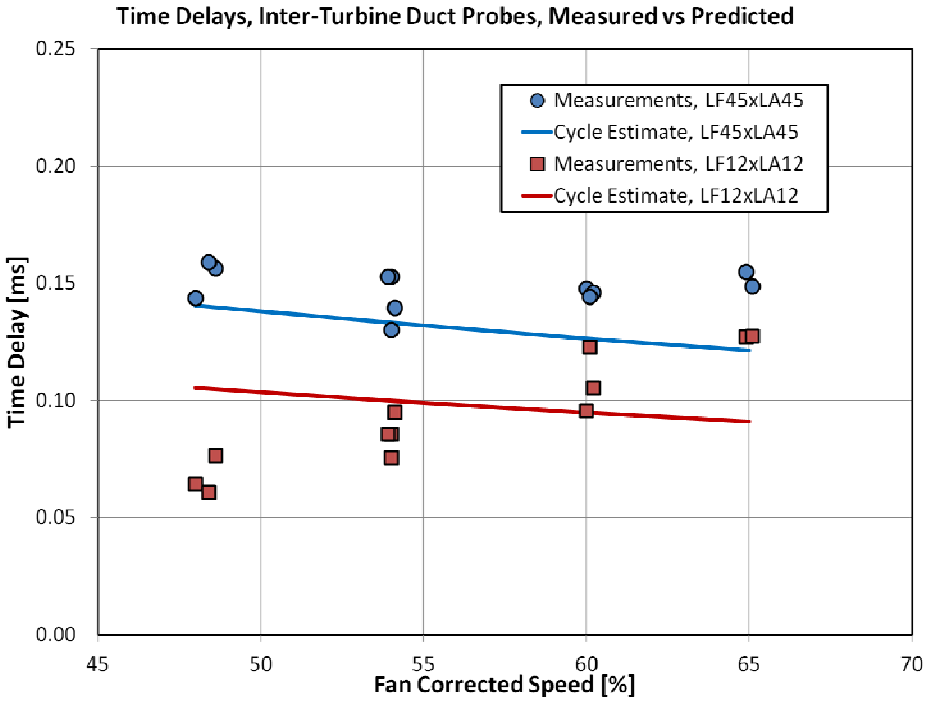

Figure 147. Measured Versus Predicted Convective Time Delays Between the Upstream and Downstream Probes in the ITD.

7.3.4 Temperature and Pressure Cross Correlations

Of particular interest to the indirect noise problem is whether there is an identifiable correlation between the dynamic temperature fluctuations and the dynamic pressure fluctuations inside the engine core. For example, a convincing argument for the existence of indirect combustion noise could be made if there is a significant correlation between the temperature fluctuations that are convected through the HPT and the pressure fluctuations that are propagating downstream of the turbine. In this section, correlations between temperature and pressure at various locations in the TECH977 core engine are examined. Reference 1 provides an early experimental investigation of coherence and cross-spectral measurements between pressure and temperature fluctuations inside a long duct downstream of a combustor. The experiment identified non-random phase relationships between pressure and temperature at low frequencies. The authors explored the coherence and cross-spectra between pressure and temperature fluctuations both at a single point and at spatially separated points. Similar explorations are considered here.

First, consider the correlation between the dynamic temperature and the dynamic pressure at the same (or nearly so) location in space. For each of the pressure/temperature probes in the TECH977 test, the temperature measurement is made *in the flow*, roughly near the centerline of the flowpath, whereas the pressure measurement is made *at the outer wall* of the duct. There may be some loss in correlation because the temperature and pressure measurements are not made at the exact same location in space. For example, the length scale of the temperature fluctuations might be smaller than the width of the annular duct, so there is no guarantee that the dynamic temperature near the duct wall will be highly coherent with the dynamic temperature in the flow. Similarly, there is no guarantee that the dynamic pressure measured at the wall would be highly coherent with the dynamic pressure measured at the flowpath centerline[1].

Figure 148 shows the coherence between the dynamic compensated temperature fluctuations measured by the small wire thermocouple in the centerline of the duct and the dynamic pressure measured at the duct wall (close to where the temperature probe enters the duct), for the four probes in the combustor, at 48 percent speed. The coherence at all four locations is very small, below 0.05 at all frequencies. Figure 149 plots the cross-spectral phase between the compensated dynamic temperature and the dynamic pressure (not adjusted for propagation time delay in the sensing tube) at the four locations, at 48 percent speed. Although the phase does not appear to be completely random, there is little indication of any strongly dominant pattern. Figure 151 plots the cross-spectral phase between the compensated dynamic temperature and the phase-corrected dynamic pressure (after adjustment for propagation time delay in the sensing tube) at 48 percent speed. There is perhaps a slight linear trend at the 4.5 location, but there is significant scatter in the data. Figure 151 plots the cross-spectral phase between the compensated dynamic temperature and the phase-corrected dynamic pressure at 54 percent speed. The results are similar to those at 48 percent speed. There does not appear to be a simple phase relationship between the dynamic pressure and dynamic temperature measured at a single point in the combustor.

[1] A higher degree of coherence might be expected between dynamic pressure measured at the wall and at the centerline, since the geometry and mean flow conditions are such that higher order radial modes do not propagate in the core ducts at low frequencies. For example, the modal measurements in the combustor show that the plane wave is dominant at frequencies below 500 Hz and the (m=±1, n=0) modes are dominant at frequencies between 500 Hz and 1000 Hz).

Figure 152 shows the coherence between the dynamic compensated temperature fluctuations measured by the small wire thermocouple on the temperature probe and the dynamic pressure measured at the duct wall, for the three locations in the inter-turbine duct. Note that the pressure tap at location LF45 was used to provide the purge flow reference pressure, so there is no dynamic pressure measurement available at that point. The frequency range is restricted to 500 Hz, because the compensated temperature is unreliable above that frequency due to the electronic noise floor. There is much greater coherence in the inter-turbine duct than in the combustor, although the coherence levels are still modest, being generally below 0.3. The cross-spectral phase between the compensated dynamic temperature and the dynamic pressure (not adjusted for propagation time delay in the sensing tube) is shown in Figure 153. Here, the results are dramatically different than those from the combustor, as is more easily seen by plots of the unwrapped cross-spectral phase shown in Figure 154. There is a very definitive phase relationship between pressure and temperature fluctuations.

At the LF12 and LA12 locations, the phase appears to be a linear function of frequency. At the LA45 location, the behavior is more complex; over certain frequency ranges, the phase changes linearly with frequency, but there are unusual step changes in the phase, e.g. at 175 Hz. The behavior of the phase is similar at other speeds, and becomes somewhat more consistent at the higher power settings. The unwrapped cross-spectral phase between the compensated dynamic temperature and the dynamic pressure (not adjusted for propagation time delay in the sensing tube) at 65 percent speed is shown in Figure 155. A linear fit of the phase data for locations LF12 and LA12 is applied over a frequency range from 100 to 350 Hz. The result of the fit is shown in Table 14. The average time delay is 2.7 ms, which corresponds very nicely with the expected time delay associated with propagation of the pressure signal from the wall location through the 3 foot long pressure sensing line to the Kulite location, summarized in Table 11.

As an additional confirmation, the cross-spectral phase between the compensated dynamic temperature and the phase-corrected dynamic pressure is shown in Figure 156 and Figure 157 for 48 percent and 65 percent speed, respectively. The phase is predominantly constant with frequency. At location LF12, the temperature and pressure are out of phase by 60 degrees. At location LA12, the temperature and pressure are out of phase by 120 degrees at 48 percent speed and by 60 degrees at 65 percent speed. Location LA45 exhibits a more complex behavior, and reveals the existence of an additional linear phase shift. An explanation for this behavior is currently lacking.

The high degree of correlation between the local pressure and temperature at the inter-turbine duct probe locations is unexpected and intriguing. Are the pressure fluctuations in the inter-turbine duct hydrodynamic or acoustic in nature? Recall that the cross-spectral measurements between upstream and downstream small wire thermocouple pairs indicated that the temperature fluctuations in the inter-turbine duct are convected with the mean flow. Since the temperature and pressure are well correlated, does this then imply that the pressure fluctuations are convected with the mean flow? Does this then imply that the pressure fluctuations are dominated by hydrodynamic disturbances? Or is it possible that indirect noise is being generated in the HP turbine, and that the residual temperature fluctuations are highly correlated with the pressure fluctuations? This is an area that requires further exploration.

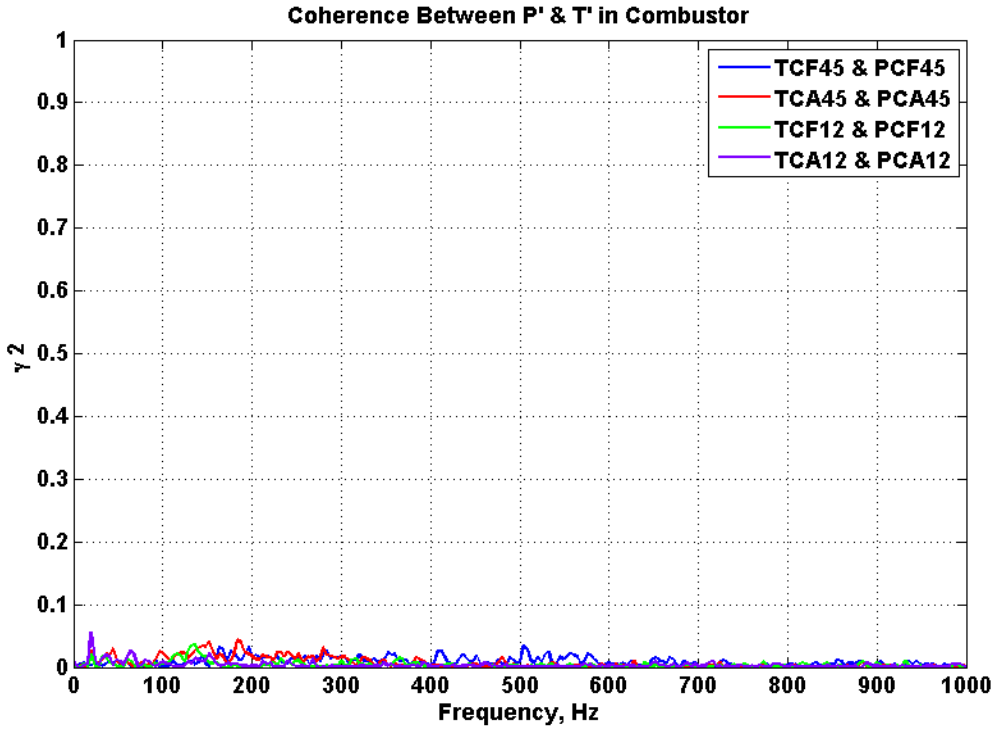

Figure 148. Coherence Between Dynamic Temperature and Dynamic Pressure at the Combustor Probe Locations, at 48 Percent Speed (March 26).

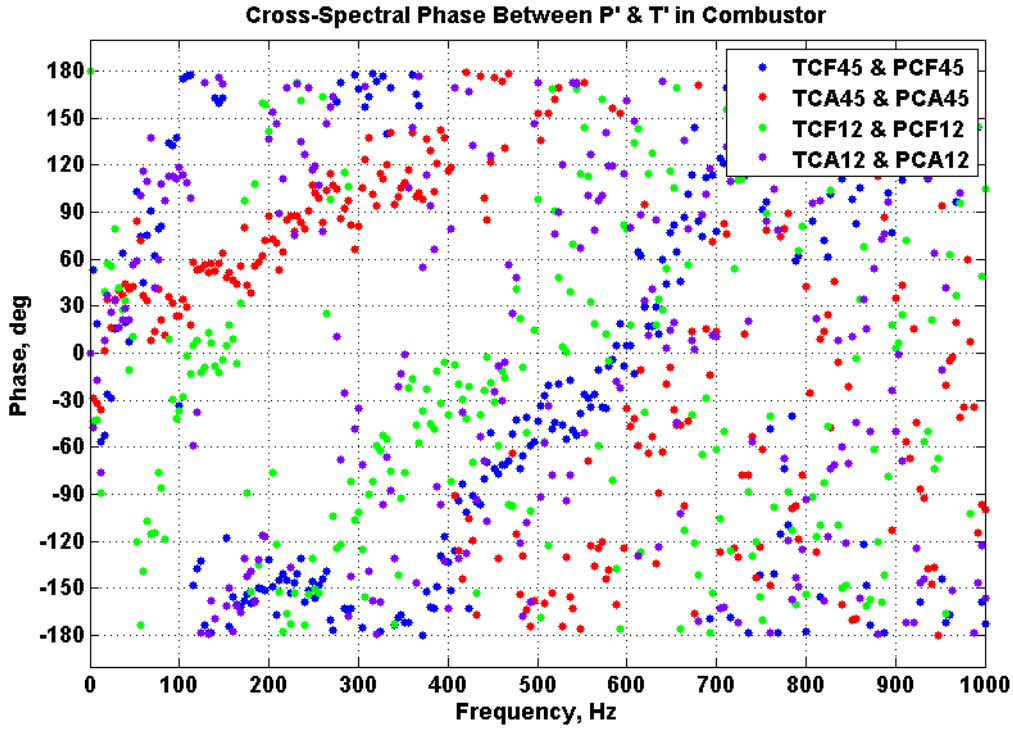

Figure 149. Cross-Spectral Phase Between Dynamic Temperature and Dynamic Pressure at the Combustor Probe Locations, at 48 Percent Speed (March 26).

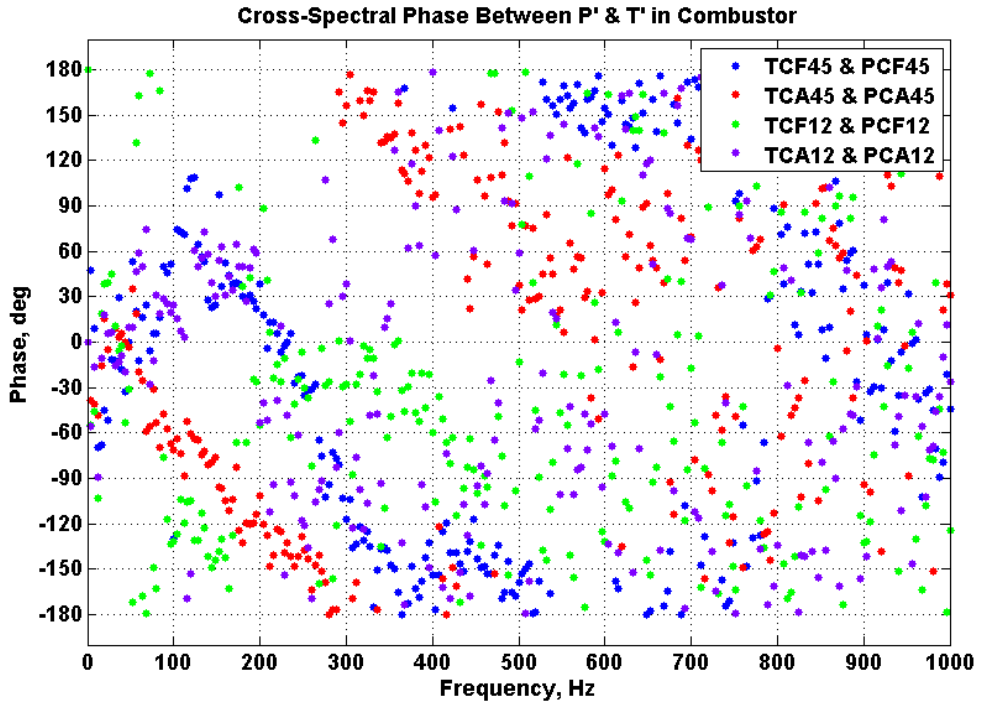

Figure 150. Cross-Spectral Phase Between Dynamic Temperature and Phase-Corrected Pressure at the Combustor Probe Locations, at 48 Percent Speed (March 26).

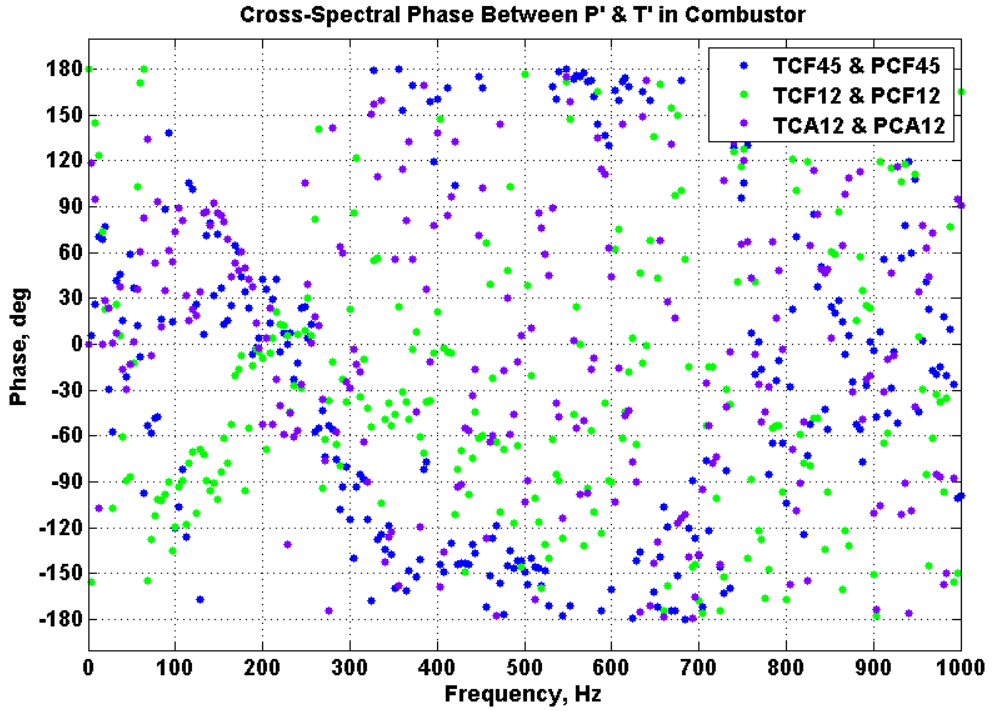

Figure 151. Cross-Spectral Phase Between Dynamic Temperature and Phase-Corrected Pressure at the Combustor Probe Locations, at 54 Percent Speed (March 28).

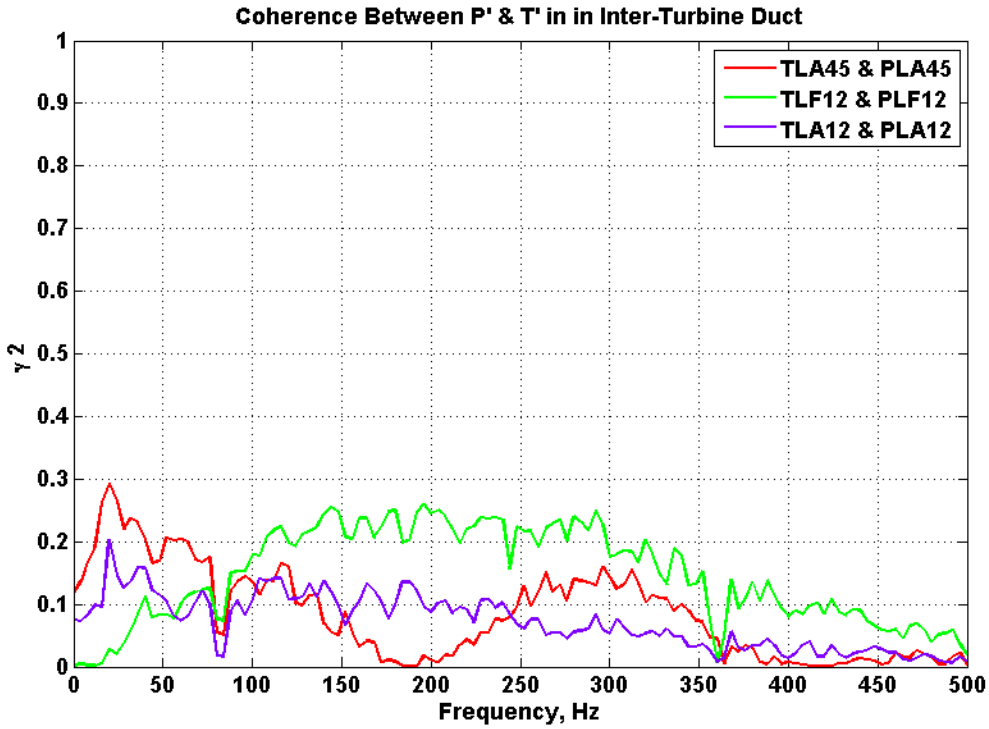

Figure 152. Coherence Between Dynamic Temperature and Dynamic Pressure at the ITD Probe Locations, at 48 Percent Speed (March 26).

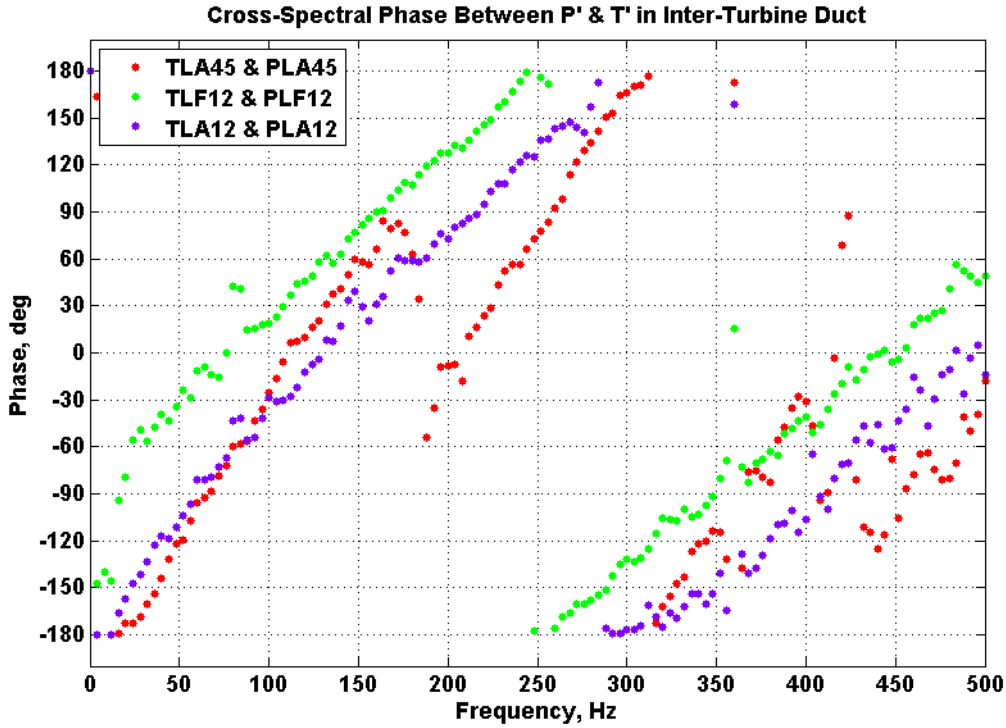

Figure 153. Cross-Spectral Phase Between Dynamic Temperature and Dynamic Pressure at the ITD Probe Locations, at 48 Percent Speed (March 26).

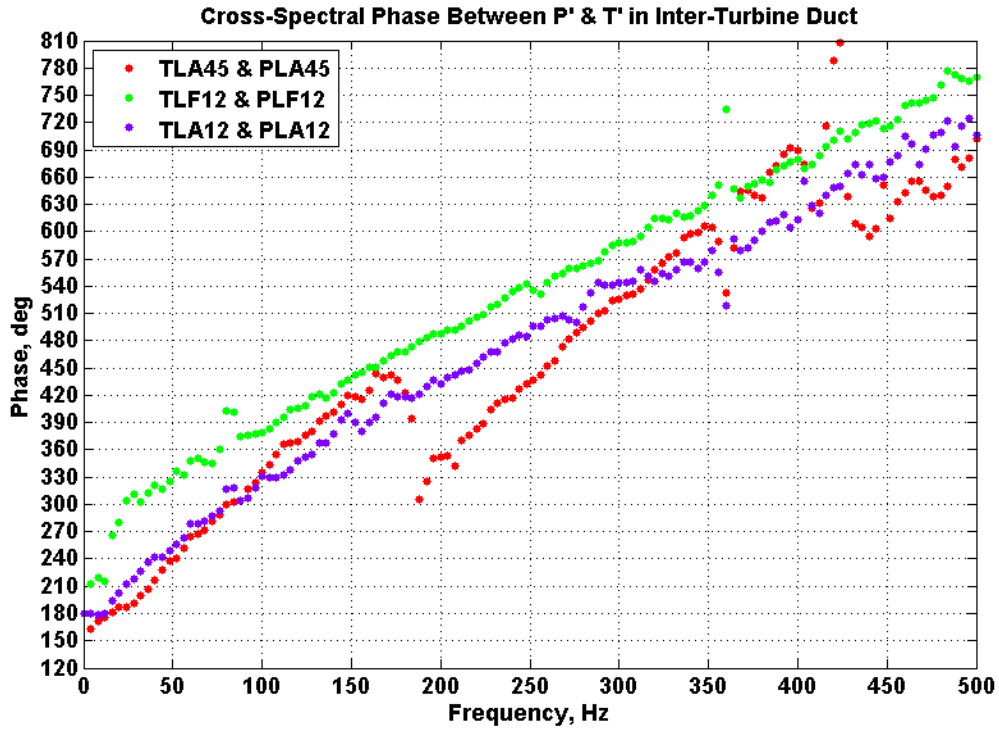

Figure 154. Unwrapped Cross-Spectral Phase Between Dynamic Temperature and Pressure at the ITD Probe Locations, at 48 Percent Speed (March 26).

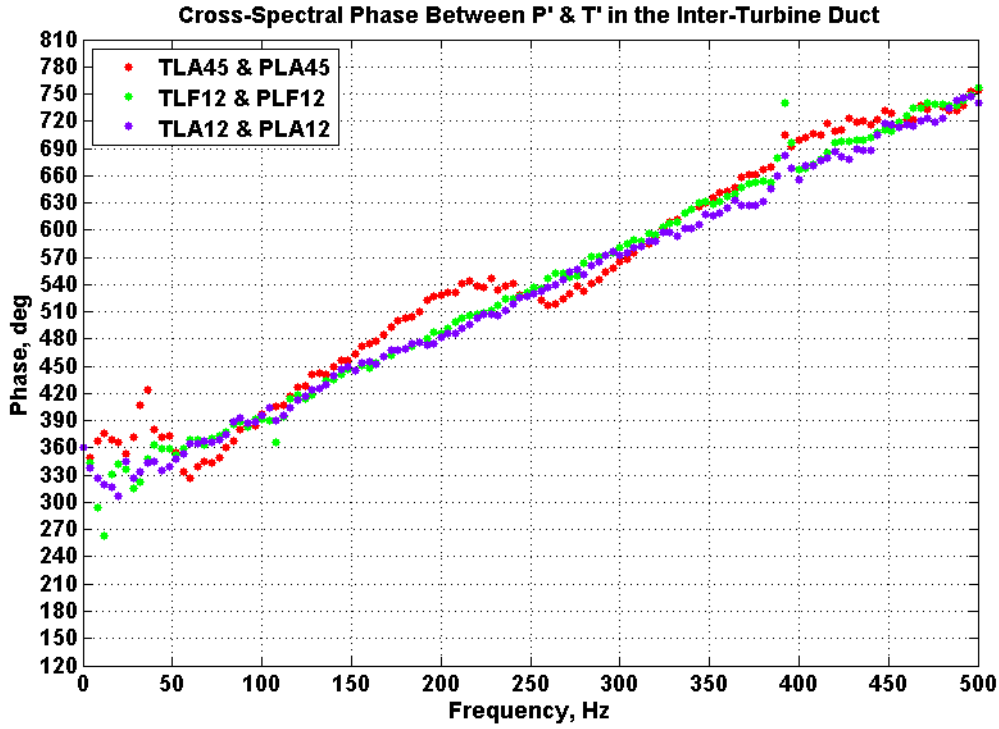

Figure 155. Unwrapped Cross-Spectral Phase Between Dynamic Temperature and Pressure at the ITD Probe Locations, at 65 Percent Speed (March 28).

Table 14. Computed Time Delays Between Local T′ and P′ in the ITD.

Test Date and Operating Point	Computed Time Delay at Location LF12, ms	Computed Time Delay at Location LA12, ms
03/26/2014 4801	2.75	2.80
03/26/2014 6001	2.72	2.58
03/26/2014 5401	2.70	2.76
03/28/2014 4801	2.77	2.95
03/28/2014 5402	2.71	2.77
03/28/2014 4802	2.77	2.86
03/28/2014 5403	2.71	2.77
03/28/2014 6001	2.66	2.59
03/28/2014 5404	2.73	2.71
03/28/2014 6002	2.73	2.71
03/28/2014 6501	2.64	2.43
03/28/2014 6502	2.52	2.44
AVERAGE	2.70	2.70

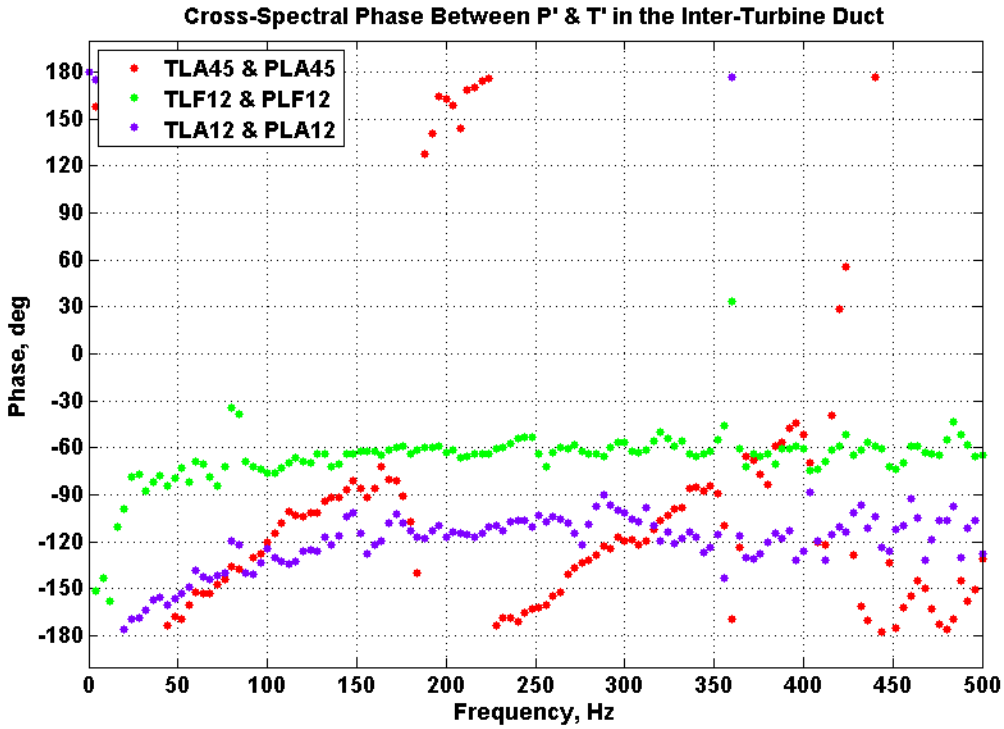

Figure 156. Cross-Spectral Phase Between Dynamic Temperature and Phase-Corrected Pressure for ITD Probe Locations, at 48 Percent Speed (March 26).

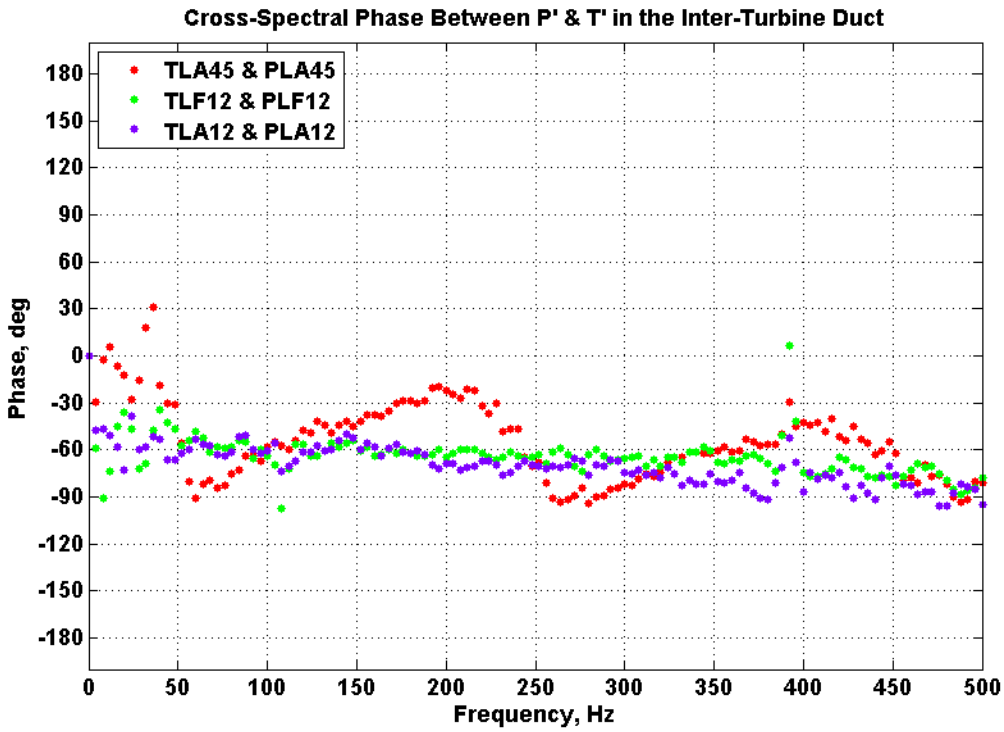

Figure 157. Cross-Spectral Phase Between Dynamic Temperature and Phase-Corrected Pressure for ITD Probe Locations, at 65 Percent Speed (March 26).

Next, the coherence and cross-spectra between pressure and temperature fluctuations at spatially separated points is examined. Perhaps the most interesting comparison is between the temperature fluctuations upstream of either the HPT or LPT, and the pressure fluctuations directly downstream of the corresponding turbine. If there is a high degree of correlation, this might indicate the presence of indirect combustion noise. However, one could expect that there will be many localized incoherent temperature fluctuations convecting through the turbine at the same time, and thus multiple incoherent sources generating noise simultaneously. Pressure measurements downstream of these sources might contain contributions from multiple incoherent sources, and thus the coherence between temperature upstream and pressure downstream of the turbine might be substantially reduced. Figure 158 presents the coherence between the compensated dynamic temperature upstream of the turbine and the phase-corrected dynamic pressure at the nearest location directly downstream of the turbine. The coherence levels are quite low in general. Figure 159 presents the corresponding cross-spectral phase between the same temperature and pressure measurements. Surprisingly, there is a fairly well defined phase relationship. Across the HPT, the relationship is not very clear, but the phase certainly does not appear to be random. There is a hint of a linear relationship between the dynamic temperature from the aft combustor probe at location 12 and the dynamic pressure from the forward pressure probe at location 12. The phase relationship between the temperature probes upstream of the LPT and the pressure probes downstream is even more definitive, with the phase dominated by a linear behavior. Further analysis is required to understand the reasons for this behavior and whether the associated time delay matches with a convective time scale.

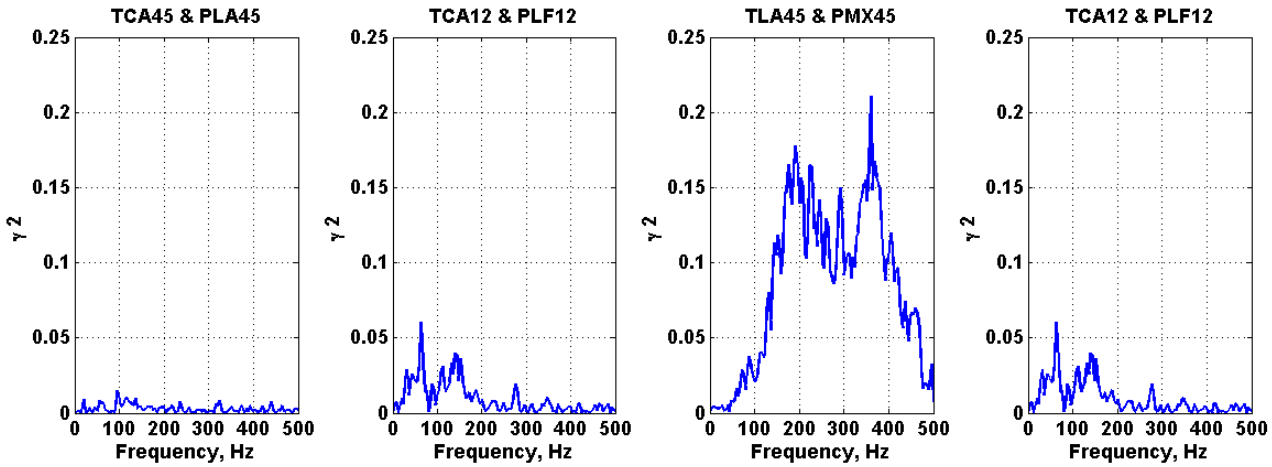

Figure 158. Coherence Between Dynamic Temperature (Compensated) Upstream and Dynamic Pressure (Phase-Corrected) Downstream of the HP and LP Turbines.

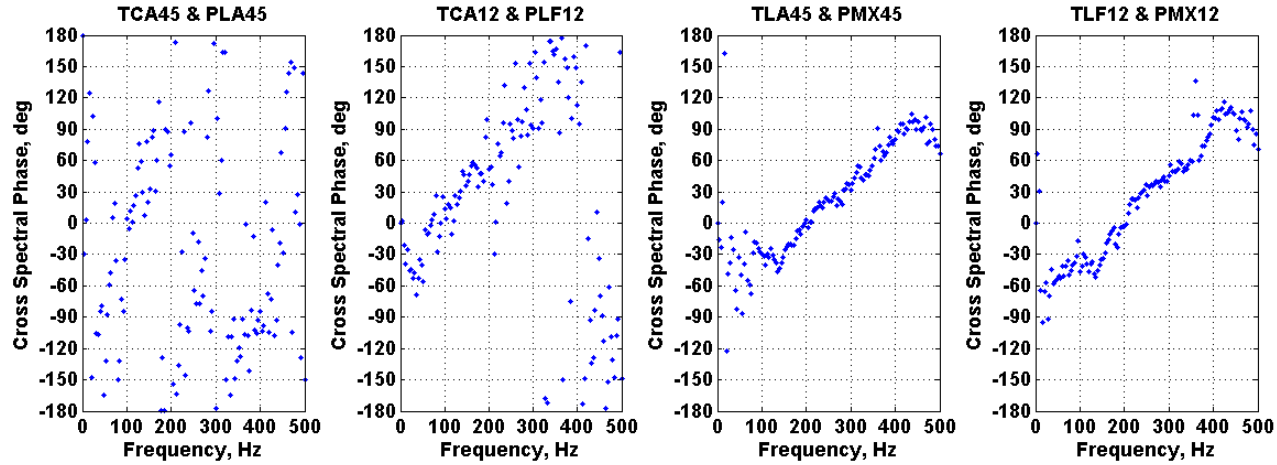

Figure 159. Cross-Spectral Phase Between Dynamic Temperature (Compensated) Upstream and Pressure (Phase-Corrected) Downstream of the HP and LP Turbines.

7.4 Task 5.4: Distribution of Data and Analysis Results

Honeywell provided NASA with an initial data package containing all of the raw dynamic pressure and dynamic temperature time history data that was acquired during the test. This data package contained the following data:

1. Dewetron Data Files from March 26, 2014 (Native Dewetron format and Matlab format exported using DEWESoft X)

2. Dewetron Data Files from March 28, 2014 (Native Dewetron format and Matlab format exported using DEWESoft X)

3. Excel spreadsheet describing details of the Matlab exported files (engine operating point, beginning and ending times)

4. B&K Pulse Data Files from March 26, 2014 (Binary Universal File Format)

5. B&K Pulse Data Files from March 28, 2014 (Binary Universal File Format)

A second package of information and analysis results was prepared containing the following data:

1. Probe dimensional characteristics

2. Relevant engine operating condition data

3. Input and output files for the DGTMS software

4. Narrowband compensated temperature and pressure spectra

5. Analysis results

6. Conclusions and recommendations for further analysis/testing (See Section 8.0)

7. Honeywell's updated version (source code) of the NASA DGTMS software

8.0 CONCLUSIONS

8.1 Major Results

A comprehensive set of dynamic temperature and dynamic pressure measurements have been acquired on the TECH977 engine. Dynamic temperature measurements were successfully acquired in the combustor, the ITD, and the mixer, using dual wire thermocouple probes. The temperature probes were constructed using 0.003-inch and 0.010-inch diameter Type B thermocouple sensing elements mounted in a ceramic stick. A pneumatic actuation system was developed to deploy the temperature probes into the middle of the annular flowpath. Dynamic pressure measurements were simultaneously acquired next to each temperature probe, and at four additional locations in the combustor, using Kulite differential pressure transducers mounted in semi-infinite tubes. The probes in the combustor and ITD were cooled using a small amount of nitrogen purge flow. Dynamic temperature and pressure time history measurements were made at four steady-state operating speeds covering the low speed regime where combustion noise is of practical interest. At each speed, the time history data were acquired for at least 70 seconds using both a Dewetron data acquisition system (primary) and a Pulse data acquisition system (backup). After the test, the NASA DGTMS software was used to process the raw thermocouple voltages and generate compensated temperature spectra corresponding to the fluctuating temperature of the gas stream. Compensated temperature spectra were generated up to a frequency range of 1000 Hz in the combustor, 500 Hz in the ITD, and 250 Hz in the mixer. Compensated time histories were also generated, representative of the fluctuating temperature of the gas stream. The compensated time history spectra at a particular measurement location were found to be fairly constant with engine speed, over the range of speeds tested.

In the combustor, fluctuating temperature data were acquired at mean temperatures up to the limits of probe survivability (3100°F). At the two higher power settings, mean temperatures at the forward combustor probe locations exceeded 3100°F, so data could not be obtained at those speeds. Mean temperatures at the aft combustor locations were between 2000°F and 2400°F and did not impose any limitations on testing. Difficulties with the actuation of the aft combustor probe on the right side of the engine limited the amount of temperature data acquired at that location. The compensated temperature spectra in the combustor have a wideband spectral content. On a narrowband basis, the spectra are relatively flat, with a slight decrease in amplitude with frequency. The temperature measurements in the combustor indicate that significant burning of fuel and/or mixing of the hot and cold gas occurs between upstream and downstream probe locations. As a result, correlations between upstream and downstream temperature probes, such as the determination of convective time delays, were not easily established. Pressure measurements made using a circumferential array of four equally spaced probes in the forward end of the combustor confirmed the modal content that was previously measured during the NASA EVNERT program, although some small differences were noted. Cross-spectra between upstream and downstream pressure probes revealed a non-random phase relationship that is more complicated than a simple propagation delay. Cross-spectra between temperature and pressure fluctuations measured at a common location did not reveal any simple phase relationship between the two.

In the ITD (downstream of the HPT) and the mixer (downstream of the LPT), the measured temperature fluctuations were an order of magnitude smaller than those measured in the combustor. Mean gas temperatures were well below the survivability limits of the probes, and did not impose any limitations on testing. A high coherence between upstream and downstream ITD probes was observed, and inspection of the cross spectral phase data showed a linear relationship with frequency indicating that the temperature fluctuations are convected by the mean flow. The measured time delays are consistent with expectations. There is very little coherence between the temperature fluctuations measured on opposite sides of the engine, suggesting that the length scales of the temperature fluctuations are much smaller than the circumference of the annulus. Interestingly, there is a strong coherence between the pressure and temperature fluctuations measured at the same location in the ITD. Inspection of the cross-spectral phases indicates that, after accounting for the propagation time delay along the sensing tube of the semi-infinite coil, the pressure and temperature fluctuations have a predominately constant phase offset. In addition, cross-spectra between the compensated temperature fluctuations measured upstream of a turbine and the phase-corrected pressure fluctuations measured directly downstream of the turbine indicated a non-random phase relationship between the two variables. An explanation for this behavior is currently lacking.

A fundamental question of interest is whether the temperature and pressure measurements acquired on the TECH977 engine provide a clear indication of the presence of indirect combustion noise. For example, can it be shown that indirect combustion noise dominates over direct combustion noise across a particular frequency range? This is a challenging question to answer, even with temperature and pressure measurements in hand. In order to answer it, one must first define what constitutes “convincing evidence” of indirect combustion noise. At the simplest of approaches, one can compare pressure spectra measured upstream and downstream of a turbine stage and look for dramatic changes in the spectra. If there is a region where the downstream spectra is higher than the upstream spectra (e.g. a broadband peak), one might consider this to be an indication of indirect noise generated by the convection of temperature fluctuations through the flow gradients in the turbine. In the current test, no clear and convincing spectral amplification was observed. However, such a comparison is complicated by the possibility of indirect noise propagating upstream of the turbine (thus

confounding the measurements upstream) and by flow and geometry changes that alter the acoustic resonances (and thus the broadband peaks) in the vicinity where the pressure measurements are made. An alternative approach is to look at correlations between variables, such as between temperature fluctuations upstream of a turbine and pressure fluctuations downstream, and consider high coherence over a particular frequency range as positive indication of indirect combustion noise. A high coherence between temperature fluctuations in the combustor and pressure fluctuations downstream of the HPT was not observed in the current test. However, this criteria also oversimplifies the problem for reasons discussed subsequently. Alternatively, one could explore more sophisticated metrics and signal processing techniques. One example is provided by the entropy wave generator [Reference 16], where indirect noise has been studied in a controlled laboratory setting with a simplified nozzle geometry and where fluctuating temperature sources could be turned on or off. The increase in noise power when the entropy sources were turned on was found to trend with nozzle Mach number according to theoretical expectations, providing convincing evidence of the presence of indirect noise. In an engine test, where the direct and indirect sources coexist and cannot be independently varied, where there are dramatic changes in the flowpath geometry, and where multiple turbine rows are present, the task of establishing “convincing evidence” is much more daunting. With the simplified approaches considered here, no convincing identification of indirect combustion noise could be made. More sophisticated analysis will have to be carried out to identify the indirect noise contribution.

8.2 Recommendations for Further Analysis

Much of the analysis presented in this report is exploratory in nature. Some fundamental conclusions have been presented, but more sophisticated signal processing techniques will be required to yield additional insights and conclusions. Although the main objective of acquiring dynamic temperature and pressure data has been achieved, the answer to the underlying question of whether indirect combustion noise can be detected remains elusive. The spectra and correlations between the dynamic pressure and dynamic temperature measurements are often non-trivial, and a more careful dissection of the data is believed to be necessary. In particular, the analyses such as those explored in References 12–15, which have proven insightful on previous TECH977 testing, are recommended.

One aspect of the indirect noise problem that probably needs thoughtful consideration is the impact of multiple noise sources. The length scales of the temperature fluctuations in the combustor are likely to be small (there are multiple fuel nozzles, each creating burning and mixing zones that are uncorrelated with the others). When multiple uncorrelated temperature fluctuations convect through the turbine and create pressure fluctuations, one would expect that the pressure fluctuations generated by each source would be uncorrelated. Furthermore, the pressure fluctuations measured at locations downstream of the HPT are likely to be a combination of multiple uncorrelated sources (not only from indirect combustion noise, but also direct combustion noise and possibly other sources). The presence of multiple uncorrelated sources will result in diminished coherence between pressure and temperature fluctuations at various points. The cross-spectral phase, time delay, or other computed quantities will also be affected, and the interpretation of the results should consider the impact of multiple sources. How the sources couple to the acoustic modes in the duct is also likely to be a relevant concern, since only low order modes are able to propagate in the engine core.

It is recommended that computational simulations of indirect combustion noise generation be explored to gain additional insight into the measurements. In particular, it would be helpful to better understand the magnitude of pressure fluctuations generated by the indirect mechanism

as a function of incident temperature fluctuations. Also, it would be helpful to explore the coherence and cross-spectra between the dynamic temperature and dynamic pressure at different locations. Although the simulations often incorporate major simplifications regarding the geometry, the mean flow, the incident disturbance field, and most notably the turbine aerodynamics, and although the simulations come with their own set of complications, there are notable advantages. The simulation datasets can be explored much more thoroughly; the indirect noise mechanism can be observed more directly in the absence of competing sources; and the limitations and uncertainties associated with physical instrumentation are not present. Furthermore, the strength, length scales, and number of sources of the incident temperature disturbances can be varied to explore how this affects the correlations between pressure and temperature. These investigations might also provide recommendations for instrumentation types and locations for future test programs, along with recommendations for data acquisition and signal processing procedures.

8.3 Recommendations for Future Testing

Based on a recommendation from previous test efforts, a probe actuation system was developed for this test effort to deploy and retract the temperature probes into the flow, with the purpose of enhancing probe survivability. Despite significant planning and risk mitigation efforts, difficulties were still encountered with some of the probe actuators. The system achieved the objective of removing the probes from the flowpath during engine startup and rapid transients, and may have contributed to the survivability of the probes. However, significant effort and expense was involved in designing, procuring, assembling, and testing the actuation system. In future testing on other engines, it may be more cost effective to use fixed probes and manufacture more spare probes to replace any that fail. Although the failure rate of probes during an engine start has not been assessed in this program, the use of a fixed probe system might be an acceptable risk.

In a realistic engine such as the TECH977 where space is a premium, significant mixing and burning of the gas occurs throughout the combustor. There is not a substantial axial distance where the flow has been fully mixed and simply convects downstream into the HPT. Additionally, hardware constraints such as the presence of flanges limit how closely probes can be placed to the turbine nozzle. As a result, it is difficult to obtain spatially separated combustor temperature measurements in a purely convective flow regime. If a rigorous determination of the convection speeds of the temperature fluctuations at the exit of the combustor is a priority, it might be better to perform a rig test where a long duct could be installed downstream of the combustor, to allow for additional stabilization of the flow.

The fluctuating temperature measurements in the ITD and the mixer had a limited frequency range due to the noise floor of the data acquisition system. This was not considered to be a limitation in the TECH977 test, since the magnitude of the fluctuating temperatures in these areas is very small, and any fluctuating pressures generated by the indirect noise process is likely small in comparison to direct and indirect noise generated by the combustor and HPT. However, if accurate measurement of low amplitude temperature fluctuations are needed at higher frequencies, (e.g. for use in a validation study of a numerical simulation) then low noise signal conditioning amplifiers that are tailored to amplifying very low voltages will need to be identified and employed.

9.0 REFERENCES

1. Miles, J.H., Wasserbauer, C.A., and Krejsa, E.A., “Cross Spectra Between Temperature and Pressure in a Constant Area Duct Downstream of a Combustor,” NASA TM 83351, 1983.

2. Miles, J.H., Wasserbauer, C.A., and Krejsa, E.A., “Cross Spectra Between Temperature and Pressure in a Constant Area Duct Downstream of a Hydrogen Fueled Combustor,” NASA TM 83463, 1983.

3. Fralick, G.C., Oberle, L.G., and Greer, L.C. III, “Dynamic Gas Temperature Measurements Using a Personal Computer for Data Acquisition and Reduction,” NASA TM106119, 1993.

4. Elmore, D.L., Robinson, W.W, and Watkins, W.B., “Dynamic Gas Temperature Measurement System, Volume I – Technical Efforts,” United Technologies Pratt & Whitney Division, NASA CR-168267, 1983.

5. Purpura, P. T., “Dynamic Gas Temperature Measurement System, Volume II – Operation and Program Manual,” United Technologies Pratt & Whitney Division, NASA CR-168267, 1983.

6. Elmore, D.L., Robinson, W.W, and Watkins, W.B., “Further Development of the Dynamic Gas Temperature Measurement System, Volume I – Technical Efforts,” United Technologies Pratt & Whitney Division, NASA CR-179513, 1986.

7. Stocks, D.R. and Elmore, D.L., “Further Development of the Dynamic Gas Temperature Measurement System, Volume II – Computer Program User’s Manual,” United Technologies Pratt & Whitney Division, NASA CR-179513, 1986.

8. Weir, D., “Engine Validation of Noise and Emission Reduction Technology Phase I,” NASA/CR—2008-215225, 2008.

9. Royalty, C. M. and Schuster, B., “Noise from a Turbofan Engine Without a Fan from the Engine Validation of Noise and Emission Reduction Technology (EVNERT) Program,” AIAA-2008-2810, 14th AIAA/CEAS Aeroacoustics Conference, Vancouver, British Columbia Canada, 5-7 May 2008.

10. Wegner, M.A., Nance, D., and Ahuja, K. K., “Characterization of Short and Infinite-line Pressure Probes for In-duct Acoustic Measurements under Hostile Environment,” AIAA 2007-3443, 13th AIAA/CEAS Aeroacoustics Conference, Rome, Italy, 21-23 May 2007.

11. Lourier, J.M., Reichling, G., Stöhr, M., Domenico, M.D., Noll, B.E., and Aigner, M., “Numerical Analysis of Probe Microphones Used for Thermoacoustic Measurements”, AIAA 2012-0545, Proc. 50th AIAA Aerospace Sciences Meeting, Nashville TN, 2012.

12. Miles, J. H., “Time Delay Analysis of Turbofan Engine Direct and Indirect Combustion Noise Sources,” J. of Propulsion and Power, V. 25, N1, Jan.-Feb. 2009.

13. Hultgren, L. S. and Miles, J. H., “Noise-Source Separation Using Internal and Far-Field Sensors for a Full-Scale Turbofan Engine,” NASA Tm 2009-215834, 2009.

14. Miles, J. H., “Separating Direct and Indirect Turbofan Engine Combustion Noise While Estimating Post-Combustion (Post-Flame) Residence Time Using the Correlation Function,” NASA TM 2011-216248, 2011.

15. Miles, J. H., “Spatial Correlation in the Ambient Core Noise Field of a Turbofan Engine,” J. Acoustical Society of America, V131, N6, June 2012.

16. Bake, F., Michel, Ulf, and Roehle, I., “Investigation of Entropy Noise in Aero-Engine Combustors,” Paper GT 2006-90093, Proceedings of the 2006 ASME Turbo Expo, May 8-11, Barcelona, Spain, 2006.